APPLICATION OF THE LOCAL MODE MODEL TO THE OVERTONE SPECTRA OF SEVERAL CLASSES OF MOLECULES

by

M. Khalique Ahmed

A Thesis submitted to
the Faculty of Graduate Studies
of the University of Manitoba
in partial fulfillment of
the requirements of the degree
Doctor of Philosophy
Winnipeg, Manitoba

 August 1986

ISBN 0-315-34000-2

APPLICATION OF THE LOCAL MODE MODEL TO THE OVERTONE SPECTRA OF SEVERAL CLASSES OF MOLECULES

BY

M. KHALIQUE AHMED

A thesis submitted to the Faculty of Graduate Studies of
the University of Manitoba in partial fulfillment of the requirements
of the degree of

DOCTOR OF PHILOSOPHY

ABSTRACT

The overtone spectra of a variety of molecules were measured and the spectral features were interpreted in terms of the local mode model.

The liquid phase spectra of $CHDCl_2$ in the regions of $\Delta v_{CH} = 2 - 4$ were used in an analysis of the Fermi resonance interactions in the overtone spectrum of dichloromethane. These interactions involve CH stretching local mode peaks and nearby combination peaks involving two quanta of HCH bending.

Liquid phase $\Delta v_{CD} = 2 - 5$ spectra of CD_2Z_2 (Z = Cl, Br or I) and CD_3Z (Z = I or CN) were studied to investigate the effects of increased interoscillator CD coupling on the symmetry splitting and intensities of the local mode states. The increased interoscillator CD coupling in deuterated molecules was found to be responsible for greater symmetry splitting between the symmetrized local mode states of these molecules as compared to the undeuterated molecules. The enhanced intensities of the local mode combination states in deuterated molecules were also accounted for by greater interoscillator CD coupling.

Liquid phase $\Delta v_{CH} = 2 - 6$ spectra of CH_3Z (Z = Cl, Br, I or CN) molecules were observed and analyzed. Integrated oscillator strengths of the spectra of methyl halides were determined and plotted against the square root of the observed energies of the pure local states. These plots and similar reported plots for dihalomethanes and trihalomethanes were used to discuss the sensitivity of the CH bond potential to the successive replacement of one, two or three hydrogen

atoms of methane with the halogens.

The liquid and gas phase spectra of $(CH_3)_3CCl$ and $(CH_3)_3SiCl$ were examined. Two types of methyl CH bonds were predicted by SCF molecular orbital calculation (4-31G and STO-3G) for both $(CH_3)_3CCl$ and $(CH_3)_3SiCl$ and were observed in the overtone spectra.

Overtone spectra (Δv_{CH} = 2 - 6) of a series of monosubstituted cyclopropanes were observed and analyzed. The analysis demonstrated the dynamical independence of the XH bonds located at different centres of these molecules.

The overtone spectra of trimethylbenzenes and benzal halides were also investigated. Features corresponding to both structurally and conformationally nonequivalent bonds were resolved. The results from the study of trimethylbenzenes revealed that absorptions from methyl groups below and above the barrier to internal rotation are resolvable in the overtone spectra.

LIST OF PUBLICATIONS

1. O. S. Mortensen, M. K. Ahmed, B. R. Henry and A. W. Tarr, "Intensities in Local Mode Overtone Spectra: Dichloromethane and Deuterated Dichloromethane", J. Chem. Phys. 82, 3903 (1985).
2. M. K. Ahmed and B. R. Henry, "A Local Mode Analysis of the CD Stretching Fundamental and Overtone Spectra of Deuterated Dihalomethanes", J. Phys. Chem. 90, 1081 (1986) and presented at 69th Canadian Chemical Conference, 1986, Saskatoon, Saskatchewan, Abstract no. PH-B5-1.
3. M. K. Ahmed and B. R. Henry, "Fermi Resonance Shifts in the Overtone Spectrum of Dichloromethane: The Overtone Spectrum of Dichloromethane-d", J. Phys. Chem. 90, 1993 (1986).
4. M. K. Ahmed and B. R. Henry, "Gas-Phase Overtone Spectral Investigation of Structurally and Conformationally Nonequivalent CH Bonds in Trimethylbenzenes", J. Phys. Chem. 90, 1737 (1986).
5. M. K. Ahmed and B. R. Henry, "A Local Mode Description of XH-Stretching Overtone Spectra of Some Monosubstituted Cyclopropanes", Abstract no. PH-B5-3, 69th Canadian Chemical Conference, 1986, Saskatoon, Saskatchewan.
6. M. K. Ahmed, D. J. Swanton and B. R. Henry, "Overtone Spectral Investigation of the Conformational Preference of Dichloromethyl and Dibromomethyl Groups in Benzal Chloride and Benzal Bromide", J. Phys. Chem., submitted.

ACKNOWLEDGEMENTS

I am extremely indebted to my supervisor, Professor Bryan Henry, for giving me the opportunity to undertake research in his laboratory and also for directing my progress and being a constant source of encouragement.

I am grateful to Dr. Ali Mohammadi, Dr. Allan Tarr, Dr. David Swanton, Dr. Kathleen Gough, Dr. Prabhat Goswami and Michael Sowa for their friendship and many interesting discussions.

I am thankful to Professor Norman Hunter and Professor Hyman Gesser for their interest in my research work and for helpful discussions.

I am grateful to the Department of Chemistry for financial assistance.

I also gratefully acknowledge the efforts of Donna Harris in the superb typing of this thesis.

Finally, I acknowledge my parents and my wife, Almas, for their encouragement and support, without which the production of this thesis would not have been such an interesting and rewarding job.

TABLE OF CONTENTS

TABLES

CHAPTER 1

INTRODUCTION

A very brief introduction to the local mode model of XH stretching vibrations will be presented in this chapter. Local mode theory of XH_2 and XH_3 system will be discussed and the principal objectives of the thesis will be outlined.

i) The Local Mode Model

The concept of a normal mode[1,2] plays an important role in the vibrational theory of polyatomic molecules. In any one normal mode vibration of a polyatomic molecule, every atom performs a simple harmonic motion with the same characteristic frequency and all the atoms move in phase with one another. In polyatomic molecules certain vibrational modes are localized. For example consider the molecules like CHZ_3 (Z = Cl, Br or I). The CH stretching vibrations of these molecules have a frequency that is so different from that of the other modes that it can effectively be considered uncoupled from the other degrees of freedom. In other words the CH stretching mode of CHZ_3 molecules can be considered as a "localized mode". Later in this section it will be emphasized that such localized modes are present in all polyatomic molecules containing XH moieties.

Interest in XH stretching overtone spectroscopy extends back almost six decades[3-8]. However, these earlier studies will not be reviewed here because a fair amount of discussion has already been presented[9,10].

In the years 1967 and 1968, interest in XH stretching overtone vibrations was renewed[11-14]. It was recognized that XH stretching overtones are important acceptor modes of the large vibrational energies associated with radiationless transitions between electronic states. Later, XH stretching overtone spectra of benzene[15], ammonia[16], and methane[16] were investigated. The observed overtone spectra were explained on the basis of independent XH oscillators. However, the final description of these overtone spectra was still made in terms of symmetry allowed normal mode components[1,2].

In 1975 Hayward and Henry[17] introduced the local mode model of XH stretching overtones through a detailed analysis of the overtone spectrum of dichloromethane. The line shapes of the observed overtone peaks were found to be best described by a model which involved local CH oscillators. Since the introduction of this model, various theoretical and experimental studies have been carried out by Henry and his coworkers and by other research groups (For reviews see references 18-22). All these studies verify the validity of the local mode model.

The local mode model considers the XH oscillators of polyatomic molecules as weakly coupled anharmonic oscillators. The essential feature of the local mode model is that high energy ($\Delta v_{XH} \geq 3$) XH stretching overtone spectra are dominated by the pure local mode peaks. The pure local mode peaks arise from transitions to states whose components have all the vibrational energy localized in one of a set of equivalent XH bonds. The transition energies $\Delta E(v)$ of pure local mode peaks fit very well to the energy equation of an anharmonic diatomic oscillator,

$$\Delta E(v) = v\omega - (v^2+v)\omega x \qquad (1.1a)$$

In Eq. (1.1a) $\omega(cm^{-1})$ is the harmonic frequency and $\omega x(cm^{-1})$ is the diagonal local mode anharmonicity constant. The vibrational quantum number is denoted by v. A somewhat different notation has been used for the local mode parameters in some local mode studies[19]. In these studies the vibrational energies of the pure local mode peaks were fitted to the following equation

$$\Delta E(v) = v\omega^{XH} + v^2X \qquad (1.1b)$$

The parameters of Eqs. (1.1a) and (1.1b) are related by

$$\omega^{XH} = \omega - \omega x \quad \text{and}$$
$$X = -\omega x \tag{1.2}$$

Local mode-local mode (LM-LM) combination peaks also occur in the XH stretching overtone spectra. These peaks arise from transitions to states, which have vibrational quanta distributed over more than one XH oscillator. The LM-LM combination peaks carry much lower intensity than the pure local mode peaks for $\Delta v_{XH} \geq 3$, and rapidly decrease in relative intensity with increasing Δv_{XH}. The vibrational energy of a LM-LM combination state can be expressed by the following equation

$$E = E_o + \sum_i v_i \omega_i^{XH} + \sum_{i>j} \sum c_{ij} \omega_{ij} + \sum_{i\geq j} \sum v_i v_j X_{ij} \tag{1.3}$$

which is a more general form of Eq. (1.1b). In Eq. (1.3), ω_i^{XH} are the local mode frequencies as defined by Eq. (1.2). X_{ij} of Eq. (1.3) are the local mode anharmonicities. E_o is the vibrational energy of the ground state and $c_{ij}\omega_{ij}$ are harmonic coupling terms. The vibrational quantum number of a specific XH oscillator is denoted by v_i. The harmonic coupling terms of Eq. (1.3) are small and can be neglected[14]. The off-diagonal local mode anharmonicity constants (X_{ij}, $i \neq j$) are much smaller than diagonal anharmonicity constants (X_{ii}) and can also be neglected[14,16,17]. With the neglect of harmonic coupling and off-diagonal anharmonicity constants, the simplified vibrational energy equation for LM-LM combination peaks can be written as,

$$\Delta E = \sum_i v_i \omega_i^{XH} + \sum_i v_i^2 X_{ii} \tag{1.4}$$

Eq. (1.4) in terms of ω_i and $\omega_i x_i$ (see Eq. 1.2) can be written as

$$\Delta E = \sum_i v_i \omega_i - \sum_i (v_i^2 + v_i)\omega_i x_i \qquad (1.5)$$

Comparison of Eqs. (1.1) and (1.5) shows that Eq. (1.5) is simply the result of summing Eq. (1.1) over excited oscillators. This comparison also shows that anharmonic contributions to the energy of LM-LM combinations are less than for a pure local mode state with the same number of vibrational quanta. Thus, for a particular overtone manifold $\Delta v_{XH} = v$, the LM-LM combination peaks are observed on the high frequency side of the pure local mode overtone peak.

Another type of peak which occurs in overtone spectra is the local mode-normal mode (LM-NM) combination. This type of combination involves simultaneous excitation of a XH stretching mode and a normal mode. LM-NM combination peaks usually occur in the close vicinity of the pure local mode peaks and "steal" intensity through resonant or near resonant interactions from these peaks.

Because of their localized nature, overtone spectra are extremely sensitive to the properties of XH bonds. Local mode overtones have been used to study intermolecular and nonbonded intramolecular interactions[23-26]. The frequencies of pure local mode peaks have been shown to decrease and increase linearly with an increase or decrease in the XH bond length[27-31]. Thus overtone spectroscopy, through the local mode model, can be used to determine XH bond lengths. These highly accurate bond lengths correlate remarkably well with geometry optimized ab initio MO calculations[32]. In the high energy overtone spectra, structurally and conformationally nonequivalent bonds display well resolved peaks which correspond to different types of XH

oscillators[9,27-43]. The local mode model has also been used extensively in studies of intramolecular vibrational energy redistribution[44-69]. However, this latter aspect of the local mode model is not relevant to the work which will be presented in this thesis.

ii) Symmetry Effects in the Local Mode Model

The local mode model in its original form[17] did not explicitly involve molecular symmetry. The principal transitions observed in the overtone spectra for $\Delta v_{XH} \geq 3$ were considered to arise from stretching excitations of single XH oscillators. Symmetry effects in the local mode picture have been introduced recently[21,70-81]. With the inclusion of symmetry, the spectral features of higher overtones ($\Delta v_{XH} \geq 3$) as well as of the fundamental and first overtone spectra are accounted for by the local mode picture. Symmetry effects on the pure local mode overtone peaks are observed in the fundamental and first overtone regions only. Symmetry splitting for the local mode combination peaks persists to higher levels of excitation. In the subsequent chapters of this thesis, symmetrized local mode theory of XH_2 and XH_3 systems will be utilized. The important features of the theory are discussed below:

a) XH_2 System

In the local mode picture*, the local mode basis states for the two coupled XH bonds which share a common X atom are taken as Morse oscillator product states, i.e., $|v_1,v_2\rangle = |v_1\rangle|v_2\rangle$, where $|v_1\rangle$ and $|v_2\rangle$ are Morse oscillator wave functions for the first and second XH bond, respectively, for a given vibrational quantum number $v = v_1 + v_2$[54,70,73,82]. Symmetrized states for the two coupled bonds are

---

*Symmetrized local mode theory for a XH_2 system was developed[70] by Mortensen, Henry and Mohammadi in 1981. The results are summarized here for completeness.

written as[54,70,73]

$$|v_1,v_2\rangle_{\pm} = \frac{1}{\sqrt{2}}\left(|v_1,v_2\rangle \pm |v_2,v_1\rangle\right) \tag{1.6}$$

The local mode Hamiltonian for the XH_2 system is taken to be[70]

$$H - E_o = (v_1+v_2)\omega - (v_1^2+v_2^2+v_1+v_2)\omega x +$$

$$(a_1^+-a_1)(a_2^+-a_2)\gamma\omega + (a_1^++a_1)(a_2^++a_2)\phi\omega \tag{1.7}$$

In Eq. (1.7), $\omega(cm^{-1})$ and $\omega x(cm^{-1})$ are the harmonic frequency and diagonal local mode anharmonicity, respectively, for an isolated XH bond, v_1 and v_2 are the quantum numbers of the two XH oscillators and E_o is the ground state energy in wavenumber units. γ and ϕ determine the kinetic energy and potential energy coupling between the two XH bonds, and are defined in terms of the Wilson G and F matrix elements[2]

$$\gamma = -\frac{1}{2}\frac{G_{12}}{G_{11}} = \frac{-\cos\theta}{2\left(1+\frac{m_X}{m_H}\right)} \tag{1.8a}$$

and

$$\phi = \frac{1}{2}\frac{F_{12}}{F_{11}} \tag{1.8b}$$

γ of Eq. (1.8a) is solely a function of molecular configuration and can be evaluated if the HXH angle θ is known. m_x and m_H of Eq. (1.8a) are the atomic masses of X and H atoms, respectively. The model Hamiltonian of Eq. (1.7) contains all of the anharmonicity that is diagonal in a single XH oscillator but evaluates the matrix elements that couple the two XH oscillators in the harmonic limit. In the

harmonic approximation, the operators a^+ and a of Eq. (1.7) have the usual step-up and step-down properties[70]:

$$\langle v+1|a^+|v\rangle = \sqrt{v+1}, \quad \langle v-1|a|v\rangle = \sqrt{v}, \quad \text{etc.} \qquad (1.9)$$

According to this "ladder" coupling scheme[70], effective coupling only occurs between states which belong to the same manifold, v, which have the same symmetry, and where the bond excitation differ by a single quantum; i.e., $|v_1,v_2\rangle_+$ effectively couples to $|v_1\pm1, v_2\mp1\rangle_+$, etc. The effective coupling decreases as the level of excitation increases. Thus, the pure local mode states, $|v,0\rangle_\pm$, which carry most of the intensity, are split at $\Delta v_{XH} = 1$ and $\Delta v_{XH} = 2$ but become effectively degenerate for higher overtones ($\Delta v_{XH} \geq 3$). The transition energies for these higher overtones can be simply described by the vibrational energy expression for a single Morse oscillator, i.e., by Eq. (1.1a).

The matrices of Eq. (1.7) in the local mode basis are given in Table 1.1 up to $\Delta v_{XH} = 6$. All these matrices involve only three parameters ω, ωx and γ' ($\gamma' = \gamma - \phi$). The first two parameters ω and ωx can be obtained by fitting the observed frequencies of the pure local mode peaks, $|v,0\rangle_\pm$, of the XH_2 system to Eq. (1.1a). The value of effective coupling, γ', with both kinetic and potential energy terms, can be obtained empirically from the observed splitting between the $|1,0\rangle_+$ and $|1,0\rangle_-$ peaks. This splitting is two times the value of γ', i.e., $\Delta E(|1,0\rangle_- - |1,0\rangle_+) = 2\gamma'$. This result is obtained simply from the diagonalization of the appropriate 2 x 2 matrix.

To calculate the energies of all the XH stretching peaks of XH_2 system ω, ωx and $\omega\gamma'$ are substituted into matrices of Table 1.1. Matrix diagonalization gives the energies of the symmetrized states.

b) XH_3 System

The local mode basis states* for a XH_3 system with local C_{3v} symmetry are of the form $|v_1,v_2,v_3\rangle = |v_1\rangle|v_2\rangle|v_3\rangle$, where $|v_1\rangle$, $|v_2\rangle$ and $|v_3\rangle$ are the Morse oscillator wave functions for the three coupled XH bonds at a given overtone manifold $\Delta v_{XH} = v_1 + v_2 + v_3 = v$. The energies of the local mode states are obtained by expanding the vibrational wave function in the local oscillator basis and diagonalizing the resulting Hamiltonian matrix. To make the analysis simple it is important that symmetry arguments be used. Thus, the first step in the calculation of the XH stretching spectra of a XH_3 system involves the formation of the symmetrized states from the equivalent product states $|v_1,v_2,v_3\rangle$. The symmetrized states for a XH_3 system with local C_{3v} symmetry can be constructed by using NONCOM (noncommuting generator) approach to molecular symmetry[83]. The C_{3v} point group can be generated by two operators C_3, a three fold rotation axis, and σ_v, a mirror plane. The operators C_3 and σ_v do not commute, but they do obey the following commutation relation:

$$C_3\sigma_v = \sigma_v C_3^{-1} \qquad (1.10)$$

As discussed in detail by Mortensen and Hassing[83], the relation (1.10) implies that the symmetry of states can be completely characterized by giving the eigenvalues λ_3 and λ_σ under the operations C_3 and σ_v, respectively. The values for λ_3 (for integer spin) and λ_σ

---

*Symmetrized local mode theory for a XH_3 system was developed[71] by Henry et al. in 1983. The results are summarized here for completeness.

are given below:

$$\lambda_3 = 1, \exp(\pm i \frac{2\pi}{3}) \tag{1.11}$$

$$\lambda_\sigma = \pm 1 \tag{1.12}$$

The eigenvalues for C_{3v} point group are tabulated in Table 1.2. The symmetrized states for a XH_3 system can straightforwardly be constructed from the entries of Table 1.2. These symmetrized states are listed in Table 1.3 for Δv_{XH} = 1-6. Note that for the states of E symmetry only one component is given in Table 1.3. The other component is the complex conjugate of the first component.

The following Hamiltonian can be used for the analysis of the XH stretching spectra of a XH_3 system

$$(H-E_o) = (v_1+v_2+v_3)\omega - (v_1^2+v_2^2+v_3^2+v_1+v_2+v_3)\omega x + (p_1p_2+p_1p_3+p_2p_3)\gamma\omega + (q_1q_2+q_1q_3+q_2q_3)\phi\omega \tag{1.13}$$

In Eq. (1.13), $\omega(cm^{-1})$ and $\omega x(cm^{-1})$ are the harmonic frequency and diagonal local mode anharmonicity, respectively, for an isolated XH bond. v_1, v_2 and v_3 are the quantum numbers of the three XH oscillators, and E_o is the ground state energy in wavenumber units. γ and ϕ determine the kinetic energy and potential energy coupling between different XH bonds and are defined in terms of the Wilson G and F matrix elements[70]

$$\gamma = -(\frac{1}{2}) \frac{G_{ij}}{G_{ii}} \tag{1.14a}$$

and

$$\phi = (\frac{1}{2})(\frac{F_{ij}}{F_{ii}}) \quad , \quad i,j = 1,2,3 \tag{1.14b}$$

Note that Eqs. (1.14a) and (1.14b) are an extension of Eqs. (1.8a) and (1.8b).

p_i and q_i of Eq. (1.13) are the normalized momentum and coordinate variables, respectively, and are defined as follow

$$p = a^+ - a \tag{1.15a}$$

$$q = a^+ + a \tag{1.15b}$$

The operators a^+ and a have the properties expressed in Eq. (1.9).

With the Hamiltonian of Eq. (1.13) and the symmetrized states of Table 1.3, the Hamiltonian matrix can be evaluated. To reduce the size of this matrix the mixing of the local mode states belonging to different manifolds (which will be extremely small) can be neglected because such states will be separated by a large energy difference. The Hamiltonian matrix of Table 1.4 can be used to calculate the XH stretching spectra of any XH_3 system with local C_{3v} symmetry. In this thesis this Hamiltonian matrix will be utilized for the analysis of the spectra of CH_3Z (Z = Cl, Br, I or CN) and CD_3Z (Z = I or CN) molecules.

iii) Objectives of the Thesis

The main objective of this thesis was to determine the applicability of an extremely simple harmonically coupled local mode description of XH_2 and XH_3 systems. This description was used in assigning the overtone spectra of polyatomic molecules which contain these moieties. This local mode theory for XH_2 systems is utilized in assigning and understanding the spectral features of the overtone spectra of some monosubstituted cyclopropanes, deuterated dihalomethanes, 2-chloro-2-methylpropane and chlorotrimethylsilane. The corresponding local mode theory for XH_3 systems is used to analyze the spectra of methyl halides, deuterated methyl iodide and deuterated methyl cyanide.

Another objective of this thesis was to extend some previous overtone studies in order to investigate molecular conformations. The time scale of the near IR experiment allows the study of processes which are much too fast to be studied by conventional techniques like NMR. In this thesis, evidence for the conformational nonequivalence of XH bonds is examined in the overtone spectra of trimethylbenzenes, 2-chloro-2-methylpropane, chlorotrimethylsilane and benzal halides.

As has already been mentioned, local mode overtone spectra are very sensitive to the properties of XH bonds. This aspect of overtone spectra is used to study the differences in bond strength/hybridization of XH bonds of some monosubstituted cyclopropanes and larger cycloalkanes and cycloalkenes. The differences in the bond strength/hybridization of XH bonds of these molecules are clearly reflected in the local mode frequencies of these molecules.

A detailed discussion regarding the individual problems will be

presented later in the appropriate chapters. In the following paragraphs only main points are outlined.

In chapter 2 the details of the experimental work and the data manipulations are discussed.

In chapter 3 the overtone spectra of dichloromethane-d are reported. With the aid of these spectra, the Fermi resonance interaction between the pure local mode peaks and local mode-bending mode combination peaks in dichloromethane is studied. This work also shows that most of the spectral features observed at low overtones arise from interoscillator couplings.

Although the local mode model has been extensively used to understand the overtone spectra of molecules containing XH oscillators, very little attention has been directed to the overtone spectra of deuterated molecules. In chapters 4 and 6 the overtone spectra of some deuterated methanes (CD_2Cl_2, CD_2Br_2, CD_2I_2, CD_3I and CD_3CN) are reported. Through the analysis of these spectra the effects of increased interoscillator coupling on the energetics and intensities of the local mode states of C_{2v} and C_{3v} symmetry are identified and discussed.

In Chapter 5 the overtone spectra of methyl halides and methyl cyanide are reported. Results from these spectra and from the previously reported spectra of dihalomethanes and trihalomethanes are used to examine the sensitivity of the CH bond potential to one, two or three halogen atoms.

Chapter 7 of this thesis discusses the liquid and gas phase CH stretching fundamental and overtone spectra of 2-chloro-2-methylpropane and chlorotrimethylsilane [$(CH_3)_3CCl$,

$(CH_3)_3SiCl$]. Molecular orbital calculations are performed and predict two types of methyl CH bonds. In the experimental spectra of each molecule two well resolved peaks corresponding to two types of nonequivalent bonds are identified. The most important aspect of this study is that the stretching vibration of the unique methyl CH bond (trans to the C-Cl(Si-Cl) bond) can be decoupled from the other local methyl vibrations. Such a decoupling of conformationally distinct CH bonds not only could be of great help in overtone spectral analysis of other molecules but also could provide direct information on the properties of the conformationally distinct bonds.

In chapter 8 overtone spectral studies on monosubstituted cyclopropanes are presented. The local mode theory of a XH_2 system is used successfully to assign the observed peaks due to the methylene oscillators. The methine oscillator peaks fit very well to the energy equation of an anharmonic Morse oscillator. These results demonstrate the dynamical independence of the XH bonds at the different centres.

The gas phase overtone spectra of trimethylbenzenes in the region of $\Delta v_{CH} = 3$ are reported in chapter 9. Spectral features due to both conformationally and structurally nonequivalent bonds are assigned. The study provides a convincing confirmation of the earlier suggestions of Gough and Henry[28] concerning the interpretation of spectral features in terms of the conformational properties of the methyl group.

The overtone spectra of benzal chloride and benzal bromide are discussed in chapter 10. Differences in the strengths of the aryl CH bonds are reflected in the overtone spectra, in agreement with recent ab initio molecular orbital results[84]. The alkyl regions of the

overtone spectra of benzal chloride suggest contributions from two conformations of the $-CHCl_2$ groups in agreement with recent Raman studies[85,86].

In Appendix A the overtone spectra of (chloromethyl) cyclopropane is discussed. This work is in fact an extension of the work reported in chapter 8 on monosubstituted cyclopropanes. Thus the results of Appendix A are interpreted on the same basis as the results of chapter 8. In Appendix B oscillator strengths of the overtones of CH_2Cl_2 and CD_2Cl_2 are reported. This work, in combination with the work of Mortensen, Henry and Tarr, was used to develop a general theory of overtone intensities[87].

Table 1.1.

Local Mode Hamiltonian Matrix for a XH_2 System. [All matrix elements are in units of XH oscillator frequency ω and $\gamma' = \gamma - \phi$.]

$\Delta v_{XH} = 1$

(+) 10 : $1-2x-\gamma'$; 10 : $1-2x+\gamma'$ (-)

$\Delta v_{XH} = 2$

(+)

	20	11
20	$2-6x$	$-2\gamma'$
11	$-2\gamma'$	$2-4x$

20 : $2-6x$ (-)

$\Delta v_{XH} = 3$

(+)

	30	21
30	$3-12x$	$-\sqrt{3}\gamma'$
21	$-\sqrt{3}\gamma'$	$3-8x-2\gamma'$

30 : $3-12x$; 21 : $3-8x+2\gamma'$ (-)

$\Delta v_{XH} = 4$

(+)

	40	31	22
40	$4-20x$	$-2\gamma'$	0
31	$-2\gamma'$	$4-14x$	$-2\sqrt{3}\gamma'$
22	0	$-2\sqrt{3}\gamma'$	$4-12x$

40 : $4-20x$; 31 : $-2\gamma'$; $4-14x$ (-)

$\Delta v_{XH} = 5$

(+)

	50	41	32
50	$5-30x$	$-\sqrt{5}\gamma'$	0
41	$-\sqrt{5}\gamma'$	$5-22x$	$-2\sqrt{2}\gamma'$
32	0	$-2\sqrt{2}\gamma'$	$5-18x-3\gamma'$

(-)

	50	41	32
50	$5-30x$	$-\sqrt{5}\gamma'$	0
41	$-\sqrt{5}\gamma'$	$5-22x$	$-2\sqrt{2}\gamma'$
32	0	$-2\sqrt{2}\gamma'$	$5-18x+3\gamma'$

Table 1.1...cont'd...

$\Delta v_{XH} = 6$

(+)

60	$6-42x$	$-\sqrt{6}\gamma'$	0	0
51	$-\sqrt{6}\gamma'$	$6-32x$	$-\sqrt{10}\gamma'$	0
42	0	$-\sqrt{10}\gamma'$	$6-26x$	$-2\sqrt{6}\gamma'$
33	0	0	$-2\sqrt{6}\gamma'$	$6-24x$

(-)

60	$6-42x$	$-\sqrt{6}\gamma'$	0
51	$-\sqrt{6}\gamma'$	$6-32x$	$-\sqrt{10}\gamma'$
42	0	$-\sqrt{10}\gamma'$	$6-26x$

Table 1.2.

Eigenvalue Table for C_{3v} Group. [$\eta = \exp(-2\pi i/3)$]

Representation	State	λ_3	λ_σ
A_1		1	1
A_2		1	-1
E	E_1	η	$\begin{pmatrix} 0 & 1 \\ 1 & 0 \end{pmatrix}$
	E_{-1}	η^*	

Table 1.3.

Symmetrized Basis States for Three Equivalent Oscillators.

[$\eta = \exp(-2\pi i/3)$]

$\Delta v_{XH} = 1$

$$|100\rangle_{A_1} = 3^{-\frac{1}{2}}(|100\rangle + |010\rangle + |001\rangle)$$

$$|100\rangle_{E} = 3^{-\frac{1}{2}}(|100\rangle + \eta^{*}|010\rangle + \eta|001\rangle)$$

$\Delta v_{XH} = 2$

$$|200\rangle_{A_1} = 3^{-\frac{1}{2}}(|200\rangle + |020\rangle + |002\rangle)$$

$$|110\rangle_{A_1} = 3^{-\frac{1}{2}}(|110\rangle + |011\rangle + |101\rangle)$$

$$|200\rangle_{E} = 3^{-\frac{1}{2}}(|200\rangle + \eta^{*}|020\rangle + \eta|002\rangle)$$

$$|110\rangle_{E} = 3^{-\frac{1}{2}}(|110\rangle + \eta^{*}|011\rangle + \eta|101\rangle)$$

$\Delta v_{XH} = 3$

$$|300\rangle_{A_1} = 3^{-\frac{1}{2}}(|300\rangle + |030\rangle + |003\rangle)$$

$$|210\rangle_{A_1} = 6^{-\frac{1}{2}}(|210\rangle + |021\rangle + |102\rangle + |201\rangle + |120\rangle + |012\rangle)$$

$$|111\rangle_{A_1} = |111\rangle$$

$$|210\rangle_{A_1} = 6^{-\frac{1}{2}}(|210\rangle + |021\rangle + |102\rangle - |201\rangle - |120\rangle - |012\rangle)$$

$$|300\rangle_{E} = 3^{-\frac{1}{2}}(|300\rangle + \eta^{*}|030\rangle + \eta|003\rangle)$$

$$|210\rangle_{E} = 3^{-\frac{1}{2}}(|210\rangle + \eta^{*}|021\rangle + \eta|102\rangle)$$

$$|201\rangle_{E} = 3^{-\frac{1}{2}}(|201\rangle + \eta^{*}|120\rangle + \eta|012\rangle)$$

$\Delta v_{XH} = 4$

$$|400\rangle_{A_1} = 3^{-\frac{1}{2}}(|400\rangle + |040\rangle + |004\rangle)$$

$$|310\rangle_{A_1} = 6^{-\frac{1}{2}}(|310\rangle + |031\rangle + |103\rangle + |301\rangle + |130\rangle + |013\rangle)$$

$$|220\rangle_{A_1} = 3^{-\frac{1}{2}}(|220\rangle + |022\rangle + |202\rangle)$$

$$|211\rangle_{A_1} = 3^{-\frac{1}{2}}(|211\rangle + |121\rangle + |112\rangle)$$

$$|310\rangle_{A_2} = 6^{-\frac{1}{2}}(|310\rangle + |031\rangle + |103\rangle - |301\rangle - |130\rangle - |013\rangle)$$

$$|400\rangle_{E} = 3^{-\frac{1}{2}}(|400\rangle + \eta^{*}|040\rangle + \eta|004\rangle)$$

Table 1.3...cont'd...

$$|310\rangle_E = 3^{-\frac{1}{2}} (|310\rangle + \eta^* |031\rangle + \eta|103\rangle)$$
$$|301\rangle_E = 3^{-\frac{1}{2}} (|301\rangle + \eta^* |130\rangle + \eta|013\rangle)$$
$$|220\rangle_E = 3^{-\frac{1}{2}} (|220\rangle + \eta^* |022\rangle + \eta|202\rangle)$$
$$|211\rangle_E = 3^{-\frac{1}{2}} (|211\rangle + \eta^* |121\rangle + \eta|112\rangle)$$

$\Delta v_{XH} = 5$

$$|500\rangle_{A_1} = 3^{-\frac{1}{2}} (|500\rangle + |050\rangle + |005\rangle)$$
$$|410\rangle_{A_1} = 6^{-\frac{1}{2}} (|410\rangle + |041\rangle + |104\rangle + |401\rangle + |140\rangle + |014\rangle)$$
$$|320\rangle_{A_1} = 6^{-\frac{1}{2}} (|320\rangle + |032\rangle + |203\rangle + |302\rangle + |230\rangle + |023\rangle)$$
$$|311\rangle_{A_1} = 3^{-\frac{1}{2}} (|311\rangle + |131\rangle + |113\rangle)$$
$$|221\rangle_{A_1} = 3^{-\frac{1}{2}} (|221\rangle + |122\rangle + |212\rangle)$$
$$|410\rangle_{A_2} = 6^{-\frac{1}{2}} (|410\rangle + |041\rangle + |104\rangle - |401\rangle - |140\rangle - |014\rangle)$$
$$|320\rangle_{A_2} = 6^{-\frac{1}{2}} (|320\rangle + |032\rangle + |203\rangle - |302\rangle - |230\rangle - |023\rangle)$$
$$|500\rangle_E = 3^{-\frac{1}{2}} (|500\rangle + \eta^* |050\rangle + \eta|005\rangle)$$
$$|410\rangle_E = 3^{-\frac{1}{2}} (|410\rangle + \eta^* |041\rangle + \eta|104\rangle)$$
$$|401\rangle_E = 3^{-\frac{1}{2}} (|401\rangle + \eta^* |140\rangle + \eta|014\rangle)$$
$$|320\rangle_E = 3^{-\frac{1}{2}} (|320\rangle + \eta^* |032\rangle + \eta|203\rangle)$$
$$|302\rangle_E = 3^{-\frac{1}{2}} (|302\rangle + \eta^* |230\rangle + \eta|023\rangle)$$
$$|311\rangle_E = 3^{-\frac{1}{2}} (|311\rangle + \eta^* |131\rangle + \eta|113\rangle)$$
$$|221\rangle_E = 3^{-\frac{1}{2}} (|221\rangle + \eta^* |122\rangle + \eta|212\rangle)$$

$\Delta v_{XH} = 6$

$$|600\rangle_{A_1} = 3^{-\frac{1}{2}} (|600\rangle + |060\rangle + |006\rangle)$$
$$|510\rangle_{A_1} = 6^{-\frac{1}{2}} (|510\rangle + |051\rangle + |105\rangle + |501\rangle + |150\rangle + |015\rangle)$$
$$|420\rangle_{A_1} = 6^{-\frac{1}{2}} (|420\rangle + |042\rangle + |204\rangle + |402\rangle + |240\rangle + |024\rangle)$$
$$|411\rangle_{A_1} = 3^{-\frac{1}{2}} (|411\rangle + |141\rangle + |114\rangle)$$
$$|330\rangle_{A_1} = 3^{-\frac{1}{2}} (|330\rangle + |033\rangle + |303\rangle)$$

Table 1.3...cont'd...

$$|321\rangle_{A_1} = 6^{-\frac{1}{2}} (|321\rangle + |132\rangle + |213\rangle + |312\rangle + |231\rangle + |123\rangle)$$

$$|222\rangle_{A_1} = |222\rangle$$

$$|510\rangle_{A_2} = 6^{-\frac{1}{2}} (|510\rangle + |051\rangle + |105\rangle - |501\rangle - |150\rangle - |015\rangle)$$

$$|420\rangle_{A_2} = 6^{-\frac{1}{2}} (|420\rangle + |042\rangle + |204\rangle - |402\rangle - |240\rangle - |024\rangle)$$

$$|321\rangle_{A_2} = 6^{-\frac{1}{2}} (|321\rangle + |132\rangle + |213\rangle - |312\rangle - |231\rangle - |123\rangle)$$

$$|600\rangle_{E} = 3^{-\frac{1}{2}} (|600\rangle + \eta^{*}|060\rangle + \eta|006\rangle)$$

$$|510\rangle_{E} = 3^{-\frac{1}{2}} (|510\rangle + \eta^{*}|051\rangle + \eta|105\rangle)$$

$$|501\rangle_{E} = 3^{-\frac{1}{2}} (|501\rangle + \eta^{*}|150\rangle + \eta|015\rangle)$$

$$|420\rangle_{E} = 3^{-\frac{1}{2}} (|420\rangle + \eta^{*}|042\rangle + \eta|204\rangle)$$

$$|402\rangle_{E} = 3^{-\frac{1}{2}} (|402\rangle + \eta^{*}|240\rangle + \eta|024\rangle)$$

$$|411\rangle_{E} = 3^{-\frac{1}{2}} (|411\rangle + \eta^{*}|141\rangle + \eta|114\rangle)$$

$$|330\rangle_{E} = 3^{-\frac{1}{2}} (|330\rangle + \eta^{*}|033\rangle + \eta|303\rangle)$$

$$|321\rangle_{E} = 3^{-\frac{1}{2}} (|321\rangle + \eta^{*}|132\rangle + \eta|213\rangle)$$

$$|312\rangle_{E} = 3^{-\frac{1}{2}} (|312\rangle + \eta^{*}|231\rangle + \eta|123\rangle)$$

In general, for $|abc\rangle$

$a = b = c$

$$|abc\rangle_{A_1} = |abc\rangle$$

$a, b = c$ $(a \neq b)$

$$|abc\rangle_{A_1} = 3^{-\frac{1}{2}} (|abc\rangle + |cab\rangle + |bca\rangle)$$

$$|abc\rangle_{E} = 3^{-\frac{1}{2}} (|abc\rangle + \eta^{*}|cab\rangle + \eta|bca\rangle)$$

a, b, c $(a \neq b \neq c, a \neq c)$

$$|abc\rangle_{A_1} = 6^{-\frac{1}{2}} (|abc\rangle + |cab\rangle + |bca\rangle + |acb\rangle + |bac\rangle + |cba\rangle)$$

$$|abc\rangle_{A_2} = 6^{-\frac{1}{2}} (|abc\rangle + |cab\rangle + |bca\rangle - |acb\rangle - |bac\rangle - |cba\rangle)$$

$$|abc\rangle_{E} = 3^{-\frac{1}{2}} (|abc\rangle + \eta^{*}|cab\rangle + \eta|bca\rangle)$$

$$|acb\rangle_{E} = 3^{-\frac{1}{2}} (|acb\rangle + \eta^{*}|bac\rangle + \eta|cba\rangle)$$

Table 1.4.

Local Mode Hamiltonian Matrix for a XH_3 System. [All matrix elements are in units of XH oscillator frequency ω, $\gamma' = \gamma - \phi$ and $\eta = \exp(\frac{-2\pi i}{3})$]

$\Delta v_{XH} = 1$

(A_1) 100 : $1-2x-2\gamma'$; 100 : $1-2x+\gamma'$ (E)

$\Delta v_{XH} = 2$

(A_1)

	200	110
200	$2-6x$	$-2\sqrt{2}\gamma'$
110	$-2\sqrt{2}\gamma'$	$2-4x-2\gamma'$

	200	110
200	$2-6x$	$-\sqrt{2}\gamma'(1+\eta^*)$
110	$-\sqrt{2}\gamma'(1+\eta)$	$2-4x+\gamma'$

(E)

$\Delta v_{XH} = 3$

(A_1)

	300	210	111
300	$3-12x$	$-\sqrt{6}\gamma'$	0
210	$-\sqrt{6}\gamma'$	$3-8x-3\gamma'$	$-2\sqrt{3}\gamma'$
111	0	$-2\sqrt{3}\gamma'$	$3-6x$

210 : $3-8x+3\gamma'$ (A_2)

(E)

	300	210	201
300	$3-12x$	$-\sqrt{3}\gamma'$	$-\sqrt{3}\gamma'$
210	$-\sqrt{3}\gamma'$	$3-8x$	$i\sqrt{3}\gamma'$
201	$-\sqrt{3}\gamma'$	$-i\sqrt{3}\gamma'$	$3-8x$

$\Delta v_{XH} = 4$

(A_1)

	400	310	220	211
400	$4-20x$	$-2\sqrt{2}\gamma'$	0	0
310	$-2\sqrt{2}\gamma'$	$4-14x-\gamma'$	$-2\sqrt{3}\gamma'$	$-\sqrt{6}\gamma'$
220	0	$-2\sqrt{3}\gamma'$	$4-12x$	$-2\sqrt{2}\gamma'$
211	0	$-6\sqrt{'}\gamma$	$-2\sqrt{2}\gamma'$	$4-10x-4\gamma'$

(A_2) 310 : $4-14x+\gamma'$

(E)

	400	310	301	220	211
400	$4-20x$	$-2\gamma'$	$-2\gamma'$	0	0
310	$-2\gamma'$	$4-14x$	$-\gamma'$	$-\sqrt{6}\gamma'$	$-\sqrt{3}\gamma'$
301	$-2\gamma'$	$-\gamma'$	$4-14x$	$-\sqrt{6}\gamma'\eta$	$-\sqrt{3}\gamma'$
220	0	$-\sqrt{6}\gamma'$	$-\sqrt{6}\gamma'\eta^*$	$4-12x$	$-\sqrt{2}\gamma'(1+\eta^*)$
211	0	$-\sqrt{3}\gamma'$	$-\sqrt{3}\gamma'$	$-\sqrt{2}\gamma'(1+\eta)$	$4-10x+2\gamma'$

Table 1.4...cont'd...

$\Delta v_{XH} = 5$

(A_1)

	500	410	320	311	221
500	$5-30x$	$-\sqrt{10}\gamma'$	0	0	0
410	$-\sqrt{10}\gamma'$	$5-22x-\gamma'$	$-2\sqrt{2}\gamma'$	$-2\sqrt{2}\gamma'$	0
320	0	$-2\sqrt{2}\gamma'$	$5-18x-3\gamma'$	$-2\gamma'$	$-\sqrt{6}\gamma'$
311	0	$-2\sqrt{2}\gamma'$	$-2\gamma'$	$5-16x$	$-2\sqrt{6}\gamma'$
221	0	0	$-\sqrt{6}\gamma'$	$-2\sqrt{6}\gamma'$	$5-14x-4\gamma'$

(A_2)

	410	320
410	$5-22x+\gamma'$	$-\sqrt{2}\gamma'/3$
320	$-\sqrt{2}\gamma'/3$	$5-18x+3\gamma'$

[E]

	500	410	401	320	302	311	221
500	$5-30x$	$-\sqrt{5}\gamma'$	$-\sqrt{5}\gamma'$	0	0	0	0
410	$-\sqrt{5}\gamma'$	$5-22x$	$-\gamma'$	$-2\sqrt{2}\gamma'$	0	$-2\gamma'$	0
401	$-\sqrt{5}\gamma'$	$-\gamma'$	$5-22x$	0	$-2\sqrt{2}\gamma'$	$-2\gamma'$	0
320	0	$-2\sqrt{2}\gamma'$	0	$5-18x$	$-3\gamma'\eta^*$	$-\sqrt{2}\gamma'$	$-\sqrt{3}\gamma'$
302	0	0	$-2\sqrt{2}\gamma'$	$-3\gamma'\eta$	$5-18x$	$-\sqrt{2}\gamma'$	$-\sqrt{3}\gamma'\eta$
311	0	$-2\gamma'$	$-2\gamma'$	$-\sqrt{2}\gamma'$	$-\sqrt{2}\gamma'$	$5-16x$	$-\sqrt{6}\gamma'(1+\eta)$
221	0	0	0	$-\sqrt{3}\gamma'$	$-\sqrt{3}\gamma'\eta^*$	$-\sqrt{6}\gamma'(1+\eta^*)$	$5-14+2\gamma'$

CHAPTER 2

EXPERIMENTAL DETAILS

In this chapter the details of the experimental work and the data manipulations will be discussed.

i) Commercially Available Compounds

All of the compounds (except dichloromethane-d) studied in this thesis were obtained commercially. All the compounds were of high purity with the exception of 1,2,3-trimethylbenzene and cyclopropyl methyl ketone. 1,2,3-Trimethylbenzene had a stated purity of 90% and was distilled prior to use. The proton NMR spectrum of the distillate confirmed the expected enhancement of purity. Cyclopropyl methyl ketone was of relatively low purity (95%) and was also distilled before making the spectral measurements. The purities of all the compounds along, with the purchase sources, are listed in Table 2.1.

Table 2.1.

Purities and Purchase Sources of Compounds

Compound	Purity	Company
Dichloromethane-d_2	99.6 + atom%D	Fisher Scientific Co.
Dibromomethane-d_2	99 + atom%D	Merck Sharpe and Dohme Canada, Ltd.
Diiodomethane-d_2	"	"
Methyl chloride	Research grade	PFALTZ and BAUER Inc.
Methyl bromide	"	"
Methyl iodide	99.9%	Fisher Scientific Co.
Methyl cyanide	99%+	Aldrich Chemical Co.
Methyl cyanide-d_3	99%	"
Methyl iodide-d_3	99%	"
2-Chloro-2-methylpropane	98%	"
Chlorotrimethylsilane	99.5%	Fisher Scientific Co.
Cyclopropylamine	98%	Aldrich Chemical Co.
Cyclopropyl bromide	99%	"
Cyclopropyl cyanide	-	"
Cyclopropyl methyl ketone*	95%	"
(Chloromethyl)cyclopropane	98%	"
1,3,5-Trimethylbenzene	99%	"
1,2,4-Trimethylbenzene	99%	"
1,2,3-Trimethylbenzene*	90%	"

Table 2.1...cont'd...

Compound	Purity	Company
Benzal chloride	99%	"
Benzal bromide	97%	"

*These samples were distilled prior to use.

ii) Synthesis of Dichloromethane-d

Dichloromethane-d was synthesized by the reduction of chloroform-d (99.8%) with acetic acid and zinc[88]. Chloroform-d (12 g) and zinc (20 g) were mixed in a round bottom flask, which was equipped with a condenser, and the acetic acid (60 mL) was added dropwise. The reaction mixture was refluxed for 8 hr at 55°C and the product was obtained through simple distillation. The ^{13}C NMR spectrum of the product (~6 mL) showed it to be a mixture of 67% $CHDCl_2$ and 33% $CDCl_3$.

iii) Liquid Phase Spectra

The liquid phase overtone spectra at room temperature were recorded with cells of various lengths from 0.10 to 10.0 cm. The longer path lengths were used for the less intense, higher overtones. The actual path lengths used to record spectra are given in the figure captions of the individual spectra.

Methyl chloride and methyl bromide are gaseous at room temperature. The spectra of these molecules in the liquid phase were measured with the samples contained in a Beckman high pressure cell (P.N.F. - 076). This cell is a hollow stainless steel block with 0.952 cm thick windows inset on Teflon seats. The cell had an effective path length of 5 cm. The relatively weak spectra (Δv_{CH} = 4 - 6) of methyl chloride and methyl bromide were measured with a fully filled cell. However, the 5 cm path length was much too long for measurement of the relatively intense Δv_{CH} = 2 and 3 spectra. The cell path length was reduced to 0.1 cm and 1 cm for recording the spectra at Δv_{CH} = 2 and 3, respectively. Reduction in path length was achieved by dismantling and then fitting the cell with solid glass cylinders. The ends of the cylinders were heat polished to increase light transmission.

Prior to condensing the sample of methyl chloride or methyl bromide into the high pressure cell, the cell was connected via a Swagelok valve to a vacuum manifold and was evacuated. The manifold was then isolated from the pump and gas sample was admitted to the evacuated system. The gas was condensed into the cell by cooling the cell with liquid nitrogen.

The liquid phase fundamental spectra were measured with a 0.1 mm path length demountable cell fitted with NaCl windows.

iv) Gas Phase Spectra

a) Room Temperature

Gas phase overtone spectra at room temperature were obtained with a Wilks 5.4 L, variable path length gas cell (Wilks Scientific Corp., South Norwalk, Connecticut, Model 5720) with KBr windows. The gas cell was connected to a vacuum manifold and pumped down for at least one hour. The sample was placed in a flask, connected to the vacuum manifold, and evacuated with several freeze-pump-thaw cycles. The vacuum manifold was then isolated from the pump. The desired pressure of sample, as monitored with a mercury manometer, was admitted into the evacuated cell directly from the flask containing the sample.

The gas cell path length is variable from 0.75 m to 21.75 m in increments of 1.5 m. The actual path lengths are given in the figure captions of the individual spectra.

The fundamental gas phase spectra were measured with a 10 cm path length gas cell fitted with KBr windows.

b) Elevated Temperature

The gas phase spectra at elevated temperature were measured with the following procedure. The gas cell was fitted with a heating jacket made up of half inch copper tubing. The cell was first evacuated and then aligned in the correct position in the spectrophotometer. The gas cell was heated to a temperature of 90°C by circulation of water from a constant temperature heating bath, (Haake, Berlin) through the heating jacket. To minimize heat loss and help stabilize the system, the cell was wrapped in several layers of black cloth, and allowed to equilibrate for three hours before spectra were measured.

The sample was placed in a 50 mL flask fitted with a stopcock and Swagelok connections and degassed. The flask was attached to the gas cell and heated in a water bath to 80°C. Sufficient amount of sample was allowed to enter the cell until the absorption signal for the desired overtone region could be observed.

v) Spectrophotometers and Treatment of Data

All overtone spectra in this thesis were measured with a Beckmann 5270 spectrophotometer. The calibration of the spectrophotometer had been checked by measuring the absorption spectrum of iodine and comparing it with the literature spectrum. The spectrophotometer was operated in the near infrared mode to record Δv_{XH} = 2 - 4 spectra. The overtone spectra in the regions of Δv_{XH} = 5 and 6 were recorded with the instrument operating in the visible mode. Narrow slitwidth and slow scan speed produce high resolution and low noise (high quality) spectra. These parameters were adjusted to optimum values in the measurement of each spectrum.

The Beckman 5270 spectrophotometer is interfaced to a Nicolet 1280 minicomputer. The wavelength spectrum from the Beckman is passed to the Nicolet 1280 computer through a pulsed signal. Variation in the scan speed allows variation in the number of pulses per nanometer. Typical pulse rates used during spectral acquisition were 12.5 pulses/nm and 50 pulses/nm in the near infrared and visible mode, respectively.

The Nicolet 1280 computer is part of a Nicolet MX3600 data system. The system constitutes a MX-1 FTIR spectrometer and an input/output interfacing device. Peripheral mass storage is provided by dual hard disk drives and a single floppy disk drive. Output components of the system include a raster display screen, a Nicolet Zeta 160 plotter, a low speed dot matrix printer, and a Model 43 teletype operating at a baud rate of 300.

The wavelength information (spectrum) from the Beckman 5270 is converted to a linear energy scale of wavenumbers (cm^{-1}) on the

Nicolet 1280 computer. The resultant spectrum is stored in the computer's dynamic memory and on the FTIR "scratch disk"[89].

The Software which transfers the wavelength spectrum from the Beckman to the Nicolet 1280 computer is a part of the BECKMA program. This program is a modified version of the FTIR36 program. The FTIR36 program[89] is provided with the MX3600 system. Most of the data manipulation subroutines available in the FTIR36 program are also available in BECKMA. The spectra can be base line corrected, added, subtracted and multiplied by calling the appropriate subroutines of the BECKMA program. These subroutines were used appropriately where required.

All the measured spectra were stored on the hard disk by using a subroutine of the BECKMA program.

The peak maxima for the well resolved overtone spectra were determined from the digital data with a Nicolet 1280 program which simply identified the wavelength setting at the highest absorbance value in the vicinity of the peak. The experimental spectra which were composed of overlapping peaks were deconvoluted with a curve analysis program NIRCAP. NIRCAP* is a Fortran 77[90] program developed for the Nicolet 1280 computer. In the program, initial values were set for the peak positions in wavenumbers, the peak amplitudes, and the peak widths. These parameters were allowed to vary freely until the best fit was obtained. The experimental and fitted spectra were plotted and compared to check the quality of the deconvolution fit.

Fundamental gas phase spectra were measured with the MX-1 FTIR

---

*NIRCAP program was written by R. K. Marat and modified by A. W. Tarr.

spectrometer. The gas cell (10 cm) was fixed in the sample compartment of the interferometer. The cell was connected to a vacuum manifold and evacuated. The sample compartment was purged with nitrogen to remove atmospheric carbon dioxide and water vapours from it.

The FTIR spectrometer is a single beam instrument. First the Fourier transformed spectrum of the evacuated cell was measured. Then the evacuated cell was filled with the sample and the Fourier transformed spectrum of the sample was measured. The single beam spectra were ratioed by the FTIR36 software to give transmittance spectra. The spectrum was converted to an absorbance spectrum and stored on the hard disk.

The liquid phase fundamental spectra were recorded on the MX-1 FTIR spectrometer with the same procedure except that evacuation of the liquid cell was not necessary. Peak frequencies for both the liquid and the gas phase spectra were obtained by the FTIR36 program.

All the spectra presented in this thesis have been plotted with a Nicolet Zeta 160 plotter.

vi) Molecular Orbital Calculations

The geometries of 2-chloro-2-methylpropane ($(CH_3)_3CCl$) and chlorotrimethylsilane ($(CH_3)_3SiCl$) were optimized to determine the CH bond lengths. The 4-31G and STO-3G basis sets were used for 2-chloro-2-methylpropane. For chlorotrimethylsilane, the calculation was done only at STO-3G level.

The STO-3G basis set[91] uses a minimal basis set of one Slater type orbital (STO) per atomic orbital. To avoid the time consuming integrals that occur with STO's each STO in the STO-3G basis set is approximated as a linear combination of three Gaussian functions.

The 4-31G basis set[91] is a split valence set. Each inner shell 1s atomic orbital is taken as a linear combination of four Gaussians with fixed coefficients. For each valence shell 2s or 2p atomic orbital, one uses a double zeta approach, taking one 2s (or 2p) function that is a fixed linear combination of three Gaussians and a second 2s (or 2p) function that consists of a single Gaussian with orbital exponent different from those in the linear combination of three Gaussians.

Molecular orbital calculations* on benzal chloride ($C_6H_5CHCl_2$) were also performed to study the conformational preference of the dichloromethyl group. The calculations were done at the SCF level with STO-3G[91] and 4-31G[91] basis sets.

The computations were done with the MONSTERGAUSS[92] ($(CH_3)_3CCl$,

---

*Molecular orbital calculations on $C_6H_5CHCl_2$ were performed by Dr. David Swanton (Department of Chemistry, University of Manitoba).

$(CH_3)_3SiCl$) and GAUSSIAN 82[92] ($C_6H_5CHCl_2$) computer programs on an Amdahl V8 system.

CHAPTER 3

OVERTONE SPECTRUM OF DICHLOROMETHANE-d

The liquid phase CH stretching overtone spectrum of dichloromethane-d in the region of Δv_{CH} = 2, 3, and 4 will be reported in this chapter. Results from this spectrum will be used in an analysis of the Fermi resonance interactions in the overtone spectrum of dichloromethane, which involve CH stretching local mode peaks and nearby combination peaks involving two quanta of HCH bending.

i) Introduction

In an earlier study Mortensen et al.[70] assigned the CH stretching overtone spectra of the dihalomethanes on the basis of a harmonically coupled local mode model. In this model[70], the CH oscillators are considered as anharmonic Morse oscillators which are harmonically coupled through Wilson F and G matrix elements. This model identified the principal peaks in the dihalomethane overtone spectra as corresponding to transitions to symmetrized states of the form

$$|v_1,v_2\rangle = \frac{1}{\sqrt{2}} |v_1,v_2\rangle \pm |v_2,v_1\rangle) \qquad (3.1)$$

Here v_1 and v_2 refer to the vibrational quanta in the two CH oscillators.

Combination peaks, which were not accounted for by the harmonic coupling model, were also observed in the Δv_{CH} = 2, 3, and 4 spectral regions of the dihalomethanes. Mortensen et al.[70] assigned these peaks as $|1,0\rangle_-|2\nu_2\rangle$, $|2,0\rangle_-|2\nu_2\rangle$, and $|3,0\rangle_\pm|2\nu_2\rangle$ for Δv_{CH} = 2, 3, and 4, respectively (ν_2 is the HCH bending mode). From Δv_{CH} = 2 to 4, the relative intensity of the combination peaks progressively increased. This observation was taken as an indication of Fermi resonance interaction of these combination peaks with the pure local mode peaks ($|2,0\rangle_-$, $|3,0\rangle_\pm$, and $|4,0\rangle_\pm$ at Δv_{CH} = 2, 3, and 4, respectively). Mortensen et al.[70] pointed out that the increase in relative intensity of the combination peaks was associated with a decrease in the energy separation between the interacting states.

In this chapter this Fermi resonance interaction will be studied with the aid of an investigation of the CH stretching overtone spectra of dichloromethane-d. Deuterium substitution has been used to

decouple the CH stretching frequency from the bending mode frequency in a variety of molecules[93,94]. [However, recent studies of CHD_3 have shown that such decoupling does not occur in every case[53,95,96].] Here a comparison of the dichloromethane-d spectra with the overtone spectra of dichloromethane[70] will be used to facilitate an analysis of the perturbation caused by Fermi resonance in dichloromethane.

ii) Results and Discussion

The CH stretching fundamental spectrum of dichloromethane-d has been reported in the literature[97,98]. The overtone spectra* of dichloromethane-d in the regions of Δv_{CH} = 2, 3, and 4 are shown in Figures 3.1-3.3. The overtone spectra of dichloromethane in the regions of Δv_{CH} = 2, 3, and 4, from previous work[70,87] are also presented in Figures 3.1-3.3 for comparison. In these figures, the combination peaks in the dichloromethane overtone spectra are marked with a "C". The spectral frequencies of the CH stretching local mode peaks for these two molecules are listed in Table 3.1.

The single peaks at Δv_{CH} = 2, 3, and 4 in the dichloromethane-d spectra correspond to transitions to Morse oscillator states $|2\rangle$, $|3\rangle$, and $|4\rangle$. The energies of these peaks can be fitted to the equation for a diatomic anharmonic Morse oscillator, i.e.,

$$\Delta E(v) = \omega v - \omega x(v^2+v) \qquad (3.2)$$

where ω, v and ωx refer to the harmonic frequency, the vibrational

---

*The overtone spectra reported here are of a mixture of 67% $CHDCl_2$ and 33% $CDCl_3$. The overtone spectra of a mixture (67% CH_2Cl_2 + 33% $CDCl_3$) in the region of Δv_{CH} = 2 was measured to investigate any effects of $CDCl_3$ on the CH stretching overtone spectra of dichloromethane. A comparison of this spectrum with the previously measured spectrum at Δv_{CH} = 2 of pure dichloromethane[70,87] revealed that the presence of $CDCl_3$ in CH_2Cl_2 has no measurable effect on the spectrum. In particular, both the frequencies and the band shapes of the CH stretching overtones of dichloromethane are unchanged.

quantum number, and the diagonal anharmonicity, respectively. The peaks at Δv_{CH} = 1 (3019 cm^{-1} from ref. 97), 2, and 4 are unperturbed. However, at Δv_{CH} = 3 in dichloromethane-d, interaction occurs with the peak corresponding to Δv_{CD} = 4. The unperturbed energy of the Δv_{CH} = 3 peak can be obtained by fitting the peaks corresponding to Δv_{CH} = 1, 2 and 4 to Eq. (3.2). The resulting values for ω and ωx are 3141.1 ± 0.4 and 60.95 ± 0.15 cm^{-1}, respectively. From these values the Fermi resonance corrected frequency for the Δv_{CH} = 3 peak in the spectrum of dichloromethane can be obtained. The corrected value (8692 cm^{-1}) differs from the observed value by 6 cm^{-1}.

In the spectra of dichloromethane-d, no evidence is found for interaction between the local mode states, $|v>$, and combination states of the type $|v-1,2B>$ (B denotes the HCD bending mode). The plot of Eq. (3.2) for the points Δv_{CH} = 1, 2, and 4 is shown in Figure 3.4. The correlation coefficient (-0.999997) for this three point fit is an indication of the absence of these local mode-combination interactions in $CHDCl_2$. The HCD bending mode frequency (1283 cm^{-1})[97] in $CHDCl_2$ is such that the states $|v>$ and $|v-1,2B>$ are not able to "tune" into resonance for the CH stretching fundamental and lower overtones. It is possible, as in the case of CHD_3 [53], that such resonances will occur for higher overtones.

The resonance shifts in the pure local mode peaks of dichloromethane are given in the last column of Table 3.1. These shifts are obtained simply by subtracting the energies of the unperturbed local mode peaks of dichloromethane-d from the energies of the perturbed local mode peaks of dichloromethane. Note that the combination peak "C" lies to the lower energy side of the $|2,0>_-$ peak

(Figure 3.1) but to the higher energy side of the $|3,0\rangle_{\pm}$ and $|4,0\rangle_{\pm}$ peaks (Figures 3.2 and 3.3). Thus the resonance shift at $\Delta v_{CH} = 2$ is opposite in sign to the shifts at $\Delta v_{CH} = 3$ and 4.

The unperturbed peak positions for $\Delta v_{CH} = 5$, 6 and 7 can be obtained from the values for ω and ωx, and Eq. (3.2) ($\Delta v_{CH} = 5$, 13877 cm^{-1}; $\Delta v_{CH} = 6$, 16287 cm^{-1}; $\Delta v_{CH} = 7$, 18574 cm^{-1}). The observed energies[99] for the corresponding peaks in dichloromethane are 13870, 16265 and 18570 cm^{-1}. Thus, the resonance shifts are -7, -22 and -4 cm^{-1} for $\Delta v_{CH} = 5$, 6 and 7, respectively. The 4 cm^{-1} shift at $\Delta v_{CH} = 7$ is within the experimental peak position error. Therefore the dichloromethane spectrum can be considered free of resonance interactions in the region of $\Delta v_{CH} = 7$. The magnitude of the resonance shift at $\Delta v_{CH} = 5$ is significantly less than that at $\Delta v_{CH} = 6$. In the region of $\Delta v_{CH} = 5$, it is likely that the pure local mode peak $|5,0\rangle_{\pm}$ is in resonance not only with the $|4,0\rangle_{\pm}|2\nu_2\rangle$ peak but also with the $|4,0\rangle_{\pm}|2\nu_8\rangle$ peak (ν_8 is the CH_2 rocking mode). On the basis of the unperturbed peak position of $|4,0\rangle_{\pm}$ (Table 3.1) and the frequencies of the ν_2 and ν_8 modes ($\nu_2 = 1428$ cm^{-1}, $\nu_8 = 1265$ cm^{-1} from ref. 97), the unperturbed state $|5,0\rangle_{\pm}$ lies between the unperturbed states $|4,0\rangle_{\pm}|2\nu_2\rangle$ and $|4,0\rangle_{\pm}|2\nu_8\rangle$. Thus the two resonance shifts for $|5,0\rangle_{\pm}$ will tend to cancel and lead to a small resultant shift.

In this analysis, it has been assumed that the CH stretching local mode frequency, ω, is the same for both CH_2Cl_2 and $CHDCl_2$. This assumption is not rigorously correct. There is a small contribution to the local mode frequency from off-diagonal anharmonicities involving other vibrational modes[1]. Of course, some of these other

modes, and the corresponding off-diagonal anharmonicities, will be different in CH_2Cl_2 and $CHDCl_2$. However, the net effect on the local mode frequency is expected to be very small and has been neglected.

The perturbed energies of the combination peaks "C" and the pure local mode peaks of dichloromethane can be expressed as[100]

$$E_{\pm} = \bar{E} \pm 1/2\ (4W^2+\delta^2)^{1/2} \qquad (3.3)$$

In Eq. (3.3), E_+ and E_- denote the observed (i.e., perturbed) energies of the combination peaks "C" or the pure local mode peaks, depending on the overtone. $\bar{E}$ is the average of the unperturbed energies. W and δ are the off-diagonal matrix element and the difference in the unperturbed energies of the interacting levels, respectively. Since the resonance shift (see Table 3.1) for the pure local mode and the combination peaks "C" of dichloromethane will be of equal magnitude but of opposite sign, the unperturbed positions of the combination peaks can also be calculated. The observed and resonance corrected energies of the combination peaks "C" of dichloromethane are given in Table 3.2. From the data of Tables 3.1 and 3.2 and Eq. 3.3, the off-diagonal matrix element W can be calculated. The values of W for Δv_{CH} = 2, 3, and 4 are 22.5, 33 and 33.5 cm^{-1}, respectively. These values are similar to those obtained by Perry et al.[53] for Δv_{CH} = 5 (30 cm^{-1}) and Δv_{CH} = 6 (35 cm^{-1}) in their analysis of interaction between stretching states and stretching-HCD bending combination states in the spectra of CHD_3.

The corrected energies of the combination bands might be expected to fit the simple energy expression for two vibrational modes

$$\Delta E(v_{CH},2) = E(v_{CH}) + 2\nu_2 + 2v_{CH}X_{12} \qquad (3.4)$$

where $E(v_{CH},2)$ and $E(v_{CH})$ are the unperturbed energies of the combination and pure local mode states, respectively. Substitution of the appropriate data from Tables 3.1 and 3.2 and the value of $2\nu_2$ (2836 cm^{-1})[98] yields X_{12} values of -14 and -30 cm^{-1} for the $|2,0\rangle_-|2\nu_2\rangle$ and $|3,0\rangle_\pm|2\nu_2\rangle$ states, respectively. However, Mortensen et al.[70] in their work on dihalomethanes have shown that the HCH-bending frequency decreases with increasing v_{CH} due to an increase in the effective mass. Inclusion of such an effect in Eq. (3.4) would lead to more nearly constant values of X_{12}.

In summary, the analysis presented in this chapter has revealed that in the region from $\Delta v_{CH} = 3$ to $\Delta v_{CH} = 6$ in the spectra of dichloromethane, there are extensive near resonance interactions between the pure local mode CH stretching states and combination states with v-1 quanta of CH stretching and two quanta of HCH bending. At $\Delta v_{CH} = 2$ this interaction is small and at $\Delta v_{CH} = 7$ it has virtually disappeared. With the exception of $\Delta v_{CH} = 5$, where three levels appear to be involved, a simple two-level Fermi resonance scheme with CH stretching motion treated within the local mode picture appears to be adequate to analyze the interactions.

Table 3.1.

Observed Local Mode Frequencies of Liquid CH_2Cl_2 and $CHDCl_2$, and Fermi Resonance Shifts in CH_2Cl_2 (cm^{-1}).

Δv_{CH}	CH_2Cl_2	$CHDCl_2$	Fermi resonance shift[c]
2	5925[a]	5917	+8
3	8661[a]	8698 (8692)[b]	-31
4	11312[a]	11345	-33

[a]Reference 87

[b]Corrected energy, see text

[c]See text

Table 3.2.

Observed and Fermi Resonance Corrected Frequencies for the $|v-1,0\rangle|2\nu_2\rangle$ States of CH_2Cl_2 (cm^{-1}).

State	Observed frequency	Corrected frequency
$\|10\rangle_-\|2\nu_2\rangle$	5836[a]	5844
$\|20\rangle_-\|2\nu_2\rangle$	8727[a]	8696
$\|30\rangle_\pm\|2\nu_2\rangle$	11379[a]	11346

[a] Reference 87

Figure 3.1.

Overtone spectrum of liquid phase dichloromethane-d, containing 33% $CDCl_3$, in the region of $\Delta v_{CH} = 2$. Spectrum was measured at room temperature with a path length of 0.1 cm. The overtone spectrum of liquid phase dichloromethane in the same region is taken from Ref. 87 and presented for comparison.

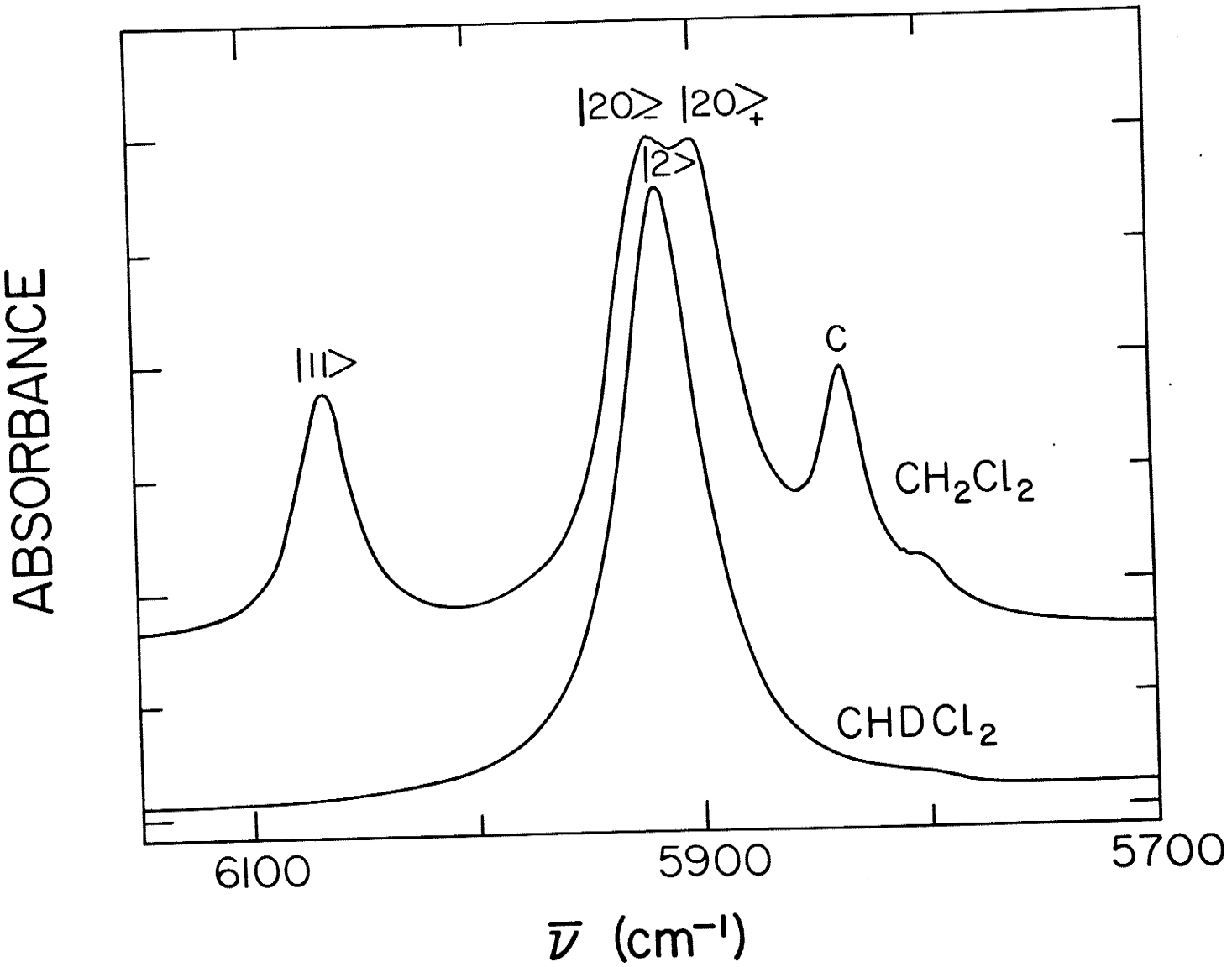
ABSORBANCE
|20> |20>+
|2>
|11>
C
CH2Cl2
CHDCl2
6100
5900
5700
ν̄ (cm⁻¹)

Figure 3.2.

Overtone spectrum of liquid phase dichloromethane-d, containing 33% $CDCl_3$, in the region of $\Delta v_{CH} = 3$. Spectrum was measured at room temperature with a path length of 3 cm. The overtone spectrum of liquid phase dichloromethane in the same region is taken from Ref. 87 and presented for comparison.

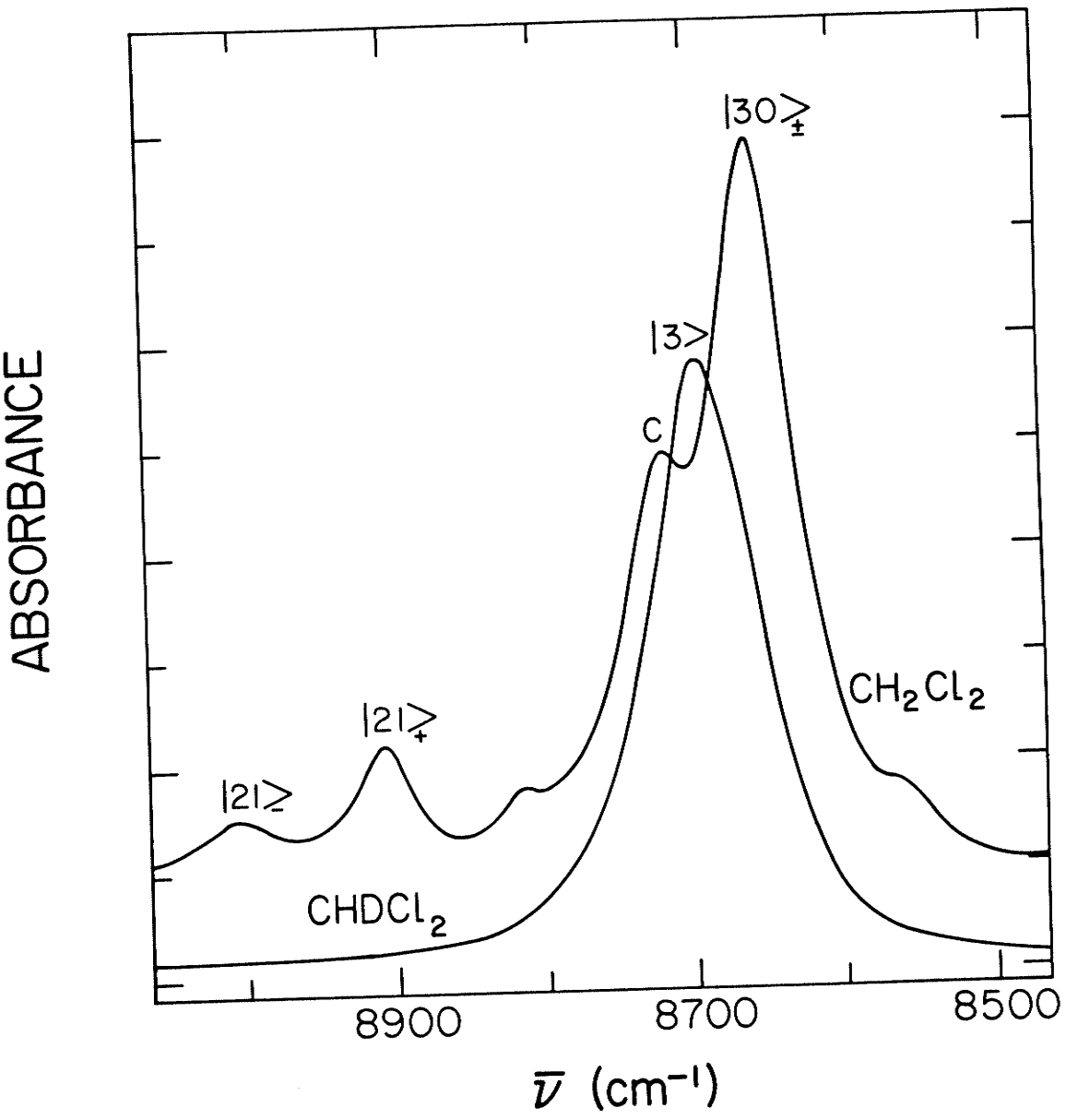
ABSORBANCE
|30>±
|3>
C
|21>+
|21>-
CH2Cl2
CHDCl2
8900
8700
8500
ν̄ (cm⁻¹)

Figure 3.3.

Overtone spectrum of liquid phase dichloromethane-d, containing 33% $CDCl_3$, in the region of the $\Delta v_{CH} = 4$. Spectrum was measured at room temperature with a path length of 3 cm. The overtone spectrum of dichloromethane in the same region is taken from Ref. 87 and presented for comparison.

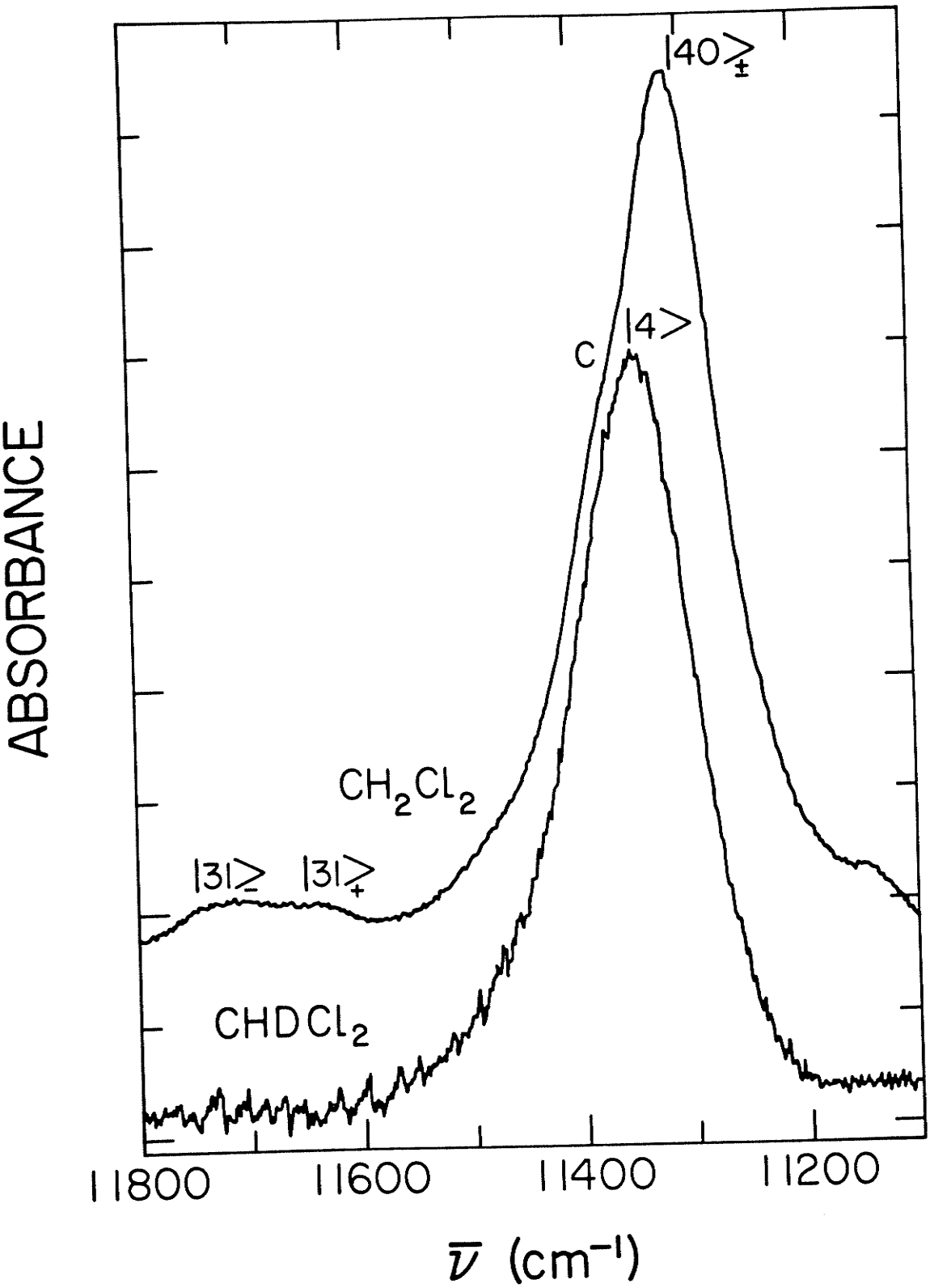
ABSORBANCE
|40>±
C |4>
CH2Cl2
|31>− |31>+
CHDCl2
11800
11600
11400
11200
ν̄ (cm⁻¹)

Figure 3.4.

A plot of Eq. (3.2) for dichloromethane-d for the points v = 1, 2 and 4.

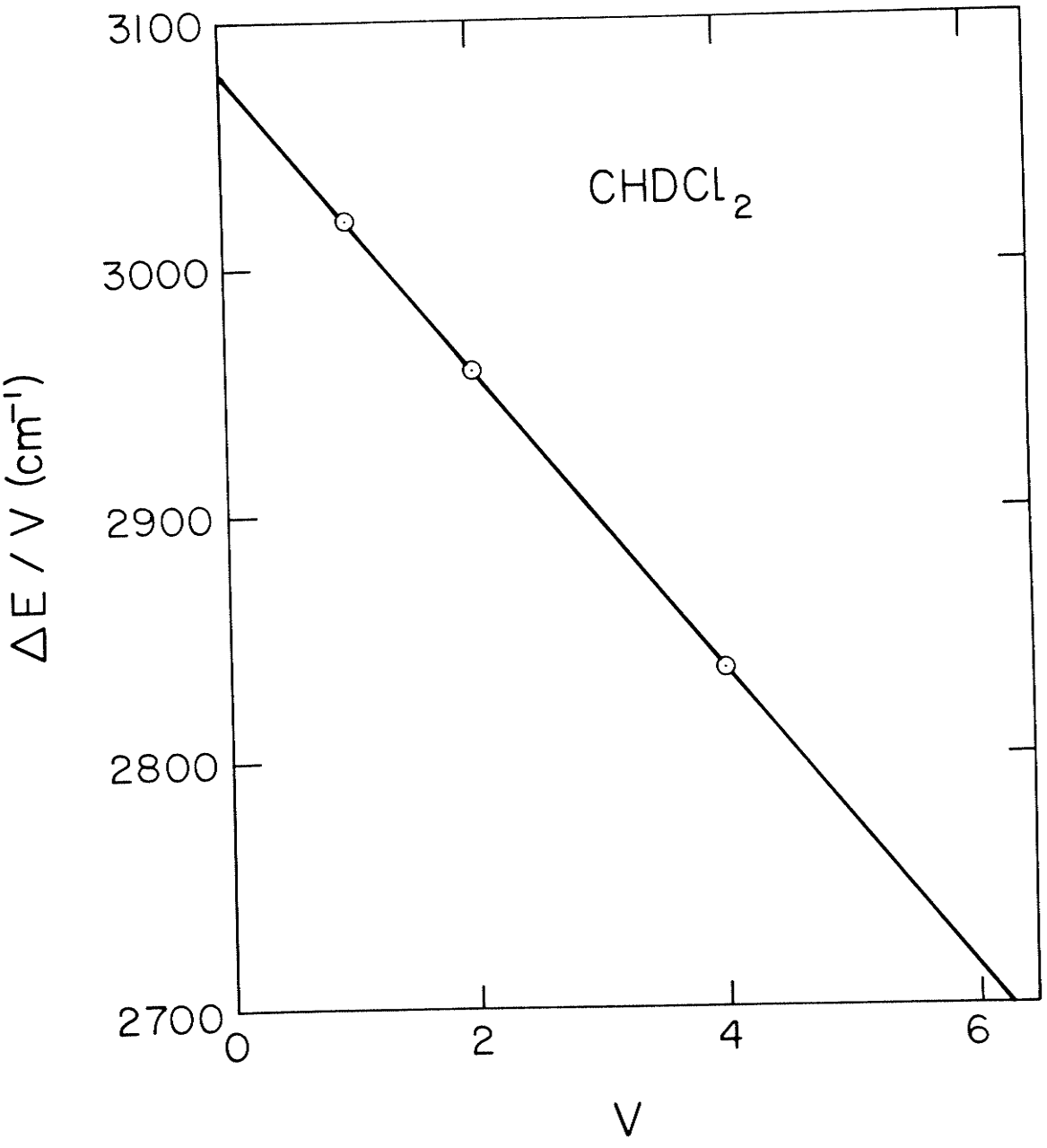
3100
3000
2900
2800
2700
0
2
4
6
V
ΔE / V (cm⁻¹)
CHDCl2

CHAPTER 4

OVERTONE SPECTRA OF DEUTERATED DIHALOMETHANES

In this chapter the overtone spectra of CD_2Z_2 (Z = Cl, Br, or I) molecules in the liquid phase in the region of CD stretching local mode overtones corresponding to Δv_{CD} = 2-5 (CD_2Cl_2 and CD_2Br_2) and Δv_{CD} = 2-4 (CD_2I_2) will be reported. These spectra , and those of previously reported fundamentals will be analyzed in terms of the local mode model. The spectra of CD_2Z_2 and CH_2Z_2 molecules will be compared and the effects of increased coupling between the CD bonds on the intensities and symmetry splittings of the local mode peaks will be pointed out.

i) Introduction

Through their work on dihalomethanes, Mortensen et al.[70] developed a general theory for the analysis of XH stretching fundamental and overtone spectra of a XH_2 system (see Chapter 1). In this chapter the theory of the XH_2 system will be used to analyze the CD stretching fundamental[97,101] and overtone spectra of CD_2Z_2 (Z = Cl, Br, or I) molecules. At a given quantum number $v = v_1 + v_2$, the vibrational states corresponding to CD stretching will be taken as symmetry-adapted states of the type $|v_1,v_2\rangle_\pm = \frac{1}{\sqrt{2}} (|v_1,v_2\rangle \pm |v_2,v_1\rangle)$, where $|v_1,v_2\rangle = |v_1\rangle|v_2\rangle$is the Morse oscillator product function of the two bond wave functions. Intramanifold coupling between the symmetrized states will be determined from the harmonic coupling model of Mortensen et al.[70] (see theory of XH_2 system in chapter 1), and intermanifold coupling will be neglected.

In their work on dihalomethanes, Mortensen et al.[70] determined that the kinetic energy is the principal source of coupling between the two CH oscillators. In the deuterated dihalomethanes, the change in mass ratio will significantly increase this coupling. In the subsequent sections of this chapter the spectral manifestations of this increased coupling will be analyzed and its effect on the applicability of the simple local mode analysis scheme will be discussed.

ii) Results and Discussion

a) Spectral Analysis

The liquid phase overtone spectra of CD_2Z_2 molecules in the regions of Δv_{CD} = 2, 3, 4, and 5 are shown in Figures 4.1-4.4. The peak positions for these spectra and for the fundamentals are given in Table 4.1. Two types of peaks are observed. The first type is only associated with CD stretching and is assigned within the local mode description to symmetrized combinations of Morse oscillator product states $|v_1,v_2>_{\pm}$. The second type of peak is marked by a C in Figures 4.1-4.4. For a given vibrational manifold, v, these peaks involve two quanta of DCD bending combined with CD stretching states with v-1 quanta.

First the CD stretching peaks are discussed. For CD_2I_2, the local mode assignments are indicated in Figures 4.1-4.3. The corresponding assignments for CD_2Br_2 and CD_2Cl_2 are obvious from the figures, and in the following discussion the arguments apply to all three molecules.

The principal peaks in the Δv_{CD} = 2 spectra (Figure 4.1) are $|2,0>_+$, $|2,0>_-$, and $|1,1>$. The splitting between the $|2,0>_+$ and $|2,0>_-$ peaks is appreciable, more than twice as large as the corresponding splitting in the spectra of the CH_2Z_2 molecules[70]. In the absence of coupling, the $|2,0>_+$ and $|2,0>_-$ states would be degenerate. However, harmonic coupling of $|2,0>_+$ and $|1,1>$ via the γ and ϕ parts of the Hamiltonian of XH_2 system (see Eq. (1.7) of chapter 1) lowers the energy of $|2,0>_+$ and provides the splitting between it and $|2,0>_-$.

At Δv_{CD} = 3 (Figure 4.2), splitting occurs between $|3,0>_+$ and

$|3,0\rangle_-$. The corresponding peaks are totally unresolved in the spectra of the CH_2Z_2 molecules[70]. However, this splitting is much smaller than the corresponding splitting at $\Delta v_{CD} = 2$. Well resolved local mode combination peaks, $|2,1\rangle_+$ and $|2,1\rangle_-$ occur on the high energy side of the $|3,0\rangle_-$ peak. The splitting for the $|2,1\rangle_\pm$ peaks is greater than for the $|3,0\rangle_\pm$ peaks because the former splitting originates from a first order coupling whereas the latter splitting originates from a third order coupling. In terms of the unsymmetrized Morse product states, $|2,1\rangle$ is directly coupled to $|1,2\rangle$ but $|3,0\rangle$ couples to $|0,3\rangle$ via the coupling route $|3,0\rangle \leftrightarrows |2,1\rangle \leftrightarrows |1,2\rangle \leftrightarrows |0,3\rangle$.

At $\Delta v_{CD} = 4$ (Figure 4.3) prominent peaks arise due to transitions to the symmetrized states $|4,0\rangle_+$, $|4,0\rangle_-$, $|3,1\rangle_+$, and $|3,1\rangle_-$. However, there are a number of combination peaks in this region, and several of the peaks overlap. This overlap is particularly severe for the peaks $|4,0\rangle_+$, $|3,0\rangle_- |2\nu_2\rangle$, and $|4,0\rangle_-$. Thus the positions of these peaks, as listed in Table 4.1, should be considered only as estimates.

At $\Delta v_{CD} = 5$, the prominent peaks in the spectra of CD_2Cl_2 and CD_2Br_2 (Figure 4.4) are the pure local mode peaks $|5,0\rangle_\pm$ and the local mode-normal mode combination peaks $|4,0\rangle_\pm |2\nu_2\rangle$. Symmetry splitting between the $|5,0\rangle_\pm$ states is not observed at $\Delta v_{CD} = 5$ due to a smaller effective coupling. The combination peak $|4,0\rangle_\pm |2\nu_2\rangle$ lies on the low energy side of the $|5,0\rangle_\pm$ peak and has considerable intensity due to near resonant interaction with the pure local mode peaks.

Most of the combination peaks with two quanta of the DCD bending mode (peaks denoted C in Figures 4.1-4.4) can be assigned to states of the form $|v-1,0\rangle_\pm |2\nu_2\rangle$ (see Table 4.1). Such peaks have been observed in the CH stretching overtone spectra of a number of polyatomic

molecules[38,52,70,99,102,103] and gain intensity principally through resonant or near resonant interactions with $|v,0\rangle_{\pm}$ states. Combination states corresponding to $|1,1\rangle|2\nu_2\rangle$ and $|2,1\rangle_{+}|2\nu_2\rangle$ can be assigned in the regions of $\Delta v_{CD} = 3$ and $\Delta v_{CD} = 4$, respectively. The assignments can be made straightforwardly on the basis of the local mode peak positions and the fundamental DCD bending frequencies (ν_2 = 995, 1026 and 1002 cm^{-1} for CD_2Cl_2 [97], CD_2Br_2 [101], and CD_2I_2 [101], respectively).

b) Local Mode Parameters and Calculated Spectra

In CH stretching overtone spectra, the pure local mode states are effectively degenerate for $\Delta v_{CH} \geq 3$. Because of this, local mode parameters (harmonic frequency, ω, and diagonal anharmonicity, ωx) can be obtained by fitting the energies of the pure local mode peaks to the vibrational energy expression of a single Morse oscillator

$$\Delta E = \omega[v - x(v^2+v)] \tag{4.1}$$

In previous work on dihalomethanes[70], Mortensen et al. obtained the effective coupling parameters $\gamma' = \gamma - \phi$ from the observed spectral splitting between the harmonically coupled $|1,0\rangle_+$ and $|1,0\rangle_-$ states ($2\gamma'\omega = E(|1,0\rangle_-) - E(|1,0\rangle_+)$). However, there are two difficulties in the application of this procedure to the calculation of the spectra of CD_2Z_2. In the first place, the pure local mode peaks $|v,0\rangle_+$ and $|v,0\rangle_-$ are spectrally resolved, even at $\Delta v_{CD} = 4$. Secondly, extensive interactions between the CD stretching states and the combination states involving DCD bending strongly perturb the peak positions in the regions of $\Delta v_{CD} = 4$ and 5. In fact, the assignments given in Table 4.1 for strongly interacting peaks are approximate in the sense that the states must be strongly mixed.

In the present case a different procedure was adopted, and the local mode parameters were determined by fitting the observed frequencies for $\Delta v_{CD} = 2$ to the following equations:

$$E(|2,0\rangle_+) = 2\omega - 5\omega x - [(\omega x)^2+(2\omega\gamma')^2]^{1/2} \tag{4.2}$$

$$E(|1,1\rangle) = 2\omega - 5\omega x + [(\omega x)^2+(2\omega\gamma')^2]^{1/2} \tag{4.3}$$

$$E(|2,0\rangle_-) = 2\omega - 6\omega x \tag{4.4}$$

Equations (4.2) and (4.3) are obtained by diagonalization of the 2 x 2 matrix[70] of the Hamiltonian of the XH_2 system over the harmonically coupled $|2,0\rangle_+$ and $|1,1\rangle$ states (see Eq. (1.7) and Table 1.1 of chapter 1). Equation (4.4) for the energy of the uncoupled $|2,0\rangle_-$ state is simply derived from Eq. (1.7) of chapter 1 by setting both γ and ϕ equal to zero, $v_1 = 2$ and $v_2 = 0$. The local mode parameters are tabulated in Table 4.2.

From the parameters of Table 4.2, it is straightforward to calculate the peak positions for all of the CD stretching states of the CD_2Z_2 molecules. The procedure involves substitution of the local mode parameters into the intramanifold coupling matrices[70] of the Hamiltonian of the XH_2 system. Matrix diagonalization yields the energies of the symmetrized states. The calculated and observed frequencies are compared in Table 4.3. The calculated and observed frequencies are in excellent agreement in the regions of $\Delta v_{CD} = 1$, 2, and 3. However, the agreement in the regions of $\Delta v_{CD} = 4$ and 5 is not as good. As has already been noted, in these regions there are strong interaction between the CD stretching states and combinations which involve the bending mode. The calculation does not take account of these interactions, and this approximation is undoubtedly a major contribution to the discrepancies. Moreover, many of the experimental peak positions are only known approximately.

c) Comparison of the CH_2Z_2 and CD_2Z_2 spectra

The two principal differences between the spectra of CH_2Z_2[70] and CD_2Z_2 molecules are that in the latter molecules there are greater splittings between the symmetrized states $|v_1,v_2\rangle_\pm$ and greater intensities for local mode combinations $|v-n,n\rangle_\pm$ relative to pure local mode states $|v,0\rangle_\pm$. Both of these effects arise because of the higher value of the effective coupling parameter, γ'. Since γ' is determined primarily by kinetic energy coupling, its marked increase for the CD_2Z_2 molecules is expected. The CD_2Z_2 values for $\omega\gamma'$ (Table 4.2) are approximately twice the corresponding values for the CH_2Z_2 molecules[70].

For example, as has already been noted, $|3,0\rangle_+$ and $|3,0\rangle_-$ are well resolved in CD_2Z_2 (Figure 4.2). $|4,0\rangle_+$ and $|4,0\rangle_-$, though not completely resolved, are clearly at different energies (Figure 4.3). According to the local mode analysis scheme, the splitting between $|v,0\rangle_+$ and $|v,0\rangle_-$ is due to coupling to the $|v-1,1\rangle_\pm$ states, which is determined by the off-diagonal terms in the matrices of Hamiltonian of the XH_2 system (see Table 1.1 of chapter 1). These matrix elements are given by $-\sqrt{v}\gamma'\omega$ for $\Delta v \geq 3$. $|v,0\rangle_+$ and $|v,0\rangle_-$ approach degeneracy, even for CD_2Z_2 molecules, but at significantly higher values of v than for the CH_2Z_2 molecules.

Another effect of the increased coupling, γ', on the peak positions is the relative ordering of the states. In CH_2Z_2, $\omega\gamma'$ is approximately half the value of ωx. However, for CD_2Z_2, $\omega\gamma'$ is approximately double the value of ωx. Because of weak coupling between the CH bonds, the ordering of states in CH_2Z_2 is always $E(|v,0\rangle) < E(|v-1,1\rangle) < E(|v-2,2\rangle)\ldots$ for both symmetric and antisymmetric

states. A change in this ordering for CD_2Z_2 is observed first at Δv_{CD} = 5 where the stronger interbond coupling lowers the energy of $|3,2\rangle_+$ below that of $|4,1\rangle_+$. Thus, in summary, although a local mode analysis can be used effectively to analyze the CD stretching peak positions in CD_2Z_2, the patterns are not as simple as for the corresponding CH_2Z_2 molecules.

The combination peaks $|v-1,1\rangle_\pm$ have significantly higher intensities relative to the pure local mode peaks $|v,0\rangle_\pm$ in CD_2Z_2 than in CH_2Z_2 molecules. Very recently a general theory for intensities in local mode overtone spectra has been developed. This theory is based upon the work of the author of this thesis and of Mortensen, Henry, and Tarr (see reference 87 and Appendix B). The authors have specifically discussed the band intensities of CD_2Cl_2 and CH_2Cl_2. The dipole moment of the two coupled oscillators of these molecules was expanded as a Taylor series in the two local coordinates R_1 and R_2. The transition dipole moment between the vibrational ground state and symmetrized local mode states involved products of dipole moment derivatives, taken with respect to the local coordinates, and single Morse oscillator matrix elements over powers of the coordinate. Dipole moment derivative values were determined numerically from distorted geometry dipole moments which were calculated with a CNDO/2 molecular orbital program. Morse oscillator matrix elements were evaluated numerically. The oscillator strengths of the overtone spectra of CD_2Cl_2 and CH_2Cl_2 were calculated with, and without, vibrational state mixing. The results clearly indicated that the dominant source of intensity for the $|v-1,1\rangle_\pm$ states is the vibrational mixing of these states with the pure local mode states

$|v,0\rangle_{\pm}$. In particular the antisymmetric states, $|v-1,1\rangle_{-}$ have no intrinsic intensity contribution[87]. Since the extent of vibrational mixing is proportional to γ',[70] the higher coupling in CD_2Z_2 provides greater intensity for these $|v-1,1\rangle_{\pm}$ states than in CH_2Z_2.

In the spectra of CD_2Br_2 and CD_2I_2, the peaks $|2,1\rangle_{+}$ and $|3,1\rangle_{+}$ correspond to the most intense peaks at $\Delta v_{CD} = 3$ and 4, respectively. It was stated in the previous paragraph that vibrational mixing is the principal source of intensity for such peaks. However, vibrational mixing alone clearly cannot account for a higher intensity for $|v-1,1\rangle_{+}$ than for $|v,0\rangle_{+}$. There are two possible additional sources of intensity for peaks $|v-1,1\rangle_{+}$. One is an intrinsic contribution through the term $(\frac{\partial^2 \vec{\mu}}{\partial R_1 \partial R_2})_0$. This term was found to be small in the previous work of Mortensen *et al.*[87], but more recent calculations[104] have indicated that CNDO/2 is not adequate to accurately map out the dipole moment function as a function of the CH/CD bond displacement. Although the CNDO/2 method provides dipole moments in agreement with experiment for the equilibrium geometry, it would appear to have difficulty in accurately determining the derivatives. Thus, the question of a significant intrinsic contribution to the intensity of $|v-1,1\rangle_{+}$ is still open and requires further study.

A second possible source of intensity for $|v-1,1\rangle_{+}$ is through intrinsic intensity contributions associated with states of the types $|v-1,0\rangle|2\nu_2\rangle$ and $|v-2,1\rangle|2\nu_2\rangle$. Such intensity could be transferred to the states $|v-1,1\rangle_{+}$ through vibrational mixing. Such a mechanism could presumably contribute to the intensity of $|3,1\rangle_{+}$ where such mixing is evident in the region of $\Delta v_{CD} = 4$. However, it is unlikely

to make a significant contribution to $|2,1>_+$ in the well resolved spectral region around $\Delta\nu_{CD} = 3$.

Table 4.1.

Observed Peak Positions (cm^{-1}) for CD_2Z_2 Molecules.

$\Delta\nu_{CD}$	CD_2Cl_2	CD_2Br_2	CD_2I_2	Assignment
	2198[a]	2195[b]	2182[b]	$\|1,0\rangle_+$
1	2304[a]	2312[b]	2297[b]	$\|1,0\rangle_-$
	-	4250	-	$\|1,0\rangle_+ \|2\nu_2\rangle$
	4286	4333	4265	$\|1,0\rangle_- \|2\nu_2\rangle$
	4367	4357	4326	$\|2,0\rangle_+$
2	4442	4445	4414	$\|2,0\rangle_-$
	4573	4589	4557	$\|1,1\rangle$
	-	6387	-	$\|2,0\rangle_+ \|2\nu_2\rangle$
	6447	6463	6380	$\|2,0\rangle_- \|2\nu_2\rangle$
	6502	6483	6429	$\|3,0\rangle_+$
3	6548	6541	6487	$\|3,0\rangle_-$
	6616	6584	-	$\|1,1\rangle \|2\nu_2\rangle$
	6672	6679	6626	$\|2,1\rangle_+$
	6807	6829	6779	$\|2,1\rangle_-$
	8411[c]	8498[c]	8392[c]	$\|3,0\rangle_+ \|2\nu_2\rangle$
4	~8555[c]	~8559[c]	~8483[c]	$\|4,0\rangle_+$, $\|3,0\rangle_- \|2\nu_2\rangle$

Table 4.1...cont'd...

Δv_{CD}	CD_2Cl_2	CD_2Br_2	CD_2I_2	Assignment
	~8555[c]	~8594[c]	~8516[c]	$\|4,0\rangle_-$
	~8618[c]	~8675[c]	~8563[c]	$\|2,1\rangle_+ \|2\nu_2\rangle$
	8702[c]	8727[c]	8660[c]	$\|3,1\rangle_+$
	~8840[c]	8869[c]	8804[c]	$\|3,1\rangle_-$
	-	~10391[c]	-	$\|4,0\rangle_\pm \|2\nu_8\rangle$[d]
	~10476[c]	~10539[c]	-	$\|4,0\rangle_\pm \|2\nu_2\rangle$
5	~10601[c]	~10609[c]	-	$\|5,0\rangle_\pm$
	~10832[c]	~10797[c]	-	$\|3,2\rangle_+$

[a] Reference 97.

[b] Reference 101.

[c] From deconvolution, see chapter 2.

[d] ν_8 is the CD_2 rocking mode.

Table 4.2.

Local Mode Parameters (cm^{-1}) for CD_2Z_2 Molecules.

Molecule	ω	ωx	$\gamma'\omega$
CD_2Cl_2	2306.5	28.5	48.4
CD_2Br_2	2306.5	28.0	55.4
CD_2I_2	2289.5	27.5	54.9

Table 4.3.

Observed and Calculated Peak Positions (cm^{-1}) for CD_2Z_2 Molecules.

CD_2Cl_2		CD_2Br_2		CD_2I_2		
observed	calculated	observed	calculated	observed	calculated	Assignment
2198	2201	2195	2195	2182	2180	$\|1,0\rangle_+$
2304	2298	2312	2306	2297	2290	$\|1,0\rangle_-$
4367	4370	4357	4359	4326	4328	$\|2,0\rangle_+$
4442	4442	4445	4445	4414	4414	$\|2,0\rangle_-$
4573	4571	4589	4587	4557	4555	$\|1,1\rangle$
6502	6502	6483	6488	6429	6444	$\|3,0\rangle_+$
6548	6548	6541	6548	6487	6503	$\|3,0\rangle_-$
6672	6670	6679	6680	6626	6634	$\|2,1\rangle_+$
6807	6818	6829	6842	6779	6794	$\|2,1\rangle_-$
~8555	8590	~8559	8577	8483	8520	$\|4,0\rangle_+$
~8555	8612	~8594	8611	8516	8553	$\|4,0\rangle_-$
8702	8741	8727	8742	8660	8683	$\|3,1\rangle_+$
~8840	8871	8869	8889	8804	8828	$\|3,1\rangle_-$
~10601	10622(+)	~10609	10616(+)	-	10546(+)	$\|5,0\rangle_\pm$
	10629(-)		10630(-)		10560(-)	
-	11046	-	11073	-	10998	$\|4,1\rangle_+$
-	10892	-	10904	-	10830	$\|4,1\rangle_-$
~10832	10789	~10797	10782	-	10709	$\|3,2\rangle_+$
-	11227	-	11270	-	11192	$\|3,2\rangle_-$

Figure 4.1.

Liquid phase overtone spectra of CD_2Cl_2, CD_2Br_2, and CD_2I_2 in the region of $\Delta v_{CD} = 2$. Spectra were measured at room temperature with a path length of 0.1 cm. Absorbances of CD_2Br_2 and CD_2I_2 have been offset by 0.3 and 0.6 absorbance units, respectively.

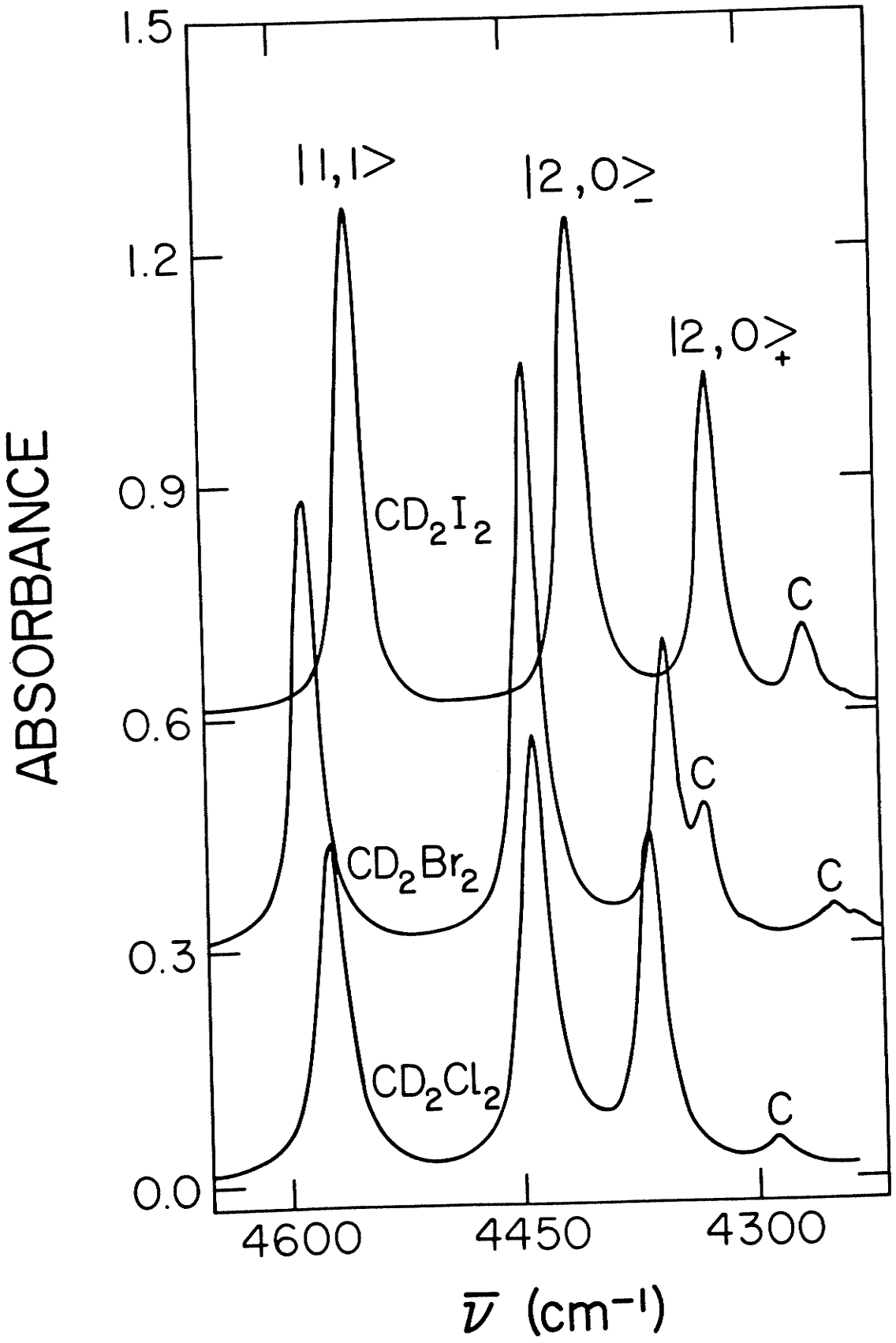
1.5
1.2
0.9
0.6
0.3
0.0
ABSORBANCE
|1,1>
|2,0>_
|2,0>+
CD2I2
CD2Br2
CD2Cl2
C
C
C
C
4600
4450
4300
ν̄ (cm⁻¹)

Figure 4.2.

Liquid phase overtone spectra of CD_2Cl_2, CD_2Br_2, and CD_2I_2 in the region of $\Delta v_{CD} = 3$. Spectra were measured at room temperature with a path length of 1.0 cm. Absorbances of CD_2Br_2 and CD_2I_2 have been offset by 0.1 and 0.2 absorbance units, respectively.

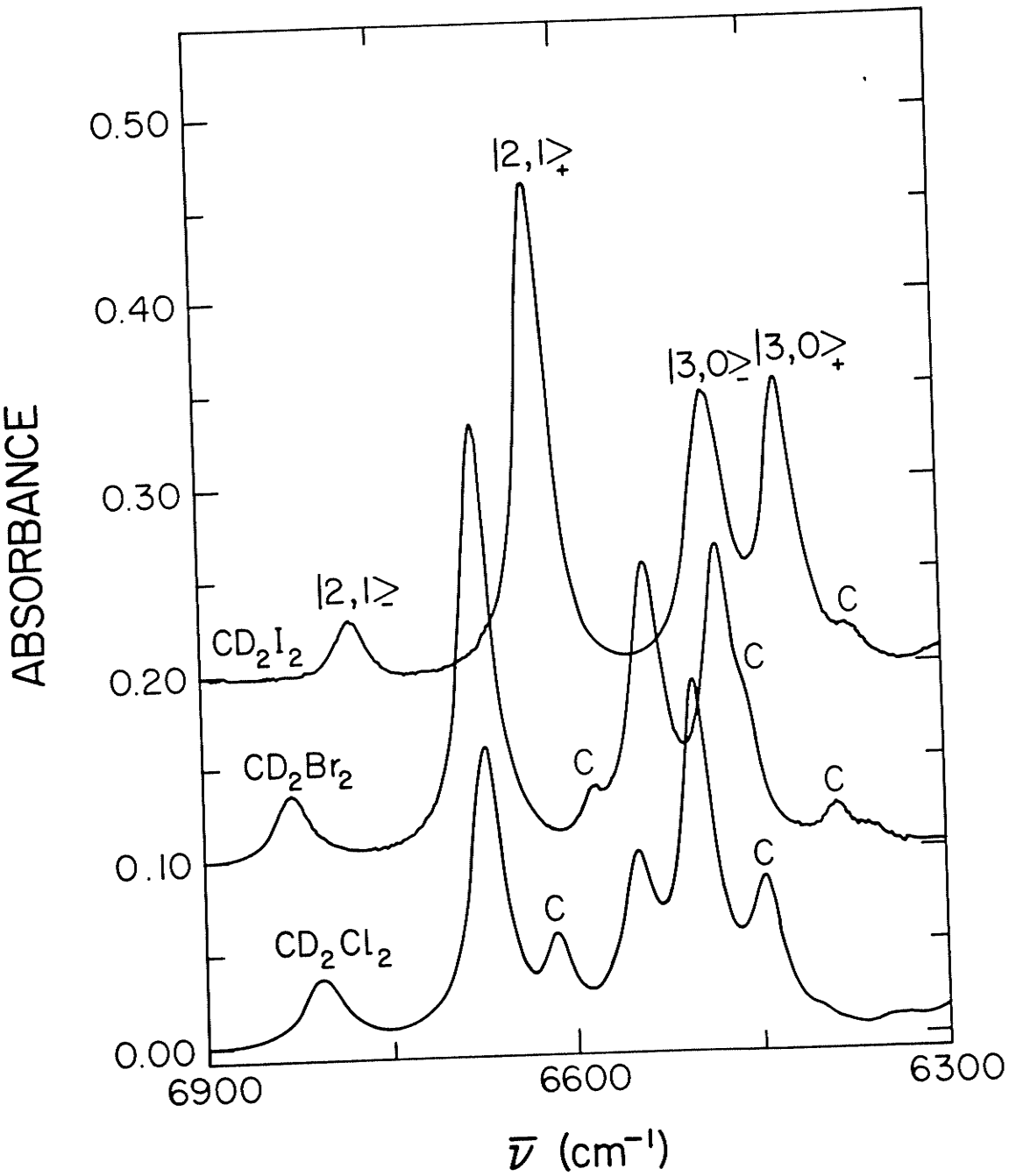
ABSORBANCE
0.50
0.40
0.30
0.20
0.10
0.00
6900
6600
6300
$\bar{\nu}$ (cm^{-1})
$|2,1\rangle_+$
$|3,0\rangle_-$
$|3,0\rangle_+$
$|2,1\rangle_-$
CD_2I_2
CD_2Br_2
CD_2Cl_2
C

Figure 4.3.

Liquid phase overtone spectra of CD_2Cl_2, CD_2Br_2, and CD_2I_2 in the region of $\Delta v_{CD} = 4$. These spectra are the sum of four base line corrected scans. Individual scans were measured at room temperature with a path length of 1.0 cm. The right hand ordinate scale represents the absorbance of CD_2I_2. The absorbance of CD_2Br_2 has been offset by 3.4×10^{-3} absorbance units with respect to the absorbance of CD_2Cl_2.

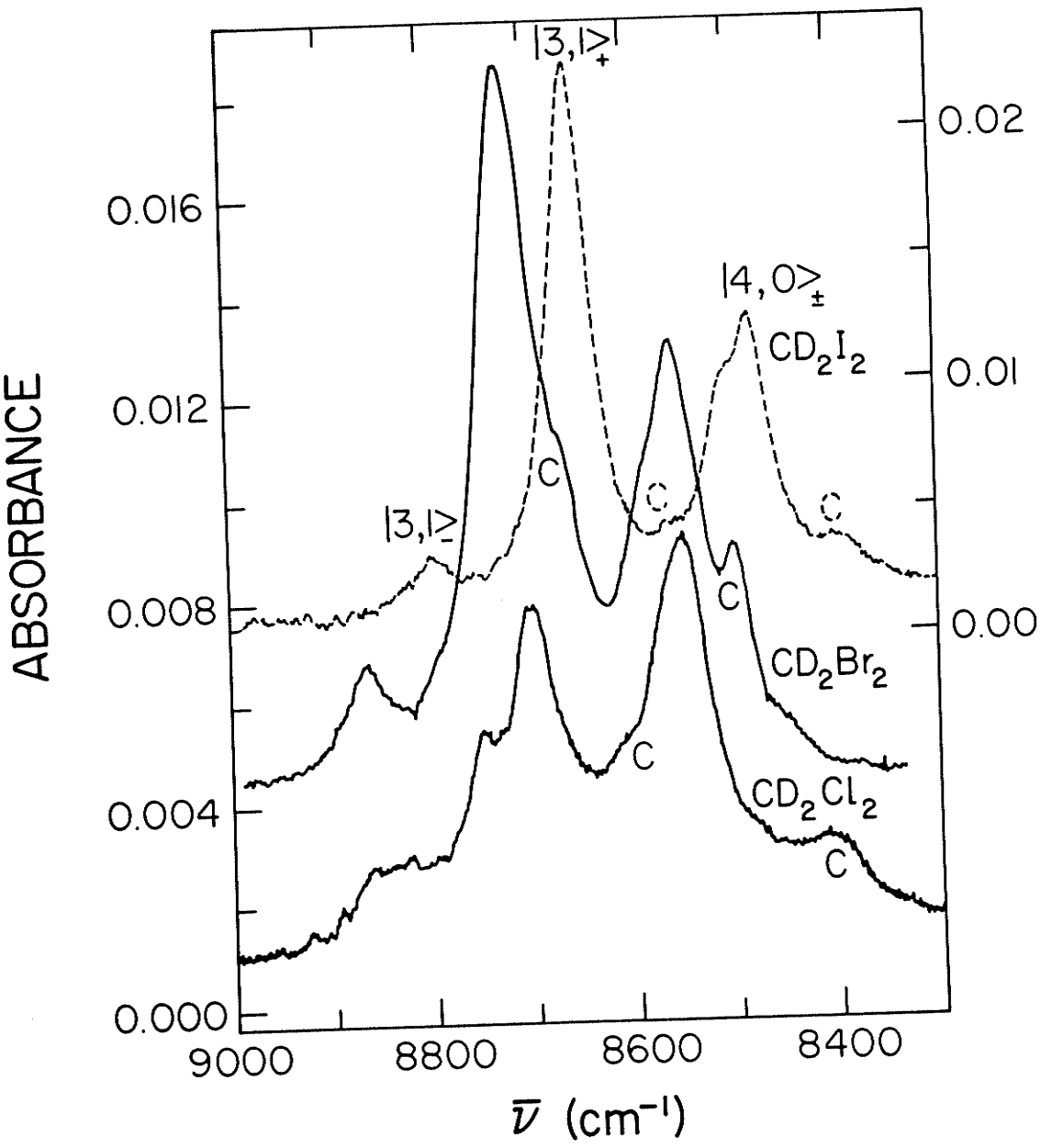
ABSORBANCE
0.016
0.012
0.008
0.004
0.000
0.02
0.01
0.00
9000
8800
8600
8400
$\bar{\nu}$ (cm^{-1})
|3,1>+
|4,0>±
|3,1>−
CD2I2
CD2Br2
CD2Cl2
C

Figure 4.4.

Liquid phase overtone spectra of CD_2Cl_2 and CD_2Br_2 in the region of $\Delta v_{CD} = 5$. These spectra are the sum of nine base line corrected scans. Individual scans were measured at room temperature with a 1.0 cm path length cell. The absorbance of CD_2Br_2 has been offset by 3.6×10^{-4} absorbance units.

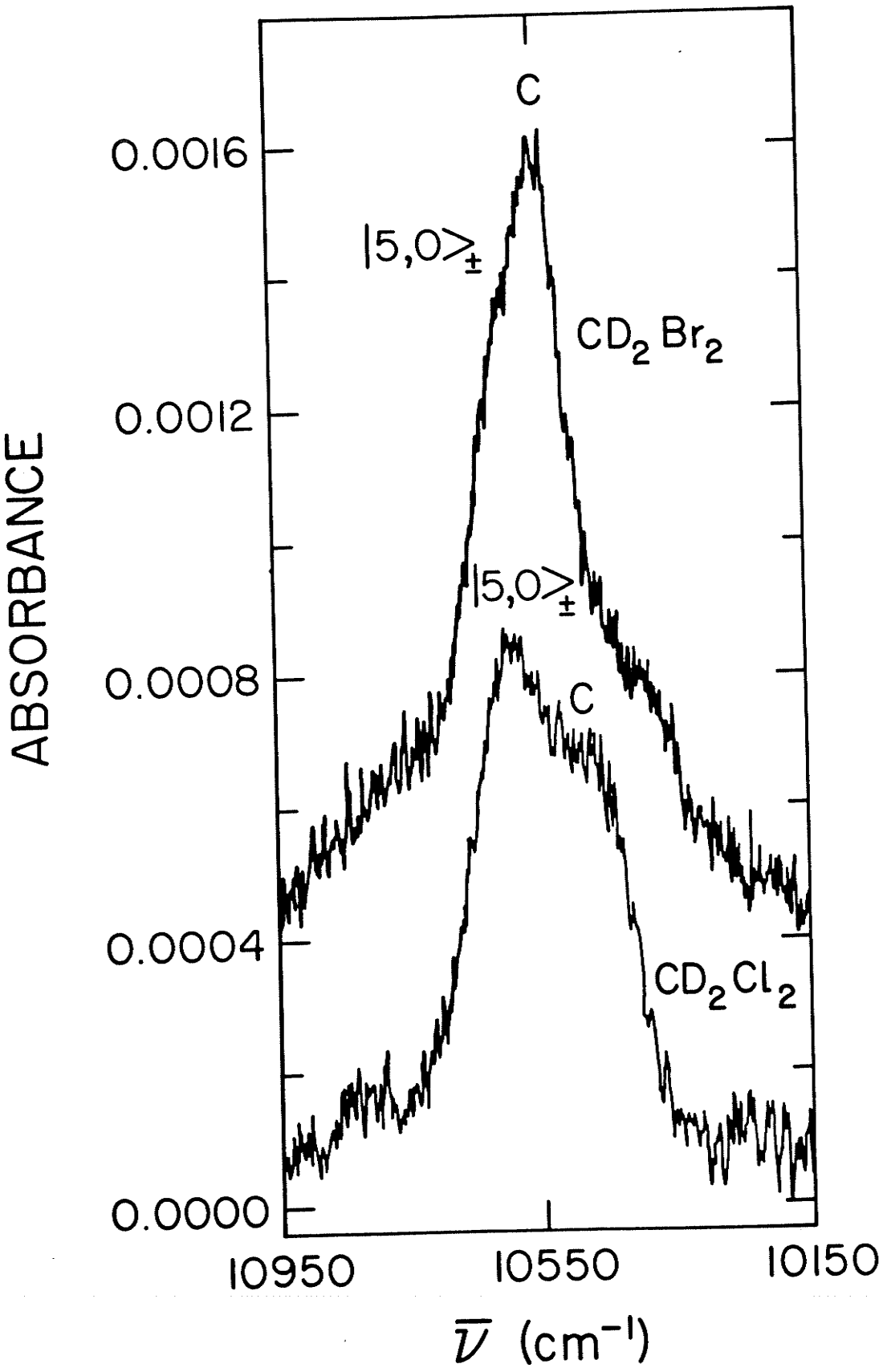
C
0.0016
|5,0>±
CD2 Br2
0.0012
ABSORBANCE
|5,0>±
0.0008
C
0.0004
CD2 Cl2
0.0000
10950
10550
10150
ν̄ (cm⁻¹)

CHAPTER 5

OVERTONE SPECTRA OF METHYL HALIDES AND METHYL CYANIDE

In this chapter, the liquid phase CH stretching overtone spectra of CH_3Cl, CH_3Br, CH_3I, and CH_3CN will be reported corresponding to the regions of Δv_{CH} = 2-6. These spectra and the reported fundamental spectra of these molecules will be analyzed in terms of the local mode model. The plots of logarithmic oscillator strengths of overtones of methyl halides against the square root of the observed energies of the pure local mode states of these molecules will be presented. These plots and similar reported plots for dihalomethanes and trihalomethanes will be used to discuss the sensitivity of the CH bond potential of the halomethanes to the number and type of halogen atoms.

i) Introduction

In very recent work[105-107], Medvedev has derived an intensity distribution law for the overtone intensities of diatomic molecules. This law is represented by a straight line on the plot of logarithmic oscillator strength log f_{ov} of observed $o \rightarrow v$ transitions versus the square root of the observed energies of these transitions, i.e.,

$$\log f_{ov} = -a \left(\frac{E_v}{\hbar\omega}\right)^{1/2} + B \qquad (5.1)$$

E_v of Eq. (5.1) is given by

$$E_v = \hbar\omega \left[(v + 1/2) - x(v + 1/2)^2\right] \qquad (5.2)$$

"B" of Eq. (5.1) is a constant and is a slowly varying function of only the initial quantum number. The slope "a" of Eq. (5.1) is given by

$$a = \frac{10.51}{\beta} (\bar{M}\,\bar{\omega})^{1/2} \qquad (5.3)$$

where "$\beta(\text{Å}^{-1})$ is a molecular parameter which describes the potential V(r) at large negative displacement where V(r) exceeds the dissociation energy D of a diatomic system ($V(r) = C\exp(-2\beta r)$ at $r < 0$ and $V(r) > D$). $\bar{M}$ and $\bar{\omega}$ of Eq. (5.3) are the reduced mass in atomic units and the harmonic frequency in units of 10^3 cm^{-1}. In deriving Eq. (5.1), a Morse potential was used to describe the diatomic system and the dipole moment matrix elements were derived from the quasiclassical approximation. The resultant expression for the dipole moment matrix elements is a product of an exponential term (which depends on the potential V(r)) and a term which arises from the dipole moment function $\mu(r)$ and is a slowly varying function of the energy

separation between the initial and final vibrational states. Two important results of Medvedev's work are summarized below:

1. Overtone band intensities are generally insensitive to the form of the dipole moment $\mu(r)$.
2. Overtone band intensities are governed by the potential at large negative displacements where the potential can be approximated as $V(r) = Ce^{-2\beta r}$.

Since, the CH bonds of highly vibrationally excited molecules behave like diatomic molecules[18-22], Medvedev applied his theory to the reported CH stretching intensities of a number of polyatomic molecules. Equation (5.1) was plotted for a number of large (C_6H_6, C_6D_5H, C_6D_6, C_6H_5D, $(CH_3)_4Si$ etc.) and relatively small (CH_2Br_2, CH_2Cl_2, $CHCl_3$, and $CHBr_3$) polyatomic molecules. From the slopes of these plots and Eq. (5.3), the values of the potential parameter β were extracted. For all large polyatomic molecules β had the same value of 3.81 Å^{-1}. From this result it was concluded that the potential, and hence the intensities, associated with the CH bonds of large polyatomic molecules are insensitive to molecular structure. For dihalomethanes (CH_2Cl_2, CH_2Br_2) and trihalomethanes ($CHCl_3$, $CHBr_3$) the value of β was found to be 3.76 $A^{\circ -1}$ and 3.10 Å^{-1}, respectively. From these results it was concluded that the CH bond potentials of dihalomethanes and of trihalomethanes are also insensitive to the type of halogen (Cl or Br). Since, the value of β obtained for the two dihalomethanes was very close to the value of β for large polyatomic molecules, Medvedev suggested that the CH bond potential of the dihalomethanes is almost the same as the CH bond potential of large polyatomic molecules. For methyl halides, Medvedev did not obtain

the potential parameter β because of unavailability of intensity data for these molecules. Nevertheless he speculated that the potential parameter β would be the same as for the other large polyatomic molecules.

In this chapter the liquid phase overtone spectra of CH_3Cl, CH_3Br, CH_3I and CH_3CN will be reported. For the first three molecules, Eq. (5.1) will be plotted to obtain the potential parameter β from Eq. (5.3). The β values of methyl halides will be compared with those reported by Medvedev for di- and tri-halomethanes. Through this comparison, it will be shown that the CH potential in halomethanes is in fact sensitive to the number of halogen atoms which replace the hydrogen atoms in methane. The observed peaks in the overtone spectra of all four molecules will be assigned by utilizing the local mode theory of the XH_3 system, which was discussed in chapter 1.

ii) Results and Discussion

a) Spectral Features

The liquid phase overtone spectra of CH_3Cl, CH_3Br, CH_3I and CH_3CN in the region of Δv_{CH} = 2 - 6 are shown in Figures 5.1 - 5.5. Most of the peaks observed in the spectra of Figures 5.1 - 5.5 can be understood as arising from the transitions to the states $|v_1,v_2,v_3>_{A_1,E}$ (see the local mode theory of a XH_3 system in chapter 1) which are symmetrized combinations of the degenerate Morse oscillator product states of the type $|v_1,v_2,v_3>$, $|v_2,v_1,v_3>$, $|v_1,v_3,v_2>$ etc., where v_1, v_2 and v_3 denote the vibrational quanta in the three CH bonds of methyl halides and methyl cyanide, $v_1,v_2,v_3 \geq 0$ and $v_1+v_2+v_3 = \Delta v_{CH}$. In the notation $|v_1,v_2,v_3>_{A_1,E}$, A_1 and E refer to the symmetry labels appropriate for the C_{3v} point group of the three equivalent CH bonds. In order to effectively explain the origin of the individual peaks of the overtone spectra of Figures 5.1 - 5.5, the observed peaks can be divided into three categories:

1. pure local mode peaks.
2. local mode combination peaks.
3. local mode - normal mode combination peaks.

The overtone spectra of CH_3Cl, CH_3Br, CH_3I and CH_3CN in the region of Δv_{CH} = 3 - 6 are dominated by the first type of peaks. These peaks arise due to transitions to the states $|v,0,0>_{A_1,E}$ whose components have all of the vibrational quanta localized in a single CH bond, e.g., in the Δv_{CH} = 3 spectrum of CH_3I (Figure 5.2), the peaks observed at 8620 cm^{-1} and 8650 cm^{-1} are $|3,0,0>_{A_1}$ and $|3,0,0>_{E}$ pure local mode peaks, respectively. The second type of peaks, i.e., the local mode combination peaks, arise from transitions to symmetrized

states whose components have vibrational quanta distributed over two or all three oscillators of the methyl halides and methyl cyanide. These peaks can be denoted by $|v-1,1,0\rangle_{A_1,E}$, $|v-2,1,1\rangle_{A_1,E}$ etc. at a given overtone manifold, Δv_{CH}. An example of such peaks are the $|2,1,0\rangle_{A_1}$, $|2,1,0\rangle_{E}$ and $|1,1,1\rangle_{A_1}$ peaks located at 8785 cm^{-1}, 8840 cm^{-1} and 9103 cm^{-1}, respectively in the $\Delta v_{CH} = 3$ spectrum of CH_3I (Figure 5.2). The third type of peak, i.e., local mode-normal mode combination peaks, are also observed in the overtone spectra of methyl halides and methyl cyanide. Most of these peaks involve v-1 quanta of CH stretching motion and two quanta of methyl deformation at a given overtone Δv_{CH}. These peaks are marked "C" in Figures 5.1-5.5 and will be discussed in a separate section.

According to the local mode theory[71,78], $|v,0,0\rangle_{A_1}$ and $|v,0,0\rangle_{E}$ states of methyl halides and methyl cyanide are initially degenerate. However, harmonic coupling of $|v,0,0\rangle_{A_1}$ and $|v,0,0\rangle_{E}$ states with the local mode combination states cause splittings between the former states at low overtones. It should be noted that the only states that can couple are those which belong to the same manifold Δv_{CH} and which have the same symmetry. With this background about the nature of coupling and the form of the local mode states, the spectral features of the observed overtones of the methyl halides and methyl cyanide can be straightforwardly assigned. For CH_3I the assignments of the pure local mode and local mode combination peaks are labelled in the spectra of Figures 5.1-5.5. The assignments of the corresponding peaks in the spectra of other molecules are obvious from the Figures.

The Δv_{CH} = 2 spectra (Figure 5.1) of methyl halides and methyl cyanide have four major peaks. From low to high energy these peaks correspond to the transitions to the states $|2,0,0\rangle_{A_1}$, $|2,0,0\rangle_{E}$, $|1,1,0\rangle_{A_1}$, and $|1,1,0\rangle_{E}$, respectively.

The most intense peak in the Δv_{CH} = 3 spectra (Figure 5.2) corresponds to transitions to either the local mode state $|3,0,0\rangle_{A_1}$ or $|3,0,0\rangle_{E}$. The highest intensity peak in the Δv_{CH} = 3 spectrum (Figure 5.2) of methyl iodide is $|3,0,0\rangle_{A_1}$. There are two unresolved shoulders to the higher energy side. The lowest energy shoulder corresponds to the $|3,0,0\rangle_{E}$ peak. In the Δv_{CH} = 3 spectrum of methyl bromide, the $|3,0,0\rangle_{E}$ peak carries the most intensity and the $|3,0,0\rangle_{A_1}$ peak appears as a low energy shoulder to this peak. $|3,0,0\rangle_{A_1}$ and $|3,0,0\rangle_{E}$ peaks are unresolved in the Δv_{CH} = 3 spectrum of CH_3Cl and CH_3CN. On the higher energy side of the pure local mode peaks $|3,0,0\rangle_{A_1}$ and $|3,0,0\rangle_{E}$ for all four molecules, the local mode combination peaks $|2,1,0\rangle_{A_1}$, $|2,1,0\rangle_{E}$ and $|1,1,1\rangle_{A_1}$ are observed.

In the region of Δv_{CH} = 4 - 6 (Figures 5.3 - 5.5), local mode combination peaks have almost totally lost their intensity and the spectra are dominated by the pure local mode peaks.

b) Local Mode Parameters and Calculated Peak Positions

The local mode parameters, harmonic frequency, ω, and diagonal anharmonicity constant, ωx, for methyl halides and methyl cyanide are given in Table 5.1. These parameters were obtained by fitting the observed energies of the pure local mode peaks to the energy equation of a diatomic anharmonic Morse oscillator[19]. This equation was quoted in three previous chapters (see Eqs. (1.1a), (3.2), and (4.1) in chapters 1, 3, and 4, respectively) and is not given here again. Note that for those spectra where the pure local mode peaks $|v,0,0\rangle_{A_1}$ and $|v,0,0\rangle_{E}$ are resolved, the weighted mean [i.e., 2/3 $E(|v,0,0\rangle_{E})$ + 1/3 $E(|v,0,0\rangle_{A_1})$] was taken as the local mode frequency in fitting the data to the energy equation of a diatomic Morse oscillator. The data of Table 5.1 show that the parameters ω and ωx for the three methyl halides are the same to within the experimental errors. In Table 5.1 the local mode parameter $\omega\gamma'$, which describes the effective interoscillator coupling in methyl halides and methyl cyanide, is also listed. This parameter was obtained from the observed splitting[108] between the fundamental CH stretching modes of A_1 and E symmetry (see entry corresponding to $\Delta v_{XH} = 1$ in Table 1.4 of Chapter 1).

Methyl halides and methyl cyanide belong to the C_{3v} point group. The local mode Hamiltonian, symmetrized local mode states, and Hamiltonian matrices for molecules of C_{3v} symmetry were given in chapter 1 (see theory of a XH_3 system in chapter 1). The Hamiltonian matrices contain the local mode parameters ω, ωx and $\omega\gamma'$. Thus from the parameters of Table 5.1, it is straightforward to calculate the peak positions for all the CH stretching states of the methyl halides and methyl cyanide. Substitution of the local mode parameters into

the intramanifold coupling matrices of Table 1.4 of chapter 1 followed by diagonalization of these matrices gives the energies of the symmetrized states. The calculated and observed frequencies are compared in Tables 5.2 and 5.3. The calculated and observed frequencies are in excellent agreement for all overtones. The observed frequencies were obtained from computer-assisted deconvolution of the experimental spectra (see chapter 2).

c) Local Mode-Normal Mode Combination Peaks

As in the overtone spectra of other polyatomic molecules[38,52,70,99,102,103], local mode-normal mode combination peaks are also observed in the spectra of Figures 5.1-5.5 of the methyl halides and methyl cyanide. Tentative assignments for all such peaks are given in Table 5.4. Among all of the combination peaks, the most prominent are those which involve v-1 quanta of pure CH stretching mode and two quanta of a CH bending mode[108] δ_A or δ_E[$\delta_A(\delta_E)$ = 1346(1444), 1297(1434), 1245(1429), and 1374(1441) cm^{-1} (from Ref. 108) for CH_3Cl, CH_3Br, CH_3I, and CH_3CN, respectively]. These peaks are denoted as $|v-1,0,0\rangle + 2\delta_A$ or $2\delta_E$ in Table 5.4 for a given value of v. These combination peaks steal intensity from the pure local mode peaks through resonant or near resonant interactions. In the spectra of CH_3CN, the effect of intensity stealing is so pronounced for the $|v-1,0,0\rangle_{A_1} + 2\delta_A$ peaks at Δv_{CH} = 3, 4, and 5 (Figures 5.2 - 5.4) that these peaks are almost as intense as the pure local mode peaks. In the spectra of methyl halides the $|v-1,0,0\rangle_{A_1} + 2\delta_E$ peaks also have considerable intensity at Δv_{CH} = 3, 4, and 5 (Figures 5.2 - 5.4).

d) Integrated Oscillator Strengths

The oscillator strength f of an absorption band can be calculated from the standard formula[109]

$$f = \left(\frac{4m_e c\varepsilon_o}{Le^2}\right) A \quad \text{or} \quad f = 6.257 \times 10^{-19}\ (m^{-2}\ \text{mol}\ s)\ A\ , \qquad (5.4)$$

where A is the integrated absorption coefficient. The integrated absorption coefficient A and the absorbance A are related through

$$A = \int \alpha d\nu = \left(\frac{2.303}{Cl}\right) \int A d\nu\ , \qquad (5.5)$$

where α is the absorption coefficient, C is the concentration of the sample, and l is the length of the cell. The integrated absorbance ($\int A d\nu$) was obtained by weighing the total area under the curve for a given overtone Δv_{CH}. The integrated oscillator strength follows straightforwardly from Eqs. (5.4) and (5.5).

The integrated oscillator strengths, f_{ov}, for the overtones of methyl halides are given in Table 5.5 along with the square roots of the energies of the upper levels, $\left(\frac{E_v}{\hbar\omega}\right)^{\frac{1}{2}}$ (see Eq. (5.2)). The plots of Eq. (5.1) (Medvedev intensity distribution law) are shown in Figure 5.6. Least squares linear regression of log f_{ov} versus $\left(\frac{E_v}{\hbar\omega}\right)^{\frac{1}{2}}$ gives the slope "a" of Eq. (5.1). The slope "a" of Eq. (5.1) for each methyl halide molecule is given in Table 5.6. The molecular parameter β (see Eq. (5.3)) is also given in Table 5.6. This parameter was obtained by substituting $\bar{M} = 0.930$ (from Ref. 107), $\bar{\omega}$ ($\bar{\omega} = \omega \times 10^{-3}\ cm^{-1}$) values from Table 5.1 and "a" values from Table 5.6 into Eq. (5.3). In Table 5.6 β and "a" values obtained by Medvedev for dihalomethanes and trihalomethanes are also listed.

The data of Table 5.6 show that β and "a" values for methyl halides do not change from one molecule to the other. Thus, in the light of Medvedev's intensity distribution law[105-107], the CH bond potential is insensitive to the type of halogen atom replacing the hydrogen in methyl halides. However, the data of Table 5.6 show that contrary to the speculation of Medvedev, the β and "a" values of methyl halides are different than those of the dihalomethanes and trihalomethanes. Thus it can be concluded that the CH bond potential of methyl halides has a different form than that of dihalomethanes and trihalomethanes. From the data of Table 5.6, it appears that successive replacement of the hydrogen atoms of methane by halogen atoms decreases the β value successively and thus the repulsive part of the CH bond potential for the less substituted halomethanes arises more rapidly than the corresponding potential of the highly substituted halomethanes ($V(r) = C\exp(-2\beta r)$ at $r<0$ and $V(r)>D$). This result is in contradiction to the conclusion reached by Medvedev for halomethanes.

The plots of Figure 5.6 show that the integrated oscillator strengths of the overtones of the methyl halides fit very well to Eq. (5.1). This result seems to be in line with the study of Amrein *et al.*[10] on a series of molecules of the type $C_nF_mCl_kH$. These authors have noticed that the intensity spread among these molecules is greatly reduced in going from the fundamental to the higher overtones, and all the intensities converge to a similar value. The present work on methyl halides is also in agreement with the study of Burberry *et al.*[110] who observed a constant absorption cross section per CH bond in

the Δv_{CH} = 3 - 6 spectra of a number of polyatomic molecules (toluene, xylene, trimethylbenzene, n-hexane, iso-octane and cyclohexane).

Table 5.1.

Local Mode Parameters (cm^{-1}) for Methyl Halides and Methyl Cyanide.

Molecule	ω	ωx	$\gamma'\omega$
CH_3Cl	3132.7±3.1	62.5±0.8	26
CH_3Br	3136.3±12.1	60.8±3.0	29
CH_3I	3128.6±4.5	60.8±1.1	32
CH_3CN	3100.5±4.3	59.2±1.1	19

Table 5.2.

Observed and Calculated Peak Positions (cm^{-1}) for Methyl Halides.

	CH_3Cl		CH_3Br		CH_3I		
Δv_{CH}	Observed	Calculated	Observed	Calculated	Observed	Calculated	Assignment
1	2956[a]	2956	2961[a]	2957	2948	2943	$\|100\rangle_{A_1}$
	3033[a]	3034	3048[a]	3044	3045	3039	$\|100\rangle_{E}$
	5861	5845	5858	5852	5845	5826	$\|200\rangle_{A_1}$
2	5914	5882	5920	5897	5911	5880	$\|200\rangle_{E}$
	6014	6009	6034	6028	6028	6016	$\|110\rangle_{A_1}$
	6061	6049	6080	6069	6082	6059	$\|110\rangle_{E}$
	8647	8625	8622	8648	8620	8617	$\|300\rangle_{A_1}$
	8647	8632	8653	8659	8650	8632	$\|300\rangle_{E}$
3	8809	8808	8808	8824	8785	8794	$\|210\rangle_{A_1}$

Table 5.2...cont'd...

Δv_{CH}	CH_3Cl		CH_3Br		CH_3I		Assignment
	Observed	Calculated	Observed	Calculated	Observed	Calculated	
3	8855	8862	8856	8883	8840	8848	$\|210\rangle_E$
	8968	8950	8996	8982	8982	8956	$\|210\rangle_E$
	-	8976	-	9009	-	8996	$\|210\rangle_{A_1}$
	9079	9059	9109	9086	9103	9070	$\|111\rangle_{A_1}$
	11265	11265	11319	11308	11287	11273	$\|400\rangle_{A_1,E}$
				11309		11274	
	11605	11568	11614	11589	11575	11543	$\|310\rangle_{A_1}$
	11605	11606	11614	11635	11575	11596	$\|310\rangle_E$
	11654	11656	11684	11693	11647	11662	$\|310\rangle_E$
4	-	11682	-	11723	-	11696	$\|310\rangle_{A_2}$

Table 5.2...cont'd...

	CH_3Cl		CH_3Br		CH_3I		
Δv_{CH}	Observed	Calculated	Observed	Calculated	Observed	Calculated	Assignment
	-	11794	-	11903	-	11877	$\|220\rangle_{A_1}$
	-	11830	-	11875	-	11854	$\|220\rangle_{E}$
	-	11866	-	11830	-	11801	$\|211\rangle_{A_1}$
	-	11975	-	12016	-	11995	$\|211\rangle_{E}$
5	13777	13788	13825	13857	13817	13819	$\|500\rangle$
6	16191	16171[b]	16261	16264[b]	16243	16218[b]	$\|600\rangle$

[a]Reference 108.

[b]Calculated from a Morse oscillator energy equation (see Eq. 4.1 in chapter 4).

Table 5.3.

Observed and Calculated Peak Positions (cm^{-1}) for Methyl Cyanide.

Δv_{CH}	Observed	Calculated	Assignment
1	2944[a]	2944	$\|100\rangle_{A_1}$
	3000[a]	3001	$\|100\rangle_{E}$
	5800	5819	$\|200\rangle_{A_1}$
2	5837	5841	$\|200\rangle_{E}$
	5958	5953	$\|110\rangle_{A_1}$
	6003	5988	$\|110\rangle_{E}$
	8608	8579	$\|300\rangle_{A_1}$
	8608	8582	$\|300\rangle_{E}$
	8753	8760	$\|210\rangle_{A_1}$
3	8793	8800	$\|210\rangle_{E}$
	8858	8865	$\|210\rangle_{E}$
	-	8885	$\|210\rangle_{A_2}$
	8996	8969	$\|111\rangle_{A_1}$
	11217	11209	$\|400\rangle_{A_1,E}$
	11491	11517	$\|310\rangle_{A_1}$
	11491	11540	$\|310\rangle_{E}$
	11600	11575	$\|310\rangle_{E}$
4	-	11592	$\|310\rangle_{A_2}$
	-	11701	$\|220\rangle_{A_1}$

Table 5.3...cont'd...

Δv_{CH}	Observed	Calculated	Assignment
	-	11721	$\|220\rangle_E$
	-	11771	$\|211\rangle_{A_1}$
	-	11858	$\|211\rangle_E$
5	13743	13719	$\|500\rangle$
6	16082	16117[b]	$\|600\rangle$

[a]Reference 108.

[b]See footnote b of Table 5.2.

Table 5.4.

Tentative Assignments of Local Mode-Normal Mode Combination Peaks of Methyl Halides and Methyl Cyanide.

Δv_{CH}	CH_3Cl	CH_3Br	CH_3I	CH_3CN	Assignment[a]
	5643	-	-	5678	$\|100>A_1+2\delta_A$
2	5697	5615	-	5716	$\|100>E+2\delta_A$
	-	5756	5685	-	$\|100>E+\delta_A+\delta_E$
	5809	5801	5776	-	$\|100>A_1+2\delta_E$
	8531	8440	8265	8529	$\|200>A_1+2\delta_A$
	8589	8559	8476	-	$\|200>A_1+\delta_A+\delta_E$
	8707	8697	8681	8651	$\|200>A_1+2\delta_E$
3	8916	8923	8914	-	$\|110>E+2\delta_E$
	-	-	-	8045	$\|200>A_1+\nu_{CN}$[b]
	-	-	-	8085	$\|200>E+\nu_{CN}$[b]
	-	-	-	8218	$\|200>A_1+\delta_A+\rho$[c]
	-	-	-	8339	$\|200>E+\delta_E+\rho$[c]
	11225	11203	-	11143	$\|300>_{A_1,E}+2\delta_A$
	11346	11410	11351	11314	$\|300>_{A_1,E}+2\delta_E$
	-	-	-	13505	$\|400>_{A_1E}+\nu_{CN}$[b]
	-	-	13690	13667	$\|400>_{A_1,E}+2\delta_A$

Table 5.4...cont'd...

Δv_{CH}	CH_3Cl	CH_3Br	CH_3I	CH_3CN	Assignment[a]
	13873	13987	13899	13582	$\|400\rangle_{A_1,E}+2\delta_E$
	-	-	16358	-	$\|500\rangle_{A_1,E}+2\delta_E$

[a] δ_A and δ_E are the CH-bending modes of A and E symmetry (see Ref. 108).

[b] ν_{CN} is the CN stretch (2256 cm^{-1}, from Ref. 108).

[c] ρ is the methyl rocking mode (1037 cm^{-1}, from Ref. 108).

Table 5.5.

Integrated Oscillator Strengths for the Overtones of Methyl Halides.

	CH_3Cl			CH_3Br			CH_3I		
Δv_{CH}	f_{ov}	log f_{ov}	$\left(\frac{E_v}{\hbar\omega}\right)^{1/2}$	f_{ov}	log f_{ov}	$\left(\frac{E_v}{\hbar\omega}\right)^{1/2}$	f_{ov}	log f_{ov}	$\left(\frac{E_v}{\hbar\omega}\right)^{1/2}$
2	2.38×10^{-7}	-6.62	1.5412	2.58×10^{-7}	-6.59	1.5423	2.76×10^{-7}	-6.56	1.5423
3	3.42×10^{-8}	-7.47	1.8043	3.97×10^{-8}	-7.40	1.8062	3.66×10^{-8}	-7.44	1.8061
4	3.45×10^{-9}	-8.46	2.0239	3.74×10^{-9}	-8.43	2.0267	4.19×10^{-9}	-8.38	2.0264
5	3.04×10^{-10}	-9.52	2.2128	3.29×10^{-10}	-9.48	2.2167	3.63×10^{-10}	-9.44	2.2163
6	5.81×10^{-11}	-10.24	2.3785	6.11×10^{-11}	-10.21	2.3855	7.49×10^{-11}	-10.13	2.3831

Table 5.6.

Slopes for the Plots of Medvedev's Intensity Distribution Law and the Molecular Spectroscopic Parameter $\beta(\text{Å}^{-1})$ of Halomethanes.

Molecule	a	β
CH_3Cl	4.43±0.25	4.05±0.23
CH_3Br	4.42±0.26	4.06±0.24
CH_3I	4.34±0.23	4.13±0.22
CH_2X_2[a]	4.80[b]	3.76±0.07[b]
CHX_3[a]	5.80[b]	3.10±0.05[b]

[a] X = Cl, Br.

[b] Reference 107.

Figure 5.1.

Liquid phase overtone spectra of CH_3CN, CH_3Cl, CH_3Br, and CH_3I in the region of $\Delta v_{CH} = 2$. Spectra were measured at room temperature with a path length of 0.1 cm. Absorbances of CH_3Cl, CH_3Br, and CH_3I have been offset by 0.5, 1.0, and 1.5 absorbance units, respectively.

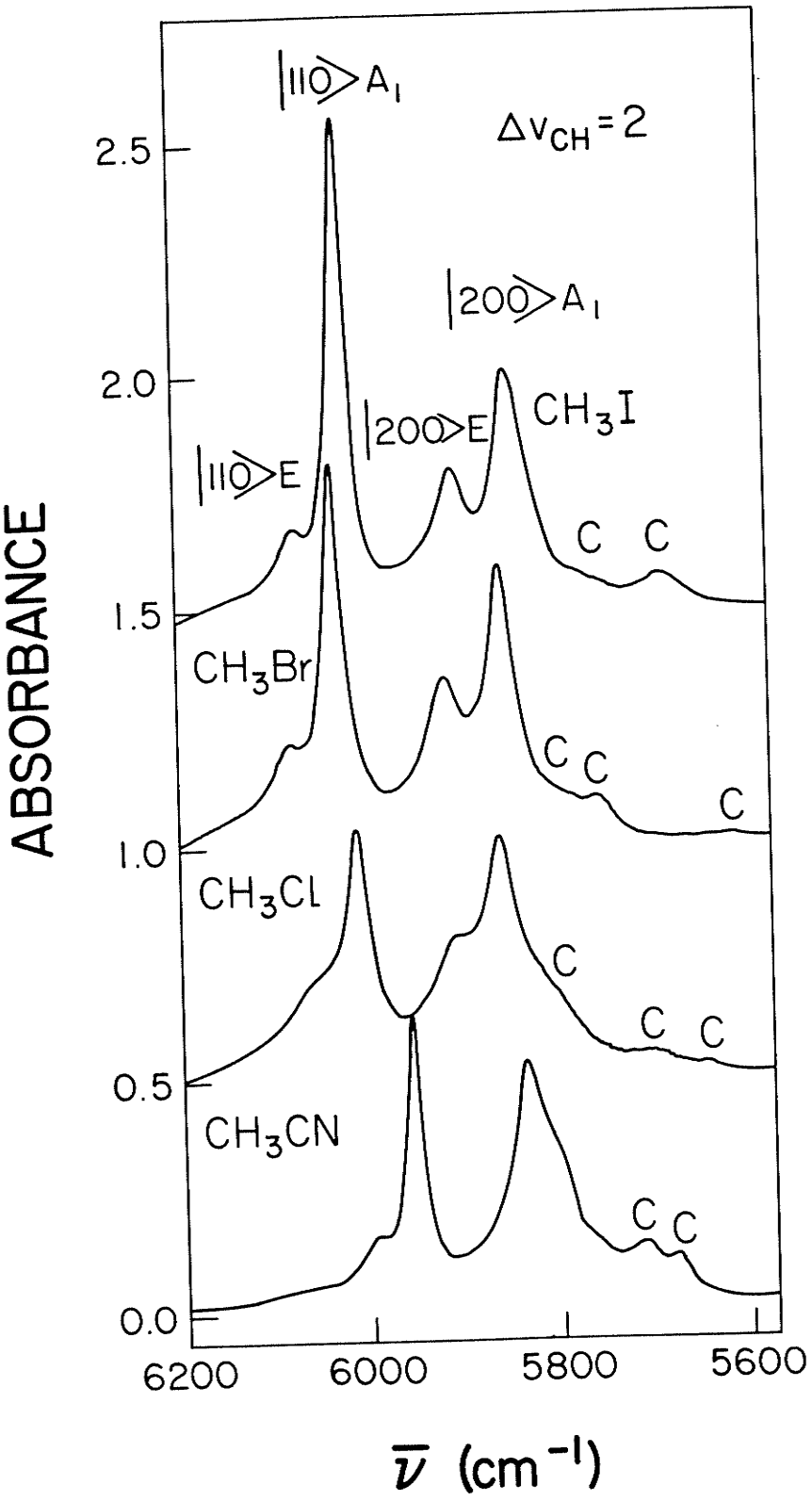
|110>A1
ΔvCH=2
|200>A1
|200>E
CH3I
|110>E
C C
CH3Br
C C C
CH3Cl
C C C
CH3CN
C C
2.5
2.0
1.5
1.0
0.5
0.0
ABSORBANCE
6200
6000
5800
5600
ν̄ (cm⁻¹)

Figure 5.2.

Liquid phase overtone spectra of CH_3CN, CH_3Cl, CH_3Br, and CH_3I in the region of $\Delta v_{CH} = 3$. Spectra were measured at room temperature with a path length of 1.0 cm. Absorbances of CH_3Cl, CH_3Br, and CH_3I have been offset by 0.5, 1.0, and 1.5 absorbance units, respectively.

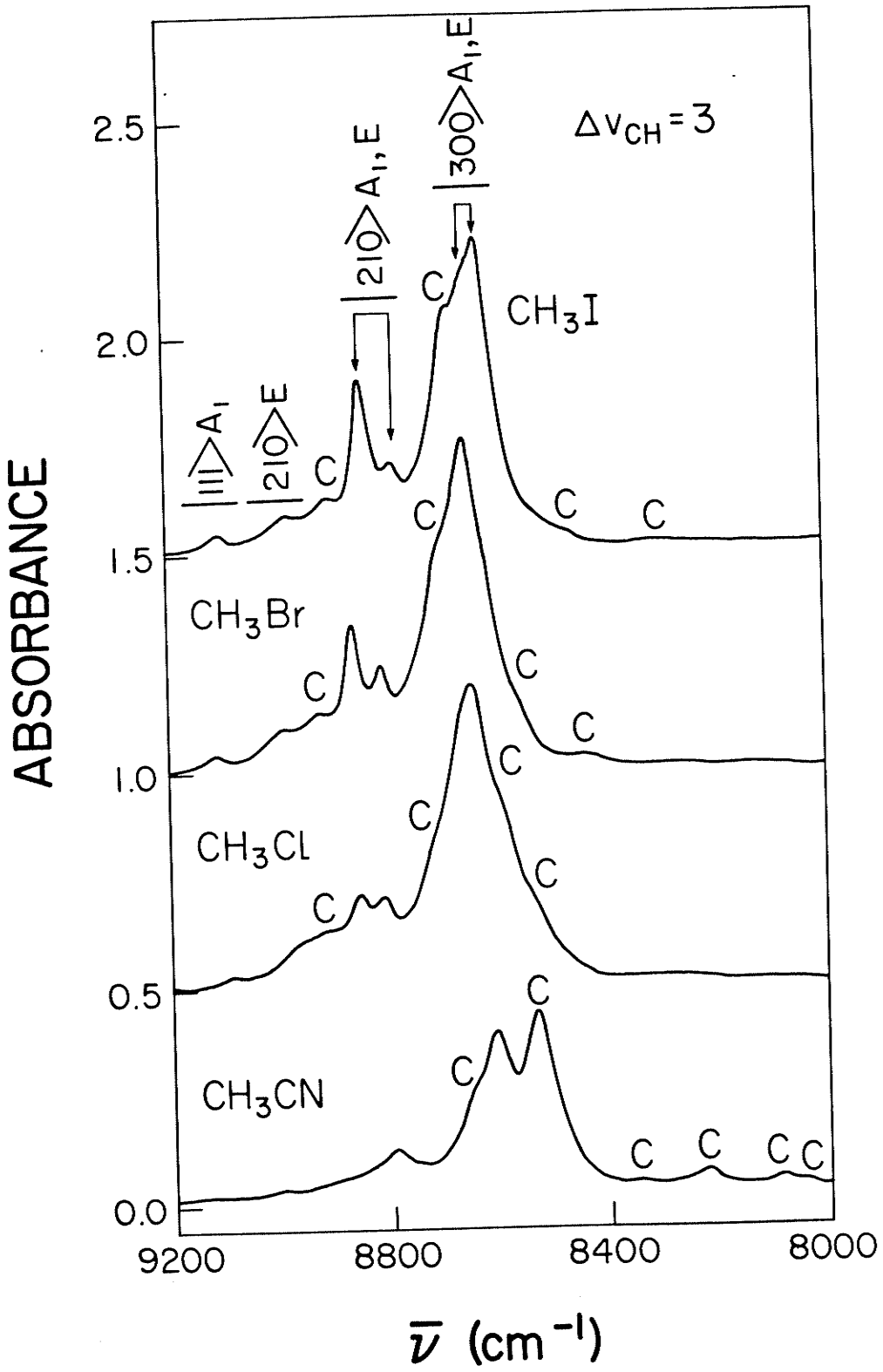
ABSORBANCE
2.5
2.0
1.5
1.0
0.5
0.0
9200
8800
8400
8000
$\bar{\nu}$ (cm^{-1})
$\Delta v_{CH} = 3$
|300⟩ A_1, E
|210⟩ A_1, E
|210⟩ E
|111⟩ A_1
CH_3I
CH_3Br
CH_3Cl
CH_3CN
C

Figure 5.3.

Liquid phase overtone spectra of CH_3CN, CH_3Cl, CH_3Br, and CH_3I in the region of $\Delta v_{CH} = 4$. Spectra were measured at room temperature with a path length of 5.0 cm. Absorbances of CH_3Cl, CH_3Br, and CH_3I have been offset by 0.27, 0.53, and 0.78 absorbance units, respectively.

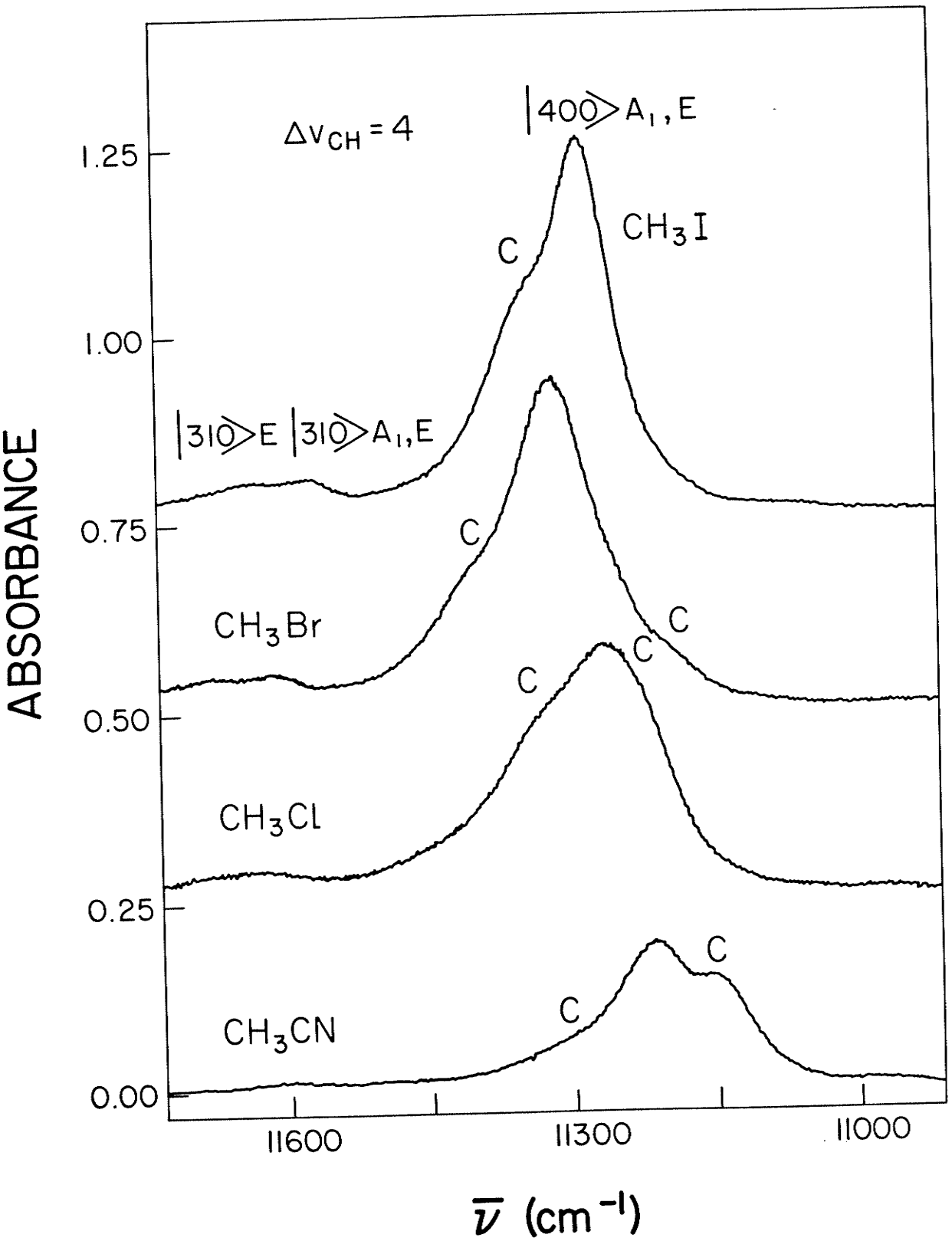
ΔvCH = 4
|400⟩A1,E
CH3I
C
|310⟩E |310⟩A1,E
CH3Br
CH3Cl
CH3CN
ABSORBANCE
1.25
1.00
0.75
0.50
0.25
0.00
11600
11300
11000
ν̄ (cm⁻¹)

Figure 5.4.

Liquid phase overtone spectra of CH_3CN, CH_3Cl, and CH_3I in the region of $\Delta v_{CH} = 5$. Spectra were measured at room temperature with a path length of 5.0 cm. Absorbances of CH_3Cl, CH_3Br, and CH_3I have been offset by 0.02, 0.04, and 0.06 absorbance units, respectively.

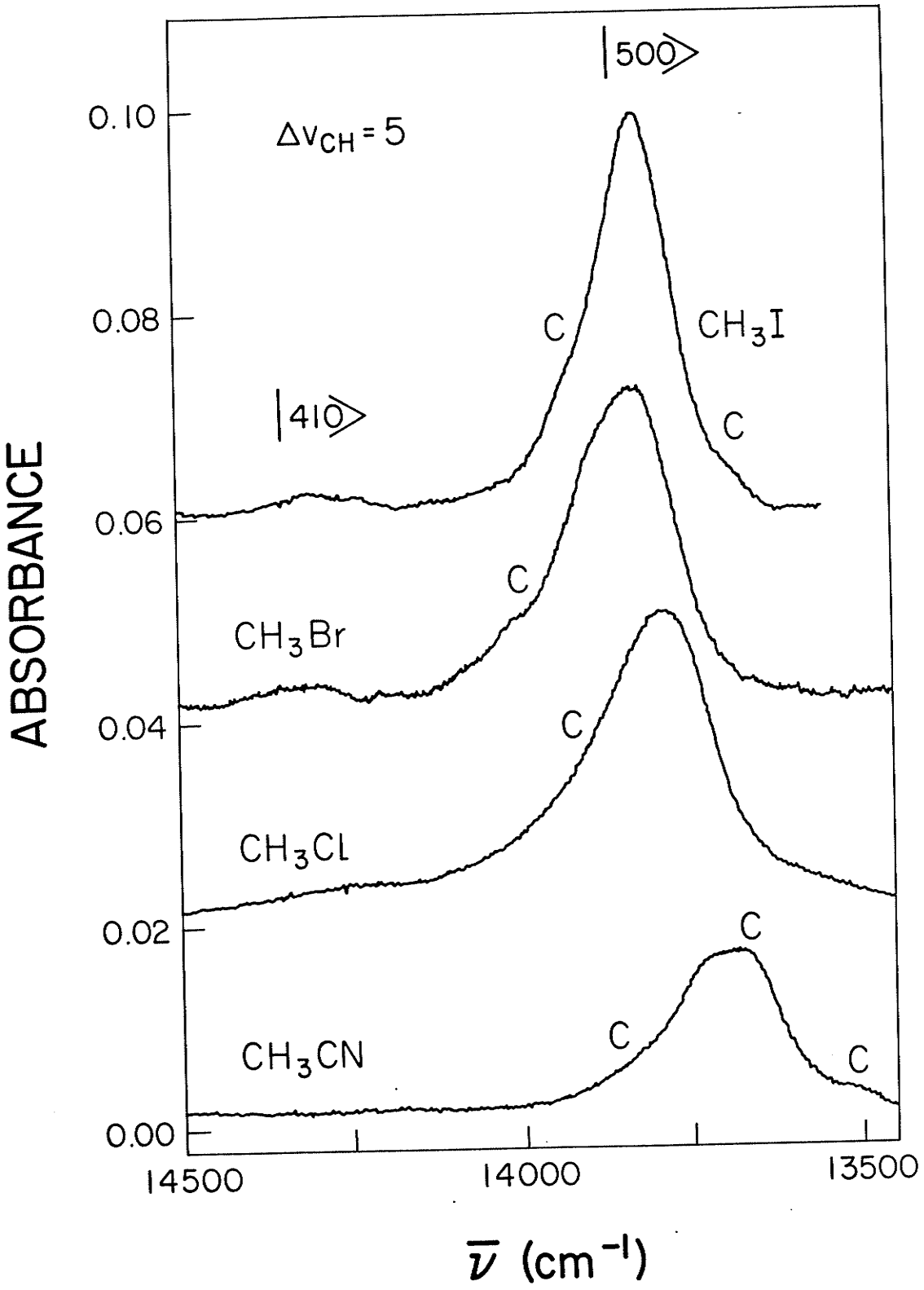
|500⟩
ΔvCH = 5
0.10
0.08
0.06
0.04
0.02
0.00
C
CH3I
|410⟩
C
C
CH3Br
C
C
CH3Cl
C
C
C
CH3CN
ABSORBANCE
14500
14000
13500
ν̄ (cm⁻¹)

Figure 5.5.

Liquid phase overtone spectra of CH_3CN, CH_3Cl, CH_3Br, and CH_3I in the region of $\Delta v_{CH} = 6$. These spectra are the sum of four base line corrected scans. Individual scans were measured at room temperature with a path length of 5.0 cm. The right hand ordinate scale represents the absorbance of CH_3I. Absorbances of CH_3Cl and CH_3Br have been offset by 0.002 and 0.004 absorbance units, respectively, with respect to the absorbance of CH_3CN.

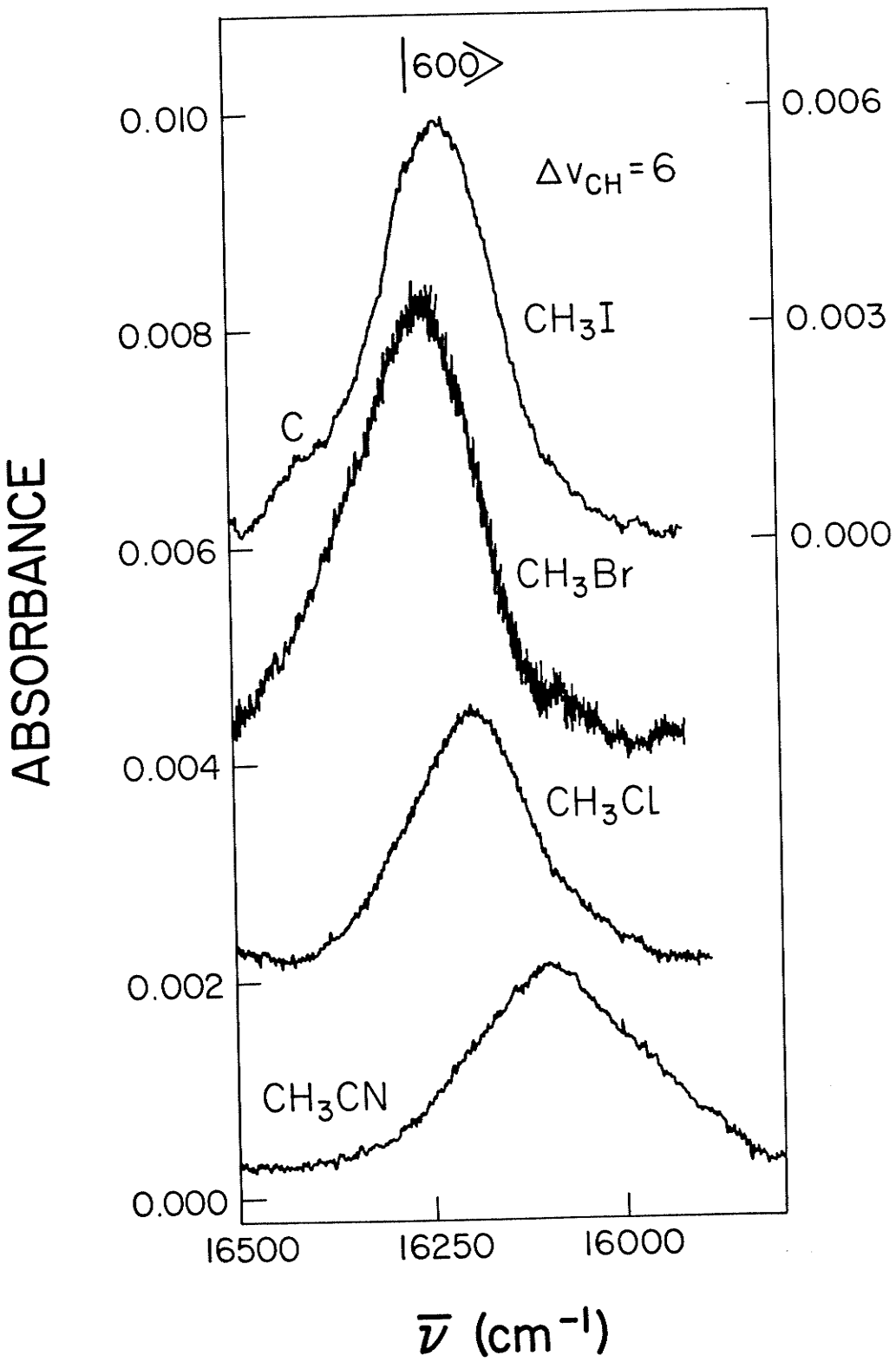
|600⟩
0.010
0.008
0.006
0.004
0.002
0.000
0.006
0.003
0.000
ABSORBANCE
$\Delta v_{CH} = 6$
CH_3I
C
CH_3Br
CH_3Cl
CH_3CN
16500
16250
16000
$\bar{\nu}$ (cm^{-1})

Figure 5.6.

Plots of integrated oscillator strengths of Δv_{CH} = 2 - 6 overtone spectra of methyl halides versus the square roots of the observed energies of the pure local mode states.

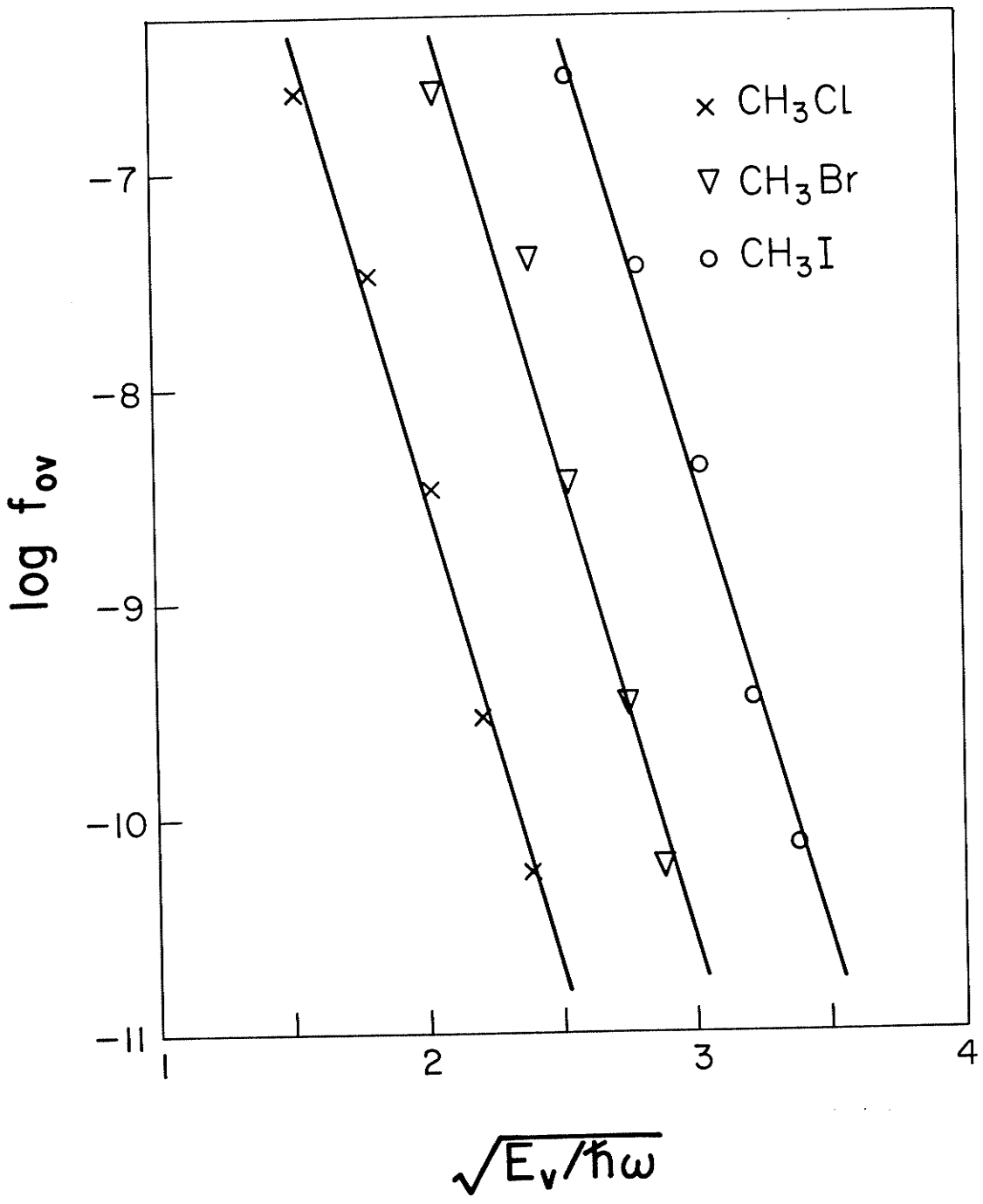
× CH3Cl
▽ CH3Br
○ CH3I
log fov
−7
−8
−9
−10
−11
1
2
3
4
√Ev/ħω

CHAPTER 6

OVERTONE SPECTRA OF DEUTERATED METHYL IODIDE AND DEUTERATED METHYL CYANIDE

In this chapter the liquid phase overtone spectra of CD_3I and CD_3CN in the region of Δv_{CD} = 2 - 5 will be reported. The spectra will be analyzed on the basis of the same local mode theory which was utilized for the analysis of the spectra of methyl halides and methyl cyanide in chapter 5. The spectra of CD_3I and CD_3CN will be compared with those of CH_3Z (Z = Cl, Br, I or CN) molecules and through this comparison, the effects of increased interoscillator coupling on the intensities and symmetry splittings of the local mode states will be discussed.

i) Introduction

Although the local mode model has been used extensively to understand the spectra of polyatomic molecules containing XH moieties[18-22], very little attention has been paid to the XD stretching overtone spectra of deuterated molecules. The study of XD stretching spectra is important in that it may provide information regarding the effect of increased kinetic coupling on the symmetry splittings, relative energies, and relative intensities of the local mode states.

In chapter 4 the liquid phase CD stretching fundamental and overtone spectra of CD_2Z_2 (Z = Cl, Br or I) molecules were analyzed within the local mode picture. The spectra of CD_2Z_2 and CH_2Z_2 molecules were compared and through this comparison, the effects of stronger interoscillator coupling on the local mode states of C_{2v} symmetry were studied. In this chapter the CD stretching overtone spectra of CD_3I and CD_3CN in the regions of Δv_{CD} = 2 - 5 will be reported. These spectra and the previously reported fundamental spectra[101,111,112] will be analyzed on the basis of the same local mode theory (see local mode theory of a XH_3 system in chapter 1) which was used for the analysis of the spectra of methyl halides and methyl cyanide in chapter 5. The features of the overtone spectra of CD_3CN and CD_3I will be compared with the overtone spectra of CH_3Z (Z = Cl, Br, I or CN) molecules. In the light of this comparison effects of increased coupling on the local mode states of C_{3v} symmetry will be discussed.

ii) Results and Discussion

a) CD Stretching Peaks

The overtone spectra of CD_3I and CD_3CN are shown in Figures 6.1 - 6.4. Three types of peaks are observed in the spectra of Figures 6.1 - 6.4. The first two types of peaks only involve CD stretching. The assignments for these peaks are given in Table 6.1. The third type of peak is marked C in Figures 6.1 - 6.4. These peaks result from transitions to states which involve pure local modes and normal modes. The assignments for these peaks will be presented later in this section.

The $\Delta v_{CD} = 2$ region of the overtone spectra is shown in Figure 6.1. The peaks observed at 4528 and 4388 cm^{-1} in CD_3I are assigned as transitions to the symmetrized pure local mode states $|2,0,0\rangle_{A_1}$ and $|2,0,0\rangle_E$. The pure local mode peaks $|2,0,0\rangle_{A_1}$ and $|2,0,0\rangle_E$ are located at 4463 and 4335 cm^{-1}, respectively, in the spectrum of CD_3CN. In addition to transitions to the pure local mode overtone states, transitions to local mode combination states are also observed. The peaks observed at 4263 and 4558 cm^{-1} in the spectrum of CD_3I are assigned as transitions to local mode states $|1,1,0\rangle_{A_1}$ and $|1,1,0\rangle_E$, respectively. The corresponding peaks in the spectrum of CD_3CN are observed at 4214 and 4513 cm^{-1}.

The $|2,0,0\rangle_{A_1}$ and $|2,0,0\rangle_E$ peaks are split and this splitting is significantly higher than the corresponding splitting in the spectra of CH_3Z (Z = Cl, Br, I or CN) molecules (see Table 5.2 in chapter 5). In the absence of any coupling, the $|2,0,0\rangle_{A_1}$ and $|2,0,0\rangle_E$ states would be degenerate. However, $|2,0,0\rangle_{A_1}$ and $|2,0,0\rangle_E$ states couple with the

$|1,1,0\rangle_{A_1}$ and $|1,1,0\rangle_E$ states, respectively and consequently $|2,0,0\rangle_{A_1}$ and $|2,0,0\rangle_E$ states become nondegenerate.

The $\Delta v_{CD} = 3$ region of the overtone spectra is shown in Figure 6.2. The pure local mode peaks $|3,0,0\rangle_{A_1}$ and $|3,0,0\rangle_E$ are observed at 6588 and 6467 cm^{-1} in the spectrum of CD_3I. The corresponding peaks in the spectrum of CD_3CN are observed at 6516 and 6362 cm^{-1}. Again splitting occurs between $|3,0,0\rangle_{A_1}$ and $|3,0,0\rangle_E$. Transitions to the local mode combination states, $|2,1,0\rangle$, of A_1 and E symmetry are observed at 6371, 6627 and 6752 cm^{-1} in the spectrum of CD_3I (see Table 6.1 and Figure 6.2). Analogous peaks in the spectrum of CD_3CN are observed at 6243, 6540 and 6656 cm^{-1}. The local mode combination peak due to transition to the state $|1,1,1\rangle_{A_1}$ is observed at 6829 and 6735 cm^{-1} in the spectrum of CD_3I and CD_3CN, respectively.

The $\Delta v_{CD} = 4$ region of the overtone spectra is shown in Figure 6.3. Due to the greater number of transitions these spectra appear complex. Several of the peaks overlap severely and thus the observed peak positions, as listed in Table 6.1, should be considered only as estimates. All the local mode combination peaks have higher frequencies (see Table 6.1) than the pure local mode peaks at $\Delta v_{CD} = 4$. This was not the case at $\Delta v_{CD} = 2$ and $\Delta v_{CD} = 3$, where the $|v-1,1,0\rangle_{A_1}$ peaks have lower frequencies than the pure local mode peaks of both A_1 and E symmetry.

The $\Delta v_{CD} = 5$ region of the overtone spectra is shown in Figure 6.4. The local mode peaks observed in each spectrum of Figure 6.4 arise from transitions to the states $|5,0,0\rangle$, $|4,1,0\rangle$ and $|3,2,0\rangle$. The splitting between the pure local mode states of A_1 and E symmetry

is not observed and thus it appears that "local mode character" starts to develop for CD_3I and CD_3CN at the Δv_{CD} = 5 level of excitation.

b) Calculated Energies of the CD Stretching Peaks

The spectra of CD_3I and CD_3CN can be calculated with the same procedure which was used to calculate the spectra of methyl halides and methyl cyanide in chapter 5. For the calculation of the spectra of CD_3I and CD_3CN knowledge of the local mode parameters of the CD oscillators of these molecules is necessary[70,71]. In chapter 5, the local mode parameters (harmonic frequency, ω, and diagonal anharmonicity, ωx) for the CH oscillators of methyl halides and methyl cyanide were obtained by fitting the energies of the pure local mode peaks of the spectra of these molecules to the vibrational energy equation of a single Morse oscillator. Morse oscillator energy equation however cannot be used to obtain ω and ωx for CD_3I and CD_3CN because extensive interactions between the CD stretching states and combination states involving deformational modes of CD_3 group strongly perturb the peak positions. The procedure which was adapted to obtain the local mode parameters for the CD oscillator of CD_3I and CD_3CN is discussed below.

When deuterium is substituted for the hydrogen of a CH oscillator, the change in the harmonic frequency is described by the following equation

$$\frac{\omega_D}{\omega_H} = \left(\frac{m_D}{m_H}\right)^{-\frac{1}{2}} = \left[\frac{\frac{24}{12}}{\frac{12}{13}}\right]^{-\frac{1}{2}} \qquad (6.1)$$

where m_D and m_H are the reduced masses for a CD and a CH oscillator, respectively. To obtain ω_D values for the CD oscillators of CD_3I and CD_3CN, ω_H values were substituted into Eq. (6.1) from Table 5.1 of chapter 5 ($\omega_H(CH_3I) = 3128.6 \pm 4.5$, $\omega_H(CH_3CN) = 3100.5 \pm 4.3$). The

resultant values of ω_D were 2295.8 cm^{-1} and 2275.1 cm^{-1} for the CD oscillators of CD_3I and CD_3CN, respectively.

The interoscillator coupling $\gamma'\omega$ can be obtained empirically from the following equation[71]

$$\gamma'\omega = \frac{1}{3}[\bar{\nu}(|1,0,0\rangle_E) - \bar{\nu}(|1,0,0\rangle_{A_1})] \qquad (6.2)$$

Eq. (6.2) is simply obtained from the local mode energy expressions for the $|1,0,0\rangle_{A_1}$ and $|1,0,0\rangle_E$ states (see Table 1.4 in chapter 1). In Eq. (6.2) $\bar{\nu}(|1,0,0\rangle_{A_1})$ and $\bar{\nu}(|1,0,0\rangle_E)$ denote the observed frequencies[101,112] for the transitions to the $|1,0,0\rangle_{A_1}$ and $|1,0,0\rangle_E$ states, respectively. The value of $\gamma'\omega$ obtained from Eq. (6.2) is 49.7 cm^{-1} and 49.0 cm^{-1} for the CD oscillators of CD_3I and CD_3CN, respectively.

The only parameter left to be determined is ωx. This parameter was determined by fitting ω, $\gamma'\omega$ and the observed frequency of $|1,0,0\rangle_E$ peak (see Table 6.1) to the following equation[71]

$$\bar{\nu}(|1,0,0\rangle_E) = \omega - 2\omega x + \gamma'\omega \qquad (6.3)$$

Eq. (6.3) expresses the expected energy of the $|1,0,0\rangle_E$ peak on the basis of the harmonic coupling model (see Table 1.4 in chapter 1). The ωx values obtained from Eq. (6.3) are 28.3 cm^{-1} (CD_3I) and 30.5 cm^{-1} (CD_3CN). Note that ωx can also be extracted from the equation analogous to Eq. (6.3) for the energy expression of the $|1,0,0\rangle_{A_1}$ peak. ωx values obtained from the energy expression of the $|1,0,0\rangle_{A_1}$ peak were the same as obtained from Eq. (6.3).

With the parameters ω, ωx, and $\gamma\omega'$ it is then straightforward to calculate the frequencies of all of the CD stretching peaks of CD_3I

and CD_3CN. The procedure is exactly the same as was used to calculate the spectra of the CH_3Z molecules in chapter 5. The calculated and observed peak positions are given in Table 6.1. The observed peak positions were obtained from the deconvolution of the experimental spectra. It is clear from the data of Table 6.1 that the calculated and observed peak positions are in reasonably good agreement.

c) Local Mode-Normal Mode Combination Peaks

The local mode-normal mode combination peaks marked C in the spectra of CD_3I and CD_3CN at a given $\Delta v_{CD} = v$ involve the $|v-1,0,0\rangle$ pure local mode state and binary combinations, or first overtones of DCD bending modes δ_A and δ_E. Since the frequencies of DCD bending modes ($\delta_A^{111}(CD_3I) = 938\ cm^{-1}$, $\delta_E^{101}(CD_3I) = 1040\ cm^{-1}$, $\delta_A^{112}(CD_3CN) = 1103\ cm^{-1}$ and $\delta_E^{112}(CD_3CN) = 1039\ cm^{-1}$) are approximately one-half of the CD stretching frequencies, these modes can effectively interact with the states $|v,0,0\rangle$. The assignments for the local mode-normal mode combination peaks observed in the spectra of CD_3I and CD_3CN are given in Tables 6.2 and 6.3, respectively.

Local mode-normal mode combinations similar to those observed in the spectra of CD_3I and CD_3CN have been observed previously in the overtone spectra of a number of polyatomic molecules[53,70,96,99,102,103,113,114]. The principal source of intensity for these combination peaks is intensity "stealing" from the local mode states through resonant or near resonant interactions.

d) Comparison of the CD_3Z (Z = I or CN) and CH_3Z (Z = Cl, Br, I or CN) Spectra

As was the case with the spectra of CD_2Z_2 and CH_2Z_2 (Z = Cl, Br or I) molecules (see chapter 4), the principal differences in the spectra of CD_3Z and CH_3Z molecules can be discussed in terms of the local mode parameters ωx and $\omega\gamma'$. In CH_3Z molecules, $\omega\gamma' < \omega x$ ($\frac{\omega x}{\omega\gamma'} \simeq 2$ for CH_3Cl, CH_3Br and CH_3I; for CH_3CN $\frac{\omega x}{\omega\gamma'} \simeq 3$). Because of this, the pure local mode states of A_1 symmetry have the lowest energy among all of the local mode states at each overtone manifold Δv (see Table 5.2 in chapter 5). In CD_3Z molecules $\omega\gamma' > \omega x$ ($\frac{\omega x}{\omega\gamma'} \simeq 0.6$) and thus the relative energy ordering of the local mode states at $\Delta v_{CD} = 2$ and $\Delta v_{CD} = 3$ of these molecules is not the same as at the corresponding overtone levels of CH_3Z molecules. This point can be understood considering the $\Delta v = 2$ overtone manifold of CD_3Z and CH_3Z molecules. The energies of the local mode states of this manifold are expressed by the following matrices (see Table 1.4 in chapter 1),

$$\begin{array}{c} |200\rangle_E \\ |110\rangle_E \end{array} \begin{bmatrix} 2\omega - 6\omega x & \sqrt{2}\gamma'\omega \\ \sqrt{2}\gamma'\omega & 2\omega - 4\omega x + \gamma'\omega \end{bmatrix} \qquad \text{(A)}$$

$$\begin{array}{c} |200\rangle_{A_1} \\ |110\rangle_{A_1} \end{array} \begin{bmatrix} 2\omega - 6\omega x & -2\sqrt{2}\gamma'\omega \\ -2\sqrt{2}\gamma'\omega & 2\omega - 4\omega x - 2\gamma'\omega \end{bmatrix}. \qquad \text{(B)}$$

First matrix (A) is considered. It is clear from this matrix that the local mode state $|2,0,0\rangle_E$ will have lower energy than the combination state $|1,1,0\rangle_E$ in CH_3Z and CD_3Z since in both cases ωx and $\omega\gamma'$ have

positive values. Consider matrix (B). It can easily be concluded that $|2,0,0\rangle_{A_1}$ state will have lower energy than $|1,1,0\rangle_{A_1}$ state in the case of CH_3Z for which $\omega x > \omega\gamma'$, but for CD_3Z the $|2,0,0\rangle_{A_1}$ state will have higher energy than $|1,1,0\rangle_{A_1}$ due to the high value of $\omega\gamma'$ compared to ωx. Thus in summary, in CH_3Z molecules the relative energy ordering of the local mode states at $\Delta v_{CH} = 2$ is $E(|2,0,0\rangle_{A_1}) < E(|2,0,0\rangle_E) < E(|1,1,0\rangle_{A_1}) < E(|1,1,0\rangle_E)$ whereas this energy ordering at $\Delta v_{CD} = 2$ of CD_3Z molecules is $E(|1,1,0\rangle_{A_1}) < E(|2,0,0\rangle_E) < E(|2,0,0\rangle_{A_1}) < E(|1,1,0\rangle_E)$.

At $\Delta v_{CD} = 3$ the energy ordering of the local mode states of CD_3Z molecules is $E(|2,1,0\rangle_{A_1}) < E(|3,0,0\rangle_E) < E(|3,0,0\rangle_{A_1}) < E(|2,1,0\rangle_E)$ $E(|2,1,0\rangle_{A_2}) < E(|1,1,1\rangle_{A_1})$. The relative energy of the local mode states at $\Delta v_{CH} = 3$ of CH_3Z molecules is $E(|3,0,0\rangle_{A_1}) < E(|3,0,0\rangle_E) < E(|2,1,0\rangle_{A_1}) < E(|2,1,0\rangle_E) < E(|2,1,0\rangle_{A_2}) < E(|1,1,1\rangle_{A_1})$. Once again the different relative energy trend of the local mode states in CH_3Z and CD_3Z molecules can be attributed to the different sets of values for ωx and $\omega\gamma'$ in CH_3Z and CD_3Z molecules.

At $\Delta v_{CD} = 4$ of CD_3Z molecules, ωx and $\omega\gamma'$ contribute to the Hamiltonian matrices in such a way that the pure local mode state, $|4,0,0\rangle$, of A_1 symmetry is of lowest energy, i.e., the situation is similar to that encountered at all overtones of CH_3Z molecules.

Halonen and Child have analyzed the spectra of CHD_3[78]. The relative ωx and $\omega\gamma'$ values for the CD oscillators of CHD_3 and CD_3Z molecules are almost the same ($\frac{\omega x}{\omega\gamma'}(CD_3Z) \simeq 0.6$, $\frac{\omega x}{\omega\gamma'}(CHD_3) \simeq 0.8$). Thus one would expect the relative energy ordering of the local mode states of CHD_3 and CD_3Z molecules to be the same. Halonen and Child report[78] that the pure local mode state $|v,0,0\rangle$ of A_1 symmetry is of

lowest energy at each overtone manifold $\Delta v_{CD} = v$. This result is highly unlikely at low overtones (Δv_{CD} = 2 and 3), and a typographical error in the work of Halonen and Child is suspected.

Another important difference between the spectra of CD_3Z and CH_3Z molecules is that in the former molecules there are greater splittings between the symmetrized states $|v,0,0\rangle_{A_1}$ and $|v,0,0\rangle_E$. According to the local mode theory which is employed for the analysis of the spectra, the local mode states of the same symmetry belonging to the same manifold harmonically couple with each other[71,78]. This coupling is determined by the off-diagonal terms of the Hamiltonian matrices of three coupled anharmonic Morse oscillators[71,78] (see Table 1.4 in chapter 1). These matrix elements involve[71,78] the coupling parameter $\omega\gamma'$. In the absence of any coupling the pure local mode states $|v,0,0\rangle_{A_1}$ and $|v,0,0\rangle_E$ would be degenerate. However, the states $|v,0,0\rangle_{A_1}$ and $|v,0,0\rangle_E$ couple with the states $|v-1,1,0\rangle_{A_1}$ and $|v-1,1,0\rangle_E$, respectively, and thus the former set of states are split. Since $\omega\gamma'$ is higher for CD_3Z molecules therefore the greater splitting between $|v,0,0\rangle_{A_1}$ and $|v,0,0\rangle_E$ is not unexpected.

In CH_3Z molecules the $|v,0,0\rangle_{A_1}$ and $|v,0,0\rangle_E$ states become degenerate at $\Delta v_{CH} = 4$ and the local mode combination peaks $|v-1,1,0\rangle$, $|v-2,1,1\rangle$ etc. almost totally loose their intensity. In other words "local mode character" develops at $\Delta v_{CH} = 4$ of CH_3Z molecules. This is not the case with CD_3Z molecules. At Δv_{CD} =4 of these molecules, the peaks $|4,0,0\rangle_{A_1}$ and $|4,0,0\rangle_E$ are still split, and the combination peaks $|3,1,0\rangle_{A_1}$, $|3,1,0\rangle_E$, $|2,1,1\rangle_{A_1}$ and $|2,1,1\rangle_E$ have considerable intensity. The local mode combination peaks of $\Delta v_{CD} = 5$ spectra of CD_3Z molecules are also quite intense. It was mentioned in chapter 4

that Mortensen et al.[87] have investigated the intensities of the local mode peaks in the spectra of CH_2Cl_2 and CD_2Cl_2. They have shown that the dominant source of intensity for the local mode combination states is the vibrational mixing of these states with the pure local mode states. As in the case of CD_2Cl_2 and CH_2Cl_2, the extent of vibrational mixing between the local mode combination and pure local mode states in CD_3Z and CH_3Z is proportional to the interoscillator coupling parameter $\omega\gamma'$. The higher value of $\omega\gamma'$ for CD_3Z molecules provides greater vibrational mixing between the pure local mode and local mode combination states. Thus the relatively higher intensity of local mode combination peaks in the spectra of CD_3Z molecules at $\Delta v_{CD} = 3 - 5$ is also accounted for by the higher value of $\omega\gamma'$ for these molecules.

Table 6.1.

Observed and Calculated Peak Positions (cm^{-1}) for CD_3I and CD_3CN.

	CD_3I		CD_3CN		
Δv_{CD}	Observed	Calculated	Observed	Calculated	Assignment
1	2140[a]	2139	2116[b]	2115	$\|100\rangle_{A_1}$
	2289[a]	2288	2263[b]	2263	$\|100\rangle_{E}$
	4263	4258	4214	4209	$\|110\rangle_{A_1}$
2	4388	4387	4335	4334	$\|200\rangle_{E}$
	4528	4543	4463	4489	$\|200\rangle_{A_1}$
	4558	4563	4513	4511	$\|110\rangle_{E}$
	6371	6354	6243	6277	$\|210\rangle_{A_1}$
	6467	6458	6362	6375	$\|300\rangle_{E}$
	5688	6594	6516	6509	$\|300\rangle_{A_1}$
3	6627	6627	6560	6546	$\|210\rangle_{E}$
	6752	6784	6656	6701	$\|210\rangle_{E}$
	-	6810	-	6729	$\|210\rangle_{A_2}$
	6829	6829	6735	6750	$\|111\rangle_{A_1}$
	8677	8424	8348	8314	$\|400\rangle_{A_1}$
	8536	8500	8391	8381	$\|400\rangle_{E}$
	8636	8616	8484	8498	$\|310\rangle_{A_1}$
	8689	8667	8597	8555	$\|310\rangle_{E}$
4	8756	8800	8677	8684	$\|310\rangle_{E}$

Table 6.1...cont'd...

Δv_{CD}	CD_3I Observed	CD_3I Calculated	CD_3CN Observed	CD_3CN Calculated	Assignment
	-	8837	-	8722	$\|310\rangle_{A_2}$
	8850	8864	8740	8755	$\|211\rangle_{A_1}$
	-	8995	-	8881	$\|220\rangle_{A_1}$
	-	9004	-	8889	$\|220\rangle_{E}$
	9057	9064	8926	8955	$\|211\rangle_{E}$
	10582	10630[c]	10419	10460[c]	$\|500\rangle$
5	10680	-	10569	-	$\|410\rangle$
	10821	-	10758	-	$\|320\rangle$

[a]Reference 101.

[b]Reference 112.

[c]Calculated from the Morse oscillator energy equation (see Eq. 4.1 in chapter 4).

Table 6.2.

Tentative Assignments for the Local Mode-Normal Mode Combination Peaks of CD_3I.

Δv_{CD}	Peak Position(cm^{-1})	Assignment[a,b]
2	4334	$\|100\rangle_E + 2\delta_E$
	6312	$\|200\rangle_E + \delta_A + \delta_E$
3	6421	$\|200\rangle_E + 2\delta_E$
	6548	$\|200\rangle_{A_1} + 2\delta_E$
	8319	$\|300\rangle_E + 2\delta_A$
	8399	$\|300\rangle_{A_1} + 2\delta_A$
4	8441	$\|300\rangle_E + 2\delta_E$
	8583	$\|300\rangle_{A_1} + 2\delta_E$
5	10438	$\|400\rangle_{A_1} + 2\delta_E$

[a] δ_A = 938 cm^{-1} (from Ref. 111), δ_E = 1040 cm^{-1} (from Ref. 101).

[b] For the frequencies of the pure local mode peaks, $|v,0,0\rangle$, see Table 6.1.

Table 6.3.

Tentative Assignments for the Local Mode-Normal Mode Combination Peaks of CD_3CN.

Δv_{CD}	Peak Position(cm^{-1})	Assignment[a,b]
	4196	comb.
	4253	comb.
2	4295	$\|100\rangle_{A_1} + 2\delta_A$
	4381	$\|100\rangle_E + \delta_A + \delta_E$
	4438	$\|100\rangle_E + 2\delta_A$
	6199	comb.
	6322	$\|200\rangle_E + 2\delta_E$
3	6397	comb.
	6459	$\|200\rangle_E + \delta_A + \delta_E$
	6484	$\|200\rangle_{A_1} + 2\delta_E$
	6616	$\|200\rangle_{A_1} + 2\delta_A$
4	8447	$\|300\rangle_E + 2\delta_E$
	8516	$\|300\rangle_{A_1} + 2\delta_E$
5	10321	$\|400\rangle_{A_1} + 2\delta_E$

[a] δ_A = 1103 cm^{-1}, δ_E = 1039 cm^{-1} (from Ref. 112).

[b] For the frequencies of the pure local mode peaks, $|v,0,0\rangle$, see Table 6.1.

Figure 6.1.

Liquid phase overtone spectra of CD_3CN and CD_3I in the region of Δv_{CD} = 2. Spectra were measured at room temperature with a path length of 0.1 cm. Absorbance of CD_3I has been offset by 0.3 absorbance units.

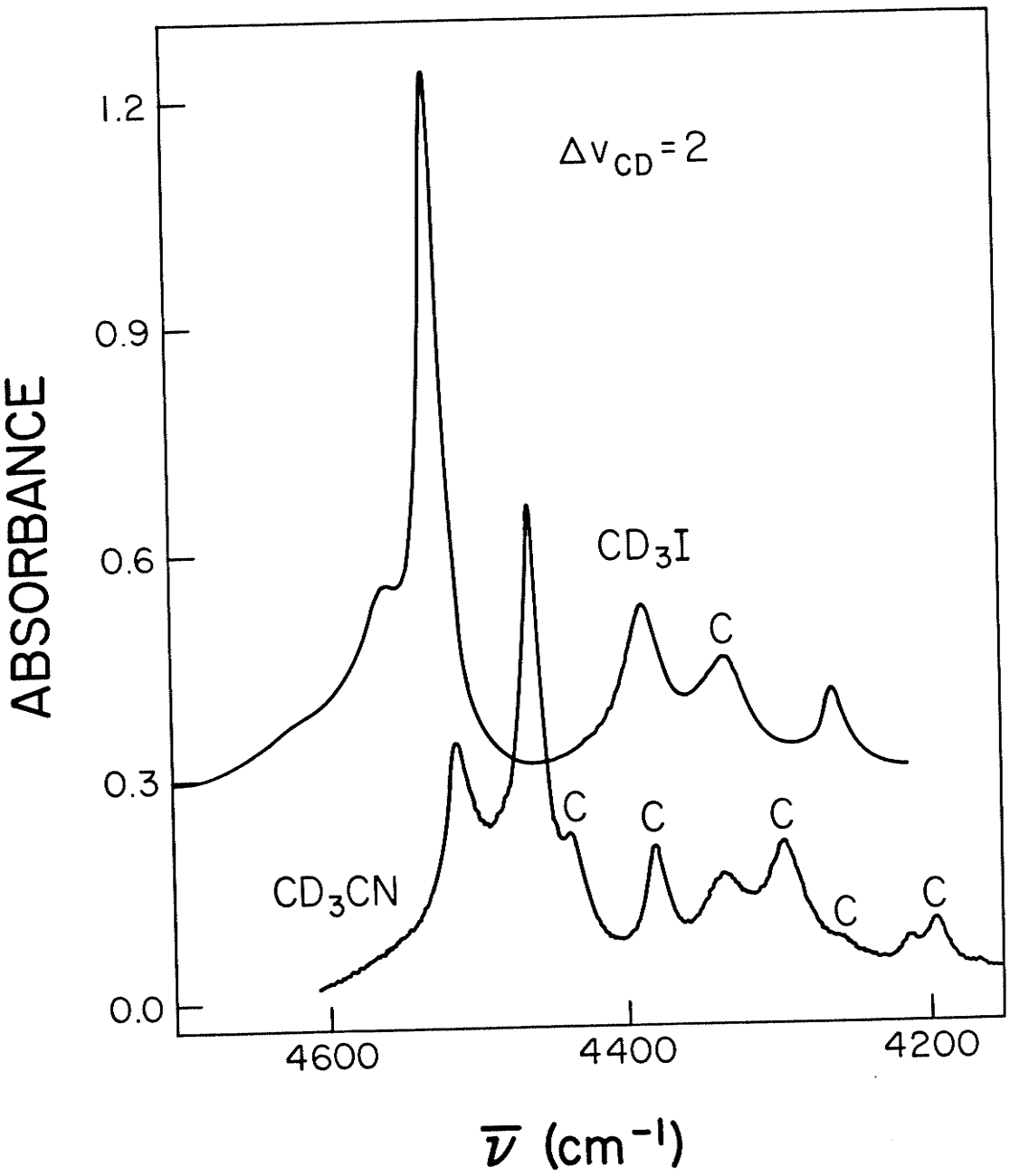
ABSORBANCE
1.2
0.9
0.6
0.3
0.0
$\Delta v_{CD} = 2$
CD_3I
CD_3CN
C
C
C
C
C
C
4600
4400
4200
$\bar{\nu}$ (cm^{-1})

Figure 6.2.

Liquid phase overtone spectra of CD_3CN and CD_3I in the region of Δv_{CD} = 3. Spectra were measured at room temperature with a path length of 3.0 cm. The right hand ordinate scale represents the absorbance of CD_3I.

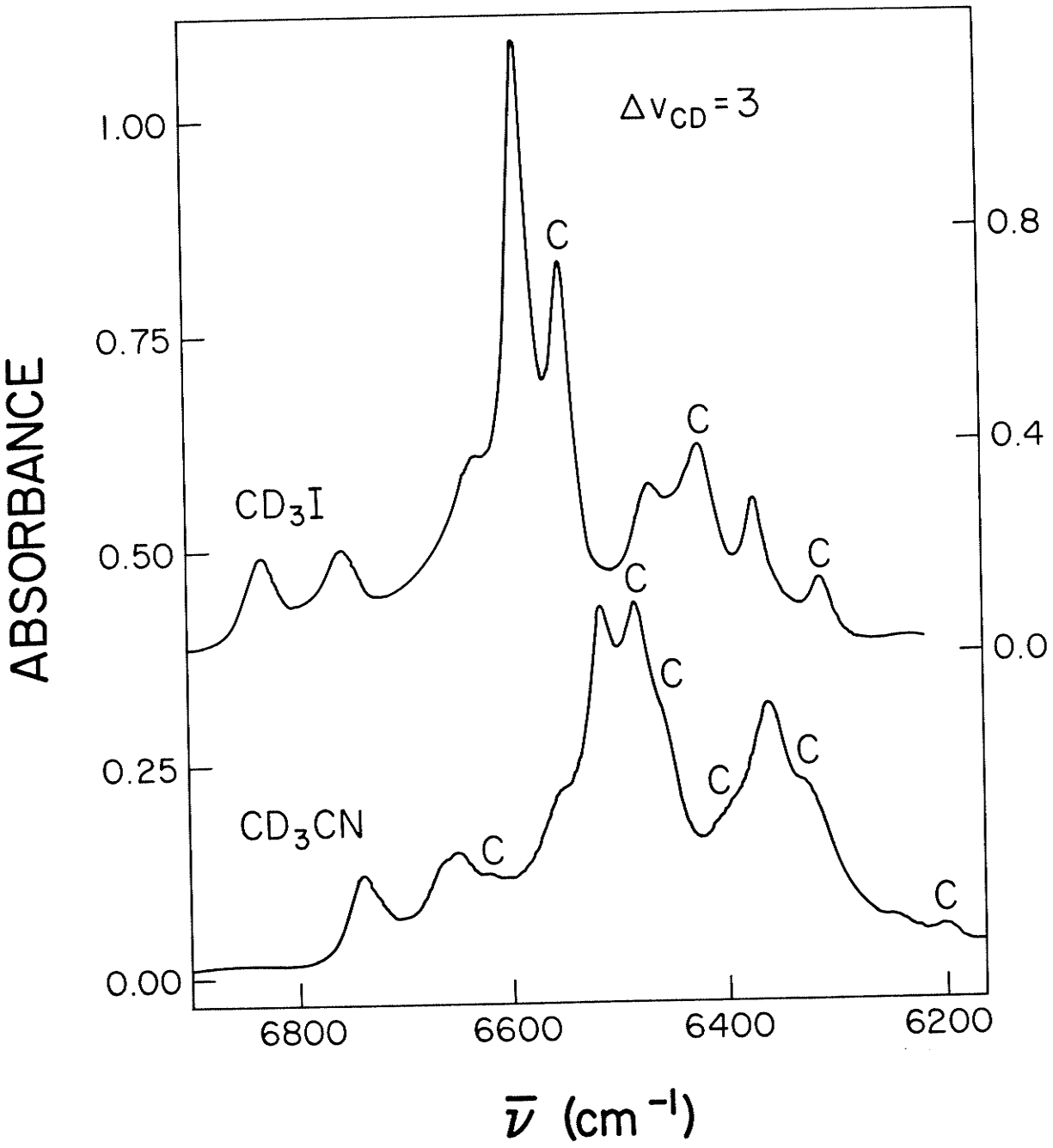
ABSORBANCE
1.00
0.75
0.50
0.25
0.00
0.8
0.4
0.0
$\Delta v_{CD} = 3$
CD_3I
CD_3CN
C
6800
6600
6400
6200
$\bar{\nu}$ (cm^{-1})

Figure 6.3.

Liquid phase overtone spectra of CD_3CN and CD_3I in the region of Δv_{CD} = 4. Spectra were measured at room temperature with a path length of 3.0 cm. The right hand ordinate scale represents the absorbance of CD_3I.

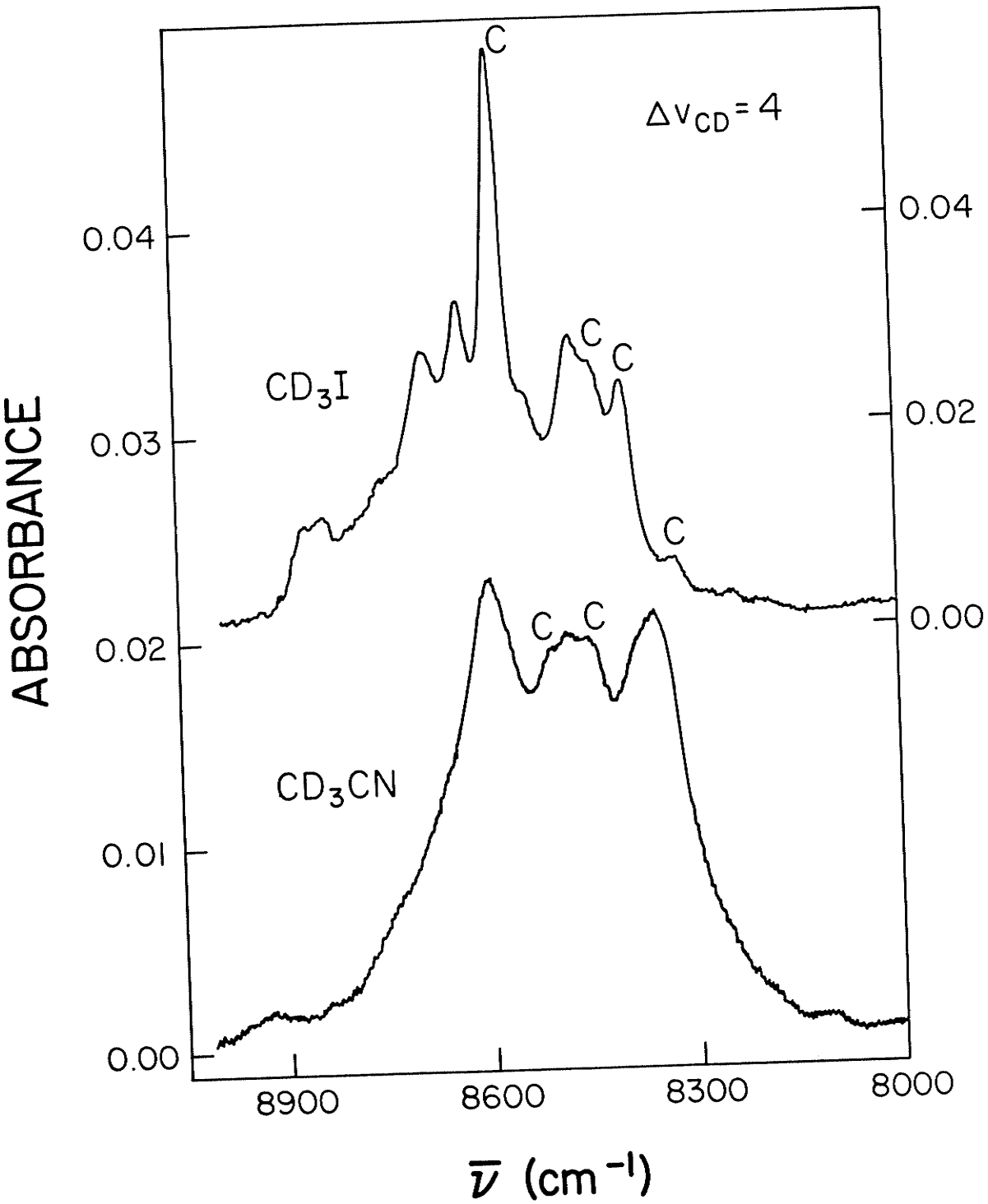
ABSORBANCE
0.04
0.03
0.02
0.01
0.00
0.04
0.02
0.00
$\Delta v_{CD} = 4$
CD_3I
CD_3CN
C
C
C
C
C
8900
8600
8300
8000
$\bar{\nu}$ (cm^{-1})

Figure 6.4.

Liquid phase overtone spectra of CD_3CN and CD_3I in the region of Δv_{CD} = 5. These spectra are the sum of four base line corrected scans. Individual scans were measured at room temperature with a path length of 3.0 cm. Absorbance of CD_3I has been offset by 0.001 absorbance units.

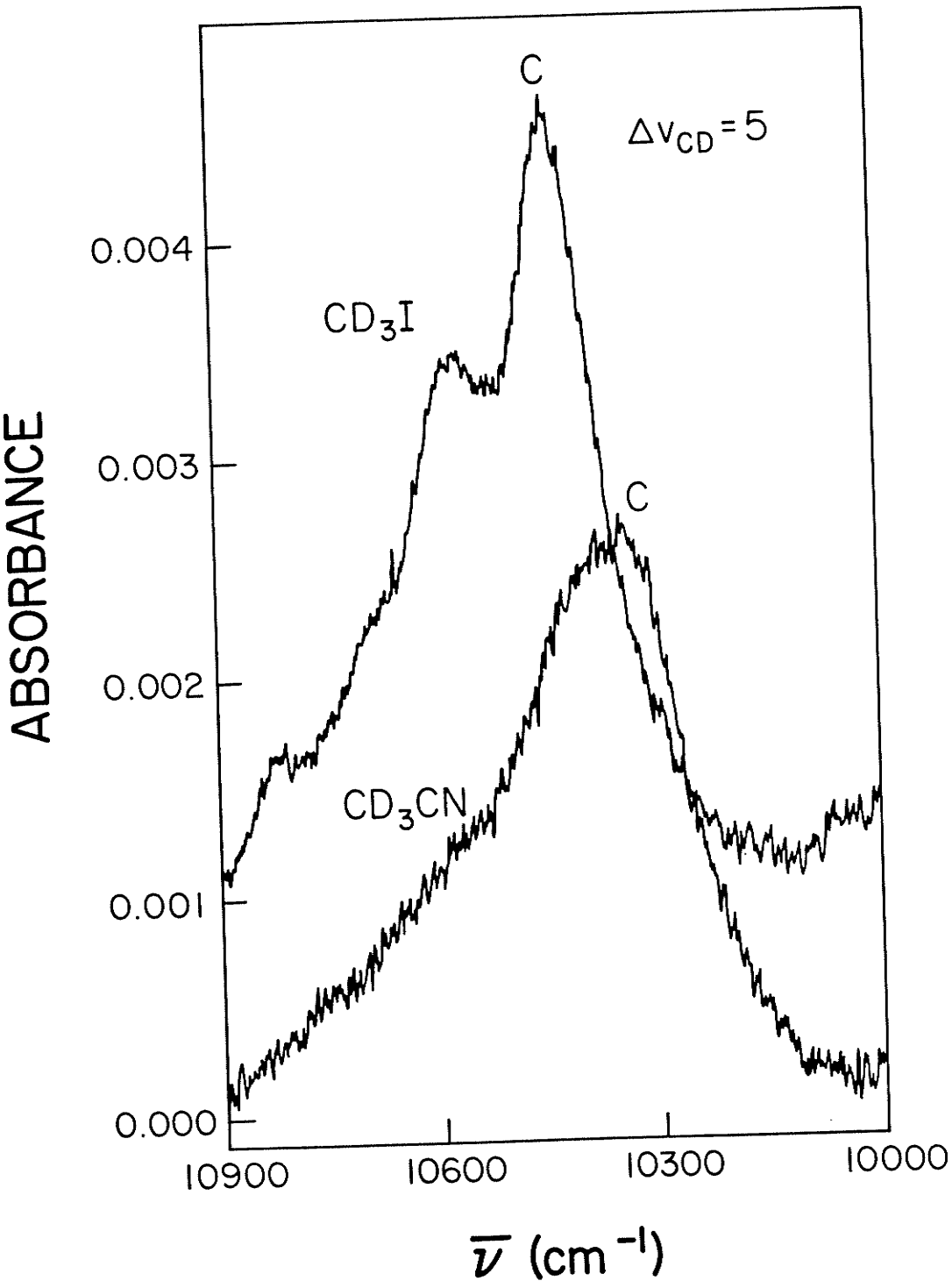
C
$\Delta\nu_{CD}=5$
0.004
CD_3I
0.003
C
ABSORBANCE
0.002
CD_3CN
0.001
0.000
10900
10600
10300
10000
$\bar{\nu}$ (cm^{-1})

CHAPTER 7

NONEQUIVALENT CH BONDS IN 2-CHLORO-2-METHYLPROPANE AND CHLOROTRIMETHYLSILANE

In this chapter, the CH stretching spectra of $(CH_3)_3CCl$ and $(CH_3)_3SiCl$ will be reported both in the liquid (Δv_{CH} = 1-6) and the gas phase (Δv_{CH} = 1-4). Bond length results from SCF molecular orbital calculations (4-31G and STO-3G) will be presented. The calculations predict two types of methyl CH bonds. It will be shown that this prediction is in agreement with the observed features of the spectra. The spectra will be analyzed by considering the stretching vibration of the unique methyl CH bond (trans to the C-Cl (Si-Cl) bond) to be uncoupled from the other local methyl vibrations.

i) Introduction

High energy XH stretching overtone spectra have been shown to provide information about the structure, conformation[9,27-43] and relative bond lengths[27-31] of polyatomic molecules. Such information can also be obtained from the fundamental spectrum by the selective deuteration method of McKean and his collaborators[93,94]. In this method all of the hydrogens of a polyatomic molecule but one are replaced by deuterium. The lone CH stretch is decoupled from the CD stretching vibrations as well as from the first overtone of bending modes. In a sense one can think of CH oscillators in such selectively deuterated molecules as chemically produced local modes.

McKean et al.[115] have shown through measurements of the fundamental gas phase CH stretching spectrum of the deuterated species $(CD_3)_2(CD_2H)CCl$ that there are two kinds of structurally nonequivalent CH bonds in $(CH_3)_3CCl$. The expected[115] structure of $(CH_3)_3CCl/(CH_3)_3SiCl$ is shown in Figure (7.1) and the nonequivalent bonds are labelled by an "a" and "s" as was done by McKean et al.[115] These authors predicted the CH_s bonds of $(CH_3)_3CCl$ to be 0.003 Å longer than the CH_a bonds through their correlation of the fundamental frequencies with the bond lengths. Since CH_s bonds are longer than the CH_a bonds, the local symmetry of the methyl groups is C_s rather than C_{3v} and the same could be expected for the methyl groups of analogous compounds, e.g., $(CH_3)_3SiCl$, $(CH_3)_3CCN$ etc.

In this chapter the CH stretching fundamental and overtone spectra of $(CH_3)_3CCl$ and $(CH_3)_3SiCl$ in the liquid (Δv_{CH} = 1-6) and the gas phase (Δv_{CH} = 1-4) will be reported. These spectra will be analyzed in terms of the local mode model with the assumption of

independent methyl groups with local C_s symmetry. It will also be assumed that the stretching motion of the unique CH_s bonds is completely decoupled from the stretching motion(s) of the CH_a bonds in $(CH_3)_3CCl$ and $(CH_3)_3SiCl$. Under these assumptions the unique CH_s bonds of the methyl groups of $(CH_3)_3)CCl$ and $(CH_3)_3SiCl$ will be represented by Morse oscillator states $|v\rangle_s$ and the CH_a bonds by symmetrized states of the type $|v,0\rangle_{\pm a}$, $|v-1,1\rangle_{\pm a}$ etc. (see chapter 1).

Overtone frequencies correlate remarkably well with XH bond lengths[27-32]. The bond length difference between the nonequivalent CH bonds of $(CH_3)_3CCl$ and $(CH_3)_3SiCl$ will be obtained from this correlation and the results will be compared with those obtained by the deuteration studies of Mckean et al.[115] and by ab initio gradient calculations at the 4-31G[91] and STO-3G[91] levels.

ii) Results

The CH stretching fundamental and the overtone spectra of $(CH_3)_3CCl$ and $(CH_3)_3SiCl$ in the liquid phase are shown in Figures (7.2) - (7.7). The gas phase spectra of these molecules in the spectral regions of Δv_{CH} = 1-4 are presented in Figures (7.8) - (7.11). Although these spectra could be assigned through the application of the local mode Hamiltonian of three coupled Morse oscillators to the symmetrized states[116-118] $|v,0,0\rangle^{*}_{\pm}$, $|0,0,v\rangle^{+}$, $|0,v-1,1\rangle^{++}_{\pm}$ etc. and diagonalization of the resultant matrices, we simplify the analysis by assuming that the stretching vibration of CH_s oscillators is decoupled from the stretching vibration(s) of the CH_a oscillators. The symmetrized states for the CH_a bonds of $(CH_3)_3CCl$ and $(CH_3)_3SiCl$ under this assumption are[70] $|v,0\rangle_{\pm a}$, $|v-1,0\rangle_{\pm a}$ etc. and

---

*Explicitly these symmetrized pure local mode states are of the form $|v,0,0\rangle_{\pm} = \frac{1}{\sqrt{2}} (|v,0,0\rangle \pm |0,v,0\rangle)$. The components of these states have all of the vibrational quanta deposited into one of the two "a" type methyl CH bonds (see Figure 7.1) of $(CH_3)_3CCl$ or $(CH_3)_3SiCl$.

$^{+}|0,0,v\rangle$ are also the pure local mode states. In these states all of the vibrational quanta are deposited into the "s" type methyl CH bond of $(CH_3)_3CCl$ or $(CH_3)_3SiCl$.

$^{++}|0,v-1,1\rangle_{\pm}$ are the symmetrized local mode combination states. In these states the vibrational quanta are distributed over both "a" and "s" type CH bonds of $(CH_3)_3CCl$ and $(CH_3)_3SiCl$. The explicit expression for these states is $|0,v-1,1\rangle_{\pm} = \frac{1}{\sqrt{2}} (|0,v-1,1\rangle \pm |0,1,v-1\rangle)$. Similar expressions for all other possible local mode combination states can be written[117].

a single Morse oscillator state $|v\rangle_s$ represents the stretching vibration of the unique CH_s bond at different vibrational manifolds. Now, the spectra of CH_s bonds can simply be calculated from the vibrational energy expression of a single Morse oscillator (see Eq. (4.1) in chapter 4). The energies of the peaks which correspond to the CH_a bonds at each overtone manifold, Δv_{CH}, can be obtained through the application of the local mode theory of a XH_2 system which was discussed in detail in chapter 1.

To obtain the numerical values of the energies of the transitions to the states $|v\rangle_s$, $|v,0\rangle_{\pm a}$, $|v-1,1\rangle_{\pm a}$ etc., what is required are the values of:

1. the anharmonicity constant ωx and the harmonic frequency ω for both the CH_a and CH_s bonds.
2. the effective coupling parameter[70] $\gamma'\omega$ ($\gamma'\omega = (\gamma - \phi)\omega$), which appear in the intramanifold coupling matrices of the Hamiltonian of a XH_2 system, for CH_a bonds only.

The parameters ω and ωx of CH_a and CH_s bonds are evaluated by fitting the observed energies of the $|v,0\rangle_{\pm a}$ and $|v\rangle_s$ peaks with a least mean squares procedure to Eq. (4.1) of chapter 4 and are given in Table 7.1. To show the quality of the fitting, the plots of Eq. (7.1) of chapter 4 for the liquid phase spectra of $(CH_3)_3CCl$ are displayed in Figure 7.12.

In Table 7.1 the values of the coupling parameter $\gamma'\omega$ for both $(CH_3)_3CCl$ and $(CH_3)_3SiCl$ are also listed. The $\gamma'\omega$ is obtained[70] from the observed splitting between the $|1,0\rangle_{+a}$ and $|1,0\rangle_{-a}$ peaks ($2\gamma'\omega = E(|1,0\rangle_{-a}) - E(|1,0\rangle_{+a})$). Unfortunately, the $|1,0\rangle_{+a}$ (and also $|1\rangle_s$) peak for $(CH_3)_3SiCl$ is not observed in the gas phase spectrum probably

due to its low intensity. It is known that the intensity of the CH stretching vibrations markedly changes on passing from the gas to the solutions in CCl_4, e.g., the intensity of the CH stretching vibration of chloroform is twenty times higher in CCl_4 solution than in the gas phase[119]. In the $\Delta v_{CH} = 1$ spectrum of a 5% solution of $(CH_3)_3SiCl$ in CCl_4, a weak broad band is seen (see Figure 7.2) at about 2930 cm^{-1}. The energy position of this band is approximately the same as is expected for the $|1,0\rangle_{+a}$ and $|1\rangle_s$ peaks of $(CH_3)_3SiCl$ on the basis of the Brige-Sponer plots (plots of Eq. (4.1)). However, due to the uncertainty involved in locating the position of the $|1,0\rangle_{+a}$ peak, this peak in combination with the $|1,0\rangle_{-a}$ peak, was not used to calculate the coupling parameter $\gamma'\omega$ for the CH_a bonds of $(CH_3)_3SiCl$. The $\gamma'\omega$ for $(CH_3)_3SiCl$ listed in Table 7.1 was evaluated by fitting the observed energy of the $|1,0\rangle_{-a}$ peak to the energy expected for this peak ($E(|1,0\rangle_{-a}) = (1-2x+\gamma')\omega$) on the basis of the local mode theory of a XH_2 system.

Substitution of the local mode parameters of the CH_a bonds from Table 7.1 into the intramanifold coupling matrices of the Hamiltonian of a XH_2 system followed by diagonalization of these matrices gives the calculated energies of the peaks corresponding to the CH_a bonds. As has already been commented, the spectra of the CH_s bonds of $(CH_3)_3CCl$ and $(CH_3)_3SiCl$ can be calculated straigthforwardly from the vibrational energy expression of a single Morse oscillator. The calculated and the observed peak positions along with the peak assignments are given in Tables 7.2 and 7.3. The experimental peak positions were obtained from the deconvolution of the observed spectra with a computer program NIRCAP (see chapter 2).

The only bands left for assignment are those which are not listed in Tables 7.2 and 7.3. All these bands are classified as "combinations". The tentative assignments and energy positions of all such peaks observed in the spectra of $(CH_3)_3CCl$ and $(CH_3)_3SiCl$ are given in Table 7.4. The weak combination peaks observed in the region of Δv_{CH} = 2-6 are of two types. The first type of peak involves v-1 quanta of a pure CH stretching mode and two quanta of symmetric or antisymmetric bending mode of a methyl group, at each overtone Δv_{CH}. The second type of peak arises when the vibrational quanta are distributed over at least two of the three methyl CH bonds of $(CH_3)_3CCl$ and $(CH_3)_3SiCl$. Such peaks are denoted as $|v_{1a},v_{2a},v_{3s}>$ in Table 7.4, where $v_{1a} + v_{2a} + v_{3s} = \Delta v_{CH}$ and v_{1a}, v_{2a} and v_{3s} represent the vibrational quanta in the CH bond of an "a" or "s" type.

McKean has established a frequency-bond length correlation[94] by observing the fundamental IR spectrum of variety of molecules where all hydrogens but one have been replaced by deuterium. According to this correlation the CH bonds which differ in length by 0.001 Å have an energy separation of 10 cm^{-1} in the fundamental spectrum. A similar correlation[29] has been observed in the CH stretching overtone spectra. It has been shown that at Δv_{CH} = 6 a frequency shift of 69 cm^{-1} corresponds to a bond length difference of 0.001 A°[27,29]. The gas phase Δv_{CH} = 4 spectra of $(CH_3)_3CCl$ and $(CH_3)_3SiCl$ consist of two well resolved peaks separated by 80 and 138 cm^{-1}, respectively. The correlation of overtone frequencies with bond lengths translates these energy separations to the bond length difference of 0.0017 and 0.003 A°. These relative bond lengths are listed in Table 7.5. For comparison, the relative bond lengths predicted by McKean et al.[115]

and ab initio gradient calculations are also given in Table 7.5. The data of Table 7.5 show that the relative bond lengths obtained for the nonequivalent bonds of $(CH_3)_3CCl$ from the overtone spectral study are in perfect agreement with those obtained by McKean et al. However, overtone spectral studies of this type are more convenient in the sense that deuteration of $(CH_3)_3CCl$ was not required for obtaining the relative bond lengths of its nonequivalent bonds. The data of Table 7.5 show that the overall agreement between the results of overtone spectral study and ab initio gradient calculations is also satisfactory.

Generally the areas of the spectral peaks observed at high overtones are proportional to the number of CH bonds of a particular type[27-29]. In some cases, it has been shown that relative peak intensities do not correspond to the number of XH oscillators of a given type. For example, in the overtone spectra of acetone and acetaldehyde, the more numerous out-of-plane methyl CH bonds give rise to less intense peaks[117,118]. The molecules $(CH_3)_3CCl$ and $(CH_3)_3SiCl$ have two types of CH bonds (see Figure 7.1) in a ratio of 2:1. When $\Delta v_{CH} = 4$ gas phase spectra (Figure 7.11) of $(CH_3)_3CCl$ and $(CH_3)_3SiCl$ were decomposed into the parent Lorentzian peaks, the areas of the high and low energy peaks were found exactly in a ratio of 2:1. As an example the decomposition of $\Delta v_{CH} = 4$ gas phase spectrum of $(CH_3)_3SiCl$ is illustrated in Figure 7.13.

iii) Discussion

a) Trans Effect, Harmonic Frequencies and Anharmonicities

In their study[115] of the fundamental CH stretching spectra of $(CD_3)_2(CHD_2)CX$ (X = Cl, F, I) molecules McKean et al. observed two bands for each molecule. The low and high frequency bands were assigned to the CH_s and CH_a bonds (see Figure 7.1) of t-butyl halides, respectively. McKean et al. observed that the "isolated" frequency of a CH_s bond in the molecules $(CD_3)_2(CD_2H)CX$ increases as X is replaced by a less electronegative halogen (more electron density at the carbon atom attached to the halogen). However, the isolated frequency of a CH_a bond was found to be almost invarient as X was changed from F to I. These observations led McKean et al.[115] to suggest that an effect analogous to the "trans lone pair effect"[120] is in operation in $(CH_3)_3CX$ compounds. Simplistically, the trans lone pair effect is the lengthening of a CH bond trans to lone pair of oxygen, nitrogen, sulphur etc.[41,42,120] According to Hamlow et al.[121] the lengthening of a CH bond trans to lone pair electrons occurs via interaction of the lone pair electron density with the antibonding orbital of the CH bond. The elegant infrared studies on nitrogen and oxygen containing compounds by McKean[94] and the overtone spectral studies by Fang et al.[41-43] on similar compounds support the phenomenon of a trans lone pair effect. J. O. Williams et al.[12] have also explained the influence of lone pair orbital interaction on molecular structure through ab initio studies on molecules containing-OH, $-OCH_3$, -NH, and $-NCH_3$ groups.

The harmonic frequencies of CH_a and CH_s bonds of $(CH_3)_3CCl$ and $(CH_3)_3SiCl$ are given in Table 7.1. The data of Table 7.1 show that,

within the experimental uncertainty, the harmonic frequencies of CH_s bonds of $(CH_3)_3CCl$ and $(CH_3)_3SiCl$ are almost of equal magnitude. The data of Table 7.1 also shows that the harmonic frequency of the CH_a bonds of $(CH_3)_3CCl$ is higher than the harmonic frequency of CH_a bonds of $(CH_3)_3SiCl$ in both liquid and the gas phases. Two conclusions can be drawn from these observations. Firstly, the relative constancy of the harmonic frequency of CH_s bonds reveals that the trans lone pair type effect of the C-Cl and Si-Cl bonds on the CH_s bonds of $(CH_3)_3CCl$ and $(CH_3)_3SiCl$ is almost of equal magnitude. Secondly, the higher frequency of the CH_a bonds of $(CH_3)_3CCl$ than the frequency of the similar bonds of $(CH_3)_3SiCl$ suggests that the chlorine atom inductively affects the strength of the CH_a bonds. Since, the Si-Cl and Si-C bond lengths* (2.0996 Å, 1.8590 Å) in $(CH_3)_3SiCl$ are longer than the bond lengths* of the corresponding bonds in $(CH_3)_3CCl$ (C-Cl = 1.8427 Å, C-C = 1.5471 Å), the bond strengthening effect of chlorine on CH_a bonds is more pronounced in $(CH_3)_3CCl$. This results in a higher value of the harmonic frequency of CH_a bonds of $(CH_3)_3CCl$.

From the harmonic frequencies of the nonequivalent CH bonds, their fundamental frequencies ($\omega-2\omega x$) can be obtained. The values (gas phase) of these frequencies for $(CH_3)_3CCl$($(CH_3)_3SiCl$) are 2969 cm^{-1} and 2940 cm^{-1} (2955 cm^{-1}, 2940 cm^{-1}). The values for $(CH_3)_3CCl$ are in excellent agreement with the results of McKean et al.[115] (2968.2 cm^{-1}, 2936.0 cm^{-1}).

---

*These bond lengths are from geometry optimization of $(CH_3)_3SiCl$ and $(CH_3)_3CCl$ at the STO-3G level.

The anharmonicity constants listed in Table 7.1 are not as sensitive to the bond strength/length of CH bonds as the harmonic frequencies. The data of Table 7.1 show that the anharmonicities of the nonequivalent CH bonds of $(CH_3)_3CCl$ or $(CH_3)_3SiCl$ in a given phase (liquid or gas) are almost equal if the experimental error is taken into consideration. Generally, the stronger bonds have low anharmonicity[29] and vice versa. This generalization, however, does not seem to work for $(CH_3)_3CCl$ and $(CH_3)_3SiCl$ probably due to the very small dissimilarity among the nonequivalent bonds of these molecules.

b) Are Nonequivalent Bonds Totally Uncoupled?

In the "Results" section of this chapter, the fundamental and the overtone spectra of $(CH_3)_3CCl$ and $(CH_3)_3SiCl$ are analyzed in terms of the local mode model with the assumption that the stretching motion of the unique CH_s bond of each methyl group is decoupled from the stretching motion(s) of the rest of the two CH_a bonds. The success of this approximation is clearly evident from the excellent agreement of the calculated spectra with the observed spectra (see Tables 7.2 and 7.3). In reality, the CH_a and CH_s bonds are coupled to some extent at low overtones and that is why the combination peaks of the type $|v_{1a},v_{2a},v_{3s}>$ are observed in the $\Delta v_{CH} = 2$ and 3 regions of the gas and liquid phase spectra (see Figures 7.3, 7.4, 7.9, 7.10, and Table 7.4).

If the anharmonicities of the CH_a and CH_s bonds are assumed equal (this is in fact very nearly the case, see Table 7.1), then the energy separation between these bonds at a given overtone Δv_{CH} is given by the following equation

$$\Delta E_{CH_a-CH_s} = v\Delta\omega \qquad (7.1)$$

Eq. (7.1) is simply obtained from Eq. (4.1) of chapter 4. $\Delta\omega$ in Eq. (7.1) denotes the difference between the harmonic frequencies of the nonequivalent bonds. According to Eq. (7.1) the energy separation between the nonequivalent bonds of $(CH_3)_3CCl$ and $(CH_3)_3SiCl$ increases linearly with v. Thus the effective coupling between CH_a and CH_s bonds decreases successively as v increases. At $\Delta v_{CH} > 3$, in the spectra of $(CH_3)_3CCl$ and $(CH_3)_3SiCl$, the combination peaks of the type

$|v_{1a},v_{2a},v_{3s}>$ are not observed at all and their disappearance provides support for the assumption of uncoupled CH_a and CH_s bonds. The fact that at high overtones the nonequivalent bonds are essentially uncoupled makes overtone spectroscopy a versatile technique for resolving structurally and conformationally nonequivalent bonds of polyatomic molecules.

In summary the local mode model accounts for all the structural details of the fundamental and overtone spectra of $(CH_3)_3CCl$ and $(CH_3)_3SiCl$ and the data of Tables 7.2 and 7.3 clearly demonstrate the success of the simple scheme which is used to analyze the spectra. It is anticipated that this simple scheme would be useful in the understanding of the spectra of other polyatomic molecules containing methyl groups of C_s symmetry.

Table 7.1.

Local Mode Parameters (cm^{-1}) for $(CH_3)_3CCl$ and $(CH_3)_3SiCl$.

Molecule	Phase	Oscillator type	ω	ωx	$\omega y'$
$(CH_3)_3CCl$	Liquid	CH_a	3080.6±4.7	61.6±1.2	14.5
		CH_s	3050.4±3.8	61.3±0.9	-
	Gas	CH_a	3095.5±6.3	63.3±2.2	12.0
		CH_s	3067.7±6.4	63.9±2.2	-
$(CH_3)_3SiCl$	Liquid[a]	CH_a	3070.7±1.4	61.5±0.3	16.4
		CH_s	3055.0±2.0	62.4±0.5	-
	Gas	CH_a	3074.1±1.0	59.7±0.3	15.5
		CH_s	3061.7±6.6	61.0±2.0	-

[a]The $\Delta v_{CH} = 5$ local mode peaks of $(CH_3)_3SiCl$ were not fit to Morse oscillator equation in obtaining ω and ωx because a combination peak at 13456 cm^{-1} (see Figure 7.6) perturbes the energy positions of these peaks.

Table 7.2.

Observed and Calculated Frequencies (cm^{-1}) for 2-Chloro-2-methylpropane.

Δv_{CH}	Liquid		Gas		
	Observed	Calculated	Observed	Calculated	Assignment
	2927	2928	2937	2940	$\|1\rangle_s$
1	2946	2943	2957	2957	$\|1,0\rangle_{+a}$
	2975	2972	2981	2981	$\|1,0\rangle_{-a}$
	5751	5733	5763	5752	$\|2\rangle_s$
2[a]	5799	5785	5817	5807	$\|2,0\rangle_{+a}$
	5799	5792	5817	5811	$\|2,0\rangle_{-a}$
	5937	5921	5953	5942	$\|1,1\rangle_a$
	8406	8414	8428	8435	$\|3\rangle_s$
3	8482	8500	8510	8525	$\|3,0\rangle_{\pm a}$
	8737	8723	8758	8758	$\|2,1\rangle_{+a}$
	8789	8780	8806	8806	$\|2,1\rangle_{-a}$
	10965	10976	10992	10992	$\|4\rangle_s$
4	11080	11088	11129	11114	$\|4,0\rangle_{\pm a}$
	11457	11444(+)	-	11485(+)	$\|3,1\rangle_{\pm a}$
		11462(-)	-	11497(-)	
	-	11601	-	11635	$\|2,2\rangle_a$

Table 7.2...cont'd...

Δv_{CH}	Liquid		Gas		
	Observed	Calculated	Observed	Calculated	Assignment
	13409	13413	-	13421	$\|5\rangle_s$
5	13556	13553	-	13577	$\|5,0\rangle_{\pm a}$
	14033	14042(+)	-	14081(+)	$\|4,1\rangle_{\pm a}$
		14044(-)		14082(-)	
6	15744	15728	-	15722	$\|6\rangle_s$
	15923	15894	-	15913	$\|6,0\rangle_{\pm a}$

[a]Some peaks at Δv_{CH} = 2(gas) spectrum show unresolved rotational fine structure. For these peaks frequencies of the band centres are quoted.

Table 7.3.

Observed and Calculated Frequencies (cm^{-1}) for Chlorotrimethylsilane.

Δv_{CH}	Liquid		Gas		
	Observed	Calculated	Observed	Calculated	Assignment
	2930[a]	2930	-	2940	$\|1\rangle_s$
1	2930[a]	2931	-	2939	$\|1,0\rangle_{+a}$
	2964	2964	2970	2970	$\|1,0\rangle_{-a}$
	5735	5736	5755	5757	$\|2\rangle_s$
2	5774	5764	5790	5782	$\|2,0\rangle_{+a}$
	5774	5772	5790	5790	$\|2,0\rangle_{-a}$
	5927	5903	5934	5917	$\|1,1\rangle_a$
	8420	8416	8460	8453	$\|3\rangle_s$
3	8471	8470(+)	8504	8502(+)	$\|3,0\rangle_{\pm a}$
		8471(-)		8503(-)	
	8709	8691	8740	8717	$\|2,1\rangle_{+a}$
	8754	8755	8780	8778	$\|2,1\rangle_{-a}$
	10966	10972	11022	11027	$\|4\rangle_s$
4	11049	11049	11102	11099	$\|4,0\rangle_{\pm a}$
	11400	11402(+)	-	11442(+)	$\|3,1\rangle_{\pm a}$
		11424(-)		11463(-)	
	-	11567	-	11600	$\|2,2\rangle_a$

Table 7.3...cont'd...

Δv_{CH}	Liquid		Gas		
	Observed	Calculated	Observed	Calculated	Assignment
	13378	13403	-	13478.5	$\|5\rangle_s$
	13524	13504	-	13576	$\|5,0\rangle_{\pm a}$
5	14004	13992(+)	-	14049(+)	$\|4,1\rangle_{\pm a}$
		13995(-)		14052(-)	
	14165	14207(+)	-	14258(+)	$\|3,2\rangle_{\pm a}$
		14302(-)		14340(-)	
6	15712	15709	-	15808	$\|6\rangle_s$
	15842	15836	-	15933	$\|6,0\rangle_{\pm a}$

[a]Approximate energy since this peak is quite broad (see Figure 7.2).

Table 7.4.

Energies (cm^{-1}) and Tentative Assignments for the Combination Peaks Observed in the Δv_{CH} = 1-6 Spectra of $(CH_3)_3CCl$ and $(CH_3)_3SiCl$.

	$(CH_3)_3CCl$		$(CH_3)SiCl$		
Δv_{CH}	Liquid	Gas	Liquid	Gas	Assignment[a,b]
	2865	-	2874	-	comb.
1	2887	-	-	2910	comb.
	2899	-	2901	2910	comb.
	2986	2993(P branch)	2969	2979(P branch)	comb.
	5587	5600	-	-	2865+2B(-)
	5650	5664	5405	5419	$\|1\rangle_s$+2B(±)
2	5688	5704	5453	5465	$\|1,0\rangle_{-a}$+2B(±)
	-	-	5607	5624	$\|1\rangle_s$+2B(-)
	5904	5916	5927	5947	$\|1,0,1\rangle$[c]
	5957	5970	-	-	$\|1,0\rangle_{-a}$+2986(2993)
	8141	8167	-	-	$\|2\rangle_s$($\|2,0\rangle_{\pm a}$)+2B(+)
3	8286	8305	8233	8254	
	8584	8604	-	-	$\|3,0\rangle_{\pm a}$+~100cm^{-1} mode
	8708	8726	8650	8660	$\|1,1,1\rangle$, $\|1,0,2\rangle$, $\|2,0,1\rangle$[c]

Table 7.4...cont'd...

Δv_{CH}	$(CH_3)_3CCl$ Liquid	$(CH_3)_3CCl$ Gas	$(CH_3)SiCl$ Liquid	$(CH_3)SiCl$ Gas	Assignment[a,b]
4	10747	-	-	-	$\|3\rangle_s(\|3,0\rangle_{\pm a})+2B(+)$
	10868	-	10880	-	
	11158	11181		-	$\|3,0\rangle_{\pm a}$+~100cm^{-1} mode
5	-	-	13456	-	$\|4\rangle_s$ +2B(-)
6	-	-	15967	-	$\|5\rangle_s$ +2B(-)

[a] B(-) and B(+) are sym. and antisym. bends of a CH_3 gp., B(-) = 1368 cm^{-1}, B(+) = 1238 cm^{-1} for $(CH_3)_3CCl$ and B(-) = 1333 cm^{-1}, B(+) = 1254 cm^{-1} for $(CH_3)_3SiCl$ (FTIR liq. phase values from the current study).

[b] When "B" appears with both "+" and "-" signs, the "+" and "-" signify $(CH_3)_3SiCl$ and $(CH_3)_3CCl$, respectively.

[c] These are the vib. states of the type $|v_{1a},v_{2a},v_{3s}\rangle$ (see text).

Table 7.5.

Bond Length Differences Δr(Å) Between the Nonequivalent Bonds of $(CH_3)_3CCl$ and $(CH_3)_3SiCl$ Obtained Through Different Techniques.

Method \ Molecule	$(CH_3)_3CCl$	$(CH_3)_3SiCl$
McKean *et al.*[a]	0.003	-
Local mode	0.003	0.0017
4-31G	0.005	-
STO-3G	0.0012	0.001

[a] From Ref. 115.

Figure 7.1.

Structure of $(CH_3)_3MCl$ (M=C,Si) molecules. The hydrogen atoms labelled by an "a" lie on opposite sides of a σ_v plane, while those labelled by "s" lie on this plane.

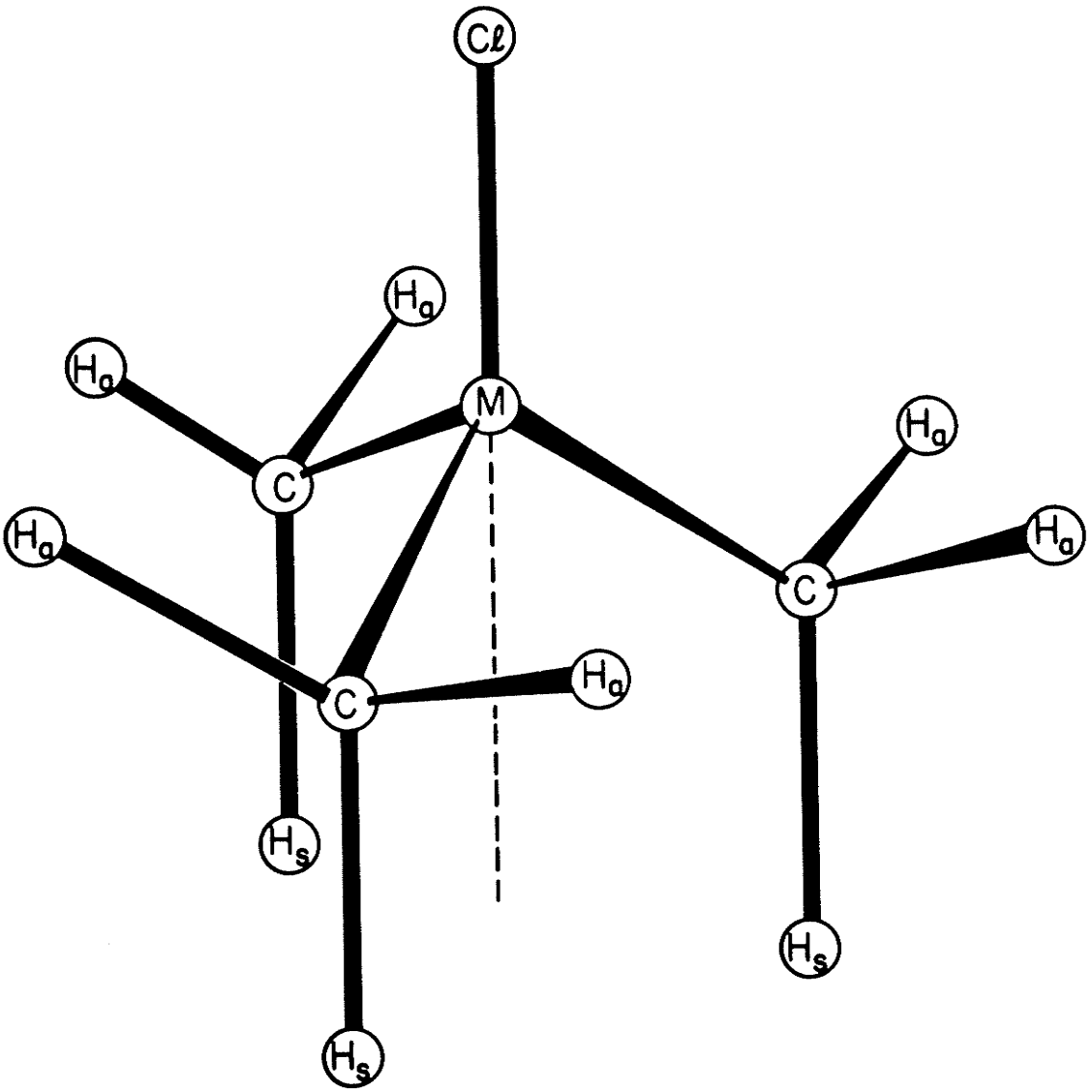

M = C, Si

Figure 7.2.

Liquid phase (5% solutions in CCl_4) fundamental spectra of $(CH_3)_3CCl$ (----) and $(CH_3)_3SiCl$ (——) in the region of $\Delta v_{CH} = 1$. Spectra were measured at room temperature with a path length of 0.1 mm.

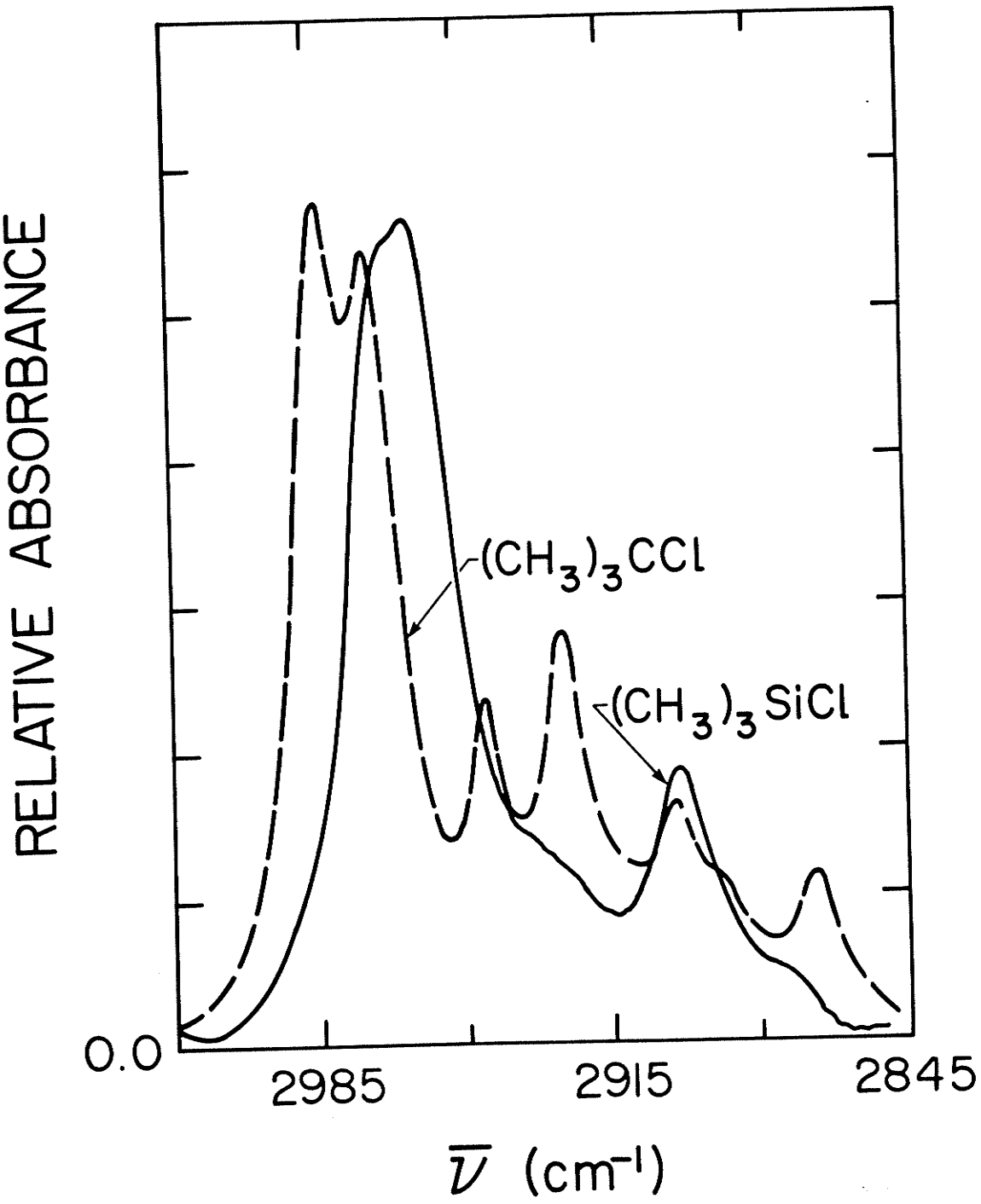
RELATIVE ABSORBANCE
0.0
2985
2915
2845
$\bar{\nu}$ (cm^{-1})
(CH$_3$)$_3$CCl
(CH$_3$)$_3$SiCl

Figure 7.3.

Liquid phase overtone spectra of $(CH_3)_3CCl$ and $(CH_3)_3SiCl$ in the region of $\Delta v_{CH} = 2$. Spectra were measured at room temperature with a path length of 0.1 cm. The absorbance of $(CH_3)_3SiCl$ has been offset by 0.3 absorbance units.

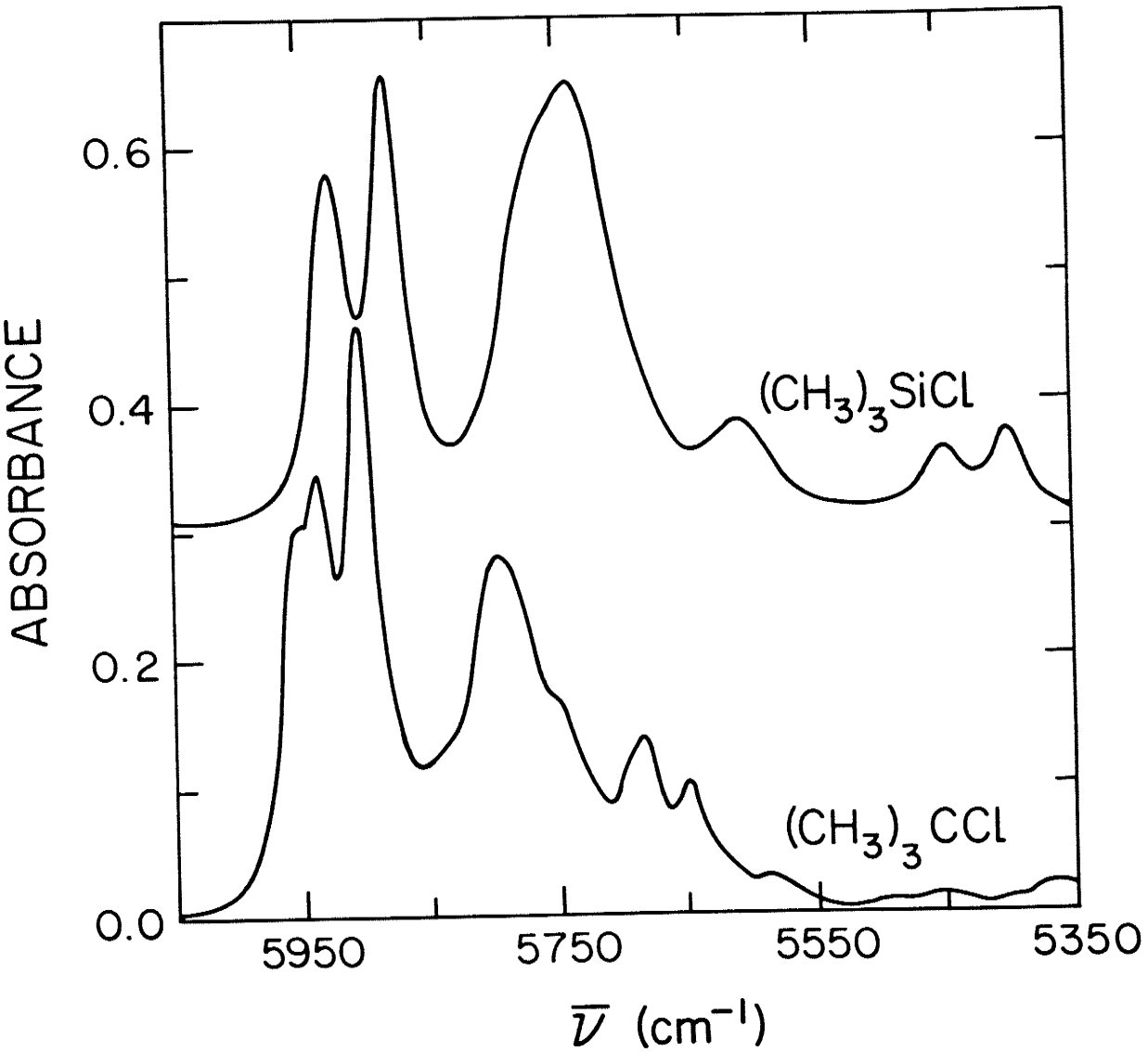
ABSORBANCE
0.6
0.4
0.2
0.0
5950
5750
5550
5350
$\bar{\nu}$ (cm^{-1})
$(CH_3)_3SiCl$
$(CH_3)_3CCl$

Figure 7.4.

Liquid phase overtone spectra of $(CH_3)_3CCl$ and $(CH_3)_3SiCl$ in the region of $\Delta v_{CH} = 3$. Spectra were measured at room temperature with a path length of 1.0 cm. The absorbance of $(CH_3)_3SiCl$ has been offset by 0.3 absorbance units.

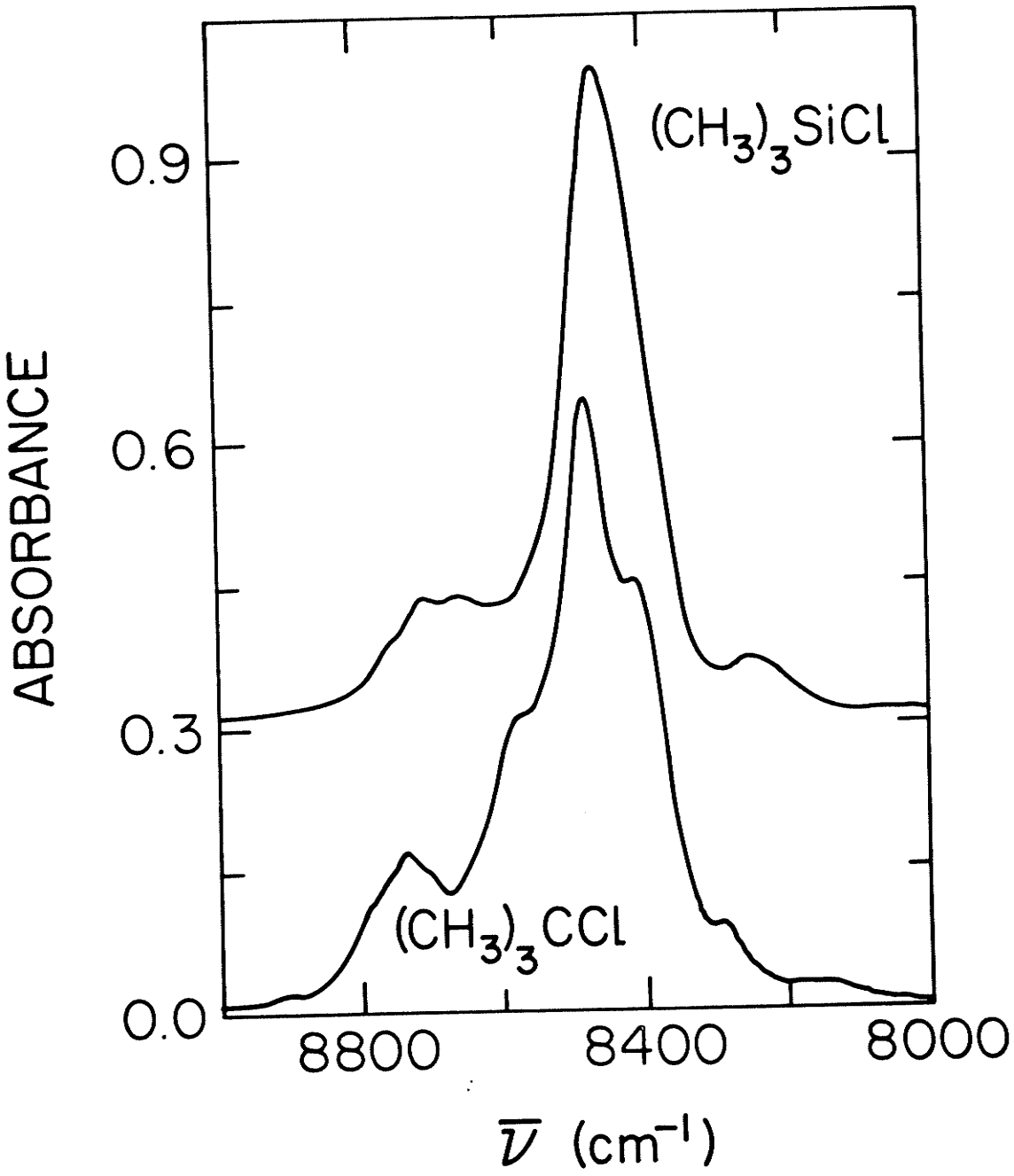
ABSORBANCE
0.9
0.6
0.3
0.0
8800
8400
8000
$\bar{\nu}$ (cm^{-1})
$(CH_3)_3SiCl$
$(CH_3)_3CCl$

Figure 7.5.

Liquid phase overtone spectra of $(CH_3)_3CCl$ and $(CH_3)_3SiCl$ in the region of $\Delta v_{CH} = 4$. Spectra were measured at room temperature with a path length of 10.0 cm. The absorbance of $(CH_3)_3SiCl$ has been offset by 0.18 absorbance units.

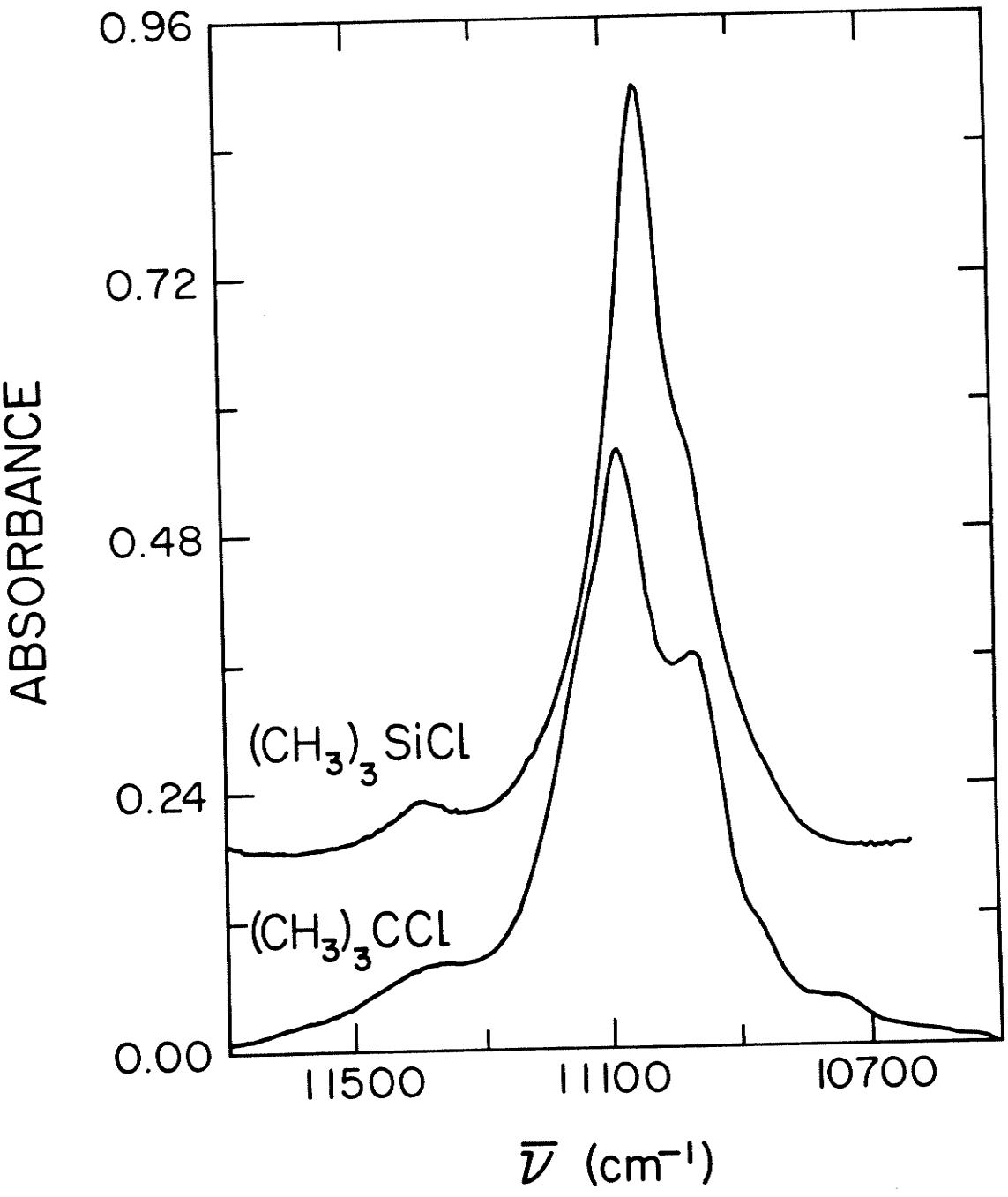
0.96
0.72
0.48
0.24
0.00
ABSORBANCE
(CH3)3SiCl
(CH3)3CCl
11500
11100
10700
ν̄ (cm⁻¹)

Figure 7.6

Liquid phase overtone spectra of $(CH_3)_3CCl$ and $(CH_3)_3SiCl$ in the region of $\Delta v_{CH} = 5$. Spectra were measured at room temperature with a path length of 10.0 cm. The absorbance of $(CH_3)_3SiCl$ has been offset by 0.022 absorbance units.

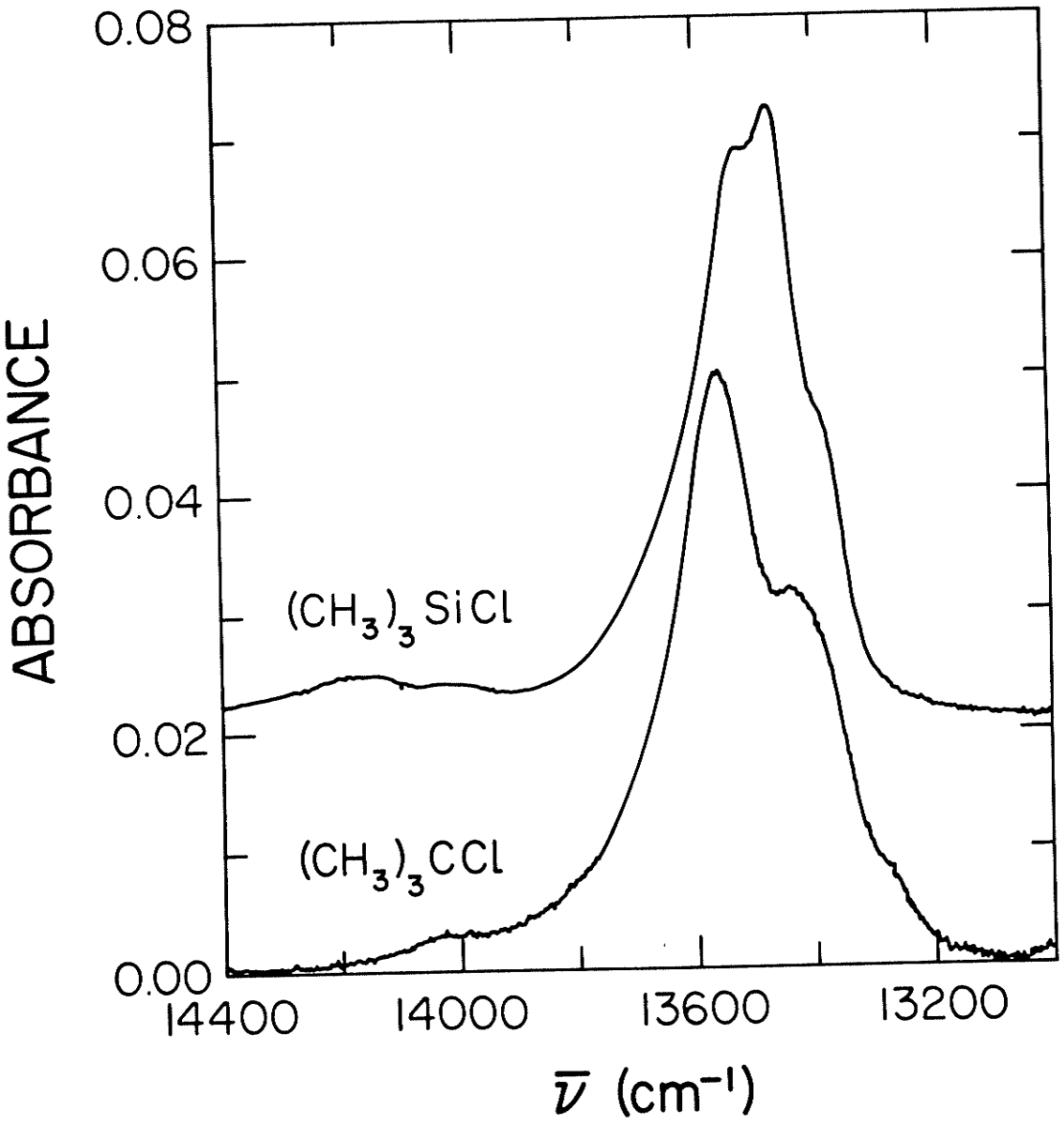
0.08
0.06
0.04
0.02
0.00
ABSORBANCE
(CH3)3SiCl
(CH3)3CCl
14400
14000
13600
13200
ν̄ (cm⁻¹)

Figure 7.7.

Liquid phase overtone spectra of $(CH_3)_3CCl$ and $(CH_3)_3SiCl$ in the region of $\Delta v_{CH} = 6$. The spectra were measured at room temperature with a path length of 10.0 cm. The spectrum of $(CH_3)_3CCl$ is an average of four base line corrected scans. The absorbance of $(CH_3)_3SiCl$ has been offset by 0.022 absorbance units.

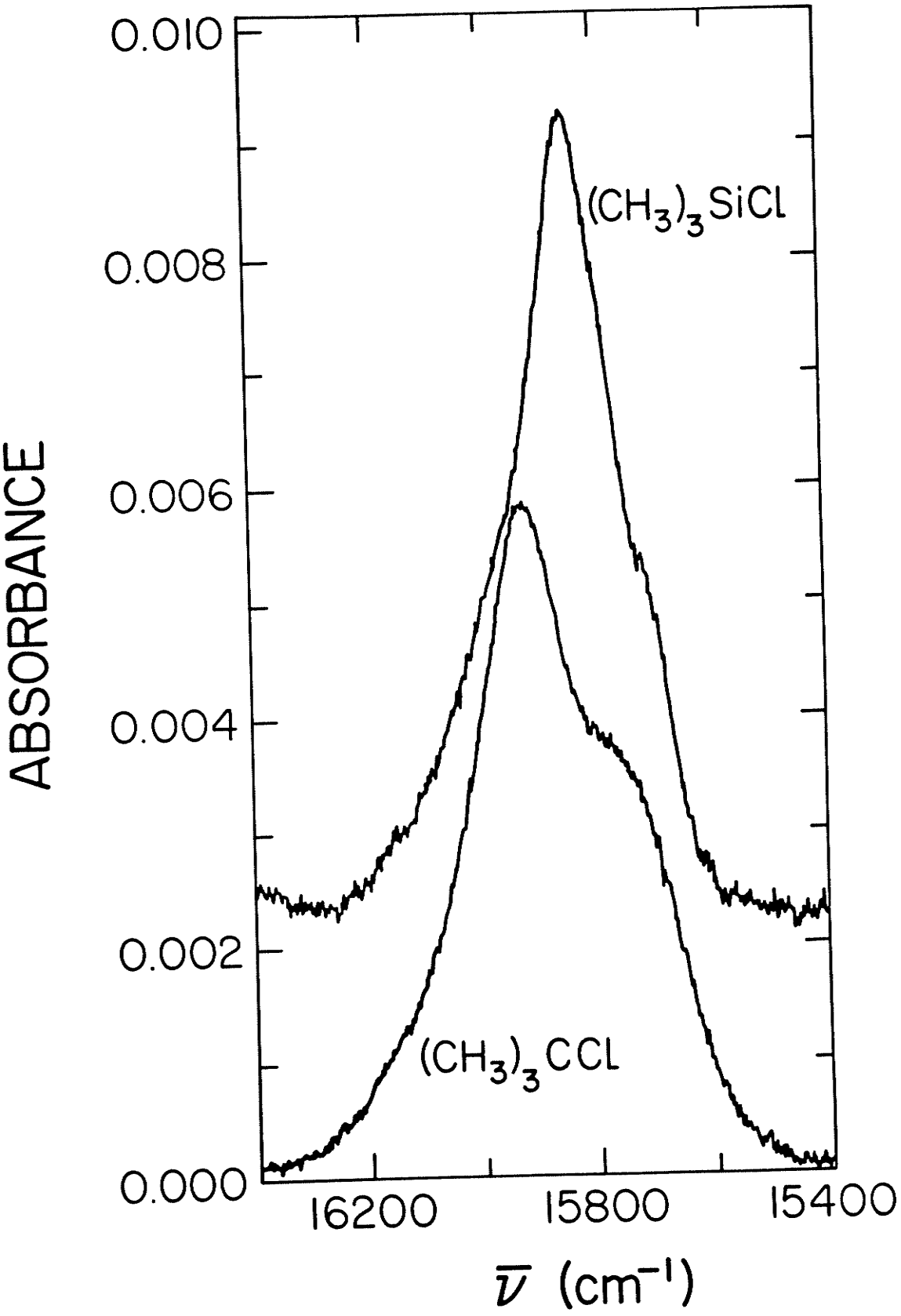
0.010
0.008
0.006
0.004
0.002
0.000
ABSORBANCE
(CH3)3SiCl
(CH3)3CCl
16200
15800
15400
ν̄ (cm⁻¹)

Figure 7.8.

Gas phase spectra of $(CH_3)_3CCl$ and $(CH_3)_3SiCl$ in the region of Δv_{CH} = 1 (10 torr pressure, 10 cm path length). Spectra were measured at room temperature.

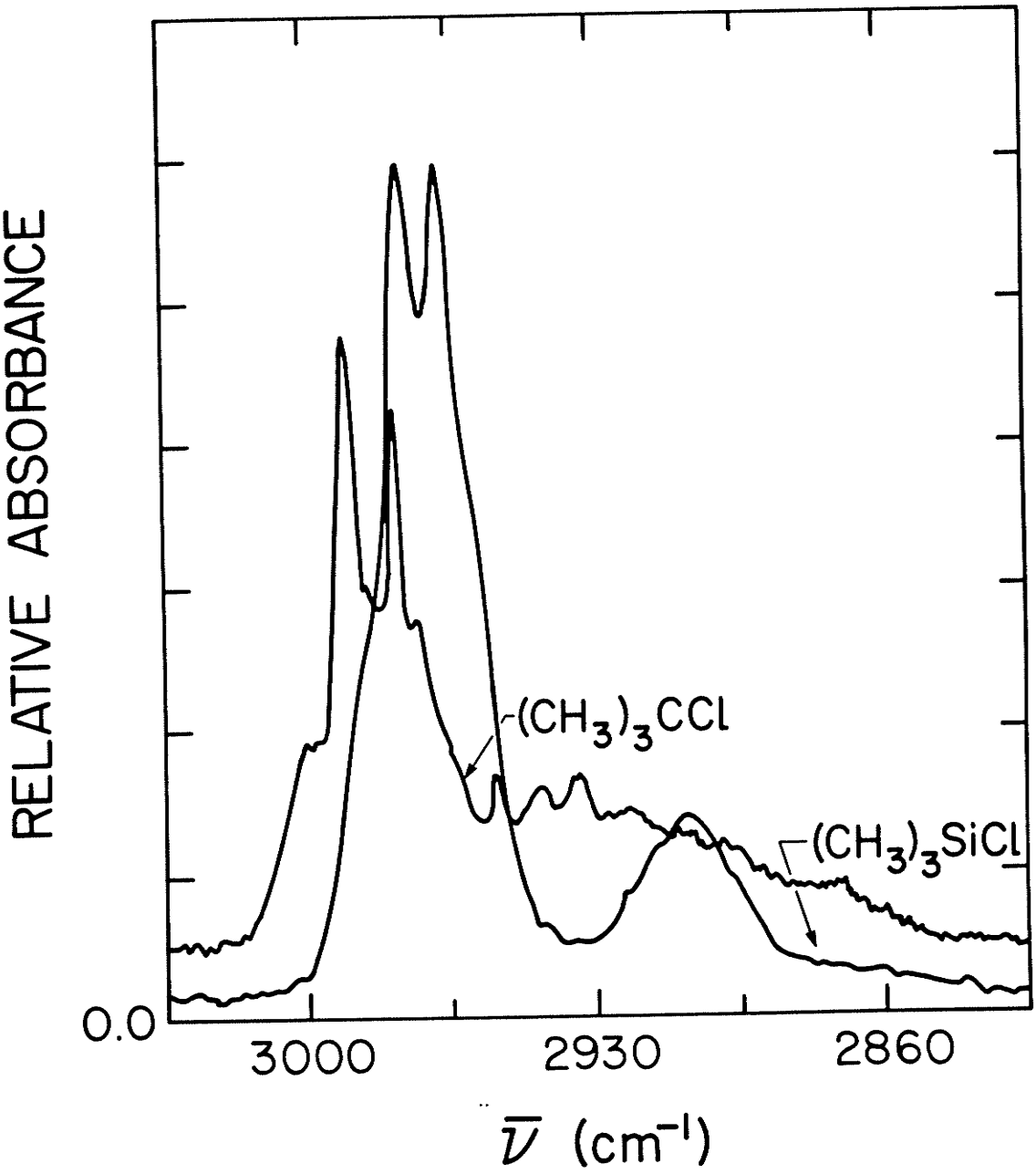
RELATIVE ABSORBANCE
0.0
3000
2930
2860
$\bar{\nu}$ (cm^{-1})
(CH$_3$)$_3$CCl
(CH$_3$)$_3$SiCl

Figure 7.9.

Gas phase overtone spectra of $(CH_3)_3CCl$ (——) and $(CH_3)_3SiCl$ (– – –) at room temperature in the region of $\Delta v_{CH} = 2$ (40 torr pressure, 10.80 m path length). The right hand ordinate scale represents the absorbance of $(CH_3)_3SiCl$.

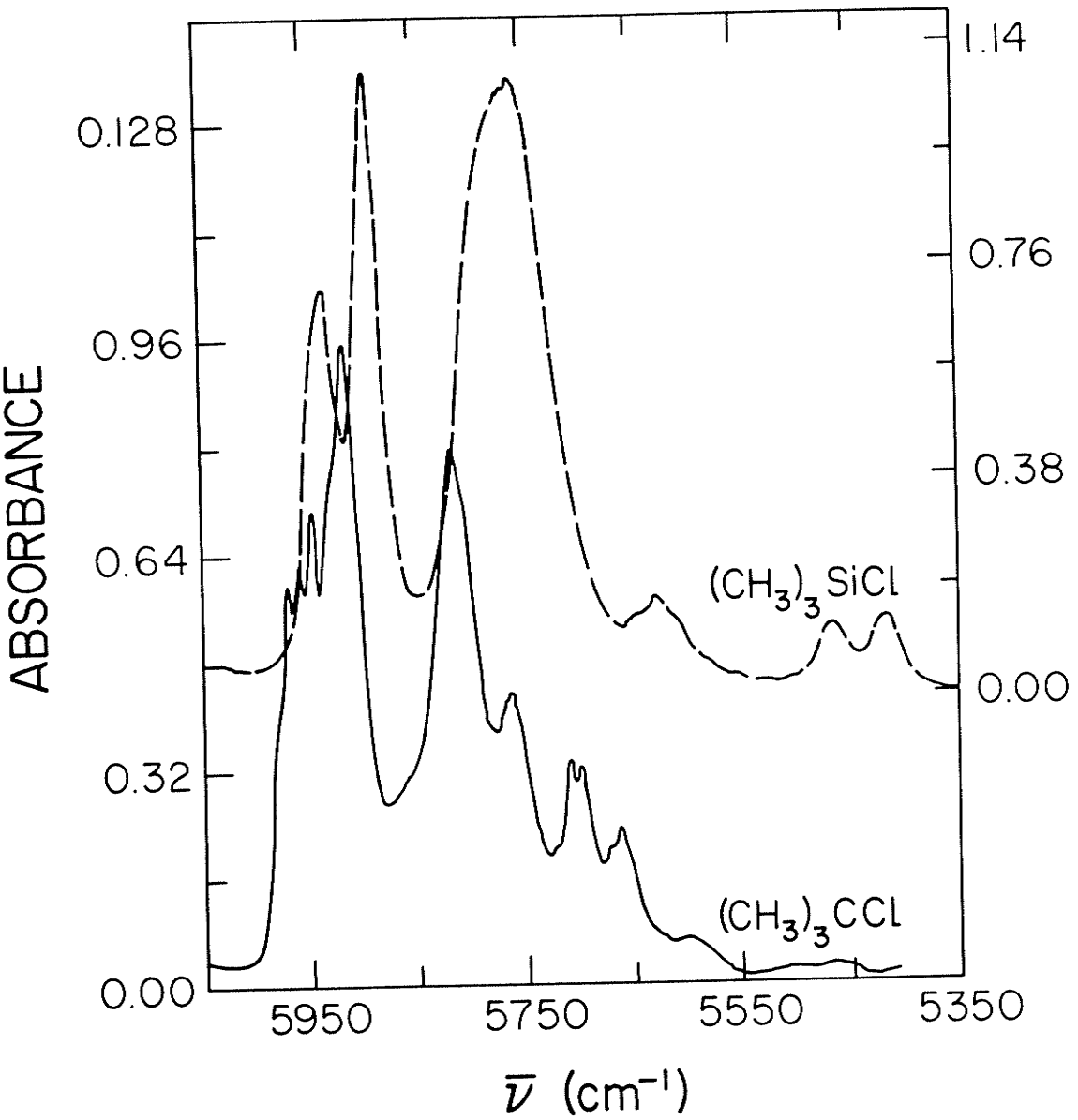
ABSORBANCE
0.128
0.96
0.64
0.32
0.00
1.14
0.76
0.38
0.00
5950
5750
5550
5350
$\bar{\nu}$ (cm^{-1})
$(CH_3)_3SiCl$
$(CH_3)_3CCl$

Figure 7.10.

Gas phase overtone spectra of $(CH_3)_3CCl$ (60 torr pressure, 12.15 m path length) and $(CH_3)_3SiCl$ (60 torr pressure, 10.89 m path length) at room temperature in the region of $\Delta v_{CH} = 3$. The right hand ordinate scale represents the absorbance of $(CH_3)_3$ SiCl.

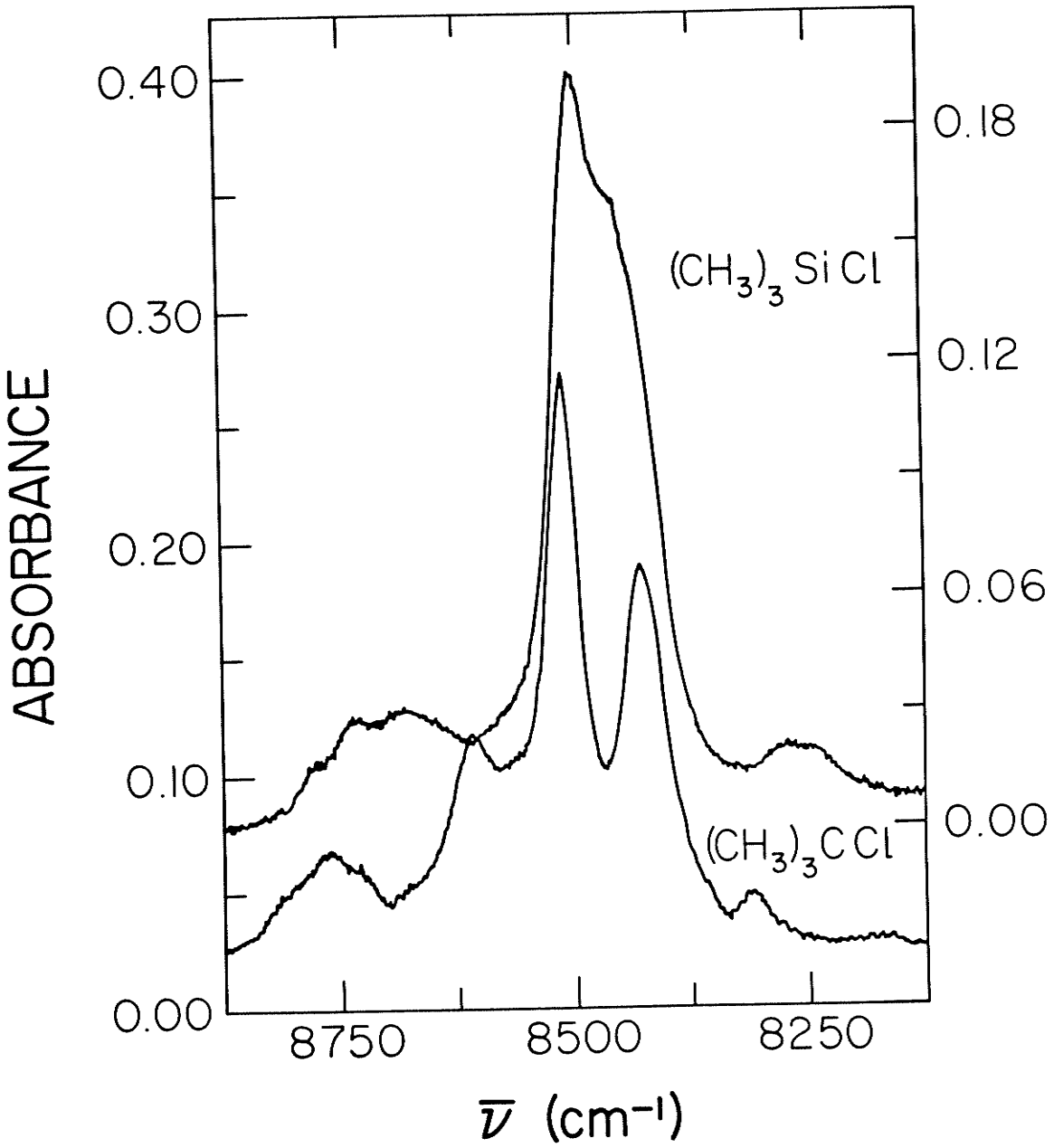
ABSORBANCE
0.40
0.30
0.20
0.10
0.00
0.18
0.12
0.06
0.00
(CH3)3 Si Cl
(CH3)3C Cl
8750
8500
8250
ν̄ (cm⁻¹)

Figure 7.11.

Gas phase overtone spectra of $(CH_3)_3CCl$ (100 torr pressure, 10.53 m path length) and $(CH_3)_3SiCl$ (70 torr pressure, 10.80 m path length) at room temperature in the region of $\Delta v_{CH} = 4$. The absorbance of $(CH_3)_3SiCl$ has been offset by 0.003 absorbance units.

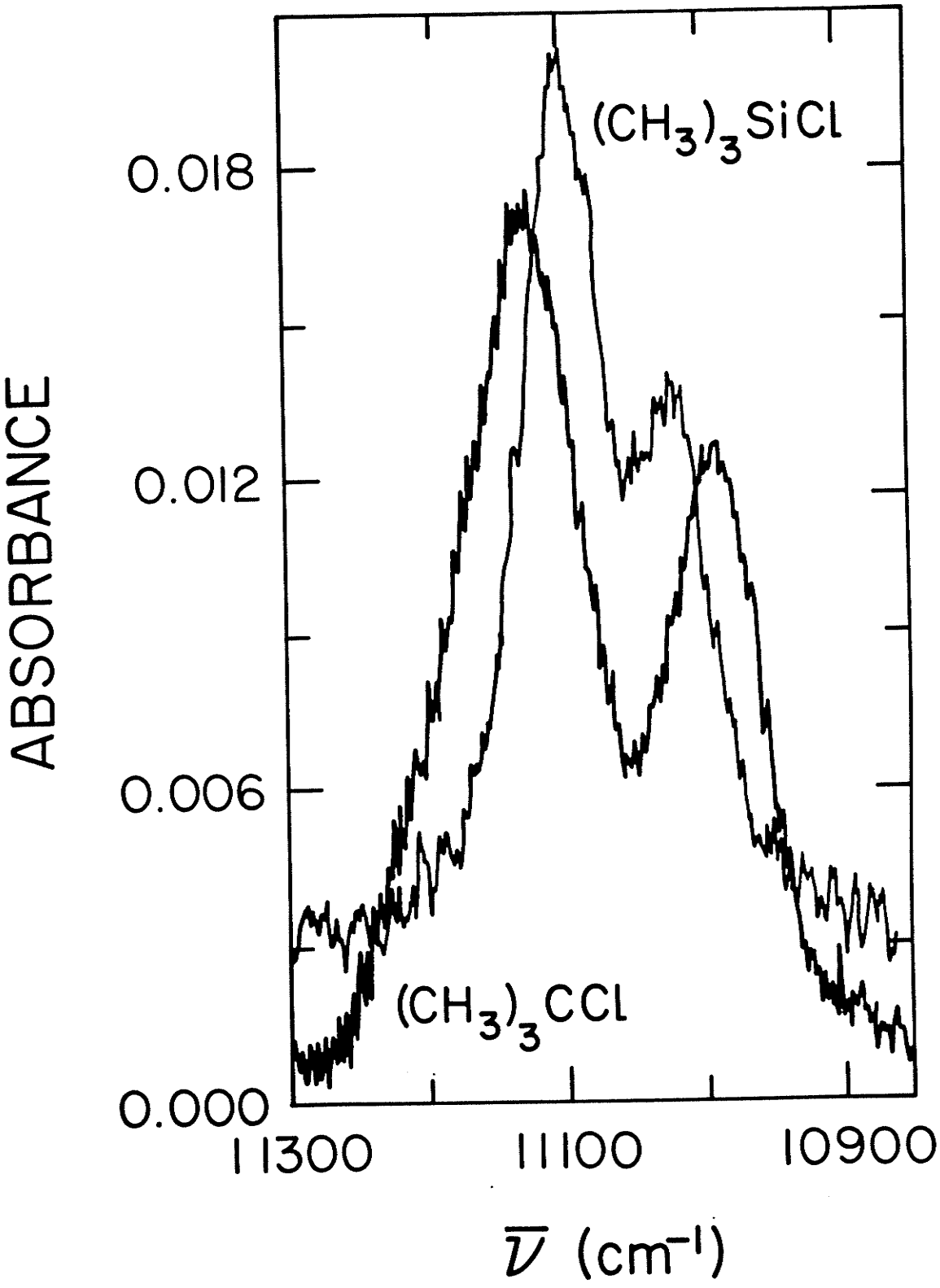
(CH3)3SiCl
(CH3)3CCl
ABSORBANCE
0.018
0.012
0.006
0.000
11300
11100
10900
ν̄ (cm⁻¹)

Figure 7.12.

Plots of the vibrational energy equation of a single Morse oscillator for the nonequivalent CH bonds of liquid phase $(CH_3)_3CCl$.

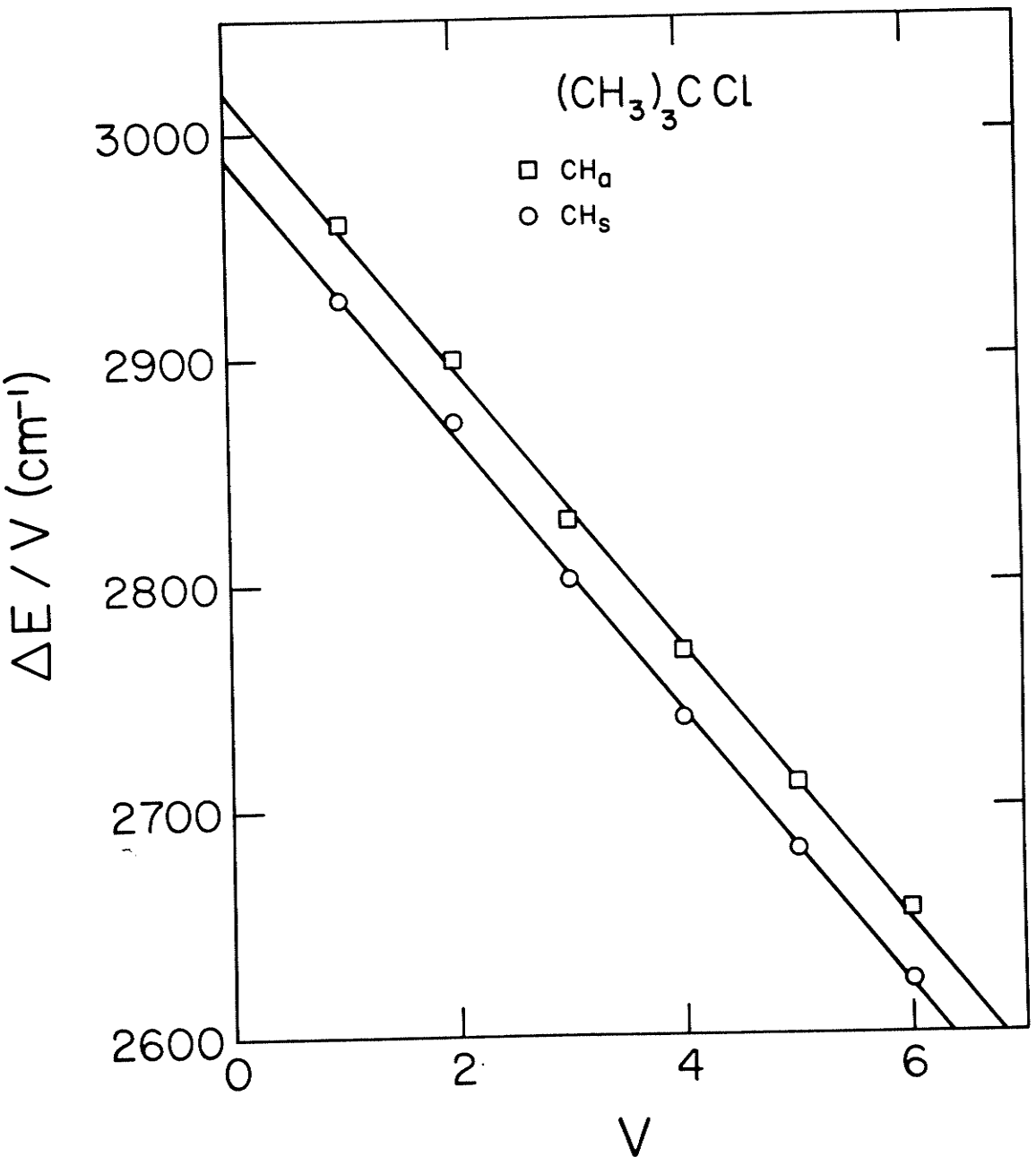
(CH3)3C Cl
CHa
CHs
3000
2900
2800
2700
2600
ΔE / V (cm-1)
0
2
4
6
V

Figure 7.13.

Upper traces: the calculated (broken curve) and experimentally observed (solid curve) overtone spectrum of $(CH_3)_3SiCl$ in the region of $\Delta v_{CH} = 4$. Lower trace: individual Lorentzian functions fit to the experimental spectrum.

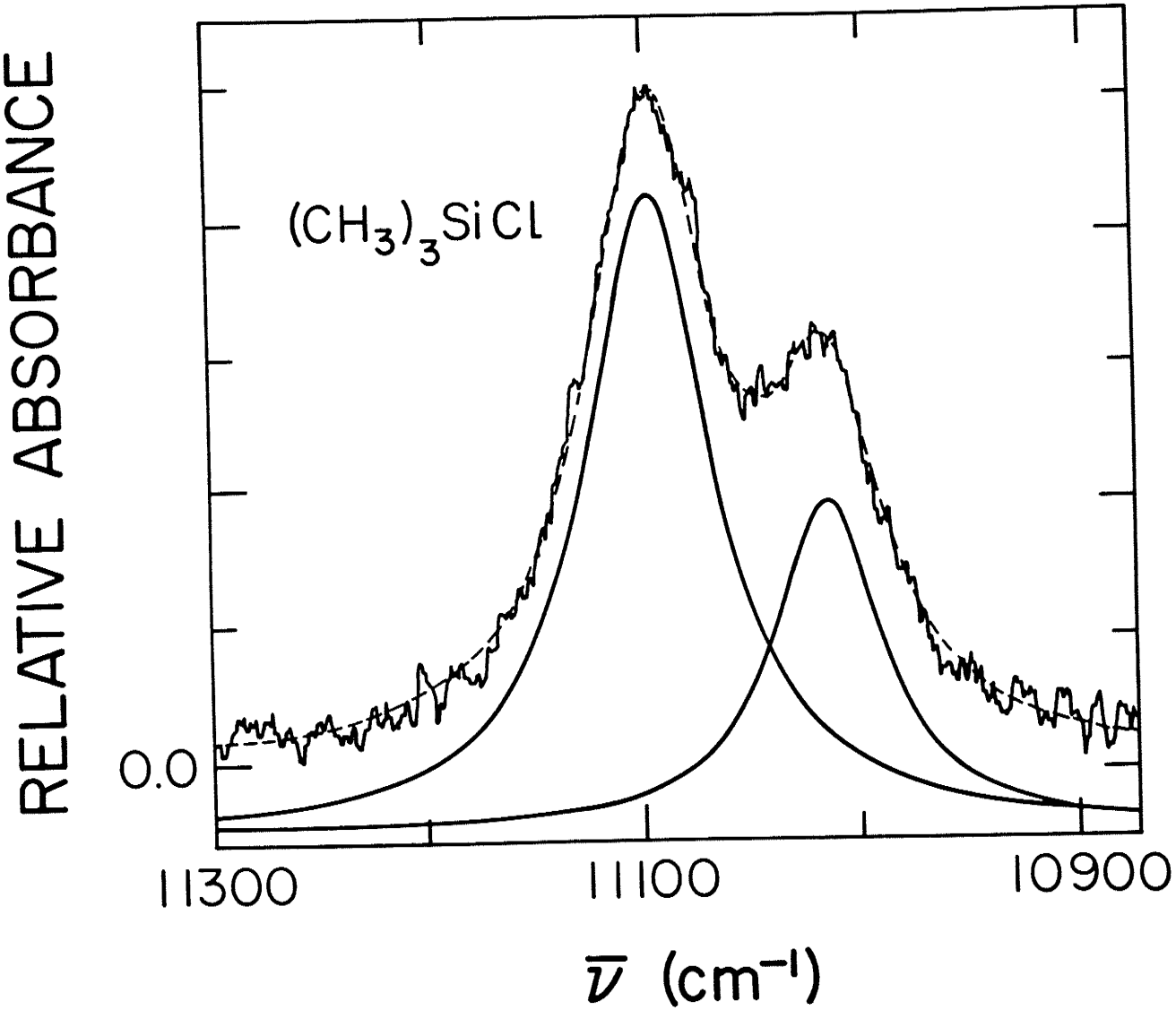
RELATIVE ABSORBANCE
$(CH_3)_3SiCl$
0.0
11300
11100
10900
$\bar{\nu}$ (cm^{-1})

CHAPTER 8

OVERTONE SPECTRA OF SOME MONOSUBSTITUTED CYCLOPROPANES

In this chapter, the CH stretching liquid phase overtone spectra of cyclopropyl bromide, cyclopropyl cyanide, cyclopropylamine, and cyclopropyl methyl ketone will be presented in the region of $\Delta v_{CH} = 2 - 6$. Spectra will also be presented for the $\Delta v_{NH} = 2 - 6$ region of the amino group of cyclopropylamine. All spectra will be analyzed in terms of the local mode model. Through this analysis, it will be shown that the XH bonds located at different centres of monosubstituted cyclopropanes behave as if they are dynamically independent.

i) Introduction

In 1980 Henry et al.[37] reported the liquid phase overtone spectra of a variety of cycloalkanes (cyclopentane to cyclooctane) and cycloalkenes (cyclopentene, cyclohexene, and cycloheptene). In 1982 Wong et al.[39] investigated the photoacoustically detected gas phase spectra of most of these molecules and of cyclobutane and cyclopropane. In both studies, spectral peaks due to structurally and conformationally nonequivalent CH bonds were identified and assigned through an analysis of the observed spectra.

In this chapter, the liquid phase overtone spectra of cyclopropyl bromide (CPBr), cyclopropyl cyanide (CPCN), cyclopropylamine (CPAM), and cyclopropyl methyl ketone (CPMK) (bracketed sets of letters are the abbreviations which will be used to denote the monosubstituted cyclopropanes) will be reported. The spectra will be analyzed in terms of the local mode model. Four main objectives for initiating this study were the following:

1. To understand to what extent the substituents (Br, CN, $-NH_2$, and CH_3CO) cause asymmetry in the bond strength of the ring CH bonds.
2. How different in strength/hybridization are the ring CH bonds of CPBr, CPCN, CPAM, and CPMK compared with the CH bonds of higher order cycloalkanes and cycloalkenes?
3. How strong is the coupling between the CH bonds located at different centres of monosubstituted cyclopropanes?
4. How successful is the local mode theory of the XH_2 system (see chapter 1) in assigning the spectra of monosubstituted cyclopropanes which contain two equivalent CH_2 groups (the theory

of the XH_2 system will also be utilized to analyze the Δv_{NH} = 2 - 6 spectra of the $-NH_2$ group of CPAM)?

For both CPAM and CPMK, the possibility of rotational isomers does exist. Wurry et al.[123] have reviewed the conformations of a number of three membered ring compounds including CPAM and CPMK. In Table 6 of their review article, they have given data about the conformational preference of CPAM and CPMK, which was collected from a number of experimental and theoretical studies[124-130] relevant to the conformations of CPAM[124-127] and CPMK[128-131]. According to their data, 94% of CPAM molecules in the vapor phase exist in a conformer (trans) in which the amino hydrogens are trans to the ring C-C bonds. This conformer is quoted to be the only one present in the solid state. No quantitative results have been given for liquid phase CPAM. However, the trans conformer is quoted to be the most favorable.

CPMK could exist in cis or trans conformers depending on whether the CO and cycloproyl groups lie on the same or opposite sides of the connecting single bond. The data of Wurrey et al.[123] show that the relative population of the cis and trans conformers of gas phase CPMK is 80% and 20%, respectively. In the solid state, CPMK exists totally in the cis form and in the liquid phase the cis conformer is the most favorable.

In this chapter, while analyzing the overtone spectra of CPAM and CPMK it will be assumed that the former molecule exists totally in the trans form and that the only conformer of CPMK is cis.

ii) Results and Discussion

a) Spectral Features of Ring CH Bonds

The CH stretching fundamental spectra of CPBr[132,133], CPCN[134], and CPAM[127], and CPMK[130] have been reported and assigned in terms of the normal mode model. Overtone spectra in the region of $\Delta v_{CH} = 2 - 6$ are displayed in Figures 8.1 - 8.5. The energies of the local mode peaks of the ring CH bonds are given in Table 8.1 along with their assignments. The observed energies were obtained from the deconvolution of the experimental spectra.

The cyclopropyl ring of monosubstituted cyclopropanes has two types of CH oscillators (methylene and methine). Within the local mode picture, the observed spectral peaks due to methylene oscillators are analogous to the local mode peaks observed in the overtone spectra of dihalomethanes[70] and deuterated dihalomethanes (see chapter 4). As in the case of dihalomethanes[70], the observed peaks of the methylene oscillators of monosubstituted cyclopropanes can be considered as arising from the transitions to symmetrized states[70],

$$|v_1,v_2\rangle_{\pm} = \frac{1}{\sqrt{2}}(|v_1,v_2\rangle \pm |v_2,v_1\rangle), \qquad (8.1)$$

where $|v_1,v_2\rangle = |v_1\rangle|v_2\rangle$ is the Morse oscillator product state corresponding to the two CH bonds. The methine CH oscillator gives rise to a single peak at each overtone level. This peak can be considered as arising from the transition to the Morse oscillator state $|v\rangle$, where $v = \Delta v_{CH}$.

The local mode peak assignments for CPBr are indicated in Figure 8.1 - 8.5. Analogous assignments can be made for the local mode peaks of the ring CH bonds of CPCN, CPAM, and CPMK although the features are

often not as well resolved in the latter three molecules. In the subsequent discussion the arguments apply to the spectra of all four cyclopropanes. The peaks marked "C" in Figures 8.1 - 8.3 are combination peaks and will be discussed separately. The peaks labelled as $|v,0,0\rangle_{\pm}$, $|0,0,v\rangle$ in the Δv_{CH} = 2 - 6 spectra of CPMK correspond to the methyl CH bonds. These peaks will be discussed in subsection C of the "Results and Discussion" section.

The Δv_{CH} = 2 spectra (Figure 8.1) are composed of four major peaks $|2,0\rangle_{+}$, $|2,0\rangle_{-}$, $|1,1\rangle$ and $|2\rangle$. All these peaks originate from the ring CH bonds. The first three peaks correspond to the excitation of methylene oscillators. The fourth peak, $|2\rangle$, corresponds to the methine CH bonds. As in the dihalomethanes[70] and deuterated dihalomethanes (see chapter 4), the $|2,0\rangle_{+}$ and $|2,0\rangle_{-}$ peaks are split. This splitting is caused by the harmonic coupling of the $|2,0\rangle_{+}$ and $|1,1\rangle$ states. If this coupling were absent, then $|2,0\rangle_{+}$ and $|2,0\rangle_{-}$ would have been degenerate. The peak, $|2\rangle$, is resolved in CPBr only. In CPCN and CPMK, this peak appears as an unresolved shoulder on the higher energy side of the $|2,0\rangle_{-}$ peak. For CPAM, $|2\rangle$ and $|2,0\rangle_{-}$ peaks are overlapped and give rise to a single broad band.

Peaks corresponding to the ring CH bonds in the Δv_{CH} = 3 spectra (Figure 8.2) are $|3,0\rangle_{\pm}$, $|2,1\rangle_{+}$, $|2,1\rangle_{-}$ and $|3\rangle$. Symmetry splitting between the $|3,0\rangle_{\pm}$ states is not observed at Δv_{CH} = 3 because of the absence of first order coupling. The local mode combination peaks, $|2,1\rangle_{+}$ and $|2,1\rangle_{-}$, are observed on the higher energy side of the Δv_{CH} = 3 spectra. Transitions to the $|2,1\rangle_{\pm}$ states are well resolved in the spectra of Figure 8.2 because these states undergo a first order coupling. As is the case at Δv_{CH} = 2, the methine CH peak, $|3\rangle$, is

only resolved for CPBr. At Δv_{CH} = 3 of the other molecules, a single asymmetric band is observed due to transitions to the pure local mode states $|3,0\rangle_{\pm}$ and $|3\rangle$. The methine CH peak, $|3\rangle$, is buried in the high energy portion of this band. As an example, the deconvoluted Δv_{CH} = 3 spectrum of CPCN is shown in Figure 8.6. The deconvoluted spectrum clearly shows that the most intense band is composed of $|3,0\rangle_{\pm}$ and $|3\rangle$ peaks.

The local mode peaks corresponding to the ring CH bonds at Δv_{CH} = 4 are $|4,0\rangle_{\pm}$, $|3,1\rangle_{\pm}$, and $|4\rangle$. The methine CH peak $|4\rangle$ is not resolved for all four molecules. For CPBr this peak appears as an unresolved shoulder to the higher energy side of the most intense, $|4,0\rangle_{\pm}$, peak. At Δv_{CH} = 4 of the other three molecules, $|4,0\rangle_{\pm}$ and $|4\rangle$ peaks form a single asymmetric band. Transitions to the local mode combination states $|3,1\rangle_{+}$ and $|3,1\rangle_{-}$ are not resolved at Δv_{CH} = 4 because of a smaller effective coupling of these states with the $|4,0\rangle_{+}$ and $|4,0\rangle_{-}$ states, respectively.

The Δv_{CH} = 5 and 6 spectra (Figures 8.4 and 8.5) are dominated by an asymmetric band. At Δv_{CH} = 5 this band arises from transitions to the states $|5,0\rangle_{\pm}$ and $|5\rangle$. At Δv_{CH} = 6 the most intense asymmetric band originates from transitions to the states $|6,0\rangle_{\pm}$ and $|6\rangle$. Relatively weak local mode combination peaks associated with the states $|4,1\rangle_{\pm}$ and $|5,1\rangle_{\pm}$ are also observed on the high energy side of the main band for Δv_{CH} = 5 and Δv_{CH} = 6, respectively.

b) Spectral Features of NH Bonds of Cyclopropylamine

The NH stretching overtone spectra of CPAM corresponding to Δv_{NH} = 2 and 3 are shown in Figure 8.7. The Δv_{NH} = 4 and 5 spectra are displayed in Figure 8.8. The Δv_{NH} = 6 spectrum is presented in Figure 8.9. The energies of the local mode peaks observed in Δv_{NH} = 2 - 6 spectra along with their assignments are given in Table 8.2. The observed local mode peaks of Figures 8.7 - 8.9 can be understood as arising from the transitions to the symmetrized states[70] $|v_1,v_2\rangle_{\pm}$, where $v_1 + v_2 = \Delta v_{NH} = v$.

The most intense asymmetric band in the Δv_{NH} = 2 spectrum (Figure 8.7) arises from transitions to the $|2,0\rangle_{\pm}$ states. A relatively weak local mode combination peak, $|1,1\rangle$, is observed on the high energy side of the $|2,0\rangle_{\pm}$ peak. Transitions to the $|2,0\rangle_{+}$ and $|2,0\rangle_{-}$ states are not resolved because of a smaller coupling between $|2,0\rangle_{+}$ and $|1,1\rangle$ states than in the analogous CH_2 case. On the lower energy side of Δv_{NH} = 2, a combination peak is observed at 6301 cm^{-1}. This peak probably arises from transition to the state which contains one quantum of the asymmetric NH stretching mode[127] ν_{16} (3368 cm^{-1}) and one quantum of the CH stretching mode[127] ν_3 (3005 cm^{-1}).

At Δv_{NH} = 3 in Figure 8.7, the highest intensity peak corresponds to both $|3,0\rangle_{+}$ and $|3,0\rangle_{-}$ pure local mode states. Very weak local mode combination peaks $|2,1\rangle_{+}$ and $|2,1\rangle_{-}$ are observed at about 9849 cm^{-1} and 9934 cm^{-1}, respectively.

The Δv_{NH} = 4, 5 and 6 spectra (Figures 8.8 and 8.9) consist essentially of a single band. The Δv_{NH} = 5 and Δv_{NH} = 6 spectra show some asymmetry about 84 cm^{-1} (Δv_{NH} = 5) and 138 cm^{-1} (Δv_{NH} = 6) away from the band maxima on the high energy side. The most probable

origin of asymmetry for both Δv_{NH} = 5 and 6 is an unresolved contribution of the combination involving v_{NH} - 1 local quanta and two quanta of the in plane bending mode[127] ν_7 (1371 cm^{-1}) of the methine CH bond of CPAM.

c) Spectral Features of Methyl CH Bonds of Cyclopropyl Methyl Ketone

The energies of the pure local mode peaks observed for the methyl CH bonds of CPMK (see Figures 8.1 - 8.5) are given in Table 8.3. The methyl CH peaks of CPMK are analogous to the CH stretching peak of acetone. Fang and Swofford[40] and Fang et al.[41] have reported and analyzed the photoacoustically detected Δv_{CH} = 4 - 7 spectra of acetone. Hanazaki et al.[117] have measured and assigned the gas phase spectra of acetone in the region of Δv_{CH} = 1 - 4. These studies have shown that the methyl groups of acetone have two kinds of conformationally nonequivalent CH bonds, ones which lie in the molecular symmetry plane and the others which lie out of this plane. Fang et al.[41] and Hanazaki et al.[117] observed two well resolved peaks at each overtone level of acetone corresponding to the two kinds of nonequivalent bonds. The higher frequency peak was assigned to the stronger in plane CH bonds and the lower frequency peak was associated with the weaker out of plane CH bonds. These assignments of Fang et al.[41] and Hanazaki et al.[117] are in agreement with the study of McKean[135], who observed two well resolved peaks in the fundamental CH stretching spectrum of $(CD_3)CO(CD_2H)$.

The methyl CH bonds of CPMK can be treated similarly to the methyl CH bonds of acetone. As in acetone[117], the local symmetry of the methyl group of CPMK is C_s. The symmetrized local mode states for the methyl CH bonds of CPMK can be written as $|v_1,v_2,v_3\rangle_{\pm}$, where $v_1 + v_2 + v_3 = \Delta v_{CH} = v$ and v_1, v_2, and v_3 represent the vibrational quanta in the first, second (out of plane) and third (in plane) CH bonds respectively. For example, at Δv_{CH} = 2 one will have states of the

type $|2,0,0\rangle_{\pm}$ ($\equiv|2,0\rangle_{\pm}|0\rangle$), $|1,1,0\rangle(\equiv|1,1\rangle|0\rangle)$, $|0,0,2\rangle(\equiv|0,0\rangle|2\rangle)$, and $|0,1,1\rangle_{\pm}(\equiv|1,0\rangle_{\pm}|1\rangle)$. The methyl CH peaks observed in the Δv_{CH} = 2 - 6 spectra of CPMK (Figures 8.1 - 8.5) arise due to transitions to the states $|v,0,0\rangle_{\pm}$ and $|0,0,v\rangle$. These are the pure local mode states where all of the vibrational quanta are deposited in one of the three methyl CH bonds. Spectral peaks corresponding to transitions to the local mode combination states where the vibrational quanta are distributed over at least two methyl CH bonds are not observed in the Δv_{CH} = 2 - 6 spectra of CPMK. Generally the local mode combination peaks are observed at low overtones. However, for the methyl CH bonds of CPMK these peaks are absent even at Δv_{CH} = 2. It has been shown[87] that the dominant source of intensity for the local mode combination states is the vibrational mixing of these states with the pure local mode states. Most of the local mode combination peaks are also absent in the Δv_{CH} = 2 and 3 spectra of acetone[117] and at Δv_{CH} > 3 such peaks are not observed at all. This shows that vibrational mixing is very small in acetone. Since the extent of vibrational mixing for the pure local mode and local mode combination states of the methyl CH bonds of CPMK will be similar in magnitude to the case of acetone, it is not surprising that local mode combination peaks are not observed in the methyl regions of the Δv_{CH} = 2 - 6 spectra of CPMK.

d) Combination Peaks

In the $\Delta v_{CH} = 2$ and $\Delta v_{CH} = 3$ spectra (Figures 8.1 and 8.2) of all the molecules, and in the $\Delta v_{CH} = 4$ spectrum of CPAM, the peaks marked by a "C" are combinations. Most of these peaks arise from transitions to states which contain v-1 quanta of a CH stretch and two quanta of a CH deformational mode. Such peaks have been previously observed in the overtone spectra of a number of polyatomic molecules[38,52,70,102]. The energy positions and the tentative assignments of the combination peaks observed in the overtone spectra of monosubstituted cyclopropanes are given in Table 8.4.

e) Local Mode Parameters

The local mode frequencies, ω, and diagonal anharmonicities, ωx, for the nonequivalent bonds of monosubstituted cyclopropanes are given in Table 8.5. The parameters ω and ωx were obtained with the standard procedure of fitting the energies of the pure local mode peaks to the vibrational energy equation of a single Morse oscillator. The correlation coefficients, r, for the fit of the energies of the pure local mode peaks of the nonequivalent bonds to the Morse oscillator energy equation are also listed in Table 8.5. The r values of table 8.5 indicate an almost perfect fit of the pure local mode peaks of nonequivalent bonds to the Morse oscillator energy equation ($r = -1$ corresponds to an exact linear correlation). The r values for the methyl CH peaks of CPMK are somewhat lower because these peaks are perturbed by a combination peak in the regions of $\Delta v_{CH} = 2$ and 3 (see Figures 8.1, 8.2 and Table 8.4). To exemplify the excellent quality of the fit of the pure local mode peaks of monosubstituted cyclopropanes to the Morse oscillator energy equation, the plots of Morse equation for the nonequivalent bonds of CPCN are shown in Figure 8.10.

In Table 8.5 ω and ωx values of a variety of cycloalkanes and cycloalkenes from previous studies[37,136] are listed for comparison with the ω and ωx values of monosubstituted cyclopropanes. The sensitivity of the local mode parameters to the molecular environment is clearly evident from the data of Table 8.5. The local mode frequencies of the methylene and methine CH oscillators of the monosubstituted cyclopropanes are higher than the local mode frequencies of methylene oscillators of all of the cycloalkanes and

cycloalkenes listed in Table 8.5. The local mode frequencies and anharmonicities of the ring CH oscillators of monosubstituted cyclopropanes are closer to the local mode frequencies and anharmonicities of the olefinic CH oscillators of cyclopentene, cyclohexene, and benzene. The higher frequencies and lower anharmonicities of the ring CH oscillators of monosubstituted cyclopropanes are a result of ring strain and the bond strengthening effect of substituents (Br, CN, $-NH_2$, and CH_3CO). The high ring strain in monosubstituted cyclopropanes increases the "p" character in the endocyclic C-C bonds to maximize the orbital overlap. Consequently the "s" character of exocyclic CH bonds increases[137-139]. The increased "s" character of CH bonds makes them shorter[140] and stronger and their vibrational energy increases. In fact, theoretical models[141] have been suggested with hybridizations of sp^2 to $sp^{2.28}$ for the CH bonds of cyclopropane. The data of Table 8.5 for monosubstituted cyclopropanes are in agreement with such models.

f) Calculated CH Stretching Spectra

First the spectra of methylene oscillators are discussed. The energies of the local mode states $|v_1,v_2>_\pm$ of methylene oscillators can be calculated by making use of the Hamiltonian of two coupled Morse oscillators. This Hamiltonian was discussed in detail in chapter 1 and is not reiterated here. The intramanifold coupling matrices of the Hamiltonian of two coupled Morse oscillators in the local mode basis states $|v_1,v_2>_\pm$ were given in Table 1.1 of chapter 1. These Hamiltonian matrices involve the local mode parameters (harmonic frequency, ω, diagonal anharmonicity, ωx, and effective interoscillator coupling, $\omega\gamma'$). Thus the first step in the calculation of the spectra of methylene oscillators involves the determination of ω, ωx, and $\omega\gamma'$. ω and ωx values for methylene oscillators which were calculated from a Morse oscillator energy equation are listed in Table 8.5. The effective interoscillator coupling parameter $\omega\gamma'$, which contains the effects of both kinetic energy and potential energy couplings, can be calculated from the following equations

$$E(|2,0>_+) = 2\omega - 5\omega x - \sqrt{(\omega x)^2 + (2\omega\gamma')^2} \qquad (8.2)$$

$$E(|1,1>) = 2\omega - 5\omega x + \sqrt{(\omega x)^2 + (2\omega\gamma')^2} \qquad (8.3)$$

Eqs. (8.2) and (8.3) are obtained by diagonalization of the 2 x 2 matrix of the Hamiltonian of the XH_2 system over the harmonically coupled $|2,0>_+$ and $|1,1>$ states (see Table 1.1 of chapter 1). Since the observed energies of $|2,0>_+$ and $|1,1>$ states and the parameters ω and ωx for the methylene CH bonds are known (see Tables 8.1 and

8.5), either Eq. (8.2) or Eq. (8.3) can be utilized to obtain $\gamma'\omega$. From Eq. (8.3), $\gamma'\omega$ values of 55.1, 49.4, 51.6, and 55.2 cm^{-1} were obtained for CPBr, CPCN, CPAM, and CPMK, respectively. Eq. (8.3) is preferred over Eq. (8.2) in obtaining $\gamma'\omega$ since the local mode peaks $|2,0\rangle_+$ are located in the close vicinity of the combination peaks "C" (see Figure 8.1) and may be under some perturbation.

Substitution of ω, ωx, and $\gamma'\omega$ in the matrices of Table 1.1 of chapter 1, followed by diagonalization of these matrices, gives the calculated energies of the peaks observed for the methylene oscillators of monosubstituted cyclopropanes. These energies are given in Table 8.6.

The spectra of the methine CH oscillators of the monosubstituted cyclopropanes can be calculated straightforwardly from the vibrational energy expression of a single Morse oscillator. The calculated energies of the local mode states $|v\rangle$ of methine CH oscillators are also listed in Table 8.6.

The energies of the methyl CH peaks of CPMK can be calculated by applying the local mode Hamiltonian of the three coupled Morse oscillators to the symmetry adapted vibrational states of the form[116-118] $|v,0,0\rangle_\pm$, $|0,0,v\rangle$, $|v_1,v_2 0\rangle_\pm$, $|v_1,0,v_3\rangle_\pm$* etc., and diagonalizing the resultant Hamiltonian matrices. This calculation

---

*In the symmetrized states $|v_1,0,v_3\rangle_\pm$, $|v_1,v_2,0\rangle_\pm$ etc. v_1, v_2, and v_3 denote the vibrational quantum numbers of the first (out of plane), second (out of plane), and the third (in plane) methyl CH bonds of CPMK, respectively, and $v_1 + v_2 + v_3 = v = \Delta v_{CH}$.

however is not presented in this chapter because a similar calculation has already been reported very recently by Sage[116] for the methyl CH oscillators of methanol. Hanazaki et al.[117] and Findsen et al.[118] have also reported the procedure for calculating the local mode peak positions for the methyl CH oscillators of acetone[117] and acetaldehyde[118].

g) Calculated NH Stretching Spectra

The energies of the local mode peaks of the Δv_{NH} = 2 - 6 spectra of CPAM can be calculated by following the same procedure that is used to calculate the spectra of the methylene oscillators of monosubstituted cyclopropanes.

The local mode parameters, ω and ωx, for the NH oscillators are listed in Table 8.5. Substitution of these parameters and the observed energy of the $|1,1\rangle$ peak (see Table 8.2) into Eq. (8.3) yields a value of 31.9 cm^{-1} for the effective interoscillator coupling parameters $\gamma'\omega$. With the known ω, ωx, and $\gamma'\omega$ values the energies of all the NH stretching local mode states corresponding to the Δv_{NH} = 2 - 6 spectra of CPAM were calculated and are compared with the observed energies in Table 8.7.

h) Supportive Arguments

Keeping in mind the simplicity of the model which is employed for the analysis, the agreement between the calculated and experimental spectra (see Tables 8.6 and 8.7) is satisfactory.

This assignment of the overtone spectra is also supported by ^{13}C NMR studies[142,143] on monosubstituted cylcopropanes. The coupling constants J_{CH} of the methine CH oscillators are significantly higher than the J_{CH} of the methylene oscillators. The higher value of J_{CH} represents high %s character[140,144] and a shorter bond length[140,145]. With these considerations, it seems reasonable to assign the high frequency peak in the local mode spectra of monosubstituted cyclopropanes to the methine CH oscillators of these molecules.

Further support for the spectral assignments which are presented in this chapter for the Δv_{CH} = 2 - 6 spectra of monosubstituted cyclopropanes comes from the photoacoustically measured Δv_{CH} = 6 (gas phase) spectrum of cyclopropane[39]. The Δv_{CH} = 6 spectrum of cyclopropane is a single symmetric peak, while the spectra of monosubstituted cyclopropanes in the same region are asymmetric bands. This asymmetry is caused by the substituents (Br, CN, NH_2, and CH_3CO) which make the methine CH oscillator stronger and increases its vibrational energy compared with the methylene oscillators. The effect of these substituents in the ^{13}C NMR studies is to increase the coupling constant J_{CH}[142,143].

Table 8.1.

Observed Energies[a] (cm^{-1}) and Assignments of the Local Mode Peaks of Ring CH Bonds of Monosubstituted Cyclopropanes.

Δv_{CH}	C_3H_5Br	C_3H_5CN	$C_3H_5NH_2$	$C_3H_5COCH_3$	Assignment
	5890	5933	5895	5897	$\|2,0\rangle_+$
	5947	5993	5947	5959	$\|2,0\rangle_-$
2	6000	6026	5976	5995	$\|2\rangle$
	6127	6164	6123	6141	$\|1,1\rangle$
	8749	8799	8734	8758	$\|3,0\rangle_\pm$
	8814	8852	8785	8822	$\|3\rangle$
3	8897	8962	8938	9006	$\|2,1\rangle_+$
	9102	9157	9092	9122	$\|2,1\rangle_-$
	11433	11498	11421	11451	$\|4,0\rangle_\pm$
	11506	11571	11508	11516	$\|4\rangle$
4	11756	11817	-	-	$\|3,1\rangle_+$

Table 8.1...cont'd...

Δv_{CH}	C_3H_5Br	C_3H_5CN	$C_3H_5NH_2$	$C_3H_5COCH_3$	Assignment
	11827	11893	11802	11820	$\|3,1\rangle_-$
	14006	14078	13972	14019	$\|5,0\rangle_\pm$
5	14100	14171	14066	14124	$\|5\rangle$
	14505	14575	14494	14521	$\|4,1\rangle_\pm$
	16469	16546	16416	16471	$\|6,0\rangle_\pm$
6	16624	16661	16539	16592	$\|6\rangle$
	17073	17173	17096	17104	$\|5,1\rangle_\pm$

[a]Observed energies are from deconvolution of the experimental spectra.

Table 8.2.

Observed Energies[a] (cm^{-1}) and Assignments of the Local Mode Peaks of the Δv_{NH} = 2 - 6 Spectra of Cyclopropylamine.

Δv_{NH}	Obs. energy (cm^{-1})	Assignment
	6501	$\|2,0\rangle_+$
2	6543	$\|2,0\rangle_-$
	6724	$\|1,1\rangle$
	9558	$\|3,0\rangle_\pm$
3	9849	$\|2,1\rangle_+$
	9934	$\|2,1\rangle_-$
	12435	$\|4,0\rangle_\pm$
4	12873	$\|3,1\rangle_\pm$
5	15115	$\|5,0\rangle_\pm$
6	17680	$\|6,0\rangle_\pm$

[a]Observed energies are from deconvolution of the experimental spectra.

Table 8.3.

Observed Energies[a] (cm^{-1}) and Assignments of the Local Mode Peaks of the Methyl CH Bonds of Cyclopropyl Methyl Ketone.

Δv_{CH}	Obs. energy (cm^{-1})	Assignment[b,c]
2	5729	$\|2,0,0\rangle_{\pm}$
	5810	$\|0,0,2\rangle$
3	8404	$\|3,0,0\rangle_{\pm}$
	8603	$\|0,0,3\rangle$
4	11020	$\|4,0,0\rangle_{\pm}$
	11198	$\|0,0,4\rangle$
5	13464	$\|5,0,0\rangle_{\pm}$
	13702	$\|0,0,5\rangle$
6	15818	$\|6,0,0\rangle_{\pm}$
	16067	$\|0,0,6\rangle$

[a] Observed energies are from deconvolution of the experimental spectra.

[b] $|v,0,0\rangle_{\pm}$ ($\equiv |v,0\rangle_{\pm} |0\rangle$) are the symmetrized pure local mode states which have all of the vibrational quanta localized into one of the two equivalent methyl CH bonds of CPMK (see text).

$^{c}|0,0,v>(\equiv|0,0>|v>)$ are the pure local mode states which have all of the vibrational quanta localized in the unique methyl CH bond of CPMK (see text).

Table 8.4.

Tentative Assignments of the Combination Peaks of Monosubstituted Cyclopropanes.

Δv_{CH}	Molecule[a]	Obs. Energy (cm^{-1})	Tentative Assignment[b]
2	CPBr	5840	Sym. CH_2 stretch ν_1 (3012 cm^{-1}) + 2 x ν_{15} asym. CH_2 def. (1422 cm^{-1})
		5860	Sym. CH_2 stretch ν_1 (1312 cm^{-1}) + 2 x ν_4 sym. CH_2 def. (1446 cm^{-1})
3		8648	$\|2,0\rangle_+$ (5890 cm^{-1}) + 2 x ν_{15} asym. CH_2 def. (1422 cm^{-1})
		8990	$\|1,1\rangle$(6127 cm^{-1}) + 2 x ν_4 sym. CH_2 def. (1446 cm^{-1})
2	CPCN	5733	Deg. CH_2 stretch ν_1 (3058 cm^{-1}) + 2 x ν_6 CH def. (1348 cm^{-1})
		5900	Sym. CH_2 stretch ν_2 (3030 cm^{-1}) + 2 x ν_5 sym. CH_2 def. (1460 cm^{-1})
3		8671	$\|2,0\rangle_+$ (5933 cm^{-1}) + 2 x ν_{17} asym. CH_2 def. (1437 cm^{-1})

Table 8.4...cont'd...

Δv_{CH}	Molecule[a]	Obs. Energy (cm^{-1})	Tentative Assignment[b]
		9044	$\|1,1\rangle$(6164 cm^{-1}) + 2 x ν_5 sym. CH_2 def. (1460 cm^{-1})
2	CPAM	5688	CH stretch ν_4 (2964 cm^{-1}) + 2 x ν_7 CH bend in plane (1371 cm^{-1})
		5777	Antisym. stretch ν_2 (3084 cm^{-1}) + 2 x ν_7 CH bend in plane (1371 cm^{-1})
		5848	Antisym. stretch ν_2 (3084 cm^{-1}) + 2 ν_{19} sym. CH_2 def. (1418 cm^{-1})
3		8463	$\|1,1\rangle$ (6123 cm^{-1}) + 2 x ν_8 Ring breathing (1213 cm^{-1})
		8982	$\|1,1\rangle$(6123 cm^{-1}) + 2 x ν_6 CH_2 def. (1453 cm^{-1})
4		11040	$\|3,0\rangle_{\pm}$ (8734 cm^{-1}) + 2 x ν_8 Ring breathing (1213 cm^{-1})
		10772	$\|3,0\rangle_{\pm}$ (8734 cm^{-1}) + 2 x ν_{21} CH_2 wag (1037 cm^{-1})

Table 8.4...cont'd...

Δv_{CH}	Molecule[a]	Obs. Energy (cm^{-1})	Tentative Assignment[b]
2	CPMK	5616	2962 cm^{-1} + 2 x 1352 cm^{-1}
		5771	2962 cm^{-1} + 2 x 1420 cm^{-1}
3		8504	$\|0,0,2\rangle$ (5810 cm^{-1}) + 2 x 1383 cm^{-1}

[a]CPBr = Cyclopropyl bromide, CPCN = Cyclopropyl cyanide

CPAM = Cyclopropyl amine, CPMK = Cyclopropyl methyl ketone

[b]Fundamental frequencies for CPBr, CPCN, CPAM, and CPMK are from Refs. 132, 134, 127, and 130, respectively.

Table 8.5.

Local Mode Harmonic Frequencies and Anharmonicity Constants of the Nonequivalent Oscillators of the Cycloalkanes and Cycloalkenes.

Molecule	Oscillator type	$\omega(cm^{-1})$	$\omega x(cm^{-1})$	Correlation coefficient
Cyclopropyl bromide	$-CH_2$	3144.6±0.7	57.2±0.2	-0.9999
	-CH	3169.4±6.5	57.7±1.5	-0.9989
Cyclopropyl cyanide	$-CH_2$	3173.1±2.9	59.5±0.6	-0.9998
	-CH	3187.9±2.2	58.9±0.5	-0.9998
Cyclopropylamine	$-CH_2$	3150.0±2.0	59.2±0.5	-0.9999
	-CH	3161.6±4.3	57.8±1.0	-0.9996
	-NH	3513.6±3.9	81.3±0.9	-0.9998
Cyclopropyl methyl ketone	$-CH_2$	3154.2±1.2	58.4±0.3	-0.9999
	-CH	3171.5±2.6	58.0±0.6	-0.9998
	$-CH_3$(op)	3032.1±5.9	56.4±1.3	-0.9991
	$-CH_3$(ip)	3087.0±10.7	57.9±2.4	-0.9973
Cyclopentane[a]	equitorial	3061 ± 7	63.1±1.3	-
	axial	3049 ± 5	67.2±0.9	-

Table 8.5...cont'd...

Molecule	Oscillator type	$\omega(cm^{-1})$	$\omega x(cm^{-1})$	Correlation coefficient
Cyclohexane[a]	equitorial	3009 ± 10	60.4±1.9	-
	axial	2987 ± 12	62.0±2.2	-
Cycloheptane[a]	$-CH_2$	3003 ± 25	62.0±4.1	-
Cyclooctane[a]	$-CH_2$	3027 ± 25	66.0±4.1	-
Cyclopentene[a]	$-CH_2$	3057 ± 9	67.3±2	
	C=CH	3163 ± 7	59.4±1.6	-
Cyclohexene[a]	$-CH_2$	2996 ± 4	60.1±0.9	-
	C=CH	3111 ± 4	59.2±0.9	-
Cycloheptene[a]	$-CH_2$	3016 ± 16	63.9±3.5	-
	C=CH	3121 ± 12	62.8±3.0	-
Benzene[b]	aryl	3148.6	57.6	-

[a] ω and ωx values from Ref. 37.

[b] ω and ωx values from Ref. 136.

Table 8.6.

Observed and Calculated Energies (cm^{-1}) of the Local Mode Peaks of Ring CH Bonds of Monosubstituted Cyclopropanes.

C_3H_5Br		C_3H_5CN		$C_3H_5NH_2$		$C_3H_5OCH_3$		
Obs.	Calc.	Obs.	Calc.	Obs.	Calc.	Obs.	Calc.	Assignment
5890	5879	5933	5934	5895	5885	5897	5892	$\|2,0\rangle_+$
5947	5946	5993	5989	5947	5945	5959	5958	$\|2,0\rangle_-$
6000	5993	6026	6022	5976	5976	5995	5995	$\|2\rangle$
6127	6127	6164	6164	6123	6123	6141	6141	$\|1,1\rangle$
8749	8694	8799	8765	8734	8695	8758	8710	$\|3,0\rangle_+$
8749	8722	8799	8785	8734	8718	8758	8737	$\|3,0\rangle_-$
8814	8816	8852	8857	8785	8791	8822	8818	$\|3\rangle$
8897	8919	8962	8985	8938	8918	9006	8937	$\|2,1\rangle_+$
9102	9111	9157	9163	9092	9102	9122	9131	$\|2,1\rangle_-$
11433	11395	11498	11473	11421	11383	11451	11410	$\|4,0\rangle_+$
11433	11402	11498	11477	11421	11388	11451	11417	$\|4,0\rangle_-$

Table 8.6...cont'd...

C_3H_5Br		C_3H_5CN		$C_3H_5NH_2$		$C_3H_5OCH_3$		
Obs.	Calc.	Obs.	Calc.	Obs.	Calc.	Obs.	Calc.	Assignment
11506	11504	11571	11574	11508	11490	11516	11526	$\|4\rangle$
11756	11667	11817	11762	-	11669	-	11689	$\|3,1\rangle_+$
11827	11810	11893	11885	11802	11799	11820	11831	$\|3,1\rangle_-$
14006	13973	14078	14054	13972	13945	14019	13986	$\|5,0\rangle_+$
14006	13974	14078	14055	13972	13946	14019	13987	$\|5,0\rangle_-$
14100	14116	14171	14173	14066	14074	14124	14117	$\|5\rangle$
14505	14362(+)	14576	14474(+)	14494	14358(+)	14521	14384(+)	$\|4,1\rangle_\pm$
	14441(-)		14535(-)		14426(-)		14463(-)	
16469	16433	16546	16515	16416	16387	16471	16441	$\|6,0\rangle_\pm$
16624	16593	16661	16654	16539	16542	16592	16592	$\|6\rangle$
17073	16965(+)	17173	17080(+)	17096	16946(+)	17104	16985(+)	$\|5,1\rangle_\pm$
	16993(-)		17099(-)		16967(-)		17012(-)	

Table 8.7.

Observed and Calculated Energies (cm^{-1}) of the Local Mode Peaks of the Δv_{NH} = 2 - 6 Spectra of Cyclopropylamine.

Δv_{NH}	Observed[a]	Calculated	Assignment
	6501	6517	$\|2,0\rangle_+$
2	6543	6540	$\|2,0\rangle_-$
	6724	6724	$\|1,1\rangle$
	9558	9554	$\|3,0\rangle_+$
	9558	9558	$\|3,0\rangle_-$
3	9849	9838	$\|2,1\rangle_+$
	9934	9962	$\|2,1\rangle_-$
	12435	12420	$\|4,0\rangle_\pm$
4	12873	12868(+)	$\|3,1\rangle_\pm$
		12924(-)	
5	15115	15121	$\|5,0\rangle_\pm$
6	17680	17659	$\|6,0\rangle_\pm$

[a]Observed energies are from deconvolution of the experimental spectra.

Figure 8.1.

Liquid phase overtone spectra of monosubstituted cyclopropanes in the region of $\Delta v_{CH} = 2$. Spectra were measured at room temperature with a path length of 0.1 cm. Absorbances of cyclopropylamine, cyclopropyl cyanide, and cyclopropyl bromide have been offset by 0.6, 1.2, and 1.8 absorbance units, respectively.

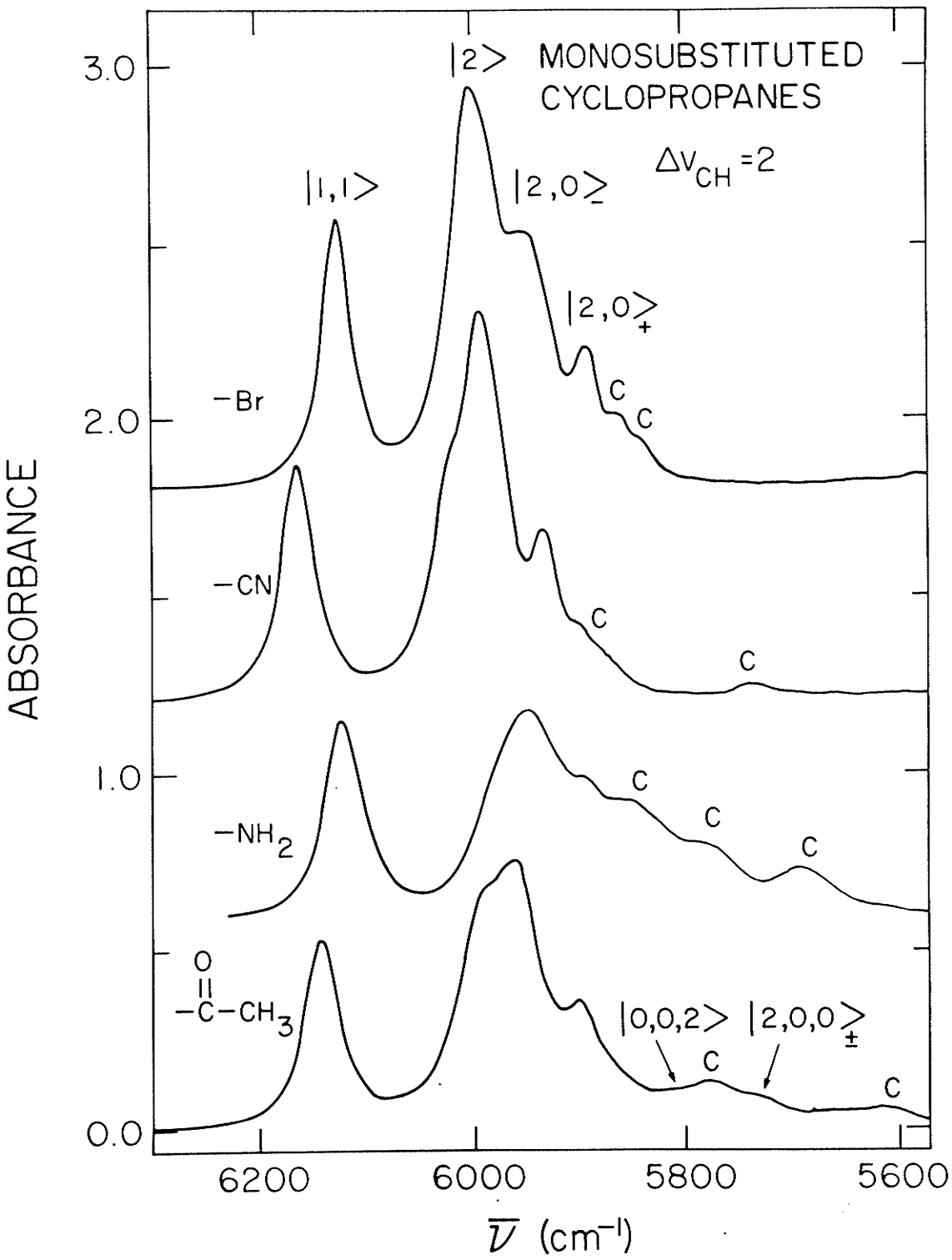
|2> MONOSUBSTITUTED
CYCLOPROPANES
ΔV_CH =2
|1,1>
|2,0>_
|2,0>+
C
C
−Br
−CN
C
C
−NH2
C
C
C
O
||
−C−CH3
|0,0,2>
|2,0,0>±
C
C
3.0
2.0
1.0
0.0
ABSORBANCE
6200
6000
5800
5600
ν̄ (cm⁻¹)

Figure 8.2.

Liquid phase overtone spectra of monosubstituted cyclopropanes in the region of $\Delta v_{CH} = 3$. Spectra were measured at room temperature with a path length of 1.0 cm. Absorbances of cyclopropylamine, cyclopropyl cyanide, and cyclopropyl bromide have been offset by 0.6, 1.2, and 1.8 absorbance units, respectively.

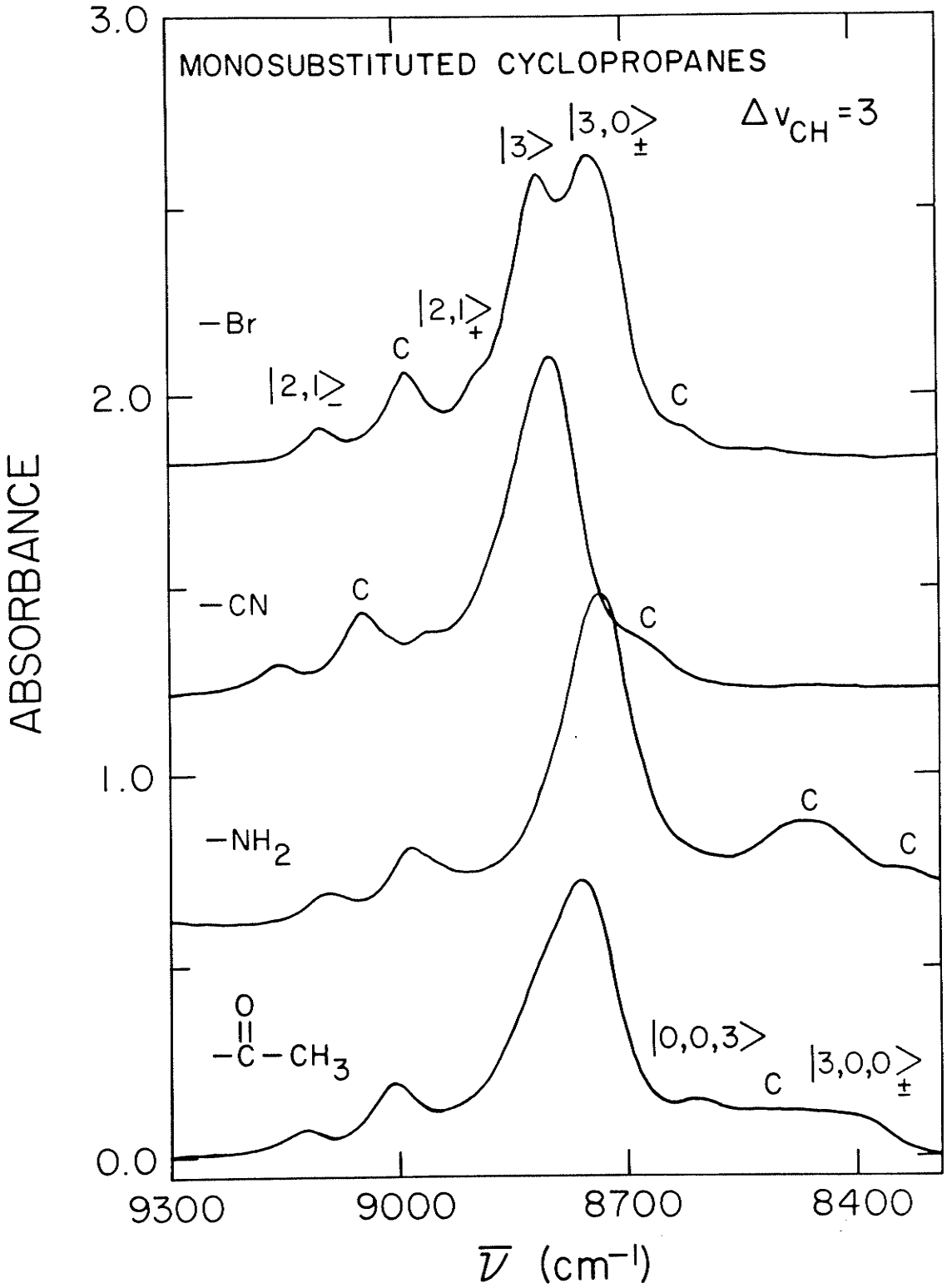
MONOSUBSTITUTED CYCLOPROPANES
$\Delta v_{CH} = 3$
$|3\rangle$
$|3,0\rangle_{\pm}$
$|2,1\rangle_{+}$
$|2,1\rangle_{-}$
C
−Br
−CN
$-NH_2$
$-\overset{O}{\overset{\|}{C}}-CH_3$
$|0,0,3\rangle$
$|3,0,0\rangle_{\pm}$
ABSORBANCE
3.0
2.0
1.0
0.0
9300
9000
8700
8400
$\bar{\nu}$ (cm^{-1})

Figure 8.3.

Liquid phase overtone spectra of monosubstituted cyclopropanes in the region of $\Delta v_{CH} = 4$. Spectra were measured at room temperature with a path length of 5.0 cm. Absorbances of cyclopropylamine, cyclopropyl cyanide, and cyclopropyl bromide have been offset by 0.2, 0.4, and 0.6 absrobance units, respectively.

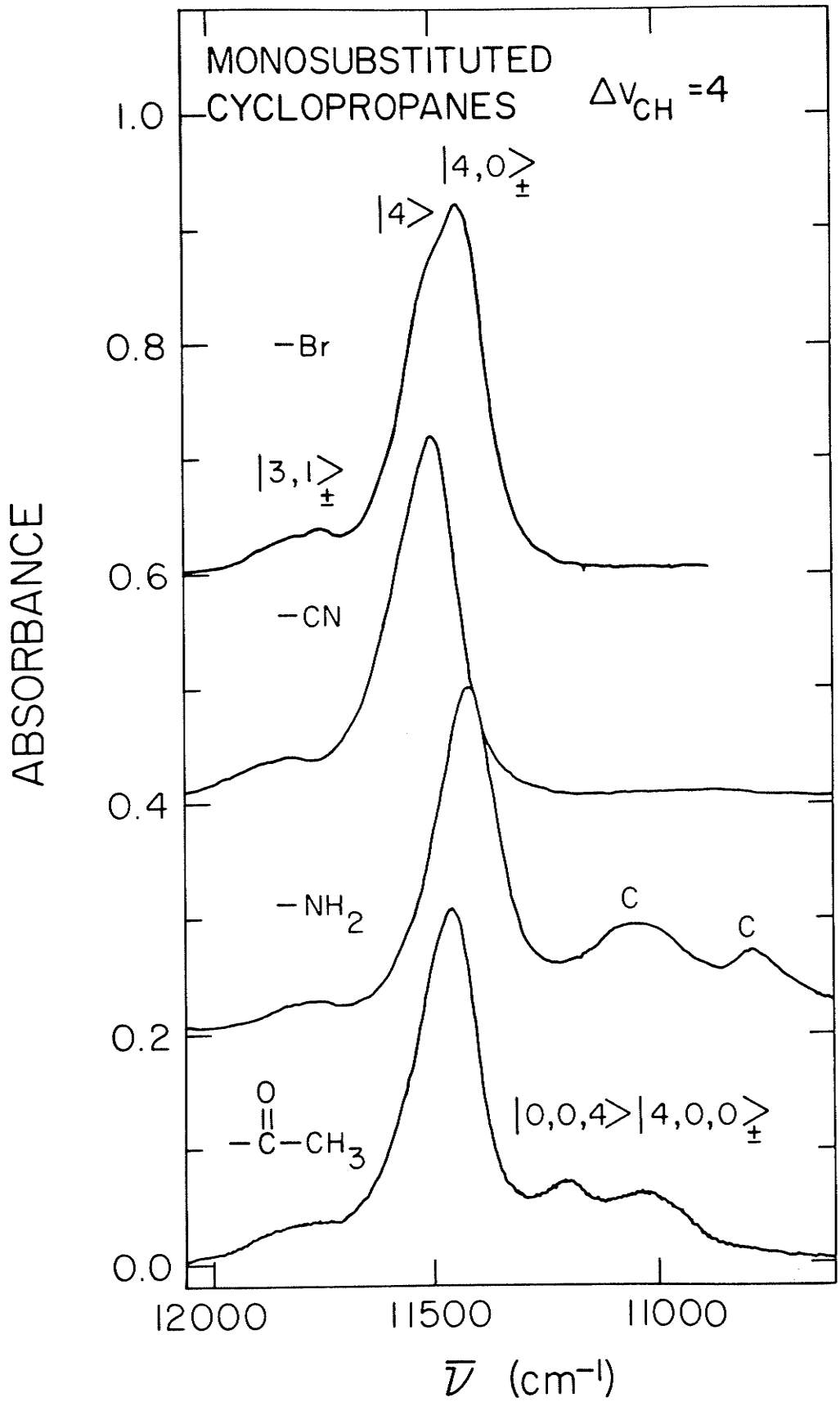
MONOSUBSTITUTED
CYCLOPROPANES
$\Delta V_{CH} = 4$
$|4,0\rangle_{\pm}$
$|4\rangle$
−Br
$|3,1\rangle_{\pm}$
−CN
−NH2
C
C
O
−C−CH3
$|0,0,4\rangle|4,0,0\rangle_{\pm}$
ABSORBANCE
1.0
0.8
0.6
0.4
0.2
0.0
12000
11500
11000
$\bar{\nu}$ (cm^{-1})

Figure 8.4.

Liquid phase overtone spectra of monosubstituted cyclopropanes in the region of $\Delta v_{CH} = 5$. Spectra were measured at room temperature with a path length of 5.0 cm. Absorbances of cyclopropylamine, cyclopropyl cyanide, and cyclopropyl bromide have been offset by 0.02, 0.04, and 0.06 absorbance units, respectively.

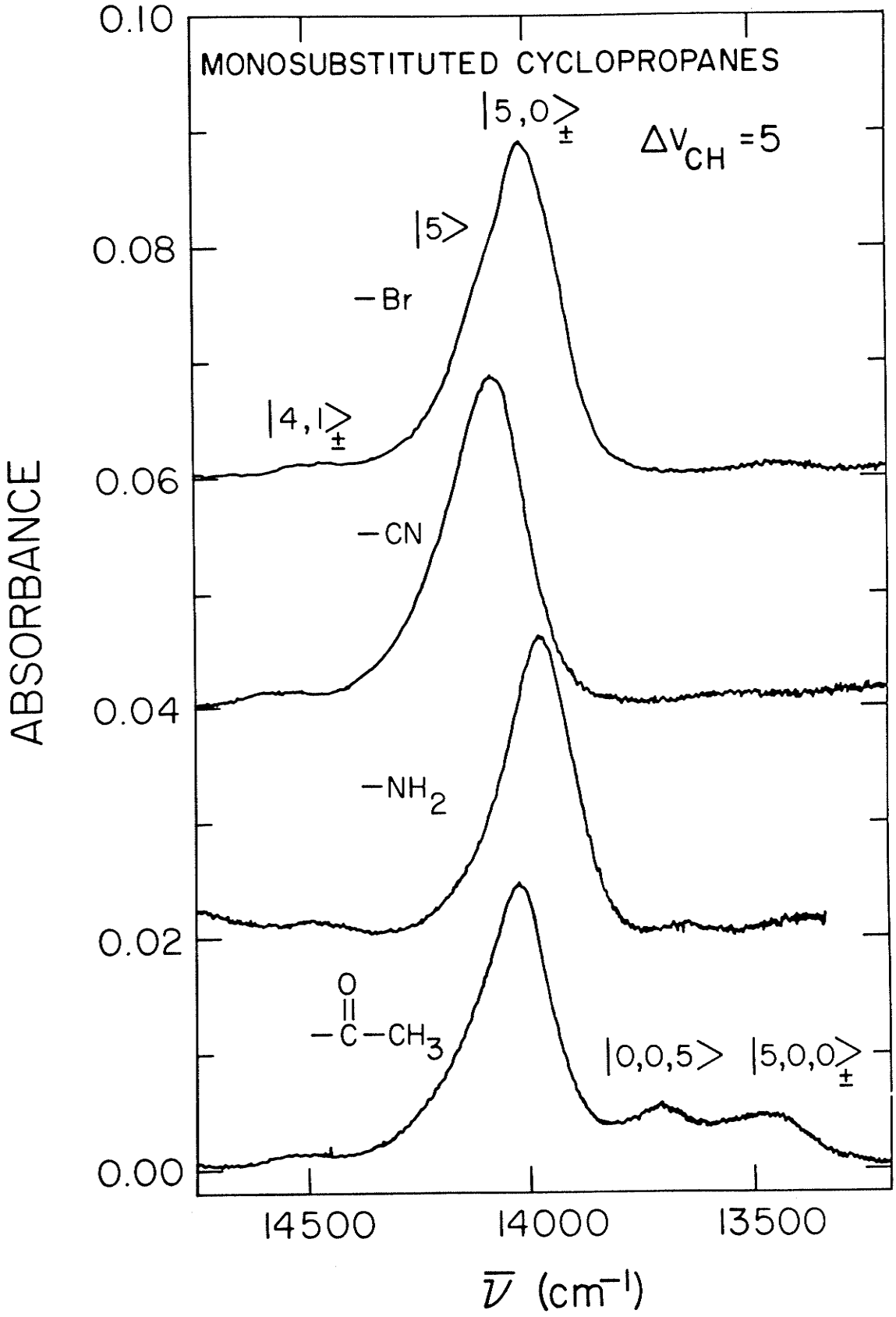
MONOSUBSTITUTED CYCLOPROPANES
$\Delta V_{CH} = 5$
$|5,0\rangle_{\pm}$
$|5\rangle$
$|4,1\rangle_{\pm}$
$|0,0,5\rangle$
$|5,0,0\rangle_{\pm}$
−Br
−CN
$-NH_2$
$-\overset{O}{\overset{\|}{C}}-CH_3$
ABSORBANCE
0.10
0.08
0.06
0.04
0.02
0.00
14500
14000
13500
$\bar{\nu}$ (cm^{-1})

Figure 8.5.

Liquid phase overtone spectra of monosubstituted cyclopropanes in the region of $\Delta v_{CH} = 6$. Spectra were measured at room temperature with a path length of 5.0 cm. All spectra are base line corrected. Absorbances of cyclopropylamine, cyclopropyl cyanide, and cyclopropyl bromide have been offset by 0.002, 0.004, and 0.006 absorbance units, respectively.

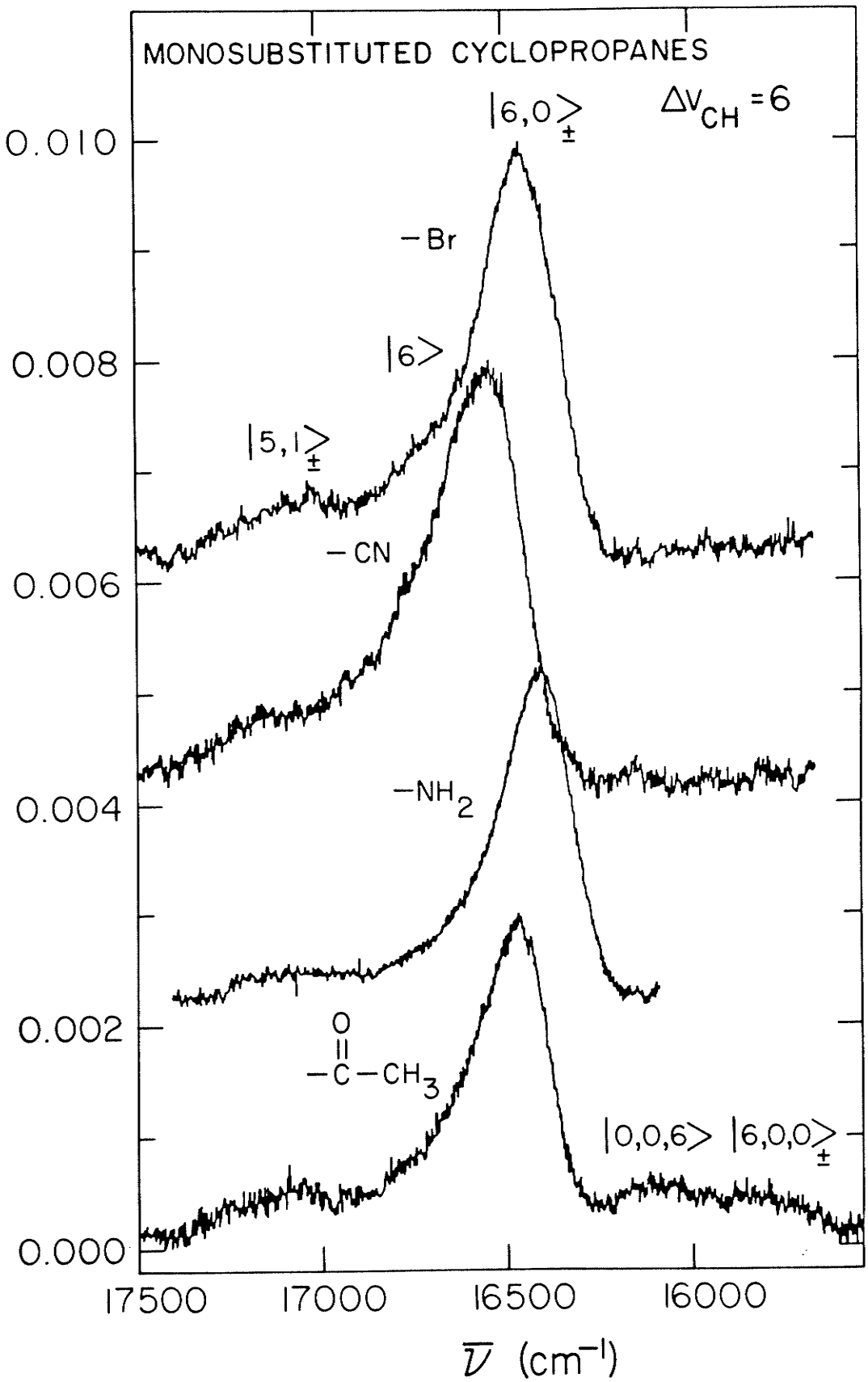
MONOSUBSTITUTED CYCLOPROPANES
$\Delta V_{CH} = 6$
$|6,0\rangle_{\pm}$
$|6\rangle$
$|5,1\rangle_{\pm}$
−Br
−CN
$-NH_2$
O
||
$-C-CH_3$
$|0,0,6\rangle$ $|6,0,0\rangle_{\pm}$
0.010
0.008
0.006
0.004
0.002
0.000
17500
17000
16500
16000
$\bar{\nu}$ (cm^{-1})

Figure 8.6.

Deconvoluted $\Delta v_{CH} = 3$ spectrum of cyclopropyl cyanide. The Lorentzian functions which were fit to the experimental (upper trace) spectrum are shown. The lower trace is the difference of the experimental and fit spectra.

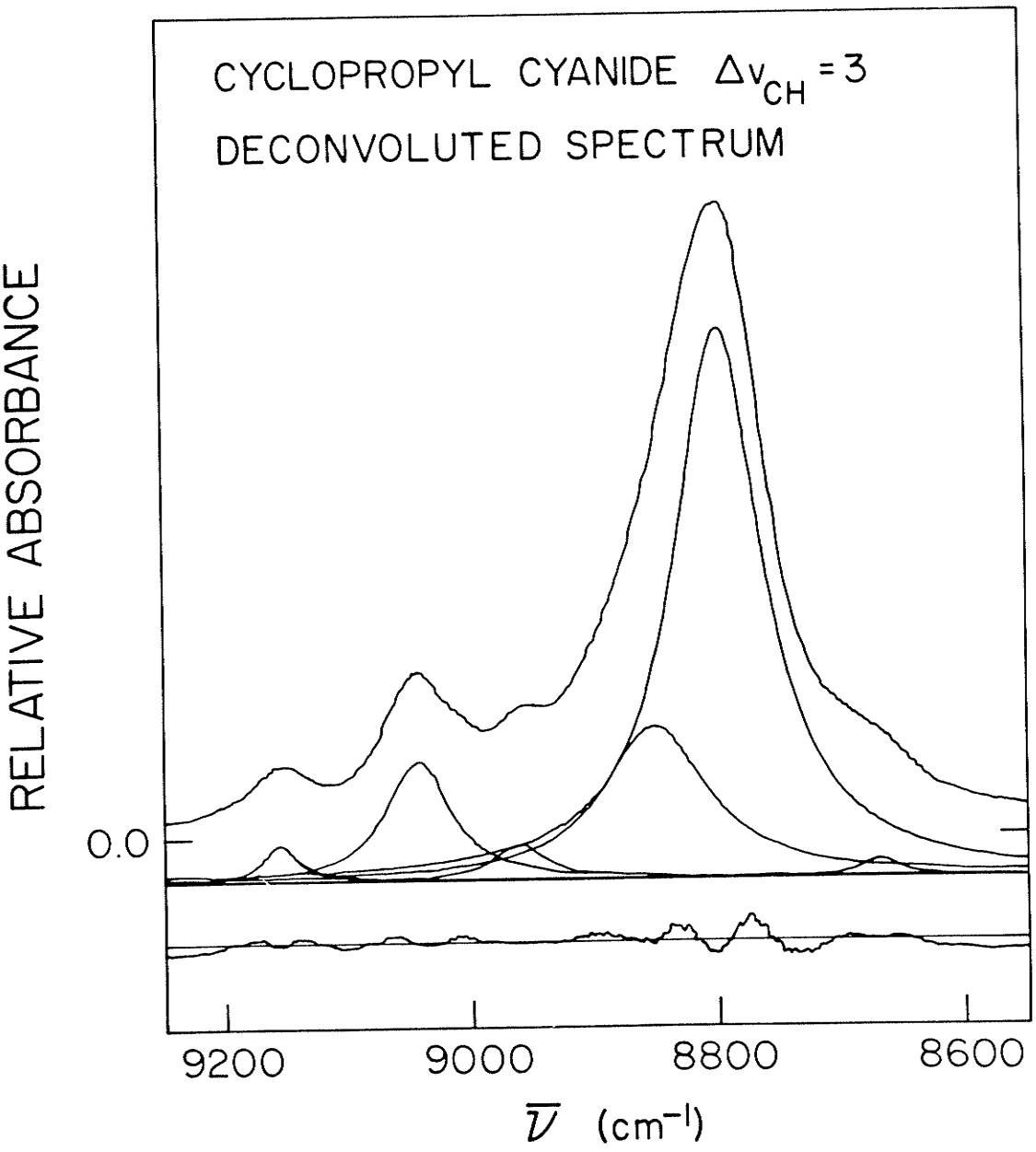
CYCLOPROPYL CYANIDE $\Delta v_{CH} = 3$
DECONVOLUTED SPECTRUM
RELATIVE ABSORBANCE
0.0
9200
9000
8800
8600
$\overline{\nu}$ (cm^{-1})

Figure 8.7.

Liquid phase overtone spectra of cyclopropylamine in the region of $\Delta v_{NH} = 2$ (lower spectrum) and $\Delta v_{NH} = 3$ (upper spectrum). Spectra were measured at room temperature. Path lengths for $\Delta v_{NH} = 2$ and $\Delta v_{NH} = 3$ were 0.1 and 1.0 cm, respectively. Lower abcissa and L.H.S. ordinate refers to $\Delta v_{NH} = 2$ spectrum; upper abcissa and R.H.S. ordinate refers to $\Delta v_{NH} = 3$ spectrum.

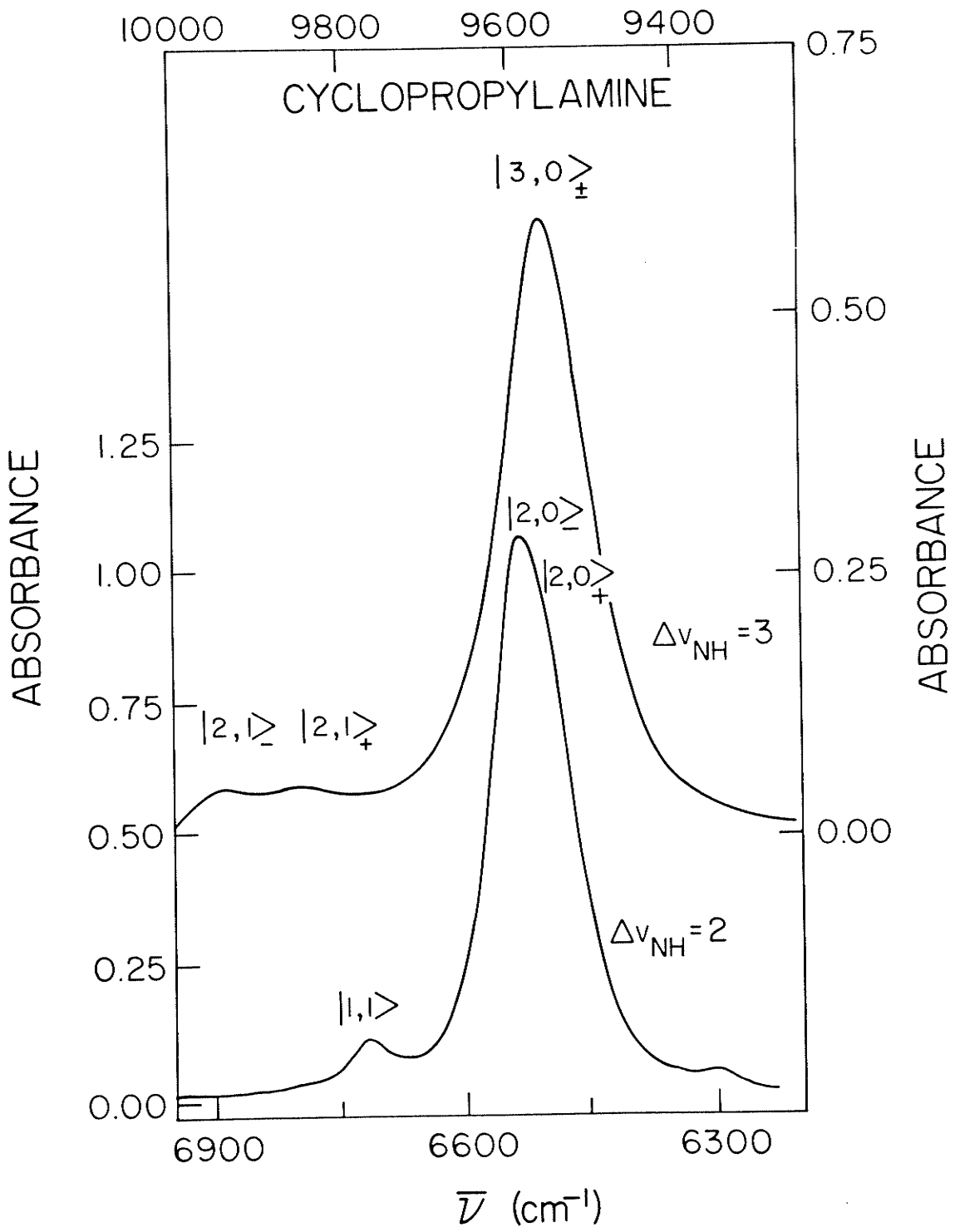
10000
9800
9600
9400
CYCLOPROPYLAMINE
|3,0>±
|2,0>−
|2,0>+
ΔνNH=3
|2,1>− |2,1>+
|1,1>
ΔνNH=2
ABSORBANCE
1.25
1.00
0.75
0.50
0.25
0.00
0.75
0.50
0.25
0.00
ABSORBANCE
6900
6600
6300
ν̄ (cm⁻¹)

Figure 8.8.

Liquid phase overtone spectra of cyclopropylamine in the region of $\Delta v_{NH} = 4$ (lower spectrum) and $\Delta v_{NH} = 5$ (upper spectrum). Spectra were measured at room temperature with a path length of 5.0 cm. Lower abcissa and L.H.S. ordinate refers to $\Delta v_{NH} = 4$ spectrum; upper abcissa and R.H.S. ordinate refers to $\Delta v_{NH} = 5$ spectrum.

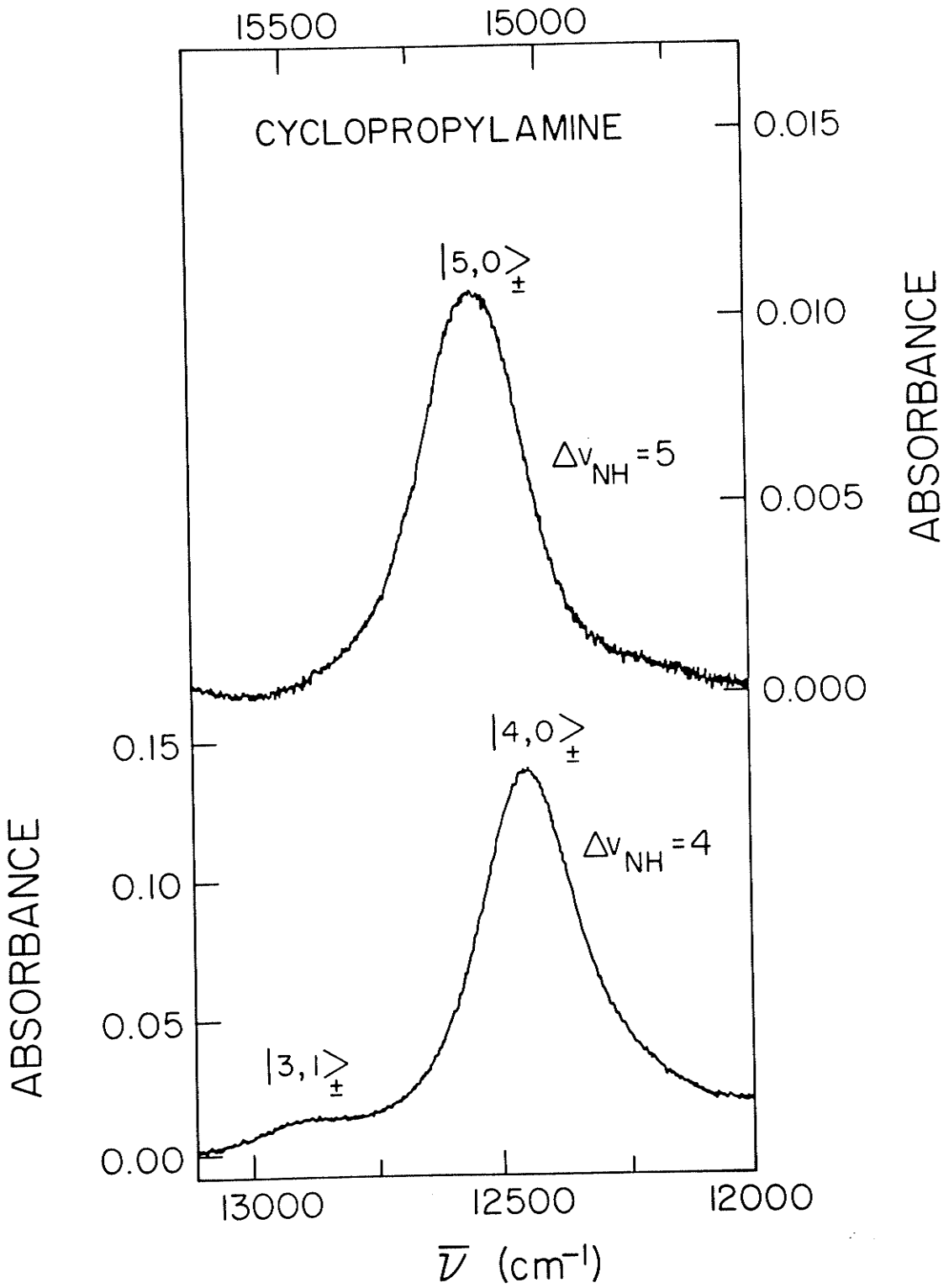
15500
15000
CYCLOPROPYLAMINE
0.015
0.010
0.005
0.000
ABSORBANCE
|5,0>±
ΔvNH=5
|4,0>±
ΔvNH=4
|3,1>±
0.15
0.10
0.05
0.00
ABSORBANCE
13000
12500
12000
ν̄ (cm⁻¹)

Figure 8.9.

Liquid phase overtone spectrum of cyclopropylamine in the region of $\Delta v_{NH} = 6$. Spectrum is base line corrected and was measured at room temperature with a path length of 5.0 cm.

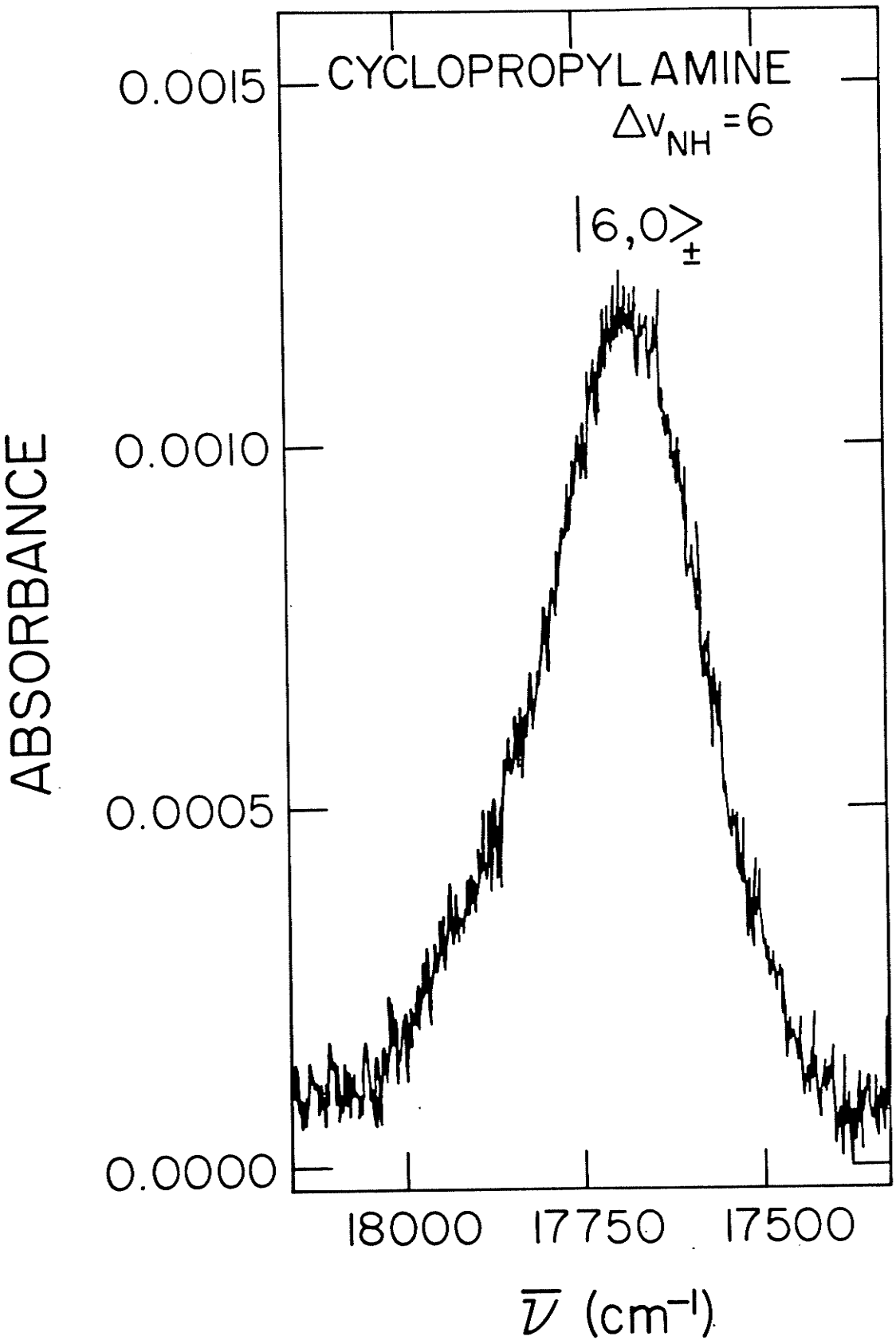
CYCLOPROPYLAMINE
$\Delta v_{NH} = 6$
$|6,0\rangle_{\pm}$
0.0015
0.0010
0.0005
0.0000
ABSORBANCE
18000
17750
17500
$\bar{\nu}$ (cm^{-1})

Figure 8.10.

Plots of the vibrational energy expression of a single Morse oscillator for the methylene and methine oscillators of cyclopropyl cyanide.

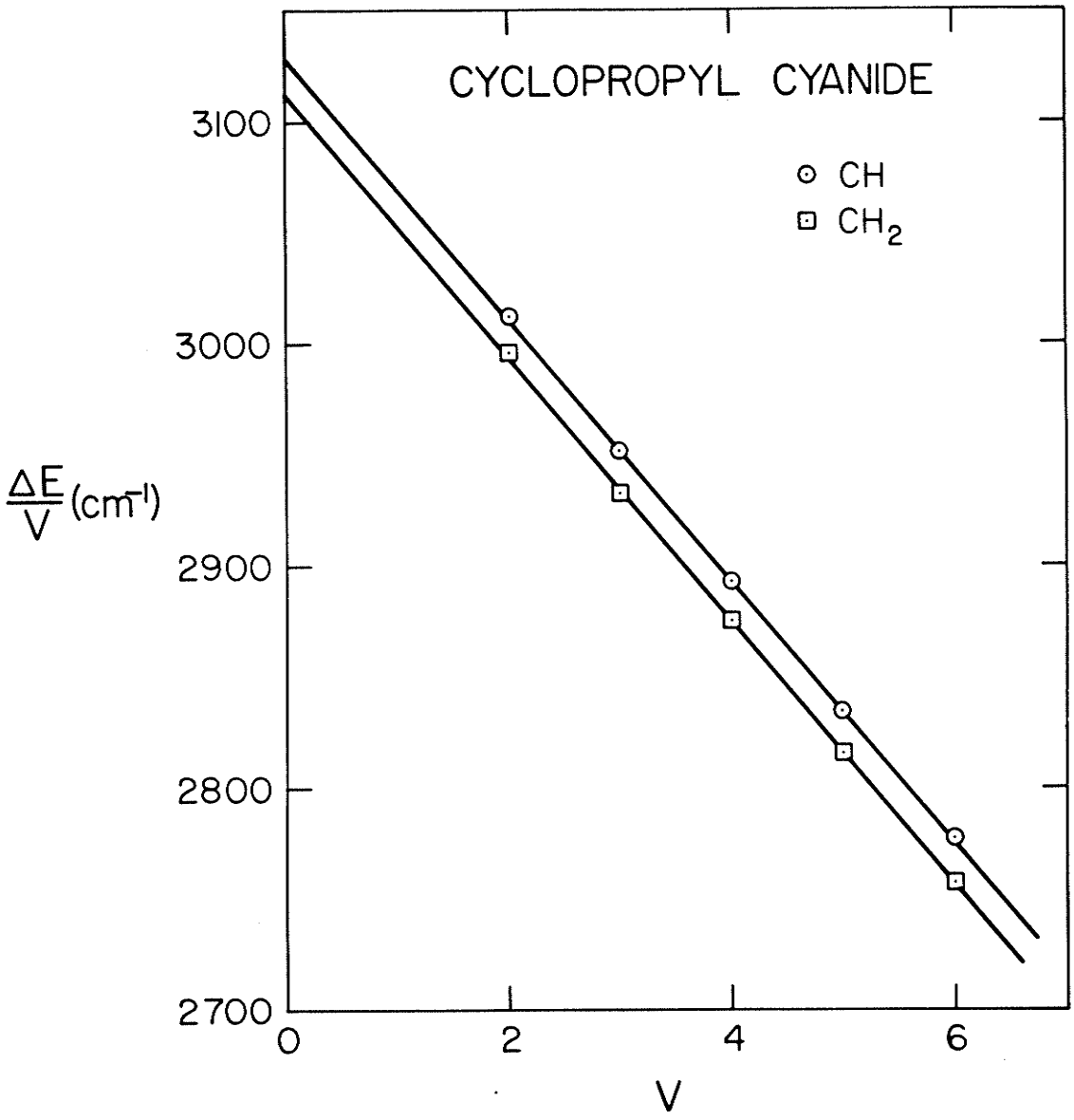
CYCLOPROPYL CYANIDE
CH
CH2
3100
3000
2900
2800
2700
ΔE/V (cm⁻¹)
0
2
4
6
V

CHAPTER 9

NONEQUIVALENT CH BONDS IN TRIMETHYLBENZENES

In this chapter the gas phase overtone spectra of the three trimethylbenzenes in the region of $\Delta v_{CH} = 3$ will be reported. The spectral features of these spectra will be related to structurally and conformationally nonequivalents bonds. Through the analysis of the methyl regions of the spectra, it will be demonstrated that absorptions from methyl groups below and above the barrier to internal rotation are resolvable in the overtone spectra.

i) Introduction

Gas phase overtone spectra with the use of the local mode model provide information about the conformational properties of molecules[27-29,32,39-43]. The time scale of the near-IR experiment permits the study of processes which are much too fast to be studied by conventional techniques like NMR. In a recent study of toluene and the xylenes[28], and in another study of the fluorotoluenes[32], Gough and Henry[28] and Henry et al.[32] found rather surprising results. In the presence of a high barrier to methyl internal rotation, they observed spectral features that could be associated with the lowest energy conformation of the methyl groups. In the presence of very low barriers to methyl internal rotation, they still observed spectral features which could be associated with a conformational preference for the methyl groups. However, they also observed other spectral features which appeared to have no other explanation than that they arose from transitions originating from rotational levels above the methyl rotational barrier.

In this chapter the gas phase overtone spectra of the three trimethylbenzenes in the region of $\Delta v_{CH} = 3$ will be reported. The liquid phase overtone spectra of these molecules have been reported previously[110,146-148]. However, intermolecular interactions in the liquid phase cause significant line broadening which obscure the details of the spectral features which relate to conformational properties. The gas phase results of this chapter provide information about the nonequivalent aryl CH bonds in the trimethylbenzenes. They also provide a convincing confirmation of earlier suggestions by Gough and Henry[28] and Henry et al.[32] concerning the interpretation of

spectral features in terms of the conformational properties of the methyl groups.

ii) Results and Discussion

The gas phase spectra of the three trimethylbenzenes in the region of $\Delta v_{CH} = 3$ are shown in Figure 9.1. The deconvoluted peak positions and the relative areas are listed in Table 9.1 along with the peak assignments. The peak positions and the relative areas of the two methyl peaks at ~8400 and ~8500 cm^{-1} are nearly the same for all three spectra. Similarly, the peak position of the center methyl peak is nearly the same in the spectra of the two molecules in which it occurs (1,3,5- and 1,2,4-trimethylbenzene). An example of the deconvolution results is presented in Figure 9.2 for the spectrum of 1,3,5-trimethylbenzene. The last column of Table 9.1 lists CH bond lengths, r_{CH}^{LM}, which are obtained from the following correlation[27-31]:

$$r_{CH}^{LM}(\text{Å}) = 1.084 - \left(\frac{\Delta\bar{\nu}}{11\Delta v_{CH}}\right) 0.001 \qquad (9.1)$$

$\Delta\bar{\nu}$ is the frequency shift relative to the $\Delta v_{CH} = 3$ transition in benzene ($\bar{\nu}$(benzene) = 8786 cm^{-1} [50]).

a) Aryl CH Bonds

In the previous work of Gough and Henry[28] with toluene and the xylenes, methyl substitution was found to shift aryl CH bond frequencies to lower values. The resultant bond lengthening (cf. Eq. (9.1)) was found to be in agreement with geometry-optimized ab initio molecular orbital results[149,150]. The effect was short range and was measurable only for aryl CH bonds ortho to methyl substituents. The results for the aryl CH bonds of the trimethylbenzenes are precisely those expected on the basis of previous observations[28].

A single peak is observed in the aryl region (8700 - 8800 cm^{-1}) of the spectrum of 1,3,5-trimethylbenzene. The three aryl CH bonds of this molecule are equivalent with an ortho influence from two of the three methyl groups and a para influence from the third. The aryl CH bonds of 1,3,5-trimethylbenzene are designated as (o+o+p) type.

The aryl region of the spectrum of 1,2,3-trimethylbenzene can be deconvoluted into two component Lorentzian peaks (see Table 9.1) with an area ratio (high to low frequency) of approximately 1:1.8. 1,2,3-Trimethylbenzene has two types of aryl CH bonds. Two bonds are of (o+m+p) type and one is of (m+m+p) type. Both on the basis of relative intensity and expected frequency shift, the (m+m+p) bond is assigned to the high frequency peak and the (o+m+p) bonds to the low frequency peak.

The aryl region of the spectrum of 1,2,4-trimethylbenzene is also a doublet for which the ratio of the deconvoluted areas (high to low frequency) is 1.7:1. The three aryl CH bonds experience (o+m+m), (o+m+p), and (o+o+m) influence. On the basis of previous work[28], the two former bond types are not expected to be spectrally resolved. Thus, once again, both on the basis of relative intensity and expected frequency shift, both the (o+m+m) bond and the (o+m+p) bond is assigned to the high frequency peak, and the (o+o+m) bond to the low frequency peak.

The data of Table 9.1 show that the frequencies corresponding to the different aryl CH bonds follow the expected order (m+m+p) > (o+m+m) $\simeq$ (o+m+p) > (o+o+m) $\simeq$ (o+o+p). Thus it appears that the net effect of the methyl substituents on the aryl CH bonds is additive in agreement with the conclusions of earlier liquid phase studies[146,148].

Moreover, in agreement with earlier results[28], only ortho methyl substituents affect aryl CH bond lengths.

b) Methyl CH Bonds

In the previous study[28] of the gas phase spectra of toluene and the xylenes, two peaks were observed in the methyl region of the spectrum of o-xylene, and three peaks in the methyl regions of the spectra of toluene, m-xylene, and p-xylene. In the o-xylene spectrum, the lower frequency peak is approximately twice as intense as the higher frequency peak. In o-xylene, the most stable conformer is a planar one[150-152] where the methyl groups have one CH bond in the ring plane and two at 60°. The spectral splitting corresponds to a bond length difference of 0.003 Å, in close agreement with the value of 0.002 Å predicted by ab initio calculations[150]. Thus the low and high frequency peaks can be associated with the out-of-plane and in-plane methyl CH bonds, respectively.

In the methyl regions of the spectra of toluene, m-xylene, and p-xylene, the frequencies of the two outside peaks are almost the same as the frequencies of the two methyl peaks in o-xylene. On this basis, these peaks were assigned also to a planar methyl conformation. Thus, the highest frequency peak was associated with the in-plane methyl CH and the lowest frequency peak with the two methyl CH bonds at 60°. Ab initio MO calculations for toluene[149,150] predict a bond length difference of 0.002 Å between the two types of methyl CH bonds, in close agreement with the value (0.003 Å) predicted by the spectral splitting. The barrier to internal rotation of the methyl groups in toluene, m-xylene, and p-xylene is very low[150,153]. The central peaks in the methyl regions of the spectra of these three molecules have been assigned[28] to transitions originating from rotational levels above this rotational barrier. Results similar to those for o-, m-,

and p-xylene have been obtained in the methyl regions of the overtone spectra of o-, m-, and p-fluorotoluene[32]. The spectra of the two ortho molecules correspond, as do the spectra of the two meta and the two para molecules.

As with the aryl CH bonds, the spectral results for the methyl CH bonds are those expected on the basis of previous observations[28]. For all three trimethylbenzenes, the relative intensity of the methyl peaks is higher than in the xylenes in accord with the increased methyl to aryl CH bond ratio. Two peaks are observed in the methyl region (8370 - 8530 cm^{-1}) of the spectrum of 1,2,3-trimethylbenzene. The peak positions and relative intensities are the same, to within experimental error, as the corresponding features in the spectrum of o-xylenes. Similarly, the methyl region spectrum of 1,3,5-trimethylbenzene corresponds closely to the spectrum of m-xylene. Thus the conformation of the methyl groups in 1,2,3- and 1,3,5-trimethylbenzenes is expected to be virtually identical with the conformation of the methyl groups in o-xylene and m-xylene, respectively. The lowest energy conformer will be a planar one. The highest frequency methyl peak is associated with the in-plane methyl CH, and the lowest frequency peak with the two methyl CH bonds at 60°, in both molecules. The spectral splitting predicts the in-plane methyl CH to be shorter by 0.003 Å. Because the barrier to internal methyl rotation is very low in 1,3,5-trimethylbenzene, a third methyl peak is observed, which is absent in 1,2,3-trimethylbenzene, and is assigned to transitions originating from rotational levels above the rotational barrier.

The methyl region of the spectrum of 1,2,4-trimethylbenzene is particularly interesting. It appears to be a superposition of the methyl regions of the spectra of toluene and o-xylene. Thus the orientation of the two adjacent methyl groups is expected to be the same as in o-xylene. The third methyl group, with a low barrier to internal rotation, will be the only one which gives rise to the central methyl peak corresponding to transitions from rotational levels above the rotational barrier. As expected, the relative intensity of this central peak is lower in 1,2,4-trimethylbenzene (0.13) than in 1,3,5-trimethylbenzene (0.19).

In addition to the peaks listed in Table 9.1, three lower intensity peaks are observed at approximately 8125, 8325, and 8600 cm^{-1} in the spectra of all three trimethylbenzenes. These peaks can be assigned to combinations involving two quanta of CH stretching and two quanta of CH bending. They have also been observed in the spectra of toluene[28], the xylenes[28], and the fluorotoluenes[32].

In summary, the spectra of the trimethylbenzenes can be interpreted on the same basis as the spectra of toluene[28], the xylenes[28], and the flurotoluenes[32]. The results provide further support for the explanation of the methyl regions of these spectra in terms of contributions from states characteristic of the lowest energy conformation as well as from "free rotor" states.

Table 9.1.

Deconvoluted Peak Positions (cm^{-1}), Peak Areas, Assignments and Bond Lengths (Å) for the Gas Phase Spectra of the Trimethylbenzenes in the Region of $\Delta v_{CH} = 3$.

Molecule	Peak Position[a]	Assignment	Bond Length[b] r_{CH}^{LM}
1,2,3-trimethylbenzene	8793 (1.0)	aryl m+m+p	1.084
	8740 (1.8)	o+m+p	1.085
	8495 (1.0)	methyl CH(in plane)	1.093
	8401 (1.6)	CH(out of plane)	1.096
1,2,4-trimethylbenzene	8744 (1.7)	aryl o+m+m, o+m+p	1.085
	8688 (1.0)	o+o+m	1.087
	8502 (1.0)	methyl CH(in plane)	1.093
	8444	CH(free)[c]	
	8399 (1.7)	CH(out of plane)	1.096
1,3,5-trimethylbenzene	8704	aryl o+o+p	1.086
	8503 (1.0)	methyl CH(in plane)	1.093
	8446	CH(free)[c]	
	8408 (1.5)	CH(out of plane)	1.095

[a]Relative areas for peaks of a given bond type are given in parenthesis.

[b]Obtained from overtone frequency-bond length correlation, see text.

[c]See text.

Figure 9.1.

The gas phase overtone spectrum of the three trimethylbenzenes at 90°C in the region of $\Delta v_{CH} = 3$. Path length, 8.7 m. Each spectrum is an average of four scans. Absorbances of 1,2,4- and 1,3,5-trimethylbenzenes have been offset by 0.04 and 0.08 absorbance units, respectively.

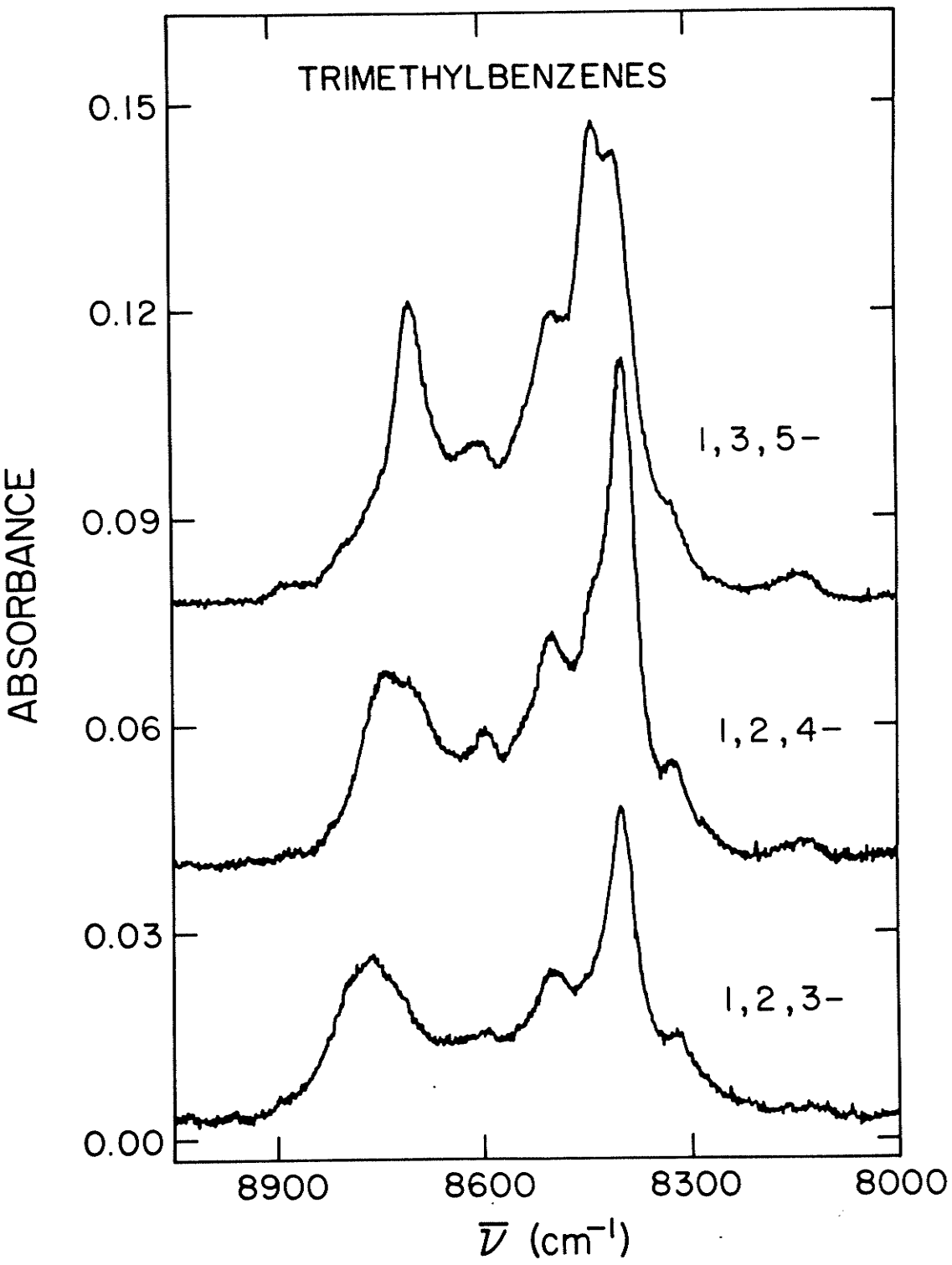
TRIMETHYLBENZENES
ABSORBANCE
0.15
0.12
0.09
0.06
0.03
0.00
1,3,5-
1,2,4-
1,2,3-
8900
8600
8300
8000
$\bar{\nu}$ (cm^{-1})

Figure 9.2.

The calculated (- - -) and experimentally observed (——) overtone spectra of 1,3,5-trimethylbenzene in the region of $\Delta v_{CH} = 3$. The calculated band envelope represents the sum of Lorentzian peaks obtained from a computer-assisted deconvolution of the experimentally observed overtone band. The individual Lorentzian functions are also shown. The lower trace is the difference of the experimental and calculated spectra.

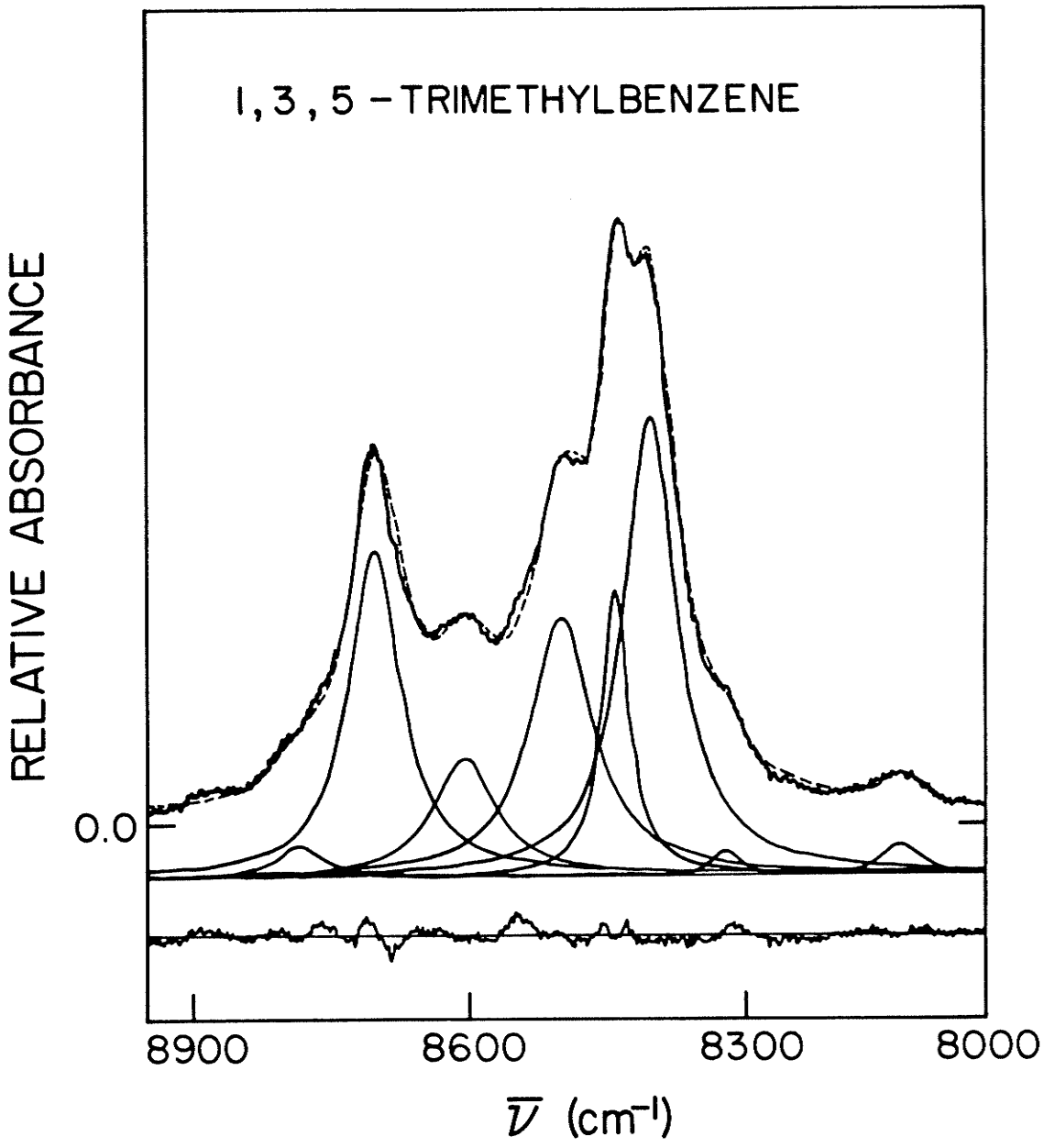
1,3,5 – TRIMETHYLBENZENE
RELATIVE ABSORBANCE
0.0
8900
8600
8300
8000
$\bar{\nu}$ (cm^{-1})

CHAPTER 10

CONFORMATIONAL PREFERENCE OF $-CHCl_2$ AND $-CHBr_2$ GROUPS IN BENZAL CHLORIDE AND BENZAL BROMIDE

In this chapter liquid phase CH-stretching overtone spectra of benzal chloride ($C_6H_5CHCl_2$) in the region of Δv_{CH} = 3 - 6 and of benzal bromide ($C_6H_5CHBr_2$) in the region of Δv_{CH} = 3 - 5 will be presented. The alkyl regions of the overtone spectra of both $C_6H_5CHCl_2$ and $C_6H_5CHBr_2$ contain information about the conformational preference of the dichloromethyl and dibromomethyl groups of these molecules. The equilibrium geometry of benzal chloride will also be reported which is determined from ab initio calculations at the SCF level with STO-3G and 4-31G basis sets.

i) Introduction

In a recent Raman study[85], Ribeiro-Claro and Teixeira-Dias have suggested that the $-CHCl_2$ group of $C_6H_5CHCl_2$ exists in two conformers, one in which the CH bond lies in the ring plane (planar) and the other in which it makes an angle of 90° with the ring plane (orthogonal). The planar and orthogonal conformers have been associated with the two bands in the CH-stretching region of the spectrum of the $-CHCl_2$ group. The authors state that the existence of two conformers is supported by solvent and temperature effects and by CNDO/2 calculations.

In another very recent study[84], Schaefer and Penner have used geometry optimized STO-3G molecular orbital computations with the benzene framework constrained to be planar and hexagonal to show that the potential for rotation of the $-CHCl_2$ group of $C_6H_5CHCl_2$ is two fold (single minimum), and that in the conformer of lowest energy the alkyl CH bond prefers the plane of benzene ring. A value of 11.6 ± 0.1 kJ mol^{-1} was derived for the internal rotational potential of $-CHCl_2$.

In this chapter the liquid phase overtone spectra of $C_6H_5CHCl_2$ (Δv_{CH} = 3 - 6) and $C_6H_5CHBr_2$ (Δv_{CH} = 3 - 5) will be reported. These spectra will be analyzed in terms of a local mode model. An analysis of the alkyl regions of the overtone spectra of $C_6H_5CHBr_2$ shows that the $-CHBr_2$ group in this molecule exists in a single conformation. However, in the alkyl regions of the overtone spectra of $C_6H_5CHCl_2$, spectral features are identified which can be assigned to absorptions due to the planar and orthogonal conformations of the $-CHCl_2$ group. The calculations of Schaefer and Penner[84] are extended to the larger

4-31G basis set to examine the effect of restricting the benzene ring to a planar hexagonal geometry.

ii) Results and Discussion

The liquid phase overtone spectra of $C_6H_5CHCl_2$ and $C_6H_5CHBr_2$ in the regions of Δv_{CH} = 3 and 4 are shown in Figures 10.1-10.4. In these Figures, the Lorentzian functions which were fitted to the experimental spectra to obtain the individual peak positions are also shown. The liquid phase overtone spectra of $C_6H_5CHCl_2$ in the regions of Δv_{CH} = 5 and Δv_{CH} = 6 are shown in Figure 10.5. The liquid phase overtone spectrum of $C_6H_5CHBr_2$ in the region of Δv_{CH} = 5 is shown in Figure 10.6. The individual peak positions for Δv_{CH} = 5 and 6 of $C_6H_5CHCl_2$ and Δv_{CH} = 5 of $C_6H_5CHBr_2$ were also obtained through deconvolution but the corresponding Lorentzian functions for these regions are not shown.

The sample of $C_6H_5CHBr_2$ had a slight yellow color. The overtone spectra of this molecule in the region of Δv_{CH} = 6 could not be obtained due to interference from the absorption tail of the visible electronic spectrum.

The deconvoluted peak positions for the spectra of $C_6H_5CHCl_2$ in the regions of Δv_{CH} = 3 - 6 are given in Table 10.1 along with the peak assignments. The deconvoluted peak positions and assignments for the spectra of $C_6H_5CHBr_2$ in the regions of Δv_{CH} = 3 - 5 are given in Table 10.2.

As was stated in chapter 2, calculations for $C_6H_5CHCl_2$ were performed at the SCF level with the ab initio gradient program GAUSSIAN 82[92b]. The STO-3G and 4-31G basis sets were used. The calculations of Schaefer and Penner[84] with the STO-3G basis set were reproduced. The calculations of Schaefer and Penner[84] were also extended in the sense that the benzene ring was not restricted to be

planar and hexagonal. However, this restriction was retained in the calculation with the larger 4-31G basis set.

The removal of the restrictions on the benzene ring to be planar and hexagonal does not make a significant difference in the calculated geometry at the STO-3G level. The largest bond length variation occurs for the ring CC bonds which changed by ±0.002 to 0.005 Å. The <CCC and <CCH angle variations were only ± 0.2° which sets an effective limit on the angular uncertainty in the calculation. Based on this relative stability of the ring system, and because of calculational limitations, geometry optimization was carried out with the 4-31G basis restricting the benzene ring to planarity and to hexagonal symmetry. The equilibrium geometries associated with both the unrestrained STO-3G calculation and the 4-31G calculation are summarized in Figures 10.7 and 10.8.

In both calculations, the planar conformer with the alkyl CH bond in the plane of the benzene ring was found to be the most stable. The difference in energy between this conformer and the highest energy perpendicular conformer with the alkyl CH bond at 90° to the benzene ring was 11.42 and 10.99 kJ $mole^{-1}$ for the STO-3G and 4-31G calculations, respectively. The alkyl CH bond length is a function of angle. As in the case of toluene[28], this bond length is shortest in the ring plane and longest at 90°. The values for this bond length at 0°, 30°, 60° and 90° are given in Table 10.3 for the two calculations.

As has been noted, the unrestrained STO-3G geometry is very similar to the restrained STO-3G geometry of Schaefer and Penner[84]. However, there is one important difference between the STO-3G and 4-31G results. In the former, the aryl CH bond lengths are all very

close with the CH bonds ortho and para to the $-CHCl_2$ group approximately the same, and longer than the two equal meta CH bonds by about 0.0006 Å. In the 4-31G calculation, the aryl bond lengths are still close, but the largest difference occurs between the two ortho CH bonds with the one closer to the planar CH bond longer by 0.0018 Å.

There is an excellent correlation between CH bond lengths and overtone frequencies[28-31,33,39]. However, in the most stable planar conformer of $C_6H_5CHCl_2$ and $C_6H_5CHBr_2$, all five aryl CH bonds are nonequivalent. Moreover, the bond length differences are predicted to be small (see Figures 10.7 and 10.8). The spectra have been obtained in the liquid phase where the bands are undoubtedly broadened by intermolecular interactions. Under these circumstances, it is not surprising that the aryl peaks are unresolved and that an unambiguous assignment of the two observed aryl features is not possible. The observed splitting between these two features increases with Δv_{CH} in the manner expected[31] for contributions from two types of nonequivalent aryl CH bonds.

Mizugai and Katayama[154,155] have investigated substituent effects on the $\Delta v_{CH} = 6$ overtones in the aryl region of the spectra of a series of monosubstituted benzenes using thermal lens techniques. For the spectrum of $C_6H_5CHCl_2$ they have reported a frequency of 16520 cm^{-1} at $\Delta v_{CH} = 6$. This value is in good agreement with our value of 16528 cm^{-1} for the lower energy, higher intensity aryl peak. However, it should be noted that Mizugai and Katayama did not attempt to deconvolute their spectra, and the frequency of 16520 cm^{-1} corresponds to the single asymmetric band due to all of the aryl CH bonds.

In their study of the CH-stretching Raman spectrum of $C_6H_5CHCl_2$, on the basis of solvent and temperature effects, Ribeiro-Claro and Teixeira-Dias have assigned the two bands observed at 2992 cm^{-1} and 3006 cm^{-1} to the two conformers, planar and orthogonal. In overtone spectra, the frequency separation between peaks corresponding to nonequivalent CH bonds increases linearly with increasing Δv_{CH}[29,31]. Thus if two rotational conformers were present, one would expect to observe an asymmetric band in the alkyl region of the spectrum, particularly at higher overtones.

The alkyl region of each overtone of $C_6H_5CHCl_2$ consists of an asymmetric band which is a result of two overlapping Lorentzian functions. This is apparent from the deconvoluted Δv_{CH} = 3 and 4 spectra of Figures 10.1 and 10.2. The geometry optimized calculations on $C_6H_5CHCl_2$ predict the CH bond of the $-CHCl_2$ group to be shortest when in the ring plane (planar conformation) (see Table 10.3). Thus on this basis and the overtone frequency bond length correlation, the higher frequency, higher intensity methyl peak at each overtone of $C_6H_5CHCl_2$ is assigned to the planar conformation.

The lower energy, lower intensity component of the alkylic asymmetric band at each overtone of $C_6H_5CHCl_2$ could possibly arise from a transition to a combination state of the type $|v-1,2B>$, where v-1 is the number of quanta in the pure local mode state and B refers to a CH bending mode. Such combination peaks have been observed previously in the overtone spectra of a number of polyatomic molecules.[38,52,53,70,71,95,96,99,102] However, such combination peaks change their relative position and intensity as a function of Δv because of different anharmonicities for the interacting modes at

different overtone levels. Neither of these effects is observed for the lower energy component peak of the alkylic band of $C_6H_5CHCl_2$.

M.O. calculations (see Table 10.3) on $C_6H_5CHCl_2$ predict the alkyl CH bond to be of maximum length when it makes an angle of 90° to the ring plane (orthogonal conformation). The predicted difference in the length of the CH bond of the planar and orthogonal conformations is 0.003 Å (STO-3G) and 0.0014 Å (4-31G) (see Table 10.3). For this bond length difference, the overtone frequency-bond length correlation[29,31] predicts energy separations of 99, 132 and 165 cm^{-1} (STO-3G) and 46, 62 and 77 cm^{-1} (4-31G) between the alkyl peaks of the planar and orthogonal conformations at Δv_{CH} = 3, 4 and 5, respectively. The observed energy separations (74, 105 and 182* cm^{-1} at Δv_{CH} = 3, 4 and 5, respectively) are in reasonably good agreement with the predicted values. Thus it appears that the lower energy component peak of the alkylic band of $C_6H_5CHCl_2$ arises from the orthogonal conformation of the $-CHCl_2$ group. The approximate intensity ratios of these peaks with respect to the higher energy alkyl peaks are 1:11, 1:9 and 1:10 at Δv_{CH} = 3, 4 and 5, respectively. On this basis, if one assumes equal intrinsic intensities for the two conformers, on the average about 10% of the molecules would be in the orthogonal conformation in

---

*The observed energy separation of 182 cm^{-1} at Δv_{CH} = 5 is subject to greater error because of poor signal noise ratio in this region of spectrum.

the liquid phase**.

Both our calculations and the earlier STO-3G calculations of Schaefer and Penner[84] predict only a single stable planar conformation. However, both the experimental results and those of Ribeiro-Claro and Teixeira-Dias indicate the existence of two stable conformers. The calculations relate to the isolated gas phase molecules. It is conceivable, as pointed out by Schaefer and Penner[84], that intermolecular interactions could stabilize the orthogonal conformer in the liquid phase.

The results of the overtone spectral study agree with the Raman study[85] of Ribeiro-Claro and Teixeira-Dias in the sense that both studies predict two stable conformations for $C_6H_5CHCl_2$. However, in principle, the assignments presented in this chapter for the alkyl regions of the overtone spectra are in contradiction to the assignments by Ribeiro-Claro and Teixeira-Dias of the alkyl region of the fundamental Raman spectrum. They assign the observed lower and higher frequency Raman peaks (2992 cm^{-1} and 3006 cm^{-1}) to the planar and orthogonal conformation, respectively, whereas the assignments of this chapter are in the reverse order. In the fundamental spectrum, due to extensive coupling between vibrational states and the large number of transitions, there is the possibility of ambiguity in the assignment of peaks to different conformers. This ambiguity might be responsible for the disagreement with the overtone results.

**Overtone intensities depend in a complicated fashion on a number of factors[87]. The danger of assigning overtone spectra on the basis of relative intensities has been emphasized by Findsen et al.[118].

In the region of $\Delta v_{CH} = 3$ in the spectrum of $C_6H_5CHCl_2$, there is an additional peak at 8753 cm^{-1} between the aryl and alkyl CH peaks. This peak is assigned to a combination which involves three quanta of alkyl CH-stretching (8619 cm^{-1}) and one quantum of $-CHCl_2$ torsion (118 cm^{-1})[86]. This peak has significant intensity, probably due to a near resonant interaction with the aryl CH-stretching local mode state(s).

It is evident from Figures 10.3 and 10.4 that the alkyl regions of both the $\Delta v_{CH} = 3$ and 4 spectra of $C_6H_5CHBr_2$ are fitted very well by a single Lorentzian function. A similar result was obtained for the $\Delta v_{CH} = 5$ spectrum. These results provide strong evidence for the existence of a single stable conformation for the $-CHBr_2$ group of $C_6H_5CHBr_2$. Such a result is in keeping with the expected larger barrier to internal rotation in benzal bromide as compared to benzal chloride. Assignments of the peaks, other than the alkyl peaks, at $\Delta v_{CH} = 3 - 5$ in the spectra of $C_6H_5CHBr_2$ are analogous to the corresponding peaks in the spectra of $C_6H_5CHCl_2$ (see Tables 10.1 and 10.2).

The local mode parameters (harmonic frequency, ω, and diagonal anharmonicity, ωx) of the nonequivalent bonds of $C_6H_5CHCl_2$ and $C_6H_5CHBr_2$ can be obtained by fitting the energies of the pure CH-stretching peaks from Tables 10.1 and 10.2 to the energy equation of a single Morse oscillator. These parameters are listed in Table 10.4. The uncertainties in the ω and ωx values for the alkyl CH oscillator of the orthogonal conformation of $C_6H_5CHCl_2$ (also to a lesser degree for the alkyl CH oscillator of $C_6H_5CHBr_2$) are significantly higher than usual[19]. These greater uncertainties are undoubtedly due to the uncertainty in the peak positions of these low

intensity peaks, particularly at $\Delta v_{CH} = 5$ (both molecules). Therefore, the ω and ωx values for the alkyl CH oscillator of the orthogonal conformer of $C_6H_5CHCl_2$ and the alkyl CH oscillator of $C_6H_5CHBr_2$ should be regarded only as estimates. It is also noted that the values of ω and ωx associated with the two aryl peaks are averages in the sense that these peaks correspond to unresolved contributions from nonequivalent aryl CH bonds.

The transition frequencies (see Tables 10.1 and 10.2) of the aryl CH oscillators of $C_6H_5CHCl_2$ and $C_6H_5CHBr_2$ are higher than the corresponding transition frequencies for the CH oscillator of benzene (ΔE(benzene) = 8760, 11442, 14015 and 16467 cm^{-1} for $\Delta v_{CH} = 3, 4, 5$ and 6, respectively[136]). Both the $-CHCl_2$ and $-CHBr_2$ groups are electron attracting relative to hydrogen. Thus, they strengthen the aryl CH bonds of $C_6H_5CHCl_2$ and $C_6H_5CHBr_2$ and increase their vibrational frequencies relative to benzene.

It would be particularly useful to observe the CH-stretching overtone spectrum of $C_6H_5CHCl_2$ in the gas phase. There is the possibility that peaks due to the nonequivalent aryl CH bonds would be resolved. Of even greater interest would be an indication of the role played by liquid phase intermolecular interactions in stabilizing the orthogonal conformer.

Table 10.1.

Deconvoluted Peak Positions (cm^{-1}) and Assignments for the Overtone Peaks of $C_6H_5CHCl_2$.

$\Delta\nu_{CH}$	Peak Position	Assignment
	8545	dichloromethyl CH (90°)[a]
	8619	dichloromethyl CH (0°)[a]
3	8753	combination
	8800	aryl CH
	8845	aryl CH
	11142	dichloromethyl CH (90°)[a]
	11247	dichloromethyl CH (0°)[a]
4	11479	aryl CH
	11551	aryl CH
	13509	dichloromethyl CH (90°)[a]
	13691	dichloromethyl CH (0°)[a]
5	14040	aryl CH
	14139	aryl CH
	16046	dichloromethyl CH (0°)[a]
6	16528	aryl CH
	16665	aryl CH

[a]See text

Table 10.2.

Deconvoluted Peak Positions (cm^{-1}) and Assignments for the Overtone Peaks of $C_6H_5CHBr_2$.

Δv_{CH}	Peak Position	Assignment
	8646	dibromomethyl CH
	8731	combination
3	8784	aryl CH
	8829	aryl CH
	11299	dibromomethyl CH
4	11454	aryl CH
	11522	aryl CH
	13788	dibromomethyl CH
5	14021	aryl CH
	14100	aryl CH

Table 10.3.

Alkyl CH Bond Lengths (r_{C-H}) in $C_6H_5CHCl_2$ as a Function of the Angle (θ) Formed With the Benzene Plane, Calculated at the SCF Level With the STO-3G and 4-31G Basis Sets.

θ(degrees)	r_{C-H}(Å)	
	STO-3G	4-31G
0	1.0940	1.0687
30	1.0946	1.0689
60	1.0963	1.0696
90	1.0972	1.0701

Table 10.4.

Local Mode Parameters (cm^{-1}) for the Nonequivalent Bonds of $C_6H_5CHCl_2$ and $C_6H_5CHBr_2$.

Molecule	Bond Type	ω	ωx
$C_6H_5CHCl_2$	dichloromethyl CH (90°)	3145 ± 25	73 ± 6.0
	dichloromethyl CH (0°)	3143 ± 7.6	67.0 ± 1.6
	aryl[a]	3170 ± 8.0	59.8 ± 1.7
	aryl	3175 ± 8.3	57.2 ± 1.8
$C_6H_5CHBr_2$	dibromomethyl CH	3132 ± 12.0	62.2 ± 2.9
	aryl[a]	3175 ± 6.3	61.9 ± 1.5
	aryl	3189 ± 2.4	61.5 ± 0.6

[a]This value refers to the higher frequency aryl peak.

Figure 10.1.

Upper trace: liquid phase overtone spectrum of $C_6H_5CHCl_2$ in the region of $\Delta v_{CH} = 3$. The spectrum was measured at room temperature with a path length of 3.0 cm. Middle trace: individual Lorentzian functions fit to the experimental spectrum; lower trace: difference of the experimental and fit spectra.

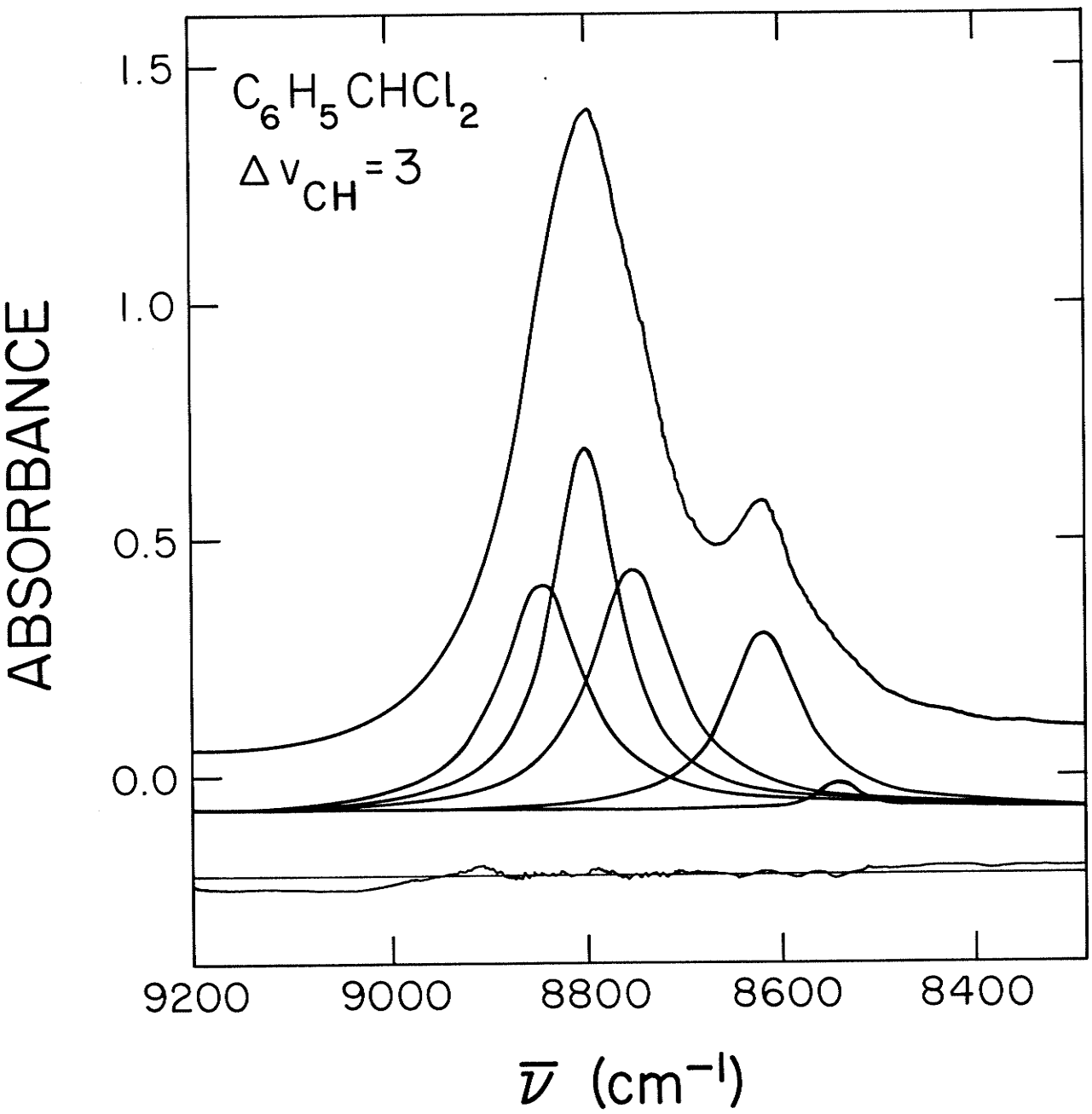
$C_6H_5CHCl_2$
$\Delta v_{CH} = 3$
ABSORBANCE
1.5
1.0
0.5
0.0
9200
9000
8800
8600
8400
$\bar{\nu}$ (cm^{-1})

Figure 10.2.

Upper trace: liquid phase overtone spectrum of $C_6H_5CHCl_2$ in the region of $\Delta v_{CH} = 4$. The spectrum was measured at room temperature with a path length of 3.0 cm. Middle trace: individual Lorentzian functions fit to the experimental spectrum; lower trace: difference of the experimental and fit spectra.

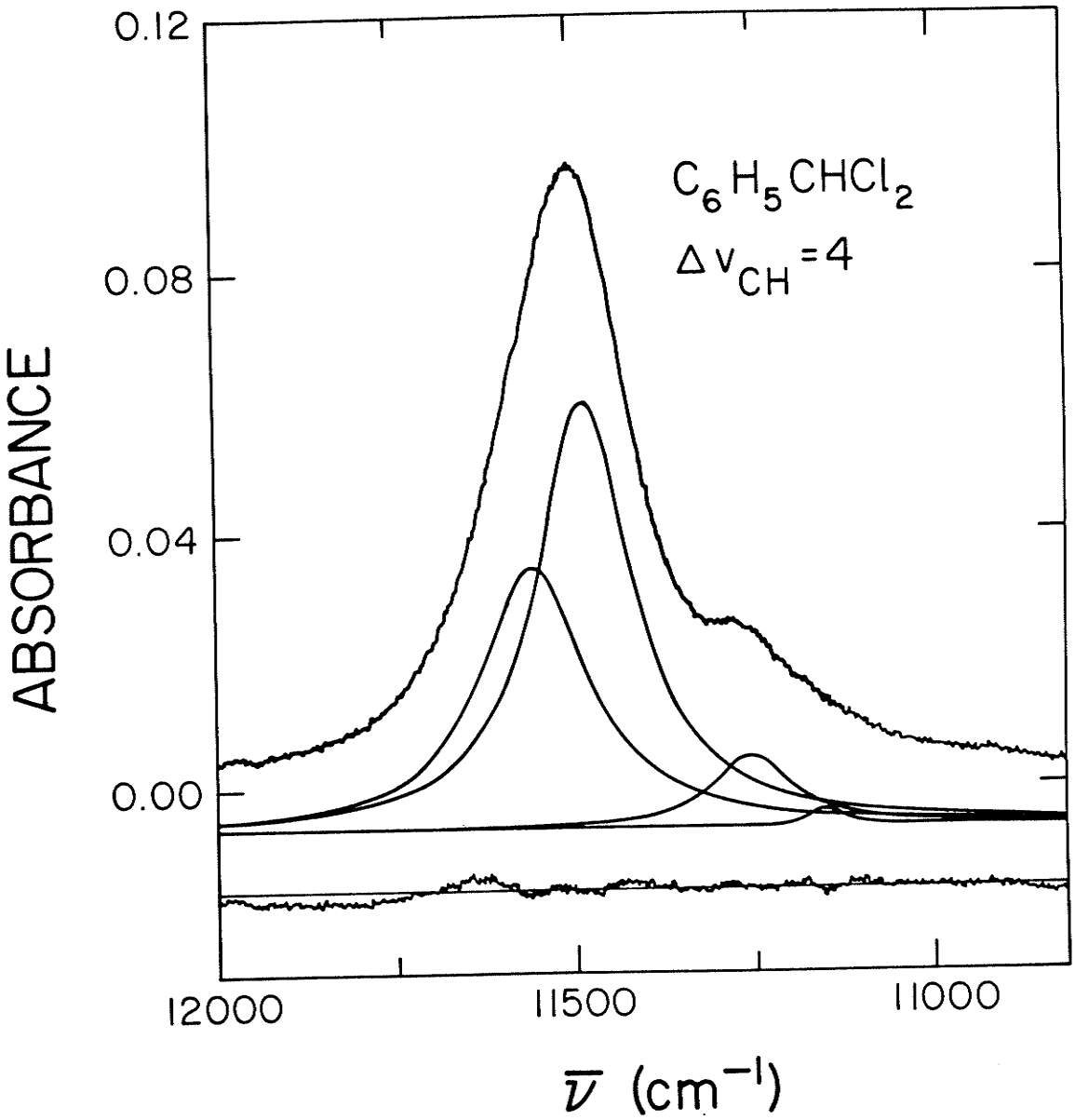
0.12
0.08
0.04
0.00
ABSORBANCE
$C_6H_5CHCl_2$
$\Delta v_{CH} = 4$
12000
11500
11000
$\bar{\nu}$ (cm^{-1})

Figure 10.3.

Upper trace: liquid phase overtone spectrum of $C_6H_5CHBr_2$ in the region of $\Delta v_{CH} = 3$. The spectrum was measured at room temperature with a path length of 3.0 cm. Middle trace: individual Lorentzian functions fit to the experimental spectrum; lower trace: difference of the experimental and fit spectra.

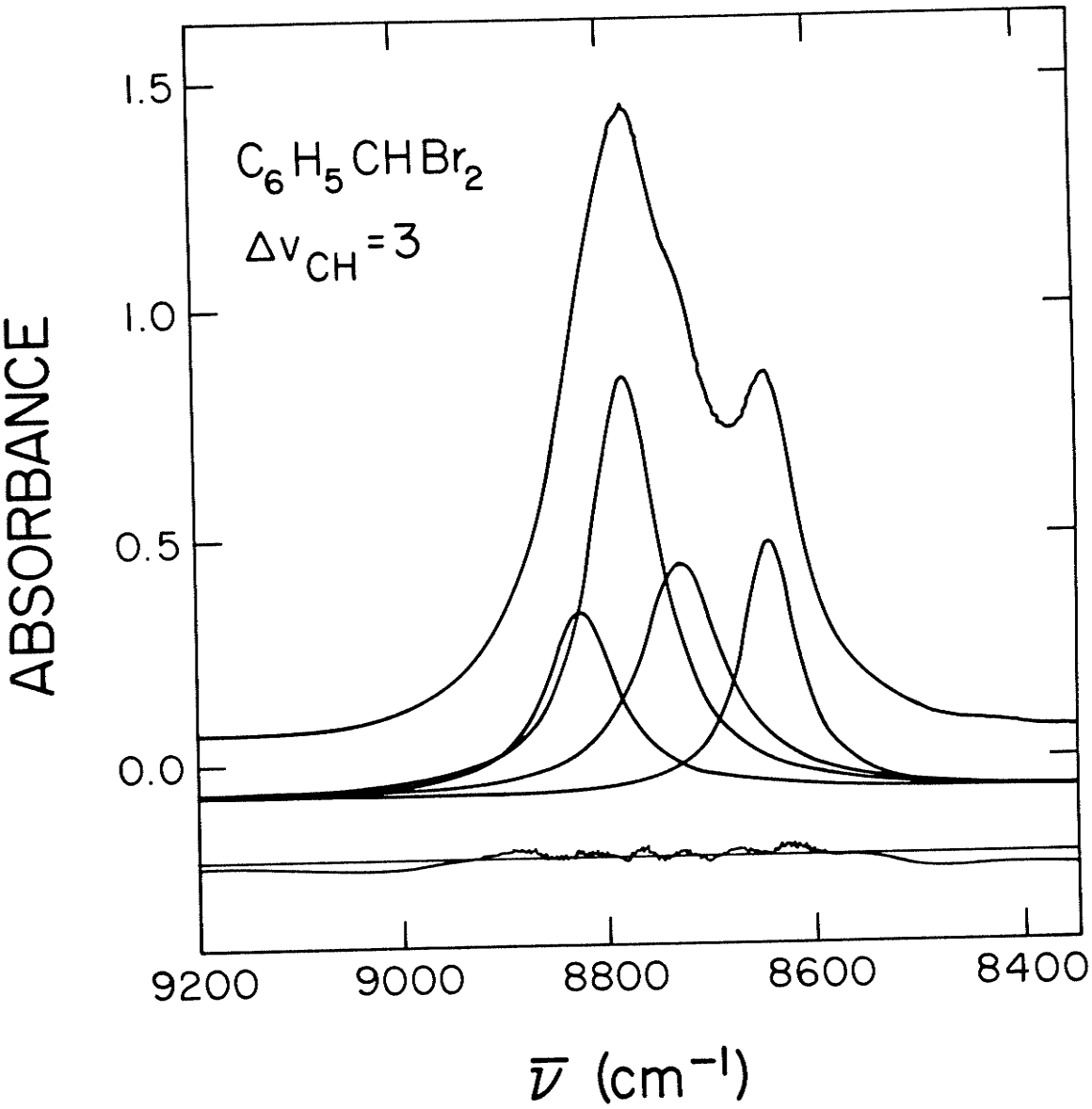
ABSORBANCE
1.5
1.0
0.5
0.0
$C_6H_5CHBr_2$
$\Delta\nu_{CH}=3$
9200
9000
8800
8600
8400
$\bar{\nu}$ (cm^{-1})

Figure 10.4.

Upper trace: liquid phase overtone spectrum of $C_6H_5CHBr_2$ in the region of $\Delta v_{CH} = 4$. The spectrum was measured at room temperature with a path length of 3.0 cm. Middle trace: individual Lorentzian functions fit to the experimental spectrum; lower trace: difference of the experimental and fit spectra.

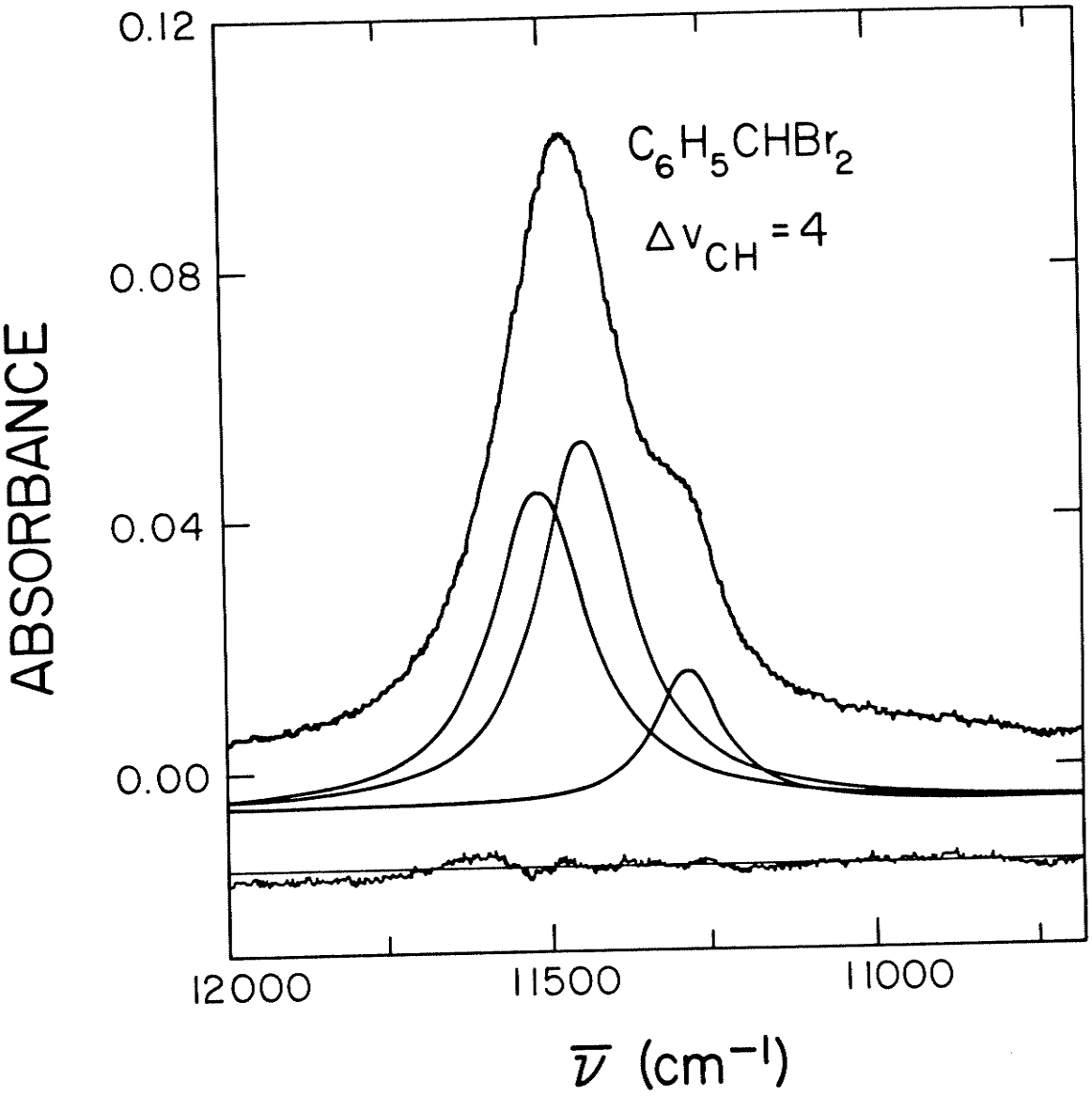
0.12
0.08
0.04
0.00
ABSORBANCE
$C_6H_5CHBr_2$
$\Delta v_{CH} = 4$
12000
11500
11000
$\bar{\nu}$ (cm^{-1})

Figure 10.5.

Base line corrected liquid phase overtone spectra of $C_6H_5CHCl_2$ in the region of Δv_{CH} = 5 and 6. The spectra were measured at room temperature with a path length of 10.0 cm. The upper abcissa and right hand ordinate scales are for the Δv_{CH} = 6 spectrum.

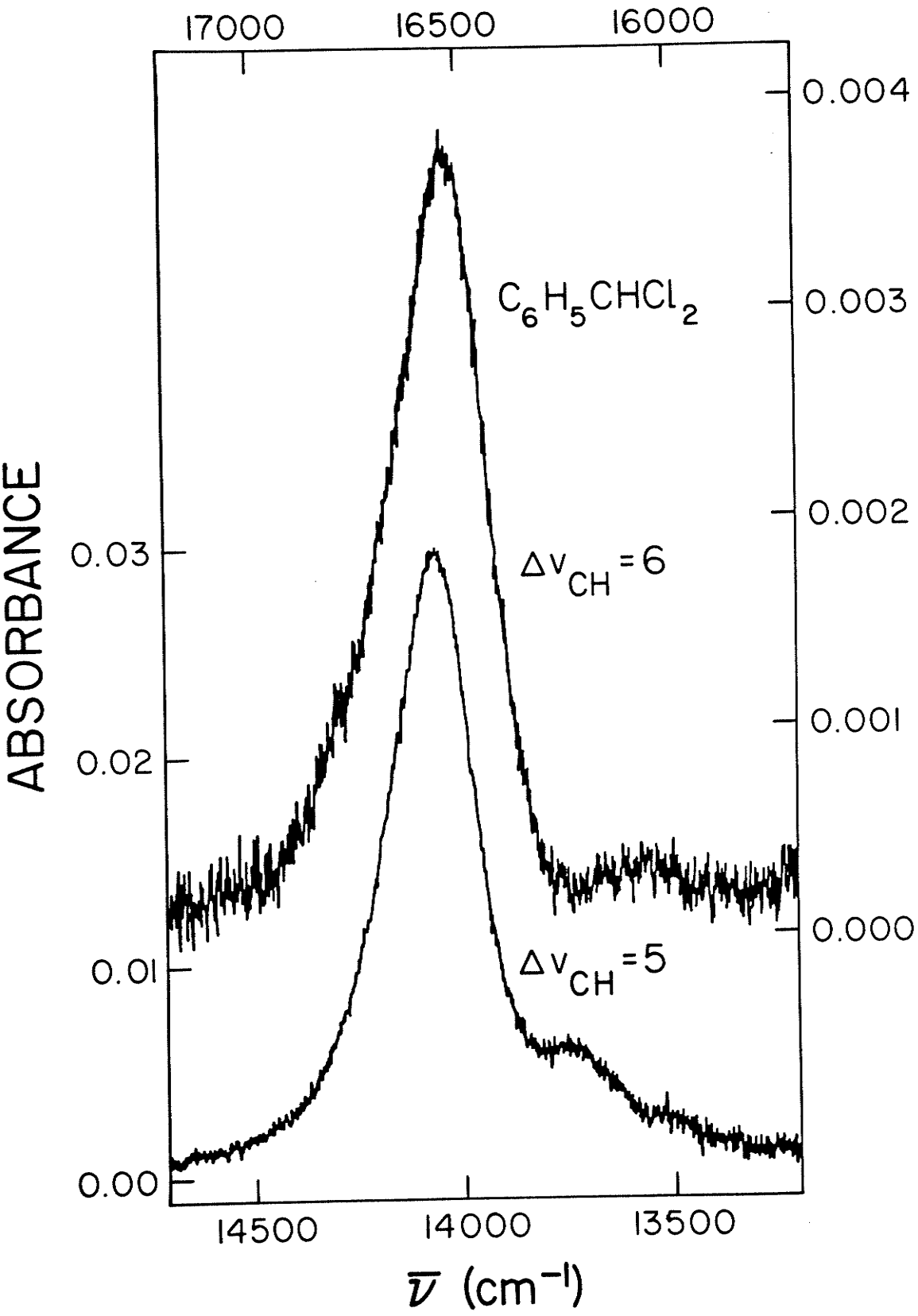
17000
16500
16000
0.004
0.003
0.002
0.001
0.000
$C_6H_5CHCl_2$
$\Delta v_{CH}=6$
$\Delta v_{CH}=5$
ABSORBANCE
0.03
0.02
0.01
0.00
14500
14000
13500
$\bar{\nu}$ (cm^{-1})

Figure 10.6.

Liquid phase overtone spectrum of $C_6H_5CHBr_2$ in the region of $\Delta v_{CH} = 5$. This spectrum is the sum of four base line corrected scans. Individual scans were measured at room temperature with a 5.0 cm path length cell.

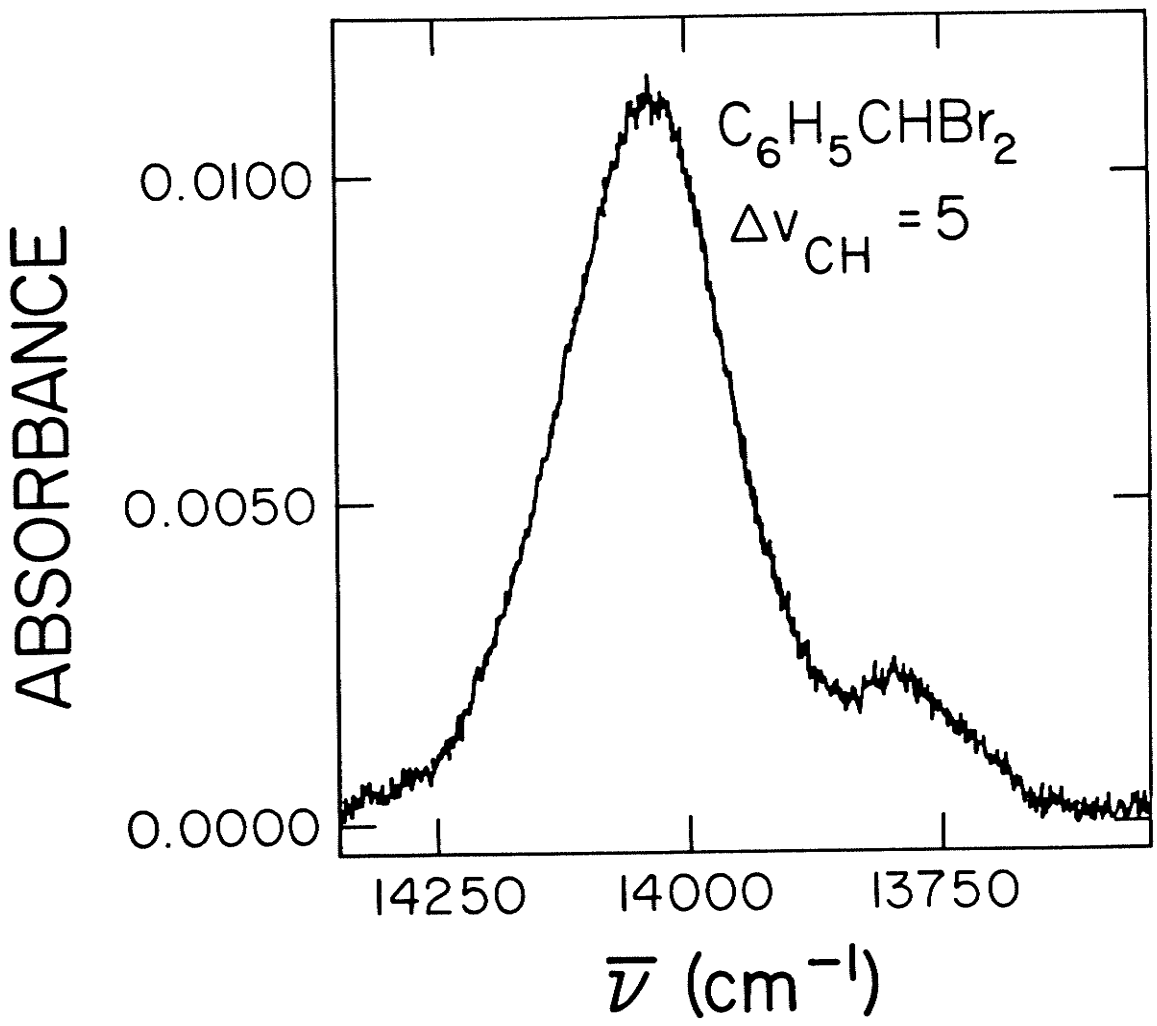
ABSORBANCE
0.0100
0.0050
0.0000
$C_6H_5CHBr_2$
$\Delta v_{CH} = 5$
14250
14000
13750
$\bar{\nu}$ (cm^{-1})

Figure 10.7.

SCF optimized geometry of benzal chloride with the STO-3G basis set. All parameters have been allowed to vary; the ring angles were all within ±0.2° of the hexagonal angle (120°). The energy* is -1174.467587 a.u. The bond lengths are given in Å and the angles are in degrees. The C-Cl bonds form an angle of 61.5° with the benzene plane.

---

*This energy is quoted to ten significant figures because conformational changes produce changes in energy of the order of 10^{-6} a.u.

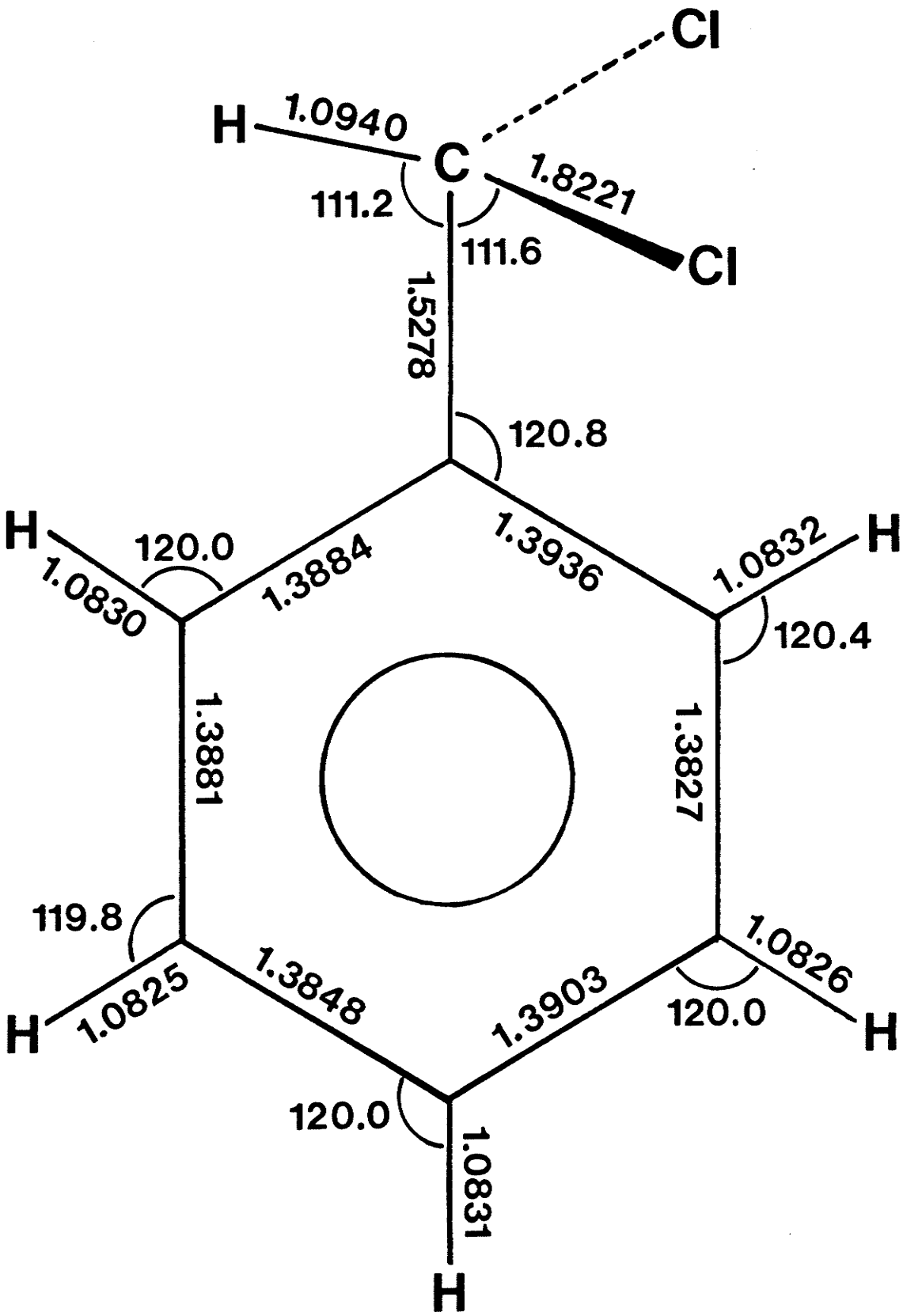
Cl
H
1.0940
C
1.8221
Cl
111.2
111.6
1.5278
120.8
H
120.0
1.0830
1.3884
1.3936
1.0832
H
120.4
1.3881
1.3827
119.8
1.0825
H
1.3848
1.3903
1.0826
120.0
H
120.0
1.0831
H

Figure 10.8.

SCF optimized geometry of benzal chloride with the 4-31G basis set. The benzene ring was constrained to be hexagonal. The energy* of this conformer is -1186.157735 a.u. The bond lengths are given in Å and the angles in degrees. The C-Cl bonds form an angle of 60.5° with the benzene ring.

---

*This energy is quoted to ten significant figures because conformational changes produce changes in energy of the order of 10^{-6} a.u.

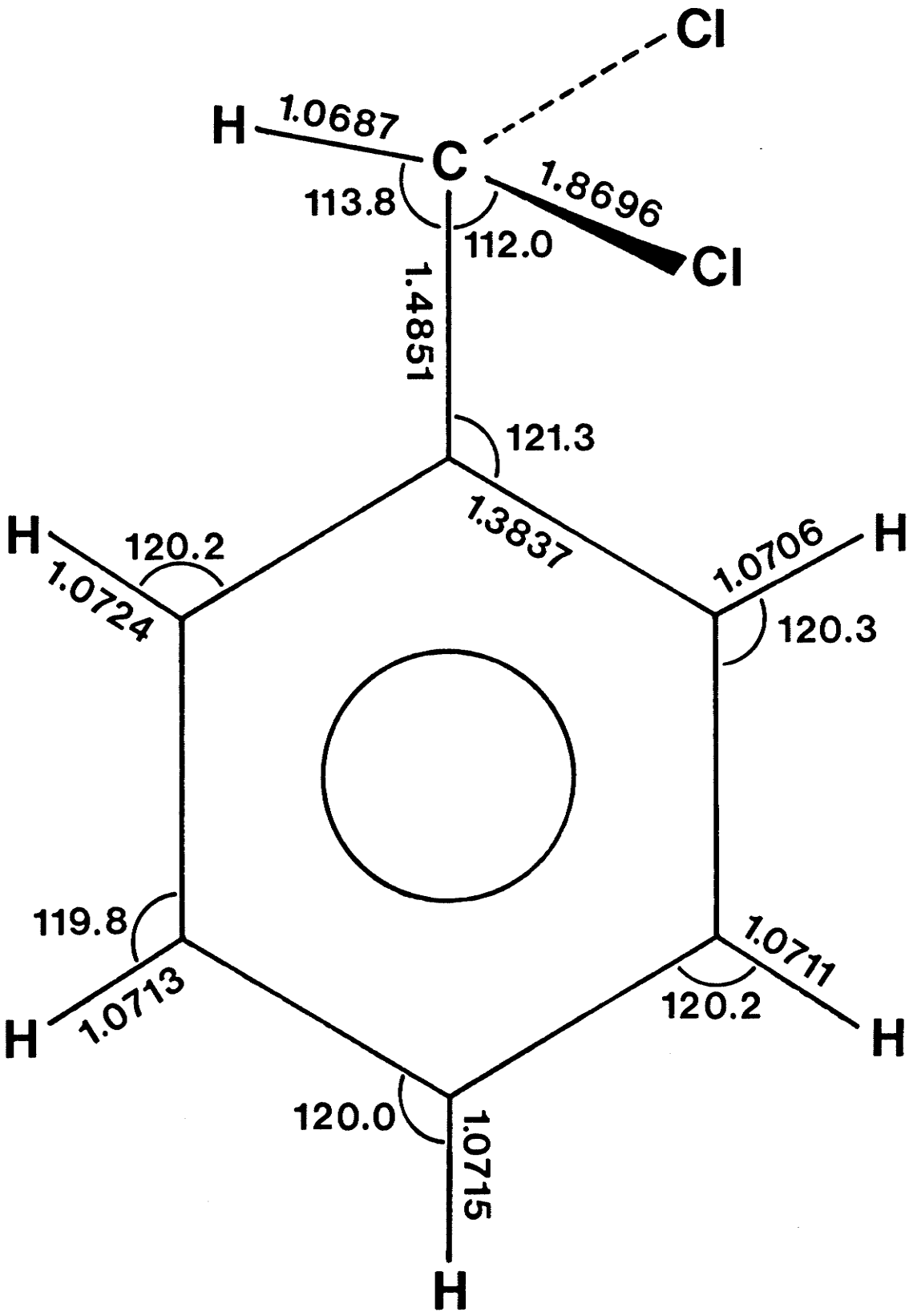
Cl
H
1.0687
C
1.8696
Cl
113.8
112.0
1.4851
121.3
1.3837
H
120.2
1.0724
1.0706
H
120.3
119.8
1.0711
H
1.0713
120.2
H
120.0
1.0715
H

APPENDIX A

OVERTONE SPECTRA OF (CHLOROMETHYL)CYCLOPROPANE

In this Appendix the liquid and gas phase overtone spectra of (chloromethyl)cyclopropane (CMCP) are reported. This work is an extension of the work which was reported in chapter 8 on cyclopropyl methyl ketone (CPMK), cyclopropylamine (CPAM), cyclopropyl cyanide (CPCN) and cyclopropyl bromide (CPBr).

The liquid and gas phase Δv_{CH} = 2 - 4 spectra of CMCP are shown in Figures A.1-A.3. The liquid phase Δv_{CH} = 5 spectrum is shown in Figure A.4. The liquid phase Δv_{CH} = 6 spectrum was measured but is not shown. The spectral features of this spectrum were similar to the spectral features of the Δv_{CH} = 4 and 5 spectra.

The spectral features due to the ring CH oscillators of CMCP resemble closely the spectral features (see chapter 8) of the ring CH oscillators of CPMK, CPAM, CPCN and CPBr. However, there is one minor difference. In the high energy spectra ($\Delta v_{CH} \geq 3$) of CPMK, CPAM, CPCN and CPBr, the ring CH oscillators give rise to asymmetric bands because of the different bond strengths of the methylene and methine oscillators. In contrast, the ring CH oscillators of CMCP give rise to single symmetric peaks in the high energy spectra. This shows that the bond strengths/bond lengths of the methylene and methine CH bonds of CMCP are nearly the same.

The local mode parameters for the ring CH bonds of CMCP are listed in Table A.1. These parameters were obtained with the same procedure which was used to determine the local mode parameters of some monosubstituted cyclopropanes in chapter 8. The local mode parameters for the CH bonds of the chloromethyl group of CMCP are also listed in Table A.1. ω and ωx for these oscillators were determined from the Morse oscillator energy equation (Eq. 4.1 of chapter 4). The

effective coupling parameter $\gamma'\omega$ for the chloromethyl oscillators was determined from the observed splitting[70] between the $|1,0\rangle_-$ (2994 cm^{-1})[156] and $|1,0\rangle_+$ (2963 cm^{-1})[156] peaks.

The calculated and observed spectra for the ring CH and chloromethyl CH oscillators of CMCP are compared in Tables A.2 and A.3, respectively. A local mode theory of two coupled XH bonds (see chapter 1) was used for calculating the spectra. In the calculation, the effective coupling parameter, $\gamma'\omega$, for the chloromethyl CH oscillators was assumed to be the same (16.0 cm^{-1}, see Table A.1) for both liquid and gas phases. The data of Tables A.2 and A.3 show that the agreement between the observed and calculated peak positions is quite good.

CMCP could exist in two conformations (cis and gauche). Kalasinsky and Wurrey[156] have studied the conformations of CMCP through fundamental IR and Raman spectra. They have concluded that CMCP exists as an equilibrium mixture of gauche (95%) and cis (5%) conformers in the liquid state and that the only conformer in the solid phase is the gauche. The analysis of the spectra of CMCP in this appendix is based upon the assumption that this molecule exists totally in the gauche form in both liquid and gas phases.

In addition to the peaks listed in Tables A.2 and A.3, local mode-normal mode combination peaks are also observed in both the liquid (5864, 8583, 8665 and 8987 cm^{-1}) and gas (5877, 8614, 8712 and 9015 cm^{-1}) phase spectra of CMCP. The assignments for these combination peaks can easily be made on the basis of the local mode peak positions (see Tables A.2 and A.3) and the frequencies of the fundamental modes[156] of CMCP.

Table A.1.

Local Mode Parameters (cm^{-1}) for the CH Oscillators of (Chloromethyl)cyclopropane.

Phase	Oscillator Type	ω	ωx	$\gamma'\omega$
Liquid	Ring CH	3159±2.0	60.5±0.4	43.8
Gas	Ring CH	3165.7±0.3	59.4±0.1	41.8
Liquid	Chloromethyl	3082±5.0	61.7±1.2	16.0[a]
Gas	Chloromethyl	3076±5.0	57.9±1.5	16.0

[a]Assumed value, see text.

Table A.2.

Observed and Calculated Peak Positions (cm^{-1}) for the Ring CH Oscillators of (Chloromethyl)cyclopropane.

	Liquid		Gas		
Δv_{CH}	Observed[a]	Calculated	Observed[a]	Calculated	Assignment
	5911	5909	5930	5932	$\|2,0\rangle_+$
2	5958	5955	5975	5975	$\|2,0\rangle_-$, $\|2\rangle$
	6122	6122	6137	6137	$\|1,1\rangle$
	8747	8720	8785	8756	$\|3,0\rangle_+$
	8747	8734	8785	8769	$\|3,0\rangle_-$, $\|3\rangle$
3	8924	8936	8961	8967	$\|2,1\rangle_+$
	9094	9097	9118	9121	$\|2,1\rangle_-$
	11426	11403	11475	11454	$\|4,0\rangle_+$
	11426	11406	11475	11456	$\|4,0\rangle_-$, $\|4\rangle$
4	-	11704	-	11751	$\|3,1\rangle_+$
	11785	11809	11833	11850	$\|3,1\rangle_-$
	-	12017	-	12050	$\|2,2\rangle$
	13978	13960	-	14028	$\|5,0\rangle_\pm$, $\|5\rangle$
5	-	14399	-	14462	$\|4,1\rangle_+$
	14484	14445	-	14504	$\|4,1\rangle_-$
6	16421	16394	-	16482	$\|6,0\rangle_\pm$, $\|6\rangle$

Table A.2....cont'd...

	Liquid		Gas		
Δv_{CH}	Observed[a]	Calculated	Observed[a]	Calculated	Assignment
	-	16978	-	17056	$\|5,1\rangle_+$
	17100	16989	-	17066	$\|5,1\rangle_-$

[a]Observed peak positions are from deconvolution of the experimental spectra.

Table A.3.

Observed and Calculated Peak Positions (cm^{-1}) for the Chloromethyl CH Oscillators of (Chloromethyl)cyclopropane.

	Liquid		Gas		
Δv_{CH}	Observed[a]	Calculated	Observed[a]	Calculated	Assignment
	5788	5787	5803	5796	$\|2,0\rangle_+$
2	5788	5795	5803	5805	$\|2,0\rangle_-$
	5911	5926	5930	5929	$\|1,1\rangle$
	8514	8503	8539	8529	$\|3,0\rangle_+$
	8514	8504	8539	8530	$\|3,0\rangle_-$
3	-	8725	-	8737	$\|2,1\rangle_+$
	-	8789	-	8800	$\|2,1\rangle_-$
4	11114	11093	11143	11143	$\|4,0\rangle_\pm$
5	13553	13559	-	13640	$\|5,0\rangle_\pm$
6	15896	15901	-	16021	$\|6,0\rangle_\pm$

[a]See footnote "a" of Table A.2.

Figure A.1.

Lower trace: liquid phase overtone spectrum of (chloromethyl)cyclopropane in the region of $\Delta v_{CH} = 2$. The spectrum was measured at room temperature with a path length of 0.1 cm. Upper trace: gas phase overtone spectrum of (chloromethyl)cyclopropane at 90°C in the region of $\Delta v_{CH} = 2$. Path length, 2.25 m.

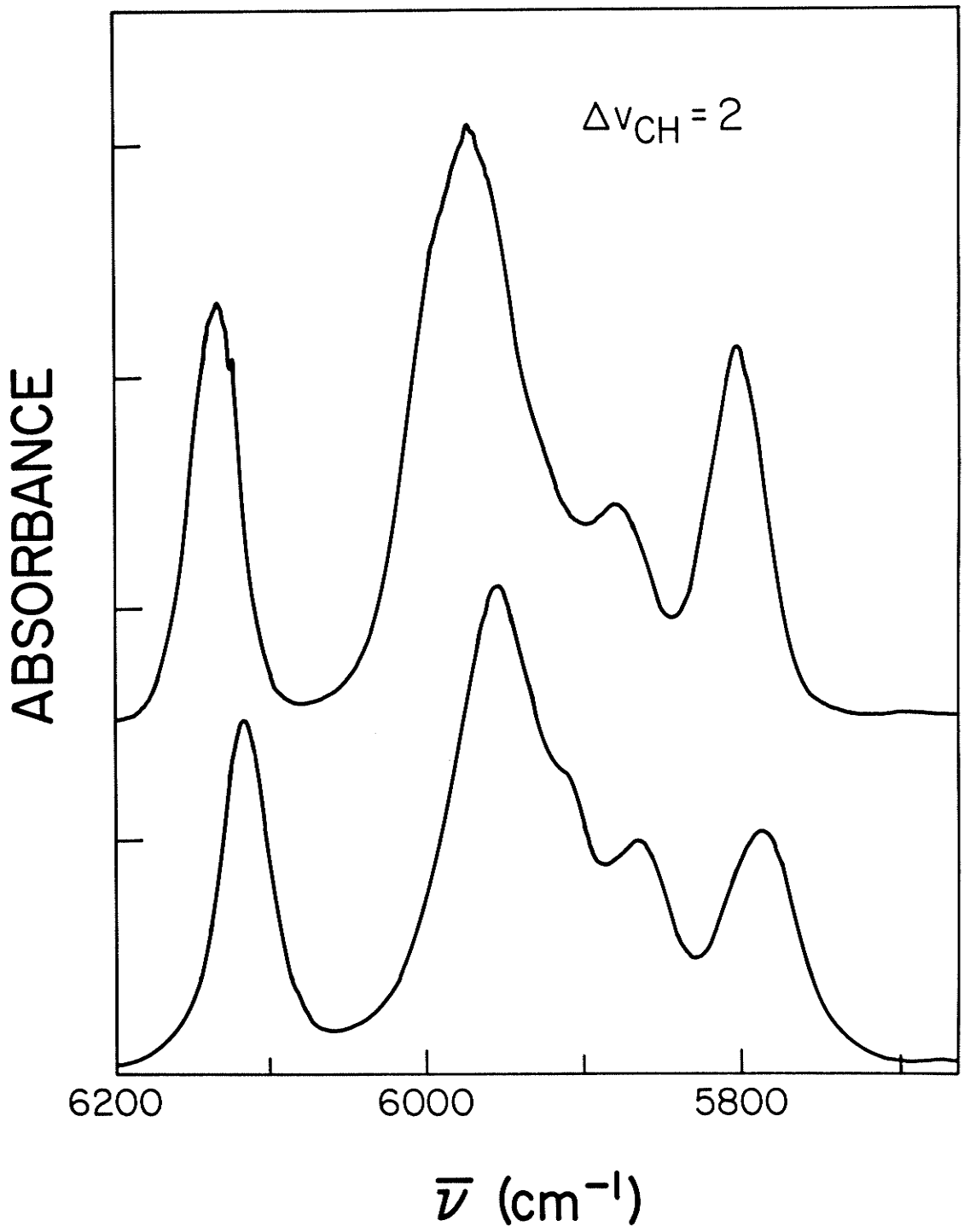
ΔvCH = 2
ABSORBANCE
6200
6000
5800
ν̄ (cm⁻¹)

Figure A.2.

Lower trace: liquid phase overtone spectrum of (chloromethyl)cyclopropane in the region of $\Delta v_{CH} = 3$. The spectrum was measured at room temperature with a path length of 1.0 cm. Upper trace: gas phase overtone spectrum of (chloromethyl)cyclopropane at 90°C in the region of $\Delta v_{CH} = 3$. Path length, 8.25 m.

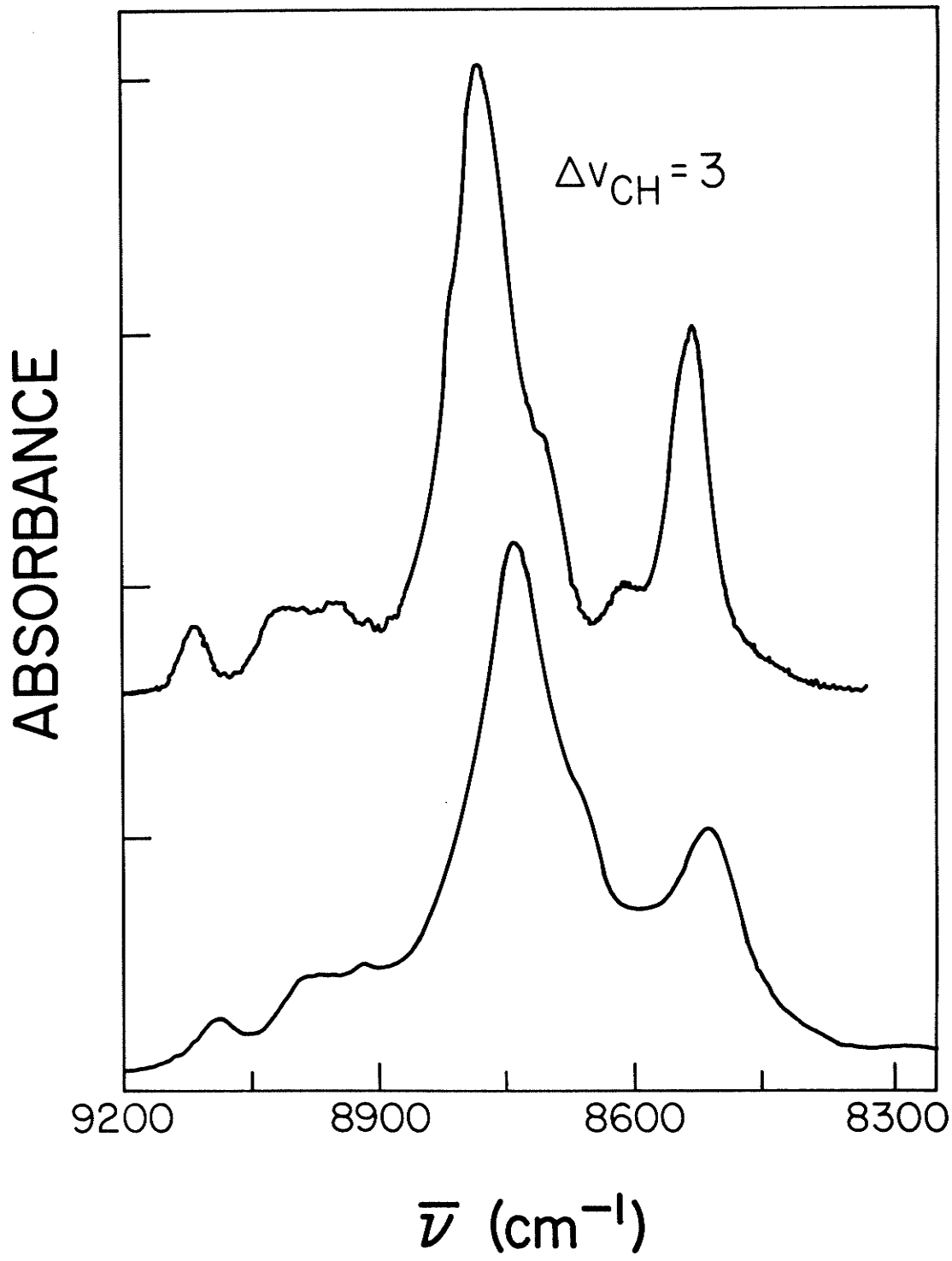
ABSORBANCE
$\Delta v_{CH} = 3$
9200
8900
8600
8300
$\bar{\nu}$ (cm^{-1})

Figure A.3.

Lower trace: liquid phase overtone spectrum of (chloromethyl)cyclopropane in the region of $\Delta v_{CH} = 4$. The spectrum was measured at room temperature with a path length of 5.0 cm. Upper trace: gas phase overtone spectrum of (chloromethyl)cyclopropane at 90°C in the region of $\Delta v_{CH} = 4$. Path length, 12.75 m.

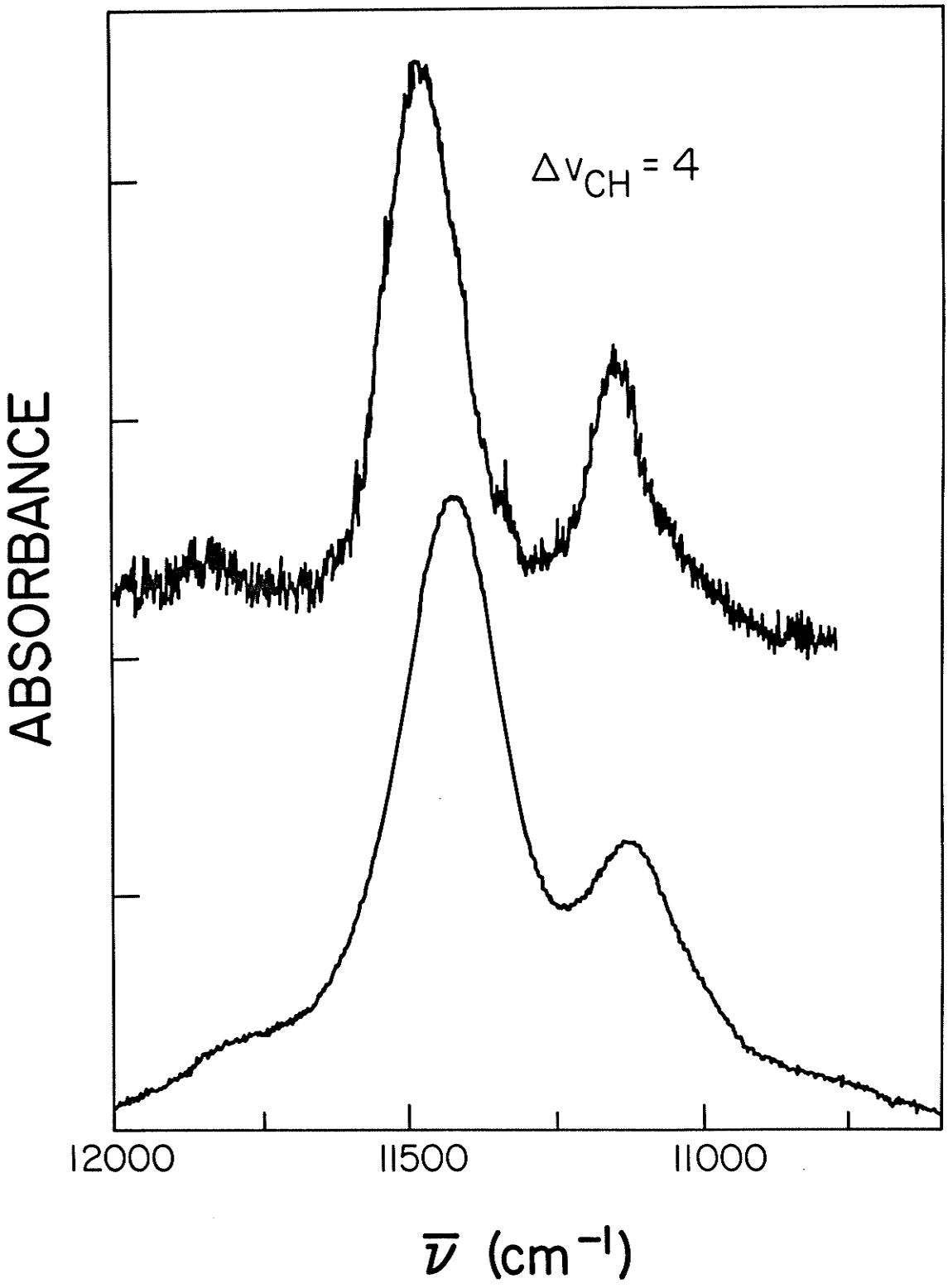
ABSORBANCE
$\Delta v_{CH} = 4$
12000
11500
11000
$\bar{\nu}$ (cm^{-1})

Figure A.4.

Liquid phase overtone spectrum of (chloromethyl)cyclopropane in the region of $\Delta v_{CH} = 5$. The spectrum was measured at room temperature with a path length of 5.0 cm.

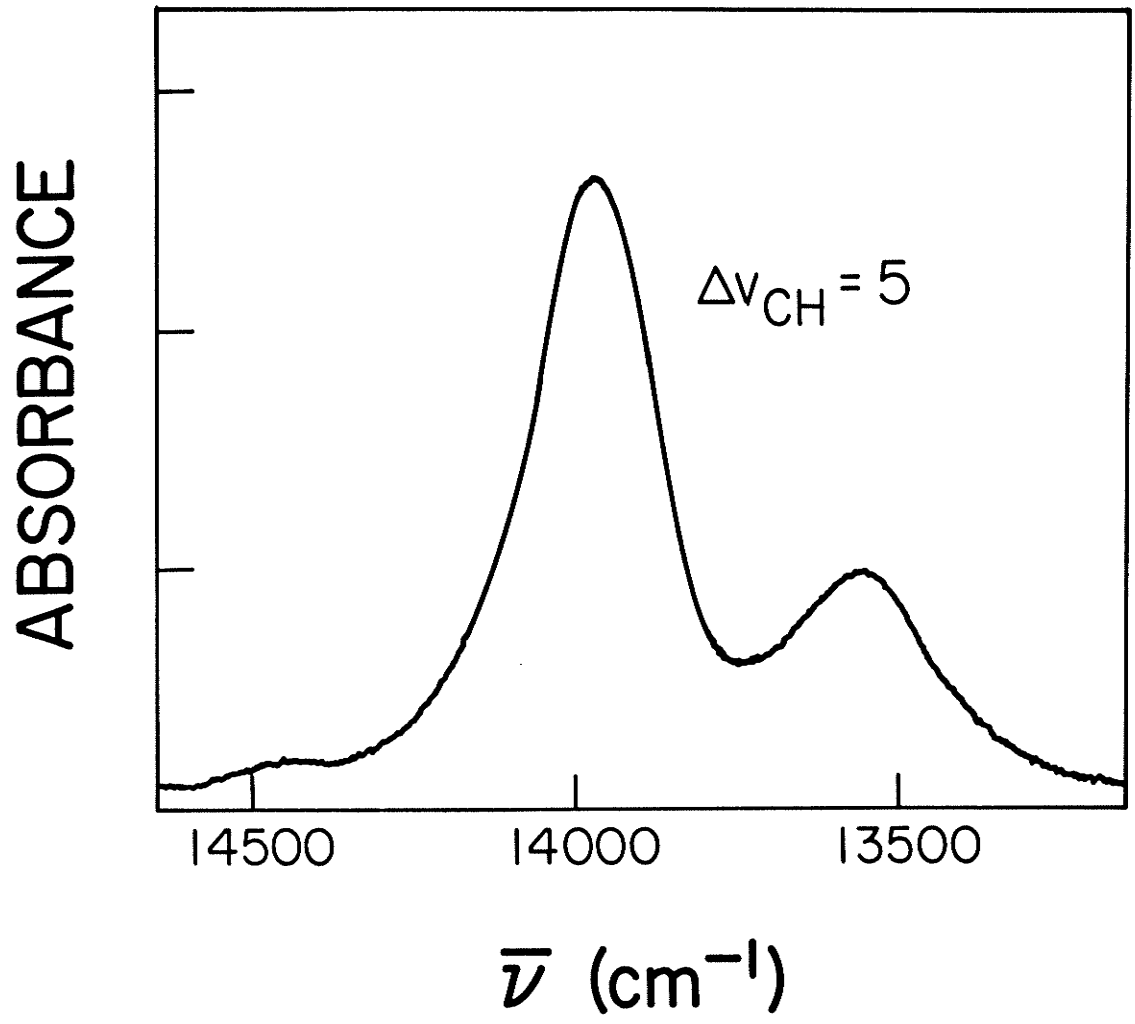
ABSORBANCE
$\Delta v_{CH} = 5$
14500
14000
13500
$\bar{\nu}$ (cm^{-1})

APPENDIX B

OSCILLATOR STRENGTHS OF OVERTONE SPECTRA OF DICHLOROMETHANE AND DEUTERATED DICHLOROMETHANE

Although the local model has been used extensively to explain the XH stretching overtone spectra of a wide variety of molecules, relatively little attention has been directed to the problem of overtone intensities. Two problems are of particular interest. The first is the fall off in intensity of local mode overtones with increasing v, and the second is the relative intensities of local mode overtones and local mode combinations within a given v manifold.

Very recently Mortensen et al.[87] have developed a general theory for overtone intensities. The main steps involved in the development of the theory were outlined very briefly in chapter 4 of this thesis while comparing the spectra of CH_2Z_2 and CD_2Z_2 (Z = Cl, Br or I) molecules. The theory predicts that vibrational mixing is more important as a source of combination intensity than off-diagonal terms in the local coordinate expansion of the electric dipole moment. In fact such mixing is the only source of intensity for the antisymmetric combination states. The predictions of the theory were tested through a comparison of the calculated and experimental oscillator strengths (intensities) of the local mode peaks of CD_2Cl_2 and CH_2Cl_2. The experimental oscillator strengths were determined by the author of this thesis and are reported in Tables B.1, B.2 and B.3.

The integrated oscillator strengths (Table B.1) were determined by following the same procedure which was used in chapter 5 to obtain integrated oscillator strengths of the overtones of CH_3Z (Z = Cl, Br or I) molecules. The oscillator strengths for the individual local mode peaks of CD_2Cl_2 and CH_2Cl_2 were obtained from the total oscillator strength and the ratios of the deconvoluted peak areas to the total areas from the deconvolution program.

In Table B.1, the theoretical and experimental oscillator strengths are compared. One notes that the calculated oscillator strengths are more than an order of magnitude too small, but that both the relative intensity of the deuterated versus the undeuterated molecule, and the fall off in intensity with Δv, is relatively well accounted for. Both the calculated and observed oscillator strengths show an exponential dependence of Δv.

Very recent work[104] indicates that the difficulty with the theoretical values arises from the use of a CNDO M.O. approach to calculate the dipole moment derivatives. Higher levels of calculations lead to good agreement with the experimental values.

Table B.1.

Experimental and Theoretical Integrated Oscillator Strengths for the $\Delta v = 2$, 3, and 4 Bands in CH_2Cl_2 and CD_2Cl_2.

		Experimental		Theoretical[a]	
Molecule	Δv	f	ln f	f	ln f
CH_2Cl_2	2	2.76×10^{-7}	-15.10	1.35×10^{-8}	-18.12
-	3	2.31×10^{-8}	-17.58	2.44×10^{-9}	-19.83
-	4	1.68×10^{-9}	-20.20	2.21×10^{-10}	-22.23
CD_2Cl_2	2	1.27×10^{-7}	-15.88	7.50×10^{-9}	-18.71
-	3	6.96×10^{-9}	-18.78	7.47×10^{-10}	-21.01
-	4	5.93×10^{-10}	-21.25	5.49×10^{-11}	-23.63

[a]From Ref. 87

Table B.2.

Oscillator Strengths of the Local Mode Overtone Peaks of CH_2Cl_2

Assignment	Frequency (cm^{-1})	Oscillator Strength
$\|1,0\rangle_+\|2\nu_2\rangle$	5796	5.24×10^{-9}
$\|1,0\rangle_-\|2\nu_2\rangle$	5836	3.62×10^{-8}
$\|2,0\rangle_+$	5900	1.08×10^{-7}
$\|2,0\rangle_-$	5925	7.67×10^{-8}
$\|1,1\rangle$	6068	4.91×10^{-8}
$\|2,0\rangle_+\|2\nu_2\rangle$	8566	3.23×10^{-10}
$\|3,0\rangle_\pm$	8661	1.38×10^{-8}
$\|2,0\rangle_-\|2\nu_2\rangle$	8727	5.87×10^{-9}
$\|1,1\rangle\|2\nu_2\rangle$	8820	3.93×10^{-10}
$\|2,1\rangle_+$	8911	1.71×10^{-9}
$\|2,1\rangle_-$	9012	9.70×10^{-10}
$\|4,0\rangle_\pm$	11312	9.48×10^{-10}
$\|3,0\rangle_-\|2\nu_2\rangle$	11379	6.12×10^{-10}
$\|3,1\rangle_+$	11669	4.70×10^{-11}
$\|3,1\rangle_-$	11754	6.72×10^{-11}

Table B.3.

Oscillator Strengths of the Local Mode Overtone Peaks of CD_2Cl_2.

Assignment	Frequency (cm^{-1})	Oscillator Strength
$\|1,0\rangle_-\|2\nu_2\rangle$	4286	4.95×10^{-9}
$\|2,0\rangle_+$	4367	3.48×10^{-8}
$\|2,0\rangle_-$	4442	4.81×10^{-8}
$\|1,1\rangle$	4573	3.92×10^{-8}
$\|2,0\rangle_-\|2\nu_2\rangle$	6447	9.55×10^{-10}
$\|3,0\rangle_+$	6502	2.11×10^{-9}
$\|3,0\rangle_-$	6548	1.09×10^{-9}
$\|1,1\rangle\|2\nu_2\rangle$	6616	4.32×10^{-10}
$\|2,1\rangle_+$	6672	1.91×10^{-9}
$\|2,1\rangle_-$	6807	4.70×10^{-10}
$\|4,0\rangle_\pm$	8555	
$\|3,1\rangle_\pm$	8702	

REFERENCES

1. G. Herzberg, "Molecular Spectra and Molecular Structure. II. Infrared and Raman Spectra of Polyatomic Molecules", (Van Nostrand Reinhold, New York, 1945).
2. E. B. Wilson, Jr., J. C. Decius and P. C. Cross, "Molecular Vibrations. The Theory of Infrared and Raman Vibrational Spectra", revised ed., (Dover, New York, 1970).
3. J. W. Ellis, Trans. Farad. Soc. 25, 88 (1929).
4. R. Mecke, Z. Physik. Chem. B17, 1 (1932).
5. G. Herzberg, F. Patat and H. Verleger, J. Phys. Chem. 41, 123 (1937).
6. R. M. Badger and S. H. Bauer, J. Chem. Phys. 8, 469 (1936).
7. E. H. Eyster, J. Chem. Phys. 6, 580 (1938).
8. H. W. Thompson, J. Chem. Phys. 7, 453 (1939).
9. K. M. Gough, "Applications of the Local Mode Model to CH-Stretching Overtone Spectra of Substituted Benzenes and Related Compounds: Analysis of Structurally and Conformationally Inequivalent CH Bonds," Ph.D. Dissertation, University of Manitoba, 1984.
10. A. Amrein, H. R. Dubal, M. Lewerenz and M. Quack, Chem. Phys. Letters 112, 387 (1984).
11. W. Siebrand, J. Chem. Phys. 46, 440 (1967).
12. W. Siebrand, J. Chem. Phys. 47, 2441 (1967).
13. W. Siebrand and D. F. Williams, J. Chem. Phys. 49, 1860 (1968).
14. B. R. Henry and W. Siebrand, J. Chem. Phys. 49, 5369 (1968).
15. R. J. Hayward, B. R. Henry and W. Siebrand, J. Mol. Spectrosc. 46, 207 (1973).
16. R. J. Hayward and B. R. Henry, J. Mol. Spectrosc. 50, 58 (1974).

17. R. J. Hayward and B. R. Henry, J. Mol. Spectorsc. 57, 221 (1975).

18. B. R. Henry, Acc. Chem. Res. 10, 207 (1977).

19. B. R. Henry, "Vibrational Spectra and Structure", ed. by J. R. Durig, (Elsevier, New York, 1981), Vol. 10, p. 269.

20. M. L. Sage and J. Jortner, Advan. Chem. Phys. 47, 293 (1981).

21. M. S. Child and L. Halonen, Advan. Chem. Phys. 57, 1 (1984).

22. M. S. Child, Acc. Chem. Res. 18, 45 (1985).

23. W. R. A. Greenlay and B. R. Henry, Chem. Phys. Letters 53, 325 (1978).

24. B. R. Henry and R. J. D. Miller, Chem. Phys. Letters 60, 81 (1978).

25. M. A. Mohammadi and B. R. Henry, Proc. Natl. Acad. Sci. U.S.A. 78, 686 (1981).

26. B. R. Henry, M. A. Mohammadi and J. A. Thomson, J. Chem. Phys. 75, 3165 (1981).

27. B. R. Henry and K. M. Gough, Laser Chem. 2, 309 (1983).

28. K. M. Gough and B. R. Henry, J. Phys. Chem. 88, 1298 (1984).

29. J. S. Wong and C. B. Moore, J. Chem. Phys. 77, 603 (1982).

30. Y. Mizugai and M. Katayama, Chem. Phys. Letters 73, 240 (1980).

31. K. M. Gough and B. R. Henry, J. Am. Chem. Soc. 106, 2781 (1984).

32. B. R. Henry, K. M. Gough and M. G. Sowa, Int. Rev. Phys. Chem. 5, 133 (1986).

33. R. J. Hayward and B. R. Henry, Chem. Phys. 12, 387 (1976).

34. W. R. A. Greenlay and B. R. Henry, J. Chem. Phys. 69, 82 (1978).

35. B. R. Henry and W. R. A. Greenlay, J. Chem. Phys. 72, 5516 (1980).

36. B. R. Henry and J. A. Thomson, Chem. Phys. Letters 69, 275 (1980).

37. B. R. Henry, I. F. Hung, R. A. McPhail and H. L. Strauss, J. Am. Chem. Soc. 102, 515 (1980).

38. B. R. Henry and M. A. Mohammadi, Chem. Phys. 55, 385 (1981).

39. J. S. Wong, R. A. McPhail, C. B. Moore and H. L. Strauss, J. Phys. Chem. 86, 1478 (1982).

40. H. L. Fang and R. L. Swofford, Applied Optics 21, 55 (1982).

41. H. L. Fang, D. M. Meister and R. L. Swofford, J. Phys. Chem. 88, 405 (1984); 88, 410 (1984).

42. H. L. Fang, R. L. Swofford and D. A. C. Compton, Chem. Phys. Letters 108, 539 (1984).

43. H. L. Fang, R. L. Swofford, M. McDevitt and A. B. Anderson, J. Phys. Chem. 89, 225 (1985).

44. J. W. Perry and A. H. Zewail, J. Chem. Phys. 70, 582 (1979).

45. J. W. Perry and A. H. Zewail, Chem. Phys. Letters 65, 31 (1979).

46. A. H. Zewail and D. J. Diestler, Chem. Phys. Letters 65, 37 (1979).

47. R. G. Bray and M. J. Berry, J. Chem. Phys. 71, 4909 (1979).

48. B. R. Henry and M. A. Mohammadi, Chem. Phys. Letters 75, 99 (1980).

49. G. A. West, R. P. Mariella, Jr., J. A. Pete, W. B. Hammond and D. F. Heller, J. Chem. Phys. 75, 2006 (1981).

50. K. V. Reddy, D. F. Heller and M. J. Berry, J. Chem. Phys. 76, 2814 (1982).

51. J. W. Perry and A. H. Zewail, J. Phys. Chem. 86, 5197 (1982).

52. B. R. Henry, M. A. Mohammadi, I. Hanazaki and R. Nakagaki, J. Phys. Chem. 87, 4827 (1983).

53. J. W. Perry, D. J. Moll, A. Kupperman, and A. H. Zewail, J. Chem. Phys. 82, 1195 (1985).

54. A. W. Tarr and B. R. Henry, Chem. Phys. Letters 112, 295 (1984).

55. J. W. Perry and A. H. Zewail, J. Chem. Phys. 80, 5333 (1984).

56. D. F. Heller and S. Mukamel, J. Chem. Phys. 70, 463 (1979).

57. K. Deguchi, A. Sado, K. Nishikawa and S. Aono, J. Chem. Phys. 75, 5584 (1981).

58. M. L. Sage and J. Jortner, Chem. Phys. Letters 62, 451 (1979).

59. J. Stone, E. Thiele and M. F. Goodman, J. Chem. Phys. 75, 1712 (1981).

60. P. R. Stannard and W. M. Gelbart, J. Phys. Chem. 85, 3592 (1981).

61. A. H. Zewail, Wm. Lambert, P. Felker, J. Perry and W. Warren, J. Phys. Chem. 86, 1184 (1982).

62. C. J. Cerjan, S. Shi and W. H. Miller, J. Phys. Chem. 86, 2244 (1982).

63. E. L. Sibert III, W. P. Reinhardt and J. T. Hynes, Chem. Phys. Letters 92, 455 (1982).

64. A. L. Sobolewski, R. Czerminski and K. Kuczera, Mol. Phys. 50, 971 (1983).

65. S. Mukamel, J. Phys. Chem. 88, 832 (1984).

66. S. Mukamel and S. Islampour, Chem. Phys. Letters 108, 161 (1984).

67. E. L. Sibert III, W. P. Reinhardt and J. T. Hynes, J. Chem. Phys. 81, 1115 (1984).

68. A. W. Tarr and B. R. Henry, J. Chem. Phys. 84, 1355 (1986).

69. A. W. Tarr, "Developments in the Local Mode Theory of XH-Stretching Overtone Spectroscopy: Symmetry Effects, Intensities and Vibratinoal Dynamics", Ph.D. Dissertation, University of Manitoba, 1985.

70. O. S. Mortensen, B. R. Henry and M. A. Mohammadi, J. Chem. Phys. 75, 4800 (1981).

71. B. R. Henry, A. W. Tarr, O. S. Mortensen, W. F. Murphy and D. A. C. Compton, J. Chem. Phys. 79, 2583 (1983).

72. R. T. Lawton and M. S. Child, Mol. Phys. 40, 773 (1980).

73. I. A. Watson, B. R. Henry and I. G. Ross, Spectrochim. Acta 37A, 857 (1981).

74. M. S. Child and R. T. Lawton, Faraday Disc. Chem. Soc. 71, 273 (1981).

75. K. Tamagake, S. Hyodo and T. Fujiyama, Bull. Chem. Soc. Jpn. 55, 1277 (1982).

76. M. S. Child and R. T. Lawton, Chem. Phys. Letters 87, 217 (1982).

77. M. S. Burberry and A. C. Albrecht, J. Chem. Phys. 71, 4631 (1979).

78. L. Halonen and M. S. Child, J. Chem. Phys. 79, 4355 (1983).

79. L. Halonen and M. S. Child, Mol. Phys. 46, 239 (1982).

80. I. Abram, A. de Martino and R. Frey, J. Chem. Phys. 76, 5727 (1982).

81. L. Halonen and M. S. Child, J. Chem. Phys. 79, 559 (1983).

82. R. Wallace, Chem. Phys. 11, 189 (1975).

83. O. S. Mortensen and S. Hassing, "Advances in Infrared and Raman Spectroscopy" ed. by R. J. H. Clark and R. E. Hester, (Heyden, London, 1979), Vol. 6, p. 1; O. S. Mortensen, to be published.

84. T. Schaefer and G. H. Penner, J. Raman Spectrosc. 16, 353 (1985).

85. P. J. A. Ribeiro-Claro and J. J. C. Teixeira-Dias, J. Raman Spectrosc. 15, 224 (1984).

86. R. J. A. Ribeiro-Claro, A. M. D'A. Rocha Gonsalves and J. J. C. Teixeira-Dias, Spectrochim. Acta 41A, 1055 (1985).

87. O. S. Mortensen, M. K. Ahmed, B. R. Henry and A. W. Tarr, J. Chem. Phys. 82, 3903 (1985).

88. R. J. Myers and W. D. Gwinn, J. Chem. Phys. 20, 420 (1952).

89. "FT-IR Software Manual", Nicolet Instrument Corporation, 5225-1 Verona Road, Madison, Wisconsin.

90. J. L. Wagener, "Principles of Fortran Seventy Seven Programming", (John Wiley and Sons, New York, 1980).

91. Ira N. Levine, "Quantum Chemistry", third edition, (Allyn and Bacon, Inc., Massachusetts, 1983).

92. (a) M. R. Petersen and R. A. Poirier, MONSTERGAUSS, Dept. of Chemistry, University of Toronto, Toronto, Ontario, Canada (1981).

(b) J. S. Binkley, M. J. Frisch, D. J. Defrees, K. Raghavachari, R. A. Whiteside, H. B. Schlegel, E. M. Fluder and J. A. Pople Gaussian 82, Department of Chemistry, Carnegie Mellon University Pittsburgh, P.A., U.S.A., 1983.

93. D. C. McKean, J. L. Duncan and L. Batt, Spectrochim. Acta, 29A, 1037 (1973).

94. D. C. McKean, Chem. Soc. Rev. 7, 399 (1978).

95. G. A. Voth, R. A. Marcus and A. H. Zewail, J. Chem. Phys. 81, 5494 (1984).

96. S. Peyerimhoff, M. Lewerenz and M. Quack, Chem. Phys. Letters 109, 563 (1984).

97. T. Shimanouchi and I. Suzuki, J. Mol. Spectrosc. 8, 222 (1962).

98. F. E. Palma, E. A. Piotrowski, S. Sundaram and F. F. Cleveland, J. Mol. Spectrosc. 13, 119 (1964).

99. H. L. Fang and R. L. Swofford, J. Chem. Phys. 72, 6382 (1980).

100. Reference 1, page 216.

101. M. Avanessof, H. D. Thang and R. Gaumann, Helv. Chim. Acta, 54, 1013 (1971).

102. H. L. Fang and R. L. Swofford, J. Chem. Phys. 73, 2607 (1980).

103. H. R. Dubal and M. Quack, J. Chem. Phys., 81, 3779 (1984).

104. A. W. Tarr, D. J. Swanton and B. R. Henry, J. Chem. Phys. in press.

105. E. S. Medvedev, Acad. Sci. USSR, Institute of Chemical Physics, Preprint (1984).

106. E. S. Medvedev, Chem. Phys. Letters 120, 173 (1985).

107. E. S. Medvedev, J. Mol. Spectrosc. 114, 1 (1985).

108. W. K. Glass and A. D. E. Pullin, Trans. Faraday Soc., 59, 25 (1963).

109. P. W. Atkins, Molecular Quantum Mechanics, 2nd ed. (Oxford University, Oxford, 1983).

110. M. S. Burberry, J. A. Morrell, A. C. Albrecht and R. L. Swofford, J. Chem. Phys. 70, 5522 (1979).

111. F. F. Cleveland and A. G. Meister, J. Chem. Phys. 19, 1561 (1951).

112. J. C. Evans and H. J. Bernstein, Can. J. Chem. 33, 1746 (1955).

113. H. R. Dubal and M. Quack, Mol. Phys. 53, 257 (1984).

114. J. E. Baggott, M. C. Chuang, R. N. Zare, H. R. Dubal and M. Quack, J. Chem. Phys. 82, 1186 (1985).

115. D. C. McKean, S. Biedermann and H. Burger, Spectrochim. Acta 30A, 845 (1974).

116. M. L. Sage, J. Chem. Phys. 80, 2872 (1984).

117. I. Hanazaki, M. Baba and U. Nagashima, J. Phys. Chem. 89, 5637 (1985).

118. L. A. Findsen, H. L. Fang, R. L. Swofford and R. L. Birge, J. Chem. Phys. 84, 16 (1986).

119. C. C. Robins, Proc. Roy. Soc. A, 269, 492 (1962).

120. L. J. Bellamy and D. W. Mayo, J. Phys. Chem., 80, 1217 (1976).

121. H. P. Hamlow, S. Okuda and N. Nakagawa, Tetrahedron Lett., No. 37, 2553 (1964).

122. J. O. Williams, J. N. Scarsdale and L. Schafer, J. Mol. Struct., 76, 11 (1981).

123. C. J. Wurrey, J. E. DeWitt and V. F. Kalasinsky, Vib. Spectra Struct., 12, 205 (1983).

124. D. K. Hendricksen and M. D. Harmony, J. Chem. Phys., 51, 700 (1969).

125. M. Pelissier, C. Leibovici and J. F. Labarre, Tetrahedron, 28, 4825 (1972).

126. A. R. Mochel, J. E. Boggs and P. N. Skancke, J. Mol. Struct., 15, 93 (1973).

127. V. F. Kalasinsky, D. E. Powers and W. C. Harris, J. Phys. Chem., 83, 506 (1979).

128. L. S. Bartell, J. P. Guillory and A. T. Parks, J. Phys Chem., 69, 3043 (1965).

129. P. L. Lee and R. H. Schwendeman, J. Mol. Spectrosc., 41, 84 (1972).

130. D. L. Powell, P. Klaboe and D. H. Christensen, J. Mol. Struct., 15, 77 (1973).

131. J. L. Pierre, Ann. Chim. (Paris), 1, 383 (1966).

132. W. G. Rothschild, J Chem. Phys., 44, 3875 (1966).

133. T. Hirokawa, M. Hayashi and H. Murata, J. Sci. Hiroshima Univ., Ser. A, 37, 301 (1973).

134. L. H. Daly and S. E. Wiberley, J. Mol. Spectrosc., 2, 177 (1958).

135. D. C. McKean, Chem. Commun. 1373 (1971).

136. C. K. N. Patel, A. C. Tam and R. J. Kerl, J. Chem. Phys., 71, 1470 (1979).

137. L. Klasinc, Z. Maksic and M. Randic, J. Chem. Soc. A, 755 (1966).

138. B. Galabov and H. Morris, J. Mol. Struct., 17, 421 (1973).

139. B. Galabov and D. Simov, J. Mol. Struct., 11, 341 (1972).

140. N. Muller and D. E. Pritchard, J. Chem. Phys., 31, 1471 (1959).

141. W. A. Bernett, J. Chem. Educ., 44, 17 (1967).

142. K. M. Crecely, V. S. Watts and J. H. Goldstein, J. Mol. Spectrosc., 30, 184 (1969).

143. P. H. Weiner and E. R. Malinowski, J. Phys. Chem., 71, 2791 (1967).

144. C. V. Alsenoy, H. P. Figeys and P. Geerlings, Theor. Chim. Acta, 55, 87 (1980).

145. N. Muller and D. E. Pritchard, J. Chem. Phys., 31, 768 (1959).

146. Y. Mizugai, M. Katayama and N. Nakagawa, J. Am. Chem. Soc. 103, 506 (1981).

147. R. Nakagaki and I. Hanazaki, Chem. Phys. 72, 93 (1982).

148. R. Nakagaki and I. Hanazaki, Spectrochim. Acta, Part A 40, 57 (1984).

149. F. Pang, J. E. Boggs, P. Pulay and G. Fogarasi, J. Mol. Struct. 66, 281 (1980).

150. K. M. Gough, B. R. Henry and T. A. Wildman, J. Mol. Struct. 124, 71 (1985).

151. W. R. Woolfenden and D. M. Grant, J. Am. Chem. Soc. 88, 1496 (1966).

152. H. D. Rudolph, K. Walzer and I. Krutzik, J. Mol. Spectrosc. 47, 314 (1973).

153. W. A. Kreiner, H. D. Rudolph and B. Tan, J. Mol. Spectrosc. 48, 86 (1973).

154. Y. Mizugai and M. Katayama, J. Am. Chem. Soc. 53, 2081 (1980).

155. Y. Mizugai and M. Katayama, J. Am. Chem. Soc. 102, 6425 (1980).

156. V. F. Kalasinsky and C. J. Wurrey, J. Raman Spectrosc. 9, 315 (1980).